STRUCTURE-PROPERTY CHARACTERISATION OF TERNARY PHASE POLYPROPYLENE COMPOSITES

A thesis submitted for the degree of
Doctor of Philosophy

by

KALYANEE PREMPHET

Department of Materials Technology
Brunel University
Uxbridge, Middlesex.

August 1995

Brunel University, Uxbridge; Department of Materials Technology; August 1995.

STRUCTURE-PROPERTY CHARACTERISATION OF TERNARY PHASE POLYPROPYLENE COMPOSITES

Kalyanee PREMPHET

ABSTRACT

An investigation to study factors controlling the structure and properties of binary- and ternary-phase polypropylene (PP) composites containing ethylene-propylene rubber (EPR) and glass beads has been carried out. The composite structure was evaluated using various techniques including SEM, DSC, XRD and DMA. While the mechanical tests included tensile and impact measurements at ambient temperature, and a fracture toughness test based on the J-integral method carried out at -20 °C.

EPR and glass beads were found to influence the structure and properties of polypropylene in different ways. Incorporation of EPR into polypropylene results in an improvement in impact strength and toughness, accompanied by a decrease in tensile strength and modulus. The opposite was found for composites containing glass beads. Polypropylene composites with balanced mechanical properties were achieved by physical blending of this polymer with both EPR and glass beads. The effect of composite structure, composition and processing variables on the properties of the ternary systems were analysed. A study of their morphology has shown that two kinds of phase structure can be formed, either a separate dispersion of the phases, or encapsulation of the filler by rubber. Factors controlling these structures are believed to be due mainly to the surface characteristics of the components. Modification of EPR by maleic-anhydride grafting results in composites with rubber encapsulation of the filler, with FTIR revealing a reaction between these phases. Composites containing unmodified EPR, on the other hand, show separate dispersion of the components. The former composites, with good adhesion at the rubber and filler interface, have noticeably higher impact strength and fracture toughness at and below ambient temperatures, while the latter variant is characterised by higher tensile strength and modulus, accompanied by a lower impact strength. Improvements in impact strength of the composites was also achieved by promoting adhesion between the polymer and filler interface using surface-coated glass beads, or by increasing the number of rubber particles adhering to the glass bead surfaces using a two-step mixing technique. Results of the present study have thus shown that mechanical properties of ternary phase polypropylene composites can be adjusted, to a certain extent, by controlling their morphologies through the use of suitable functionalised materials and also by using an appropriate compounding methodology.

ACKNOWLEDGEMENTS

I am deeply indebted to my supervisor Dr. P.R. Hornsby for his constant guidance and encouragement throughout the course of this work. I would also like to thank Dr. K. Tarverdi of Wolfson Centre and the technicians of Materials Technology Department for their technical assistance and useful advice, and finally to the Royal Thai Government for providing financial support.

CONTENTS

Contents

page

CHAPTER 1

INTRODUCTION

1.1 MULTIPHASE POLYMER COMPOSITES

Multiphase polymer composites are composites consisting of at least one component which is a polymer. They may be two-phase systems such as polymer blends, rubber toughened polymers or filled polymers, or three-phase systems where both rubber and filler are present in the systems. Furthermore, rubbers may be modified to contain reactive groups which will interact with the matrix in which they are dispersed. In the same way fillers may be modified by some surface treatment or by coating with an interfacial agent. In this way, four or more - phase systems may be obtained.

Multiphase polymer composites have both commercial and scientific significance. A wide range of product properties can be developed by incorporating two or more suitable materials into the system. Also, due to the ease of mixing and blending the cost in the production of multiphase polymer composites is much lower compared to synthesising a new polymer of required properties.

Properties of multiphase polymer composites are governed by many variables interrelated to each other, apart from the properties of the constituents and of the interaction between them, processing conditions as well as their morphology also play an important role.

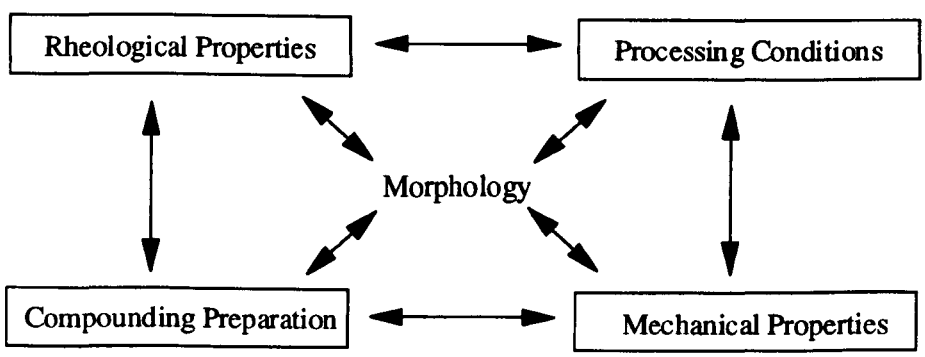

Figure 1.1 Schematic pointing out processing-morphology-property relationship in multiphase polymer composites.

As shown in *Figure 1.1* the method of composite preparation controls the morphology (e.g. the state of dispersion, rubber particle size and its distribution) which in turn controls the rheological and mechanical properties. On the other hand, the rheological properties strongly dictate the choice of processing conditions (e.g. temperature, shear

stress) which in turn strongly influence the morphology, and therefore the ultimate mechanical properties of the composites. Therefore, a scientific understanding of the relationship between processing, structure and property in multiphase polymer composites is necessary for optimising compounding conditions and composite properties.

In the present study structure and properties of the ternary phase polypropylene composites were investigated. Polypropylene is a commercially important polymer which finds use in a wide range of applications including automotive interiors and domestic appliances. The success of polypropylene is owed in part to its good mechanical properties at relatively low cost. However, under sub-ambient temperature conditions its usefulness is limited by the embrittlement behaviour. One of the most often used methods to overcome this drawback is blending with rubbery materials such as ethylene-propylene-diene terpolymer (EPDM), ethylene-propylene rubber (EPR) and polyisobutylene (PiB). Rubber modification increases polypropylene's low temperature impact strength, but lowers its stiffness. To compensate this effect, filler is added to the composite, i.e. ternary phase polymer composites are prepared. Ternary phase polypropylene composites have been investigated to some extent [141-159], but the contradictory results still remain to be verified especially their phase microstructures.

The ultimate aim of this study was to understand the relationships between the microstructure and mechanical properties of the ternary phase polypropylene composites containing ethylene-propylene rubber and glass beads. Particular attention has been directed to studying the influence of composite formulation, processing conditions, and interfacial modification of constituents.

1.2 THESIS OUTLINE

This thesis is divided into eight chapters.

Chapter 1 presents a general knowledge on multiphase polymer composites, including their advantages in both practical and theoretical points of view. The concept and the ultimate aim of the research work are included.

Chapter 2 contains a comprehensive review of the existing literature concerned with polypropylene composites. The structure and mechanical properties of polypropylene are described first, followed by the modification of polypropylene properties for both rubber

modified polypropylene and particulate filled polypropylene composites. Finally the current investigations on multiphase polypropylene composites involving both rubber and filler in the system are considered.

Chapter 3 is concerned with details of materials used throughout the work, composite preparation, and a detailed explanation of the characterisation techniques and experimental procedure employed. In some cases preliminary studies are also included to provide useful guidelines on the interpretation and quantification of results.

Chapter 4 presents the results and discussion of studies on the two-phase polypropylene and ethylene-propylene rubber (PP/EPR) blends. Two grades of polypropylene and two grades of ethylene-propylene rubber, differing in melt viscosity, were investigated. Influence of ethylene-propylene rubber on the morphology and mechanical properties of polypropylene are discussed. An attempt has been made to explain the toughening mechanisms in such blends.

Chapter 5 contains the results and discussion of studies on glass bead filled polypropylene composites. Again, the effect of glass beads on the microstructure and mechanical properties of polypropylene is discussed. The influence of bead particle size and composition are also considered. Various theoretical models were used in analysing the mechanical property data.

Chapter 6 is concerned with studies on the ternary phase composites of polypropylene, ethylene-propylene rubber and glass beads. The results gained from Chapters 4 and 5 are used in this chapter as background knowledge for the selection of suitable materials and also in the interpretation of results. The emphasis has been given to understand the relationship between the composite microstructure and properties, as well as factors controlling them. Influence of composite formulation and processing variables are discussed, including screw configuration, screw speed, feed rate, and the sequence in which each component was mixed in the extruder.

Chapter 7 presents the results and discussion of studies on the modified ternary phase polypropylene composites, in which surface-coated glass beads and functionalised rubber were used. The aim of the work is to investigate whether the phase microstructure of the composite can be altered by these modified components. Also, it is known that mechanical properties in polymer composites are limited by the strength of the interface, the ability to understand and optimise the interface is recognised as a key in developing materials of improved properties. For this reason, effect of surface-coated glass beads

and functionalised ethylene-propylene rubber are described in terms of the composite properties both at room temperature and at low temperature (-20 °C). Finally, the role of an interfacial modification and processing conditions in controlling composite microstructure and in turns composite properties are discussed.

Chapter 8 summarises tentative conclusions of the results based on present study and recommendations for further study are proposed.

CHAPTER 2

LITERATURE REVIEW

2.1 INTRODUCTION

This chapter contains a comprehensive review of the existing literature concerned with polypropylene composites. The structure and mechanical properties of polypropylene are described first. The modification of polypropylene properties is then discussed for both rubber modified polypropylene and filled polypropylene composites. Finally the current investigations on multiphase polypropylene composites where both rubber and filler are involved in the system are considered. Emphasis is placed upon morphology and property relationships as well as factors controlling them.

2.2 POLYPROPYLENE [1]

Polypropylene is one of the most important commercial thermoplastics prepared by polymerisation of propylene (CH_2=CH-CH_3) using Ziegler-Natta catalyst. Three different stereoregular configurations can be obtained in respect to the position of methyl (-CH_3) groups on the chain. They are either atactic, in which the methyl groups are randomly positioned along the chain polypropylene; syndiotactic, with the methyl groups appearing alternatively on both sides of one chain; and isotactic polypropylene where all the methyl groups are on the same side of one chain. Among these configurations, the isotactic form is the most important commercially. It takes more than 90% of polypropylene market. Syndiotactic form is only of scientific interest. Commercial polypropylenes generally have approximately 0.95 or higher isotactic indices. High isotactic index contributes to higher crystallisation and can lead to much improvement in mechanical properties.

2.2.1 Crystal structure of isotactic polypropylene

Isotactic polypropylene (iPP) is a polymorphic material which can crystallise in a number of crystal modifications [2], such as monoclinic (α), hexagonal (β) and triclinic (γ). The conventional and most widely occurring crystal structure of polypropylene is the α structure, first observed by Natta [3] in melt crystallised materials. The α crystal structure is monoclinic and the chains assume a helical conformation which arranged in a regular pattern, a left handed helix always facing a right-handed one. The hexagonal β-modification only occurs occasionally. It was known [4-6] to be favoured by high shear rate [7], fast cooling [8] and certain heterogeneous nucleating agents [9-12] such as chinacridine permanent red E3B [12-14]. The third crystalline modification of iPP is the

triclinic γ-structure, identified by Turner-Jones et.al.[2]. This modification may form in degraded, low molecular weight polypropylene [15], or in highly oriented polypropylene [127] or in samples crystallised under high pressure [16]. Quenching the molten polymer can lead to an intermediate crystalline order (between amorphous and crystalline) which has been described as "smectic form" . The interpretation of this structure is still disputed in the literature [17-18].

2.2.1.1 The spherulitic and lamella morphology of isotactic polypropylene

Spherulitic structure generally appears when crystallisation is conducted in the viscous state and/or at a high undercooling. The term "spherulite" indicates an aggregate of primary crystallites of spherical shape or spherical symmetry consisting of crystallites growing from central nuclei uniformly in all steric directions. Complete filling of the space is provided by further branching of fibrils from the main growth of fibrils at small non-crystallographic angles [19].

On the resolution level of the polarising microscope, the development of birefringent disc-like formations on randomly formed crystal nuclei can be revealed. Depending on the birefringence, spherulites can be optically positive or negative. The optical character, i.e. the sign of birefringence of the spherulites can be determined by using a primary red filter located diagonally between crossed polarisers. In this way the first and third quarter of the sight are blue and the second and fourth ones are yellow when the spherulites are positive, while a reversed arrangement of the quarter is observed for negative spherulites.

Padden and Keith [20] were the first to report five different types of polypropylene spherulites consisting of α- and β-modifications. Spherulites type I and II, known as the α-modifications are composed of monoclinic unit cells. Their birefringence is low, positive for the first and negative for the second. The spherulites of type III and IV are of β-modification. They are much more negative in birefringence and are easily distinguished by their highly luminous appearance in polarised light, surrounded by much less bright α-spherulites. Type V is a mixed type spherulite of α-modification in the intermediate range. The spherulite exhibits random distributions of positively and negatively birefringent regions where the birefringence is low and often not measurable value. The observations of Padden and Keith [20] were essentially supported by other investigations [21], however, the temperature ranges for the formation of the particular types of spherulites have been corrected more or less, presumably due to the variability in the characteristics of the molecular structure of iPP types studied [21]. The

characteristics of all the spherulites, perceived by the studies of Norton and Keller [21] are given in *Table 2.1*.

The lamella morphology of iPP on the resolution level of the electron microscope is also complex. The feature of cross-hatch type lamella is believed [21] to occur in all types of monoclinic α-spherulites (I, II, Mixed). In this feature, radial fibrils were accompanied by a great number of tangential ones. Norton and Keller [21] demonstrated that α-spherulites formed in the melt grown specimen contained fibrils with large-angle branches even at about 80° to radius of the spherulite. This was in good agreement with Khoury's data [22] for twin crystals grown by crystallisation in solution. The optical character (positive or negative) of α-spherulites is controlled by the ratio of radial to tangential fibrils. Raising the temperature of crystallisation leads to a reduction in the proportion of tangential fibrils [21] and, simultaneously, a positive to negative character transformation.

The work by Norton and Keller [21] also revealed the lamella texture of β-spherulites. The arrangement of the fibrils in β-spherulites is radial, as is usual in polymeric spherulites, and no traces of cross-hatched structure can be detected. The central region of β-spherulites comprises non-homogenous and sheaf-like branched fibrils.

Table 2.1 - Characteristics of polypropylene spherulites [21]

Spherulite type	I	Mixed	II	III	IV
	Monoclinic			Hexagonal	
Crystal structure	α	α	α	β	β
Magnitude of birefringence	-0.003	±0.002	0.002	0.007	0.007
Concentric banding	No	No	No	No	Yes
Sign of birefringence	+ve	+ve/-ve	-ve	-ve	-ve
Isothermal temperature of crystallisation	<134°C	134-138°C	>138°C	<122°C	126-132°C

2.2.1.2 Thermal behaviour of iPP spherulites

The melting behaviour of α- and β-spherulites differs significantly. In a sample subjected to the usual crystallisation, the melting points of the α- and β-spherulites are ~167° and ~152°C, respectively [19]. It should be noted that the experimental melting point of spherulites (the temperature of the complete disappearance of birefringence) depends on the temperature or temperature range of crystallisation. The melting characteristics of iPP spherulites were studied by Padden and Keith [20]. They observed the transformation of positive and mixed α-spherulites to the negative type when the sample was warmed and melted. On the other hand, β-spherulites recrystallised into the α-modification during heating. This observation was supported by other researchers [8, 23]. The reason for recrystallisation was reported [8, 23] to be due to thermodynamic instability of the β-modification. Subsequently, Varga [9] pointed out that melting of β-modification had a specific feature including a much more complicated process than that outline above. He concluded that when heating begins from the temperature of crystallisation, the β-modification does not recrystallise into the α-form. Instead, they melt separately, like the thermodynamically stable modification. However if samples containing β-PP are cooled below a critical temperature (~100-110°C) before heating, the partial melting is accompanied by a recrystallisation into α-form (βα-recrystallisation), and finally they melt in the α-form.

The α-modification recrystallised from β-spherulites has a higher melting point than α-spherulites originally present in the sample formed isothermally. The higher melting point of the α-modification formed by recrystallisation is thought to be due to its higher (re)crystallisation temperature.

The thermal conditions of crystallisation govern not only the type and optical character of spherulites, but also influence the size and size distribution of the spherulites. By reducing the crystallisation temperature or by increasing rate of recrystallisation, the average spherulite size decreases due to an increase in the average density of nuclei. As a theoretical interpretation of the size reduction of spherulites with increasing undercooling ($\Delta T = T_m - T_c$), the thermodynamic barrier of nucleation is proportional to ΔT^{-2} while that of the growth is linear with ΔT^{-1} [24]. In other words, the rate of nucleation increases at a considerably greater extent than that of growth of nuclei when the temperature decreases.

2.2.2 *Properties of isotactic polypropylene*

Polypropylene has an excellent balance of properties at relatively low cost. It has high tensile strength, stiffness and hardness due to its high crystallinity. It has a low specific gravity ~0.902. This leads to high strength-to-weight ratio and low cost per unit volume. Polypropylene has a high melting temperature T_m (~165°C) therefore it is able to retain high strength at elevated temperature. Polypropylene has good chemical properties. It is highly resistant to chemicals and also moisture. It dissolves in high boiling aliphatic and aromatic hydrocarbon at elevated temperature. However, because of containing tertiary hydrogens in the chains, it is easy to react with oxygen in several ways causing the chain to break and the polymer to become brittle. Stabilisers and antioxidants are required for protection.

Apart from the above excellent properties, polypropylene also possesses some characteristics which make it more commercially interesting. It can be processed easily in most commercial fabrication techniques. Furthermore, it can be modified for a variety of applications. Through various techniques the physical properties of the product can be varied to meet a wide range of thermal and mechanical requirements.

The usefulness of polypropylene is limited at low temperatures by the embrittlement at its glass transition temperature (about 0-6°C). Many attempts have been made to overcome this problem either by co-polymerisation with ethylene or melt-blending with rubbery materials. Incorporation of a rubbery phase with a sufficiently low glass transition temperature to polypropylene by melt blending is of economically and a wide range of properties can be gained by altering blend compositions or processing conditions used. However, the improved low temperature impact strength of such blends may accompany with a reduction of other mechanical properties such as stiffness, hardness, etc.

Modification of polypropylene can also be achieved by incorporation of mineral fillers. This usually gives rise to higher stiffness and harder products. However, the major problem in mineral filled polypropylene is that of poor impact strength. Products with balance properties, such as good impact strength and stiffness at room and low temperature, can be obtained by a concept of ternary blend which contains both rubber and mineral filler in the polypropylene matrix.

2.3 RUBBER MODIFIED POLYPROPYLENE

Based on Polypropylene/Ethylene-Propylene Copolymer, PP/EPR, Blends.

Rubber-thermoplastic blends have recently stimulated much interest because they offer the simplest route to achieve outstanding properties and low cost. The main property improvements sought through rubber/polymer blending include impact strength and toughness. Examples of rubber modified thermoplastics are shown in *Table 2.2*. One of the largest families of such blends is that made from polypropylene blends [25]. In the present review, blends based on polypropylene (PP) and ethylene-propylene rubber (EPR) are considered.

Table 2.2 - Examples of elastomer-thermoplastic blends

Thermoplastics	Elastomers
Isotactic polypropylene (iPP)	Ethylene-propylene copolymer (EPR); ethylene-propylene-diene terpolymer (EPDM); polyisobutylene (PiB)
Polyamide-6 (PA-6)	Ethylene-propylene copolymer (EPR); functionalised ethylene-propylene copolymer (EPR-g-SA); styrene-b-(ethylene-co-butene-1)-b-styrene (SEBS); styrene-acrylonitrile rubber (SAN)
Polybutylene terephthalate (PBT)	Functionalised ethylene-propylene copolymer (EPR-g-SA)
Polycarbonate (PC)	Ethylene-propylene copolymer (EPR); ethylene-propylene-diene terpolymer (EPDM); acrylonitrile-butadiene-styrene rubber (ABS); methacrylate-butadiene-styrene grafted copolymer (MBS)
Polyvinyl chloride (PVC)	Nitrile rubber; epoxidised natural rubber (ENR); butadiene rubber; acrylonitrile butadiene rubber (ABR)

Although polypropylene has a most remarkable combination in physical properties, the inherently high glass transition temperature and high crystallinity of this polymer limit its usefulness in low temperature applications. Blending of polypropylene with various

elastomers is one of the commonly used methods to improve its performance. A variety of blends of polypropylene with ethylene-propylene-diene terpolymer (EPDM), ethylene-propylene copolymer (EPR), styrene block copolymer (SBS), polyisoprene, have been commercialised for automotive applications such as bumpers and dashboards. The properties of these blends generally depend on the composition and level of dispersion of the two phases. It was established [26] that the highest increment in the impact strength of polypropylene was achieved by using ethylene-propylene copolymer (EPR) and ethylene-propylene-diene terpolymer (EPDM). Moderate effects were obtained from styrene block copolymer (SBS) and butyl rubber while polybutadiene, polyisoprene and polyisobutylene did not increase the impact strength of polypropylene much. In practice, EPR and EPDM are mainly included in polypropylene matrices as rubber impact modifiers, while styrene-butadiene is used as a based matrix in thermoplastic elastomers.

EPR is a copolymer of ethylene and propylene. It is an inherently stable, rubbery material with good heat resistance, weatherability, electrical properties and chemical resistance. Polypropylene is rendered impact resistant when EPR is incorporated, commonly at a 5-30% level. This can be done either by melt-blending or by synthesising ethylene-propylene rubber *in situ* in polypropylene homopolymers.

Production of *in situ* blends can be accompanied by several methods. A simple example is the production of isotactic polypropylene in the first stage of the reactor which is then conveyed, along with the still-active Ziegler-Natta catalyst, to a second stage into which ethylene and propylene monomers are introduced [27]. There, a noncrystalline elastomeric copolymer is made which is blended intimately with the polypropylene powder. A small amount of hydrogen, present as a chain-transfer agent in the first stage, is swept into the second stage along with polypropylene powder. Thus, the final product is an intimate mixture of polypropylene homopolymer and ethylene-propylene rubber.

Generally, blends of PP and EPR in various proportions are usually prepared by melt-mixing. Where polymer and rubber have similar melt viscosities and are both in particulate form, it may be possible to mix them in low shear mixing sections or even directly through an extruder or injection moulding machine used in making the final product. However if polymer and rubber have different viscosities, intensive mixing may be required.

2.3.1 Melt-blending techniques

(i) Internal mixer

This type of mixer is often used for dispersing rubber in liquids or in rubber compounding applications. The Banbury mixer is a typical example. The Banbury mixer is a batch mixer with temperature, pressure, shear level controlled by rotating rotors turning at different speeds. An increase in the rotation velocity of the blades increases the shear rate, which leads to more frequent dividing of the mass and renewal of its surface. This promotes rapid distribution of ingredients in the mass. An increase in rotational velocity also leads to temperature rise in the mixture as well as increasing the pressure exerted against the walls of the chamber. The Banbury mixer has also been adapted for continuous processing in the Farrel Continuous Mixer (FCM). The degree of mixing is related to the rotor speed, temperature, pressure and time of mixing.

(ii) Single-screw extruder

The single screw extruder remains a very common tool for blending polymers, due to its widespread availability, low cost, and straightforward design. It is, however, a relatively poor mixing device, due to the low imposed shear strain. Also, during mixing the sample in a single screw extruder may experience a wide range of conditions. For example, some of the material that passes between the flights and the barrel can experience high rates of shear, while material passing along the channel will be subjected to lower rates of shear. The improvement of blending on the single screw extruder can be achieved through the use of various modified screw designs. Barrier screws, for example, are fitted perpendicular to the screw axis providing separation of the flow and enhancing distributive mixing.

(iii) Twin-screw extruder

An increasing number of compounding tasks is being undertaken on twin-screw extruders, due to their continuous operation, versatility and effective mixing action. These machines offer several advantages over single screw extruders. Better feeding and more positive conveying characteristics allow the machine to process hard-to-feed materials such as powders, slippery materials, etc. and yield short residence times and a narrow time distribution spectrum. Better mixing resulting from high shear input and larger heat transfer areas allow good control of the stock temperatures. Good control over residence times and stock temperatures obviously are key elements in the profile

extrusion of thermally sensitive materials such as unplasticised PVC. The behaviour of PVC during either single or twin screw extrusions had been reported elsewhere [219-220].

There are various types of twin-screw extruders available commercially. They differ in their design and operating principles, thus in their abilities for distributive and dispersive mixing and hence their application areas. The available twin-screw extruders can be classified as co-rotating and counter-rotating, on the basis of the direction of the rotating of the screws. The counter-rotating extruders can again be classified in terms of the degree of intermeshing of the screws, ranging from fully intermeshed, where the flight of one screw fits tightly into the channel of the other screw, to non-intermeshing "tangential", where the two screws rotate freely in their barrel sections. The co-rotating twin screw extruders are not produced in the non-intermeshing mode. Further differences can be found in the form of screw flight. Co-rotating designs, for example, may have rounded or so-called self-wiping screw flights, which have large channel clearances across the intermeshing zone, or trapezoidal shaped channels and flights with more restricted interchannel flow (see *Figure 2.1a*). This can have important implications with regard to their positive conveying efficiency and the nature of mixing between the screws. Trapezoidal shaped screws are generally more effective in both these respects.

Figure 2.2 shows different types of twin-screw extruders. Here distinction is made between the axially open machines, where there is continuous passage between the inlet and outlet and the axially closed machines, where the passage is interrupted at regular intervals. The development of these twin-screw extruders, dating back to the 19th century was discussed by White et.al. [167] and recently published in a monograph by the same author [168]. The theoretical basis of twin-screw extruders were given by Cheremisinoff [169], Martelli [170], Janssen [165] and Rauwendaal [166]. While experimental evaluation on the twin-screw extrusion performance was presented by Sakai and co-workers [171] and Rauwendaal [172]. In this context the intermeshing co-rotating twin screw extruder will be highlighted.

Co-rotating twin screw extruders are commonly produced on the fully intermeshing mode and operate on the building-block (modular) principle. The barrel can be assembled in sections, with each section individually heated and cooled. Screw elements are selected and assembled on two keyed screw shafts to fit the requirements of mixing task. Commonly employed elements include right-handed and left-handed (forward and reverse) regular flighted elements, forward and reverse kneading discs, and mixing and shearing pins. Element designs also come in with various shapes and dimensions.

Corotating elements convey the feed material toward the lower wedge where the material is compressed and further conveyed by the other screw as shown in *Figure 2.1b*. The material continues to be moved downstream from one screw to the other in a figure-eight pattern. Very little material passes through the close clearance between the screws that rotate in opposite directions in the area of intermesh. Virtually all of the material is therefore transferred from one screw to the other at each revolution, resulting in a complete renewal of surfaces. Mixing and kneading effects in the extruder can be altered by arranging and selecting discs. These discs, arranged in a staggered configuration, provide intensive transverse mixing by shear forces of varying intensity. Depending on the staggered angle, neutral, forward or reversing screw sections can be generated. In the neutral mode, the material is transferred from one half of the barrel to the other half in figure-eight form before being pressured to move on in the axial direction by the following melt elements. The calendering action (i.e. passage of the material through the high-shear-rate gap between the two discs) generates excellent dispersive mixing. The introduction of reverse elements will generate further extensive mixing in the axial direction.

Because of the design flexibility and effective mixing action, co-rotating twin screw extruders are widely used currently for a multitude of applications, including incorporation of fillers and reinforcements to commodity plastics, additive concentrates, polymer blending, PVC formulations, and reaction extrusion.

Hornsby and co-workers [173-178], using a co-rotating twin screw extruder with a trapezoidal-shaped screw channel, investigated dispersive mixing of highly filled polypropylene composites [174-176], distributive mixing phenomena [177], and polymer degradation during flow in the extruder [178]. Bartilla et.al. [63] studied effect of compounding conditions in a ZSK 30 twin-screw extruder on the properties of PP/EPDM blends. Lim and White [179] using the same ZSK 30 machine, investigated the development of phase morphology of a polyethylene/polyamide blend.

2.3.2 Blend morphology

Since PP and EPR are immiscible, its blends tend to phase-separate and two-phase systems are obtained where EPR forms a discontinuous phase within a continuous PP matrix. These blends are reported [28] immiscible also in the melt, even when the ethylene content of the copolymer is as low as 8 percent.

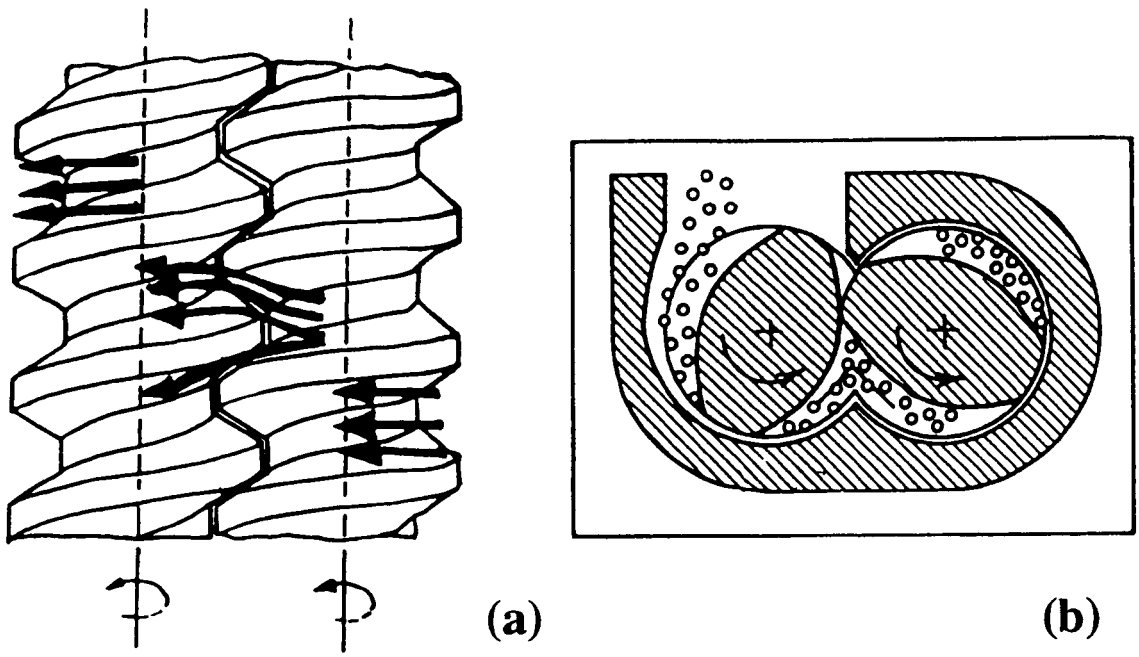

Figure 2.1 *(a)* Interchannel flow paths through the intermeshing zone of a co-rotating twin screw extruder with trapezoidal screws [180]. *(b)* Feed intake of co-rotating screws [181].

Screw engagement		System	Counterrotating	Corotating
Intermeshing	Fully intermeshing	Lengthwise and crosswise closed	1	Theoretically not possible 2
		Lengthwise open and crosswise closed	Theoretically not possible 3	Screws 4
		Lengthwise and crosswise open	Theoretically possible but practically not realized 5	Kneading disks 6
	Partially intermeshing	Lengthwise open and crosswise closed	7	Theoretically not possible 8
		Lengthwise and crosswise open	9A	10A
			9B	10B
Not intermeshing	Not intermeshing	Lengthwise and crosswise open	11	12

Figure 2.2 Twin screw design concepts [181].

In examining blend morphology and degree of dispersion in the immiscible blends, microscopy is frequently used. Both light (optical) and electron microscopy can be used. Light microscopy provides many techniques for polymer characterisation. In crystalline polymers, spherulitic structure is often studied by using a polarised or reflected light microscope. Phase-contrast is used for determining the structure of two phase systems. Interference contrast is used in the study of surface structures.

Karger-Kocsis et.al. [29] investigated the structure and location of the impact modifier in PP/EPR blends using optical microscopy. Due to the low glass-transition temperature of EPR (~ -40°C), a thin specimen was sectioned using an ultramicrotome equipped with a cryogenic adapter at -50°C.

However, optical microscopy has limited application in morphological investigations because of the low resolution. When one of the components of a blend is unsaturated, as in terpolymers of acrylonitrile-butadiene-styrene rubber or ethylene-propylene-diene (EPDM), then the morphology can be clearly seen by using osmium tetraoxide stained thin sections viewed by transmission electron microscopy (TEM). This technique has been applied to binary PP/EPDM blends [30-32] and ternary PP/EPDM/HDPE blends [33].

Although TEM observation of stained thin sections is a powerful technique for examining morphology of polymer blends, it suffers several disadvantages. Fundamentally, the method is not applicable to systems composed of saturated polymers that cannot be selectively stained, such as the PP/EPR system. It also requires considerable skill in ultramicrotomy to cut suitable thin sections.

Scanning electron microscopy (SEM) does not suffer these limitations. Surfaces for SEM investigations can be prepared by fracturing the sample. The fracture surface may be examined directly, or after removal of the rubbery component by selective solvents. The use of SEM on etched samples where the minor phase was removed is an excellent method of achieving a good contrast. The etching efficiency required for the analysis of phase morphology depends on the domain size of the dispersed phase. For polymer blends with a large domain of the dispersed phase, strong oxidising agents provide a more effective etching system [34]. The use of SEM to evaluate the interfacial interaction in polymer blends was studied by Hudec et al. [35].

The SEM analysis [26, 36-39] showed that PP/EPR blends are two phase system consisting of spherical shaped EPR particles distributed in the continuous PP matrix.

However, different observations have been reported on the location of the elastomer phase. Laus [40] demonstrated that the elastomeric impact modifier is situated between the spherulites in the inter-spherulitic boundary causing a reduction in the average size and formation of modified spherulitic morphologies. On the other hand, Karger-Kocsis et al. [26] and Martuscelli et al. [39] found that the elastomer may also be located inside the spherulites. Recently Karger-Kocsis et al. [41] concluded that impact modifier in PP/elastomer blends can be located both in intra- and inter-spherulitic situations depending on type, chemical structure and molecular characteristics of the impact modifier used.

Apart from microscopy, other experimental techniques may be used for the investigation of blend morphology. These include wide-angle X-ray scattering (WAXS) and small-angle X-ray scattering (SAXS) [30, 37, 42-44], small-angle neutron scattering (SANS) [27], differential scanning calorimetry (DSC) [30, 37, 45] and dynamic mechanical analysis (DMA) [43, 46].

WAXS have been widely used by many researchers [30, 37, 42]. Pukanszky et al. [30] investigated PP/EPDM blends using WAXS and SAXS. They found that EPDM seems to promote the formation of hexagonal (β-form) modification of polypropylene. An increase in elastomer contents only gives slightly changes in crystalline structure of polypropylene in the blend quickly cooled from the melt. Greco et al. [37] found the alteration in proportion of the monoclinic (α-form) and hexagonal (β-form) phases in the polypropylene matrix with the incorporation of EPR.

2.3.3 Factors controlling blend morphology

The physical behaviour as well as the final use-properties of the blends are related to the blend morphology which is affected by many factors. Apart from the nature of components (both molecular structure and chemical nature), viscosity ratio of plastic and rubber (or elastomer), blend composition and level of dispersion are major factors controlling the blend morphology. The dispersion level is in turn affected by the technique and conditions of compounding.

(i) Viscosity ratio

The viscosity ratio has been shown to be one of the most critical variables in controlling blend morphology. The size and size distribution of the disperse phase were found to be determined mainly by the value of viscosity ratio [36, 38, 47]. Generally matching the viscosities results in a fine morphology. There have been extensive studies on the rheological behaviour of mechanical blends of molten polymers; reviews are given by Han [48] and White et.al. [49].

Karger-Kocsis et al. [38] found for an iPP/EPDM system that there was a linear relationship between the number average diameter of the minor phase (EPDM) and the viscosity ratio. The particle size increased with increasing viscosity ratio. Fine dispersions could be achieved if the ethylene content of EPDM is low and the viscosity ratio value is near unity. A similar trend was also observed by D'Orazio [36] in iPP/EPR blends. The melt viscosity values of the blends were found to be lower than the mean value of the simple components. Danesi and Porter [47] reported that as the amount of rubber in the blend increased (80 EPR/20 PP) the viscosity ratio became less important in determining the state of dispersion.

(ii) Effect of composition on the blend morphology

The changes in blend composition can influence the state of dispersion of the phases in the blend via the changes in viscosity of polymer melts. There have been extensive reports on the dependence of viscosity on the blend composition. Many experimental studies [50-51] have indicated that the viscosity function varies monotonically with blend composition. However, there is little literature attempting quantify this relationship. The most widely quoted relation is that given by Hayashida et.al. [51] as shown below.

$$1/\eta = \phi/\eta_A + (1-\phi)/\eta_B \qquad (2.1)$$

where ϕ is the volume fraction of phase A and η_A and η_B are the shear viscosities of phases A and B at the same shear stress.

Pukanszky et al. [52] reported for PP/EPDM blends that a continuous PP phase was obtained at low EPDM content (less than 25-30 vol%) and continuous elastomer phase seen at high EPDM content (higher than 80 vol%) with a transitional structure is observed in between. Fortelny and Kovar [53] also found that in an PP/EPR blend the

phase structure changes in the composition ranging from 60/40 to 50/50 in the case where the viscosity of PP is more than that of EPR and from 50/50 to 60/40 in the case of viscosity of PP is lower than that of EPR. Their result was supported by Danesi and Porter [47]. They found that by increasing the EPR concentration, the size of elastomeric particles increases. Further increases in the elastomer concentration the elastomeric phase becomes continuous and the system has a structure comprising physically interpenetrating networks.

(iii) Crystallisation and thermal behaviour

The influence of impact modifiers such as EPR or EPDM on crystallisation and thermal behaviour of polypropylene blends has been studied by many researchers [54-57]. Their results can be summarised as follows:

Incorporation of impact modifier leads to a change in the structure of polypropylene in the blends. The proportion of α-form (monoclinic) and β-form (hexagonal) alters. Most researchers [26,37,45,58] reported that impact modifier significantly promotes the formation of α-form spherulites. The extent of α-form (spherulite type I) increases with increasing concentration of the impact modifier. Onogi et.al. [59] have reported that although quenched samples of virgin polypropylene crystallised in the hexagonal structure (β-form), the PP in the melt-blended PP/EPR samples crystallised in a monoclinic α-structure under similar conditions of quenching. In the α-spherulite form, however, some β-form (spherulite type III) can also be observed, its amount decreasing with increasing concentration of impact modifier. However, Pukanszky et al. reported findings contrary to these results [30]. They found that EPDM seems to promote the formation of β-form spherulites of PP in PP/EPDM blends.

Both the spherulitic fine structure, and the size of spherulites changes after EPR is incorporated. Bartczak et.al. [60], Martuscelli et.al. [61] and Kalfoglou [62] have investigated crystallisation behaviour in PP/EPR blends prepared by solution blending. Martuscelli et.al [61] have reported that the addition of EPR and polyisobutylene to PP results in a monotonic increase in the nucleation density of polypropylene as per optical microscopic studies carried out at 123 to 135°C. The incorporation of elastomer was found to decrease the average spherulite size. Recently, Kalfoglou [62] has also observed a reduction in the spherulite size of PP with increasing EPR content. Bartczak [45] concluded that these effects are not the result of the activity of EPR as a nucleating agent, but due to the migration of impurities from EPR phase to the iPP. Such impurities

induce the heterogeneous nucleation of iPP spherulites. Greco [37] , on the other hand, demonstrated that even in the system in which impurity-free elastomer was used, a reduction of spherulite size in the blend was still observed.

Thermal behaviour of the blends is mainly concerned with the crystalline phase in the blends. The incorporation of EPR into PP is known to alter the structure of polypropylene crystalline phase [26,37,45]. Therefore its thermal behaviour is altered. Since smaller spherulites, having lower heat capacity, are present in the blend, the melting range of the polymer blend should shift to a lower temperature. DSC results [26] showed that increasing the concentration of impact modifier shifted the melting peak of the polymer blend to a lower temperature. On the other hand, the crystallisation peak shifted to a higher temperature. As a result of these two effects, the extent of undercooling, which is defined as the difference between the melting temperature (T_m) and crystallisation temperature (T_c), decreases.

(iv) Blending procedure and processing conditions

Both processing equipment and compounding conditions used, such as type of mixing device, screw configuration, rotor speed, mixing time and energy input, play an important role in determining the morphology of polymer blends. Only a few studies exist on dispersion in polymer melt blends as a function of mixing regime, but those that do generally show that shear mixing in an internal mixer or mixing with a combined screw extruder can yield dispersions with phase sizes of the order of microns [41, 63-64].

Bartilla et. al. [63] studied the effect of processing variables in 70/30 (by weight) PP/EPDM blends on a co-rotating twin screw extruder. They found that the presence of built-in baffles (left-handed elements located downstream of the kneading blocks of the melting zone) provided finer EPDM particles with more uniform distribution. This result was due to the drag flow which took place in these left-handed elements, acts in opposition to the actual transport direction. As a result, a quasi circular flow was established leading to an increase in average residence time. Increasing the screw speed also resulted in more uniform EPDM distribution because the material was exposed to more shearing. On the other hand, increasing the material throughput produced a coarsening of the EPDM structure.

Jang [58] studied the morphology of rubber-modified polypropylene prepared using a Brabender extruder. The samples were subsequently injection moulded. It was found that the morphology of injection moulded samples in the core differed from that in the skin layer (shear zone). The spherulites in the skin layer were oriented while those in the core were randomly nucleated. In PP/EPR systems, the β-form (spherulite type III) was observed in the skin layer while the α-form (spherulite type I) was found in the core. The β-form of spherulites was stimulated by the high pressure inside the mould cavity.

Ho and Salovey [64] examined the morphology of PP/EPDM blends processed by injection and compression moulding. Droplets of EPDM were found to be elongated in the flow direction within 400 μm of the mould surface in injection moulding, while the spherical EPDM inclusions were observed in compression moulding. The size of spherical EPDM increased with increasing time under compression in the mould.

2.3.4 Structure-Property Relationships

2.3.4.1 Improvement in impact strength and toughness

The overwhelming number of rubber-modified thermoplastics are produced to improve the mechanical properties of a given (dominant) thermoplastic component which already has useful properties. Strength and toughness are perhaps the most important mechanical properties; they are both influenced by molecular architecture, polymer microstructure and sample homogeneity. Needless to mention that sample geometry, experimental parameters (rate of stress or strain, temperature) and environment can also influence the mechanical properties.

(i) Impact strength

Rubber-modified thermoplastics, in particular, can offer added impact resistance while maintaining stiffness, strength and processability at a desired level. The influence of EPR on the mechanical properties of PP has been studied by many researchers [36,37,52,65] and can be summarised as follows :

Increasing in rubber content leads to an increase in impact strength. At high rubber content the impact strength depends markedly on its particle size than at low rubber content. Strong dependence of blend properties on rubber particle size and size distribution (dispersion) were reported [31,36,40,64-69]. For each type of material, there

appears to be an optimum particle size for toughening. Impact strength falls drastically if the average particle diameter is reduced below a critical value, and there is evidence for a rather slow fall in fracture resistance as the particle size is increased above the optimum diameter. Speri and Patrick [31] have explored to a limited degree the behaviour of polypropylene blends containing EPR. They found impact strength of PP/EPR blends to be favoured by small rubber particle size (0.5 μm) and a narrow distribution (0.1 μm to 1.0 μm and centred around 0.5 μm). They also acknowledge that dispersed rubbers cause a decrease in average crystallite size in polypropylene and thereby result in an improvement in impact strength.

(ii) Toughness

The toughness of a material is its capacity to withstand brittle fracture. A fracture process consists of at least two steps : crack initiation and crack propagation or crack growth. Fracture mechanics describe the behaviour of cracks when a body is loaded on a more quantitative basis than is possible using conventional impact tests. Its application in design is based on the assumption that all bodies contain imperfections such as flaws or voids which could make the component unsafe or unserviceable.

There are two approaches used in describing fracture : the balance of energy released from the elastic deformation during the creation of the new surface including some which is absorbed by the area created, and the local stress field around the crack tip.

The criteria describing fracture toughness for polymers have been extensively investigated. One of the most practically used procedures for brittle and ductile fractures is that based on the J-integral concept, proposed by Rice [70] and standardised by the ASTM [101] for metallic materials testing. The J-integral is an energy input parameter which can be used as a measure of crack initiation in the fracture process of materials. The objective of the J-integral test is to determine the value of J at initiation of crack growth (J_c) which is the energy required for the onset of crack growth. (Details of fracture toughness measurement procedures are described in Chapter 3). More recently, interest has centred on its application to plastics testing. In particular, Williams and co-authors [71-75] have shown it to be effective for this purpose. The J- integral concept has received considerable attention in relation to ductile and toughened polymers [74-84], such as polypropylene [76,83], polypropylene copolymer [74,75,83], polyethylene [74,75,82,83], acrylonitrile-butadiene-styrene polymer [74,80], nylon [74-76], toughened nylon [77], modified polycarbonate [78,79] and polypropylene blends [84].

Kim and co-workers [76] studied the fracture toughness of various polymers by measuring fracture energy in terms of J_c. Included in this was a polypropylene which a J_c value of 1.1 kJ/m^2 was achieved.

Hashemi and Williams [74] investigated the fracture characteristics of several toughened polymers including polypropylene copolymer. The J_c value of 15.5 kJ/m^2 of polypropylene copolymer (at test temperature 20°C) was reported. This report showed a good agreement with that published by Kim and Joe [81].

2.3.4.2 Toughening Mechanisms

The various theories have been proposed to explain the concept of rubber toughening. A number of excellent comprehensive review articles [54,85,86] and research papers [69,88-90], have been reported on rubber toughening and a brief outline of theories are given below :

(i) Energy absorption by the rubber particles.
(ii) Energy absorption by yielding of the continuous phase; ductility enhanced by strain induced dilatation near the rubber occlusion.
(iii) Craze formation involving cavitation and polymer deformation within the crazes.
(iv) Shear yielding as a source of energy absorption and crack termination.
(v) Stress distribution and relief.
(vi) Rubber particles acts as craze terminating points and obstacles to crack propagation.

No one of these alone should be considered adequate to provide a total theory of rubber toughening. Early theories of toughening tended to concentrate on the rubber phase, and its role in preventing brittle fracture. The idea was developed by Merz et.al. [91] for the system of butadiene-styrene rubber in a polystyrene matrix. They suggested that the rubber particles held together the opposite faces of a growing crack, being stretched out as the matrix material parted, and thus inhibiting brittle crack propagation. The stabilising effect of the rubber permitted the formation of a large number of microcracks instead of a single catastrophic crack.

However, Newman and Strella [92] showed that this model was inadequate since the energy absorbed by rubber presented only one-tenth of the total energy absorbed by the composite. These authors asserted that the presence of the dispersed particle served to

trigger yielding in the continuous phase, and the enhanced toughness could be attributed to the large energy absorption involved in the local deformation of the matrix.

It is now generally recognised that energy absorption occurs almost entirely in the polymer matrix. The function of the rubber particles is to promote and control deformation in the matrix, by providing a large number of stress concentrations, where localised deformation can be initiated.

Crazing is the first stage of fracture in glassy polymers. Craze has been identified by Kambour [93] as regions of porous, plastically deformed matter. It is possible to consider crazes as microcracks bridged by fibrils and their deformation is accompanied by an increase in specimen volume. Under a sufficiently high stress, the fibrillar structure of craze breaks down, and a true crack forms.

Shear yielding, in the form of shear bands or more diffuse shear yielding, is another important mechanism which can lead to plastic deformation in polymers. There is a translation of molecules past each other during shear yielding but on annealing a deformed polymer above its glass transition temperature, it often completely recovers to its original shape. Both shear yielding and crazing involve localised, or inhomogeneous, plastic deformation of the material and arises from strain softening and geometric considerations. The difference between the two mechanisms is that shear yielding occurs essentially at constant volume whereas crazing occurs with an increase in volume. Thus, unlike shear yielding, crazing is a cavitation process in which the initiation step requires the presence of a dilatational component of the stress tensor.

2.3.4.3 Important requirements for rubber toughening

A qualitative study of rubber-toughened polymers shows that phase separation is an essential feature i.e. rubber must be dispersed randomly as small discrete particles in the continuous matrix phase if satisfactory resistance is to be achieved [85]. Other necessary features of the rubber phase are : (a) low shear modulus in relation to the matrix polymer; (b) good adhesion to the polymer matrix; (c) average particle diameter near the optimum value for the material; and (d) low glass transition temperature. In this section, only the effect of rubber particle size and rubber-matrix adhesion are described in detail.

(i) Effect of particle size

It is generally recognised that the size of rubber particles (and their size distribution) has a strong influence upon the mechanical properties, especially impact strength and toughness [64-69]. At fixed volume fraction, increasing the average diameter of rubber particles from 0.2 to 2.0 μm results in a marked increase in the impact strength of toughened polystyrene [223], but a marked decrease in the impact strength of toughened nylon [94]. The basic reason for this difference is that the two polymers deform by different mechanisms. At low loading rates, type I polymers [e.g. polymethyl-methacrylate (PMMA), polystyrene (PS)] exhibit brittle fracture and dissipate energy through crazing while type II polymers [e.g. polypropylene (PP), polyamide (PA), polycarbonate (PC)] undergo ductile fracture and shear yielding. Rubber toughening for the former occurs through increased matrix crazing, while for type II it allows for increased matrix yielding. For type I there exists an optimum size of the rubber particle for maximum toughness. For type II a sharp tough-to brittle transition can occur at a critical particle size. For example, in 15% rubber/PA blends a fourfold drop in the notched Izod impact strength was observed increasing the number average particle size from 0.7 μm to 0.8 μm [94].

Possible toughness improvements, can be achieved by controlling particle size and size distribution (dispersion) of the dispersed phase. In general, the rubber particle size in the blends is determined by the dynamic equilibrium between the break-up and coalescence of particles in the flow field [53,95-97].

The particle break-up process is fast, so mixing time has only secondary effect. The main factors are the shear conditions and the relative viscosity of the polymers. By increasing the mixing time the average size of the particles decreases and an equilibrium is reached between particle break-up and coalescence. Coalescence can be neglected at very low dispersed phase concentration. With increasing mixing time the possibility of thermal degradation increases. Thus, as a consequence of degradation, the viscosity of the matrix decreases resulting in a change in the shearing conditions and an increase in the viscosity ratio of the components [95]. In an analysis of the factors influencing the particle size and in the prediction of an equilibrium value, all these processes must be taken into consideration.

Taylor [96] analysed the forces using to deform a droplet in a viscous liquid matrix under well-defined deformation conditions. He developed an equation which describes the

deformation of the particle as a function of its size (r), the viscosity of the polymer matrix (η_m) and the interfacial tension of the components (γ_{AB}), as follows.

$$r = C\gamma_{AB} / \eta_m \dot{\gamma} f(\eta_{rel}) \qquad (2.2)$$

Where: $\dot{\gamma}$ is the shear rate; η_{rel} is the relative viscosity between the dispersed phase (η_d) and the matrix (η_m), and C is a constant.

Tokita [97] proposed a correlation between the equilibrium particle size and the dynamic equilibrium of the break-up and coalescence processes as a function of blend compositions. Tokita's equation is as follows.

$$r = 12\alpha\gamma_{AB}\phi_d / (\eta_m \dot{\gamma}\pi - 4\alpha\phi_d E_{dk}) \qquad (2.3)$$

Where: ϕ_d is the volume fraction of the dispersed phase; α is the coalescence probability and E_{dk} is the break-up energy of the particles.

Fortelny and Kovar [53] derived a more realistic expression for the droplet radius taking to account the theoretically and experimentally verified assumption that the break-up of particles in shear flow is controlled by Weber's number (W_e).

$$W_e = \eta_m \dot{\gamma} r / \gamma_{AB} \qquad (2.4)$$

For each blend of two polymers there is a critical Weber's number $(W_e)_c$. At $W_e > (W_e)_c$ particles break up in the system, at $W_e \leq (W_e)_c$ the flow field cannot induce a break up of the particles any more.

In practice, by controlling processing conditions and rubber/polymer rheology the particle parameters (size and size distribution) can be tailored. The general conclusions are that strong shear fields developed during intense melt extrusion and moulding will produce fine dispersion [31,98-99] and large disparity in viscosity between rubber and polymer and low viscosity rubbers will also result in small particles [47,66].

(ii) Role of adhesion

The toughening mechanism also fails when the bond between the rubber and the matrix is weak. Instead of stabilising the craze, a void would form at the weak bonding interface, and a crack would be initiated. Once such a crack developed, it would run from one rubber particle to the next with little hindrance from the poorly anchored particles in its path.

Interfacial adhesion between the two phases may be improved through one of the following routes :

(i) by blending suitably functionalised polymers capable of enhanced specific interactions, and/or chemical reactions,

(ii) by adding a third component (e.g. block, graft copolymers) having its sequences identical to or chemically compatible with each of the molecular chains of the two major components. The third component acts as an "interfacial agent" producing a fine rubber dispersion and improving the adhesion of the rubber particles to the matrix.

D'Orazio et.al. [100] showed that the addition of ethylene-propylene rubber (EPR) to high-density polyethylene (HDPE) / isotactic polypropylene (PP) blends improves the impact strength of compression-moulded specimens. They suggested that EPR may act as an interfacial agent in this system.

In the case of polymers exhibiting shear deformation, in which the entire material in the matrix bridges between the particles is involved in the plastic deformation, strong adhesion alone does not ensure toughening [94]. The interparticular distance must also be smaller than the critical value to achieve a transition from brittle to tough behaviour. Even if the rubber particles are chemically bonded to the matrix, a polymer blend will still be brittle, if the interparticular distance is greater than the critical value. Wu [94] proposed the interparticular distance model for determining the onset of tough-brittle transition in polymer-rubber blends.

In this model, the tough-brittle transition is assumed to occur when the interparticular distance between two nearest neighbouring particles is at a critical value. The critical particle diameter, d_C , is given by

$$\mathbf{d_c = T_c [(\pi/(6\phi_r))]^{1/3} - 1]^{-1}} \qquad \mathbf{(2.5)}$$

where T_c is the critical interparticular distance between the surfaces of two nearest neighbouring particles (as shown in *Figure 2.3*) and ϕ_r is the rubber volume fraction. For nylon-rubber blends, T_c is found to be 0.304 μm for notched Izod impact fracture. The minimum adhesion required for toughening is proposed to be 1000 Jm^{-2}, typical for van der Waals adhesion [94].

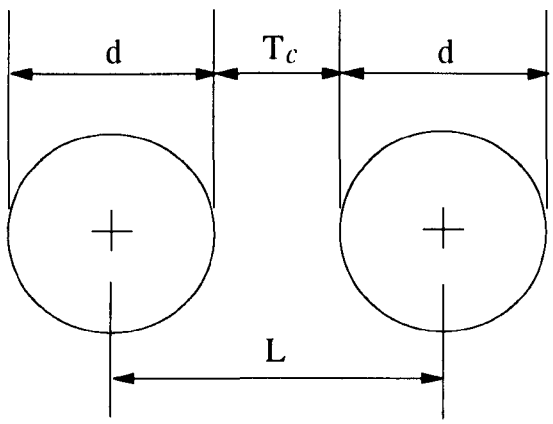

Figure 2.3 Model for (surface-to-surface) interparticular distance (T_c), centre-to-centre particle separation (L) and rubber particle diameter (d).

2.4 PARTICULATE FILLED POLYPROPYLENE

Filler is defined as a solid substance which is added to polymer to increase bulk (extenders) or improve properties (reinforcing fillers) [102]. Vast quantities of fillers are used. These include mineral fillers such as calcium carbonate, kaolin, talc, etc.; metallic fillers; carbon-type fillers and glass fillers. The properties and applications of these fillers have been reported elsewhere [102].

Extending fillers are traditionally used to lower the cost of a final product, while reinforcing fillers, such as glass fibres, are used to improve mechanical properties. In this context glass fibre reinforced polymers are not discussed. Details on the subject had been presented by Folkes [182-183]. By incorporating fillers the properties of polymers are modified and with the development of new chemicals for filler surface treatment it has now become possible to improve the mechanical properties of filled polymer composites.

2.4.1 Effect of filler on polymer properties

In general, incorporation of filler increases modulus and stiffness, compressive and flexural strength, hardness, heat distortion temperature, wear resistance and decreases shrinkage of the base polymer. On the other hand, the addition of fillers can result in disadvantages such as a reduction in impact resistance, elongation to break and tensile strength.

Fillers affect these properties in two ways. Firstly, the properties of fillers themselves (size, shape, and modulus) can have a profound effect on the polymer properties, especially on mechanical properties. Secondly, the filler particles cause a change in the polymer morphology leading to differences in mechanical properties. For example, the filler surface may act as a nucleator for semi-crystalline polymer and thereby alter the amount or type of crystallinity in the composites. The degree to which these properties are affected depend upon a number of factors, including, for example [103] :

- Filler type, shape and surface structure.
- Particle size, size distribution and content.
- Mechanical properties of filler itself (strength, stiffness).
- Interaction or bonding between filler and polymer matrix. This interaction can be influenced by coupling agent used.
- Polymer properties, e.g., ductile polymers will behave differently than brittle ones when adding fillers.
- Compounding and moulding methods used.

The factors affecting the modulus of filled composites are well understood, aspect ratio of the filler particles and their modulus relative to the polymer matrix being main factors, in addition to the filler loading. To achieve a high modulus requires the filler particles of high modulus and high aspect ratio, preferably at a high loading.

Pukanszky et al. [104] studied the effect of different fillers on the modulus of polypropylene composites. It was found that the composites filled with talc have a higher modulus than those containing calcium carbonate. This was explained by a high aspect ratio, platelike geometry of talc particles. Similar results were also found by Chartoff and Eriksen [105] and Jilken et.al.[103] for mica and wollastonite filled polypropylenes.

Busigin et.al. [106] found that larger aspect ratio particles impart a correspondingly greater modulus in mica-filled polypropylene composites, surprisingly, aspect ratio has a

minor influence on the tensile strength. Rather, the tensile strength is more dependent on the particle size of mica, with the smallest particles imparting the largest increase in strength to polypropylene.

In determining impact properties, the particle size is one of the major important factors. There is a marked relationship between decreasing particle size and increasing impact strength in mineral-filled polypropylenes [103]. Large particles (or a large aggregate of fine ones) seem to act as flaws which will reduce the stress needed to cause the composites to fracture and fail. Hence, it is important to prepare a composite with a good dispersion of filler. Riley et. al. [107] found that talc filled polypropylene composites prepared by a twin screw extruder has better filler dispersion and properties than that compounded on the Brabender where the aggregates of fillers are present. In addition to particle size, particle aspect ratio also affects impact strength. Low aspect ratio filler particles can act as blockers of cracks resulting in a lowering of stress. High aspect ratio filler particles, which are generally needed to achieve stiffness in a composite, may cause high stresses in the polymer matrix near the particle edges and facilitate failure under impact conditions. Therefore, composites with high stiffness usually have low impact strength.

2.4.2 Prediction of mechanical properties

A number of theoretical models have been proposed for the prediction of mechanical properties of a filled polymer. In many cases the changes in mechanical properties can be predicted from basic principles. However, in some cases, the property changes must be experimentally measured, since there is insufficient knowledge about the polymer-filler interactions available in order to calculate the effect of filler on property changes.

(i) Modulus

A number of investigators [108-110] have shown that the modulus is the easiest mechanical property to estimate, because it is a bulk property which depends mainly on the geometry, modulus, particle size and size distribution, and concentration of filler. Among the most prominent models are those developed by Einstein, Guth, Mooney, Kerner, and Nielsen [111-115]. These models are listed in *Figure 2.4*.

Model	Equation
Einstein	$E_R = 1+k_E \phi$ $k_E = 2.50$ for dispersed spheres
Guth	$E_R = 1+ k_E \phi+B\phi^2$ B- usually 14.1
Mooney	$E_R = \exp [k_E\phi / (1-\phi/\phi_m)]$
Kerner	$E_R = \dfrac{G_f \phi/[(7-5\nu) G_p + (8-10\nu) G_f] + \phi/[15(1-\nu)]}{G_p \phi/[7-5\nu) G_p + (8-10\nu) G_f] + \phi/[15(1-\nu)]}$
Nielsen	$E_R = (1+AB\phi)/(1-B\psi\phi)$ $\psi = 1+[(1-\phi_m)/\phi_m^2] \phi$

Figure 2.4 Frequently used models for predicting the modulus of filled polymers. E_R = relative modulus, ϕ = volume fraction of filler, G_f = shear modulus of filler, G_p = shear modulus of polymer matrix, ν = Poisson's ratio of polymer and ϕ_m = maximum packing fraction of filler.

Einstein's equation is applicable only for rigid particles at very low concentration. Guth's equation is an expansion of Einstein's to account for the interaction between particles at higher filler concentrations. Mooney introduces the concept of maximum packing fraction to account for differences in particle geometry. Nielsen's modification of Kerner's equation takes into account both the maximum packing fraction of the filler, interaction between particles, and the relative modulus of the two constituents. The maximum packing fractions for a number of common geometries are given in *Table 2.3*.

Table 2.3. - Maximum packing fraction of selected fillers

Filler Type	Packing Geometry	ϕ_m
Spheres	Hexagonal	0.74
Spheres	Face centred cubic	0.74
Spheres	Body centred cubic	0.60
Spheres	Simple cubic	0.52
Spheres	Random	0.64
Irregular	Random	0.64
Fibres	Random (L/D = 5:1)	0.52
Fibres	Random (L/D = 20:1)	0.20
Fibres	Unidirectional random	0.64
Flakes	Random	0.33

(ii) Tensile Strength

Tensile strength of a filled polymer is more difficult to predict than modulus since it also depends strongly on polymer-filler interactions. In general, two tensile strength-filler concentration responses are possible [116]. These responses are shown by the curves drawn in *Figure 2.5*. The upper bound response assumes strong adhesion between polymer and filler while the lower bound response assumes weak, or no, adhesion between the two materials.

The lower bound response of a filled polymer is often represented by Nicolais and Nicodemo's equation [117] as shown below.

$$\sigma_c = \sigma_p(1-a\phi^b) \qquad (2.6)$$

where:

σ_c is the tensile strength of the filled composite,

σ_p is the tensile strength of the polymer matrix,

a is a constant related to stress concentrations,

ϕ is the volume fraction of the filler,

b is a constant related to the geometry of the filler.

For spherical filler particles with no adhesion "a" is found equal to 1.21. When there is some adhesion between polymer and filler, there is less stress induced in the polymer by filler and "a" is smaller than 1.21. "b" has been found equal to 2/3 when the sample fails by random fracture through the composition, while "b" equals to 1 when the sample fails by planar fracture.

The upper bound response is more difficult to predict because it depends on quantitative information regarding the adhesion between polymer and filler. When an upper bound response is observed it implies some degree of reinforcement. Leidner and Woodhams [118] proposed the following relationship for an upper bound response of polymer filled with spherical particles.

$$\sigma_c = (\sigma_I + C\tau_m)\,\phi + \sigma_p\,(1 - \phi) \qquad (2.7)$$

where:
σ_I is the interfacial tensile strength between polymer and filler,
C is a constant,
τ_m is the shear strength of the polymer

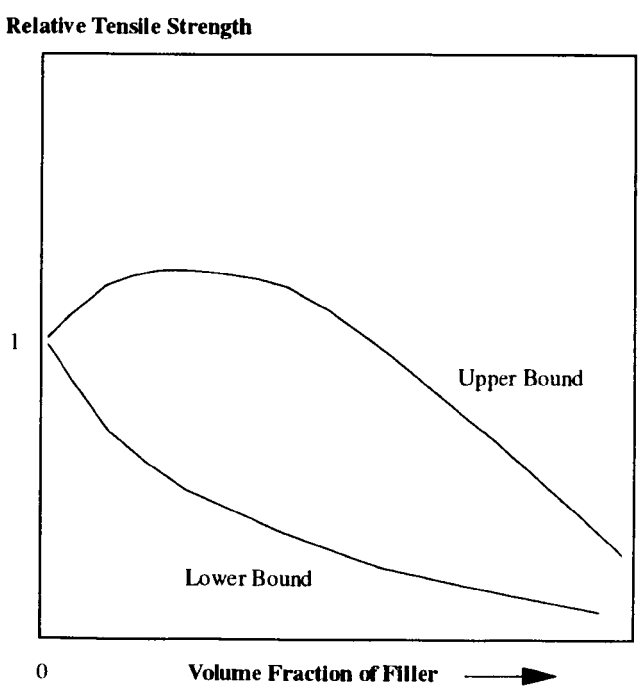

Figure 2.5 Typical tensile strength against filler concentration curves for filled polymers showing upper and lower bound responses.

(iii) Elongation at break

It is known that rigid particulate fillers generally, but not always reduce both elongation at break and tensile strength of a polymer. The decrease in elongation at break found in filled polymer, results from the true elongation of the polymer being more than the elongation of the specimen because all the elongation comes from the polymer and little from the filler. If there is a good adhesion between filler and polymer, the elongation at break can be calculated roughly by the following equation [119] :

$$\varepsilon_{bc} / \varepsilon_{bp} = 1 - \phi^{1/3} \qquad (2.8)$$

Where:
ε_{bc} and ε_{bp} are the elongation at break of the filled composite and polymer matrix, respectively.

(iv) Impact strength

Impact strength is another important mechanical property that is difficult to predict in a filled polymer. The impact strength of a filled polymer also depends on the degree of polymer-filler adhesion, but in a more complex manner than the tensile strength [120]. Other factors such as specimen geometry, mode of testing and morphological changes in the polymer causing by filler, affect the impact strength too. There are no practicable theoretical relationships between filler characteristics and concentration that can be used to predict the impact strength of filled polymers.

2.4.3 Modification of filler surface

A fundamental difficulty in producing filled polymers with improved mechanical properties is the lack of adhesion between polymer and filler, which is normally due to the hydrophilic character of the filler surface. Adhesion between phases is determined by physical and chemical characteristics of the interface and the interphase regions. An interface is a surface which is formed by a common boundary of two homogeneous phases in contact. By definition an interface has area but no volume. An interphase is a region or boundary between two phases which has a characteristic of thickness and properties differing from those of either of the continuous phases. According to Kendall

and Sherliker [121], the role of a filler as a reinforcement is influenced by the surface interaction between polymer and filler, resulting in a layer of polymer adhering to the filler surface. This polymer interphase causes energy dissipation and toughness in a filled material.

To enhance the interaction between polymer matrix and filler, two options are possible. One is to chemically modify the polymer matrix, and the other is to treat the surface of fillers. The modification of the filler surface can be achieved by the application of coupling agents. The basic role of coupling agents is to promote interaction between filler surface and polymer, also to reduce the filler-filler interactions improving the dispersion, thus overcoming many of the disadvantages associated with high filler loadings. Metal stearates and stearic acid are used [124] to promote improved wetting of the filler surface and achieve enhanced dispersion.

Two main groups of coupling agents used commercially are organofunctional silanes and titanates. Silane coupling agents are monomeric silicon chemicals and are usually bifunctional materials of the general structure R'-$Si(OR)_3$ in which two distinct centres of reactivity exist. The first site, R', is a common organofunctional group such as amino, vinyl, epoxy, methacryloxy, etc., bonded to the silicon atom by a short alkyl chain. The second reactive site is centred around the silicon atom and consists of hydrolysable alkoxy groups, $Si(OR)_3$.

The alkoxy groups hydrolyse to form silanols (Si-OH) which can react or otherwise condense to form a covalent bond on the filler surface. At the other end of the silane molecule, the functional organic groups described above react with suitable groups in the polymer matrix. The stability of the composites appears to be related to the strength of these covalent bonds via the coupling agent. Silane coupling agents are believed to be compatible with almost every type of organic polymer, ranging from thermosets through elastomers to thermoplastics. In practice, they may be applied to the substrate as a pretreatment or, in many systems, added directly to the polymer during processing. Mechanisms of adhesion using silane coupling agent has been recently reviewed by Plueddemann [184].

Titanate coupling agents are monoalkoxy organochemicals. Although claimed to promote adhesion, titanates are generally used to aid plasticisation or dispersion by lowering the surface energy of fillers. Similar to the silanes, titanates react with free protons at the inorganic interface, resulting in monomolecular layers of organofunctionality which, in turn, bond the inorganic and organic components. They

have the advantage of being applicable in either organic or water phases during polymer manufacture or as pretreatment to the fillers.

The influence of filler surface-treatment on the properties of polymer composites has been studied by many researchers [122-124]. In most cases, the addition of coupling agents promotes the interfacial interactions between filler and polymer matrix, thus enhancing some of the composite properties [122-123]. However, contradictory results have also been observed [124].

Miller and Ishida [122] used silanes as coupling agents in glass sphere/HDPE composites. An increase in composite modulus was obtained. For the 0.5, 20 and 100 layer modifications, the modulus in melt state is over that of unmodified composite 5.2%, 54% and 320%, respectively. As well as in glass bead filled SAN composite with an applied EVA interfacial layer, the viscoelastic properties and composite modulus are improved [50]. In contrast, Pukanszky et al.[124] found that stearic acid surface treatment of calcium carbonate filler in polypropylene composites results not only in a decrease of their surface tension, but also in decreased interaction with the polymer matrix. This results in the decrease of tensile strength and modulus.

Recent investigations [132] on crack propagation in particulate filled polypropylene composites revealed that incorporation of fillers, such as talc, calcium carbonate, or mica, can enhance the ductility of PP and enable the filled composites undergo a stable crack propagation instead of a brittle failure. This behaviour can be explained in terms of a "crack pinning mechanism" [86], in that the rigid particles act as obstacles and force the crack to bow (see *Figure 2.6*). The crack-pinning mechanism is influenced by the nature of the filler, the filler concentration and also by the filler-surface treatment.

Apart from influencing the mechanical properties, coupling agents also have a significant effect on the rheological properties of the composites. Han et.al.[125] studied filled polypropylene composites. They found that the addition of coupling agents to calcium carbonate filled polypropylene composites decreased the composite melt viscosity. Two reasons for this observation may be due to the act of coupling agent as a surface modifier inhibiting frictional resistance to flow, or the coupling agent might have diffused into the polymer matrix, playing the role of an internal plasticiser, decreasing the viscosity of polypropylene phase. Szijarto and Kiss [126] compared the effect of silane and titanate coupling agents on the rheological properties and impact properties of calcium carbonate filled polypropylenes. They found a great difference between the effectiveness of the two treatments. In both cases the titanate had more effect especially on the flow properties.

Effect of coupling agents on the rheological properties of filled polymers have been reported in detail elsewhere [48].

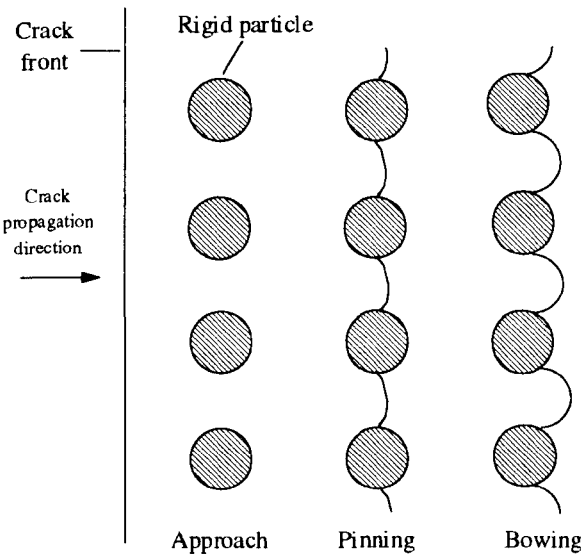

Figure 2.6 Schematic representation of the crack-pinning mechanism [84].

2.4.4 Influence of filler on the polypropylene structure

As described earlier, fillers can affect the properties of polymer in two ways. One of them is due to the properties of fillers themselves, and the other way is by changing the micromorphology of the polymer matrix such as crystal structure, crystallinity and orientation state of the crystals.

Alonso et.al. [128] studied the morphology of talc filled polypropylene composites prepared by compression moulding. They found that in such materials talc acts as a heterogeneous nucleating agent markedly enhancing the α-modification of polypropylene and suppressing the β-crystalline variant. The nucleating action of talc not only affects the morphological structures of polypropylene, but also influences the crystallisation temperature and crystallinity of polypropylene.

Ronca [138] investigated the effect of talc, sodium benzoate, boron nitride, saccharin and sorbitol on the nucleation and crystallisation of polypropylene. It has been reported that the crystallisation temperature of nucleated polymer is exponentially dependent on the

concentration of the nucleating particles. This has been explained by the decrease in the average distance between the nuclei, with no change in the crystallisation kinetics.

Hutley and Darlington [129,130] have observed a correlation between the temperature of onset of crystallisation and impact strength in a calcium carbonate filled polypropylene composite. A higher onset temperature was observed in composites of poor impact strength. They concluded that all the filler variables (shape, size, filler surface treatment and filler volume fraction) affect the falling weight impact strength through their influence on the rate of crystallisation. This correlation was confirmed by Riley et.al. [107] for a range of calcium carbonate fillers.

Khunova et.al. [131] studied the nucleating effect of different types of fillers (benzonite, zeolite, calcium carbonate, china-clay) in polypropylene-based composites. In all types of filler employed, increasing in the filler content raises the rate of crystallisation but no influence on the mechanism of crystal growth was observed, thus resulting in a diminution in the spherulite size. By increasing the filler content the extent of crystallinity also decreased. This phenomenon was related to the reduction in mobility and change in density of the macromolecules at the polymer-filler interface. These macromolecules due to conformational restrictions, do not take part in the process of crystallisation.

The reduction in polymer chain mobility after the addition of fillers was confirmed by the work of Paakkonen et al. [56]. The changes in the glass transition process which related to the molecular mobility were studied by using DSC and DMA. It was found that talc and mica elevated the glass-transition temperature (T_g) peak of polypropylene to a higher temperature and lowered and broadened the loss tangent peak of polypropylene composites. This observation was not found in a wollastonite filled PP system.

There seems to be no general rule for the effect of fillers on the molecular mobility of a polymer matrix in the T_g region. Morales et.al. [133] studied dynamic mechanical behaviour of a sepiolite filled polypropylene composite. They found that a value of the PP glass transition temperature in the composite is lower than that of an unfilled polypropylene. While in calcium carbonate and magnesium hydroxide filled polypropylenes, Jancar [134] found no change in polypropylene molecular mobility pattern in the Tg region. A new significant loss peak at around 50°C was found in the composite containing filler content higher than 25 vol%. This peak was reported to be connected with the segmental mobility of polypropylene molecules immobilised on the filler surface.

2.5 MULTIPHASE POLYPROPYLENE COMPOSITES

Multiphase polymer composites are composites which include at least one component which is a polymer. They can be two-phase systems such as polymer blends, rubber toughened polymers or filled polymers; or three-phase systems where both rubber and filler are incorporated into the system; or more. Advantages of multiphase polymer composites are; firstly, a wide-range of product properties can be developed by incorporating two or more suitable materials into the system; secondly, the composites can be easily produced by basic mixing processes such as blending using conventional extruders; and thirdly, the cost in the production of multiphase composites is much lower relative to synthesising a new homopolymer with required properties. This section reviews current investigations on multiphase polypropylene-based composites. For general information on multiphase composites, the reader is referred to the books by Utracki [139] and by Miles and Rostami [140].

Polypropylene, although, extensively used in many fields of application, is limited by its low temperature impact strength, which significantly hinders even wider utilisation. One of the most often used methods to overcome this drawback is its blending with other polymers, especially with rubbers or elastomers as discussed earlier in *section 2.3*. Rubber modification of polypropylene increases its low temperature impact strength, but lowers its stiffness. To compensate this effect from the rubber, filler is added to the blend; i.e. three component composites are prepared. Various fillers so far have been employed in three-phase polypropylene composites, i.e. talc [141-143], calcium carbonate [144-151], mica [152,153], kaolin [154-158], etc. Toughened polypropylene composites reinforced with short glass fibres have also been investigated [143,159]. Ethylene-propylene (EPR) or ethylene-propylene-diène (EPDM) copolymers have been mostly used as elastomers, though the effects of polar elastomers [142,143,151] or block ethylene-propylene (E-P) copolymers [149] have also been studied. Apart from polypropylene-based composites, three-phase of polyethylene/elastomer/filler have been investigated [160-162].

Three-phase polymer composites, recently, have both theoretical and practical significance due to the possibility of producing composites with increasing stiffness and impact strength. The properties of the three-phase composites are dominated mainly by their morphological structures. In the next section, possible structures which may be formed in three-phase composites will be reviewed followed by discussion of these effects on the composite properties. The last section will focus on how to improve the composites properties by controlling their microstructures.

2.5.1 Morphological structures of the three-phase polymer composites

Three-phase polymer composites may possess a complex morphology that depends on many factors such as the composition, characteristics of the components, processing conditions, etc. In such systems, two different phase structures can take place : *separate dispersion* where filler and rubber particles are separately dispersed in a polymer matrix; and *encapsulation* in which the filler particle is encapsulated by rubber forming core-shell inclusions and both dispersed in a polymer matrix as shown in *Figure 2.7.*

Earlier studies on three-phase (polymer/elastomer/filler) composites have produced contradictory results in the phase structures in such composites. In some investigations, separate dispersion of the components was observed [135,148], while in others the encapsulation was perceived [136,137,144]. Recently, Pukanszky [145], has proved that under certain conditions both structures can be formed.

The factors that affect the formation and stability of the composite structure are collision of rubber and filler to bring about encapsulation, the energy balance of thermodynamic processes and the stability of the structure formed, in relation to external forces such as shear generated during mixing. Although encapsulation is thermodynamically favoured [145], the final structure is determined by the dynamic equilibrium and stability of encapsulation and de-encapsulation which depends on the magnitude of adhesion and shear forces. The strength of adhesion is mainly dependent on the particle size and surface characteristics of the filler, while the shear force is determined by shear rate and the viscosity of the mixture.

From the work of Kolarik et.al. [146] on PP/EPDM/calcium carbonate composites, the surface treatment of the filler proved to be one of the most important factors determining the phase structure of the composites. Separate dispersion was observed in the system containing surface-treated calcium carbonate [146], while encapsulation of filler particles by elastomer was found in composites with unmodified calcium carbonate [144].

An increase in the amount of any of the components results in an increase of collision probability, thereby promoting encapsulation. However, it also leads to increased shear giving increased dispersion. The final structure, thus, will be determined by the combined effect of all these processes. It was also mentioned by Pukanszky et.al. [145] that fillers frequently used in practice (particle size distribution between 0.1 and 10 μm) can never be completely encapsulated by the elastomer. At the upper end of the particle size

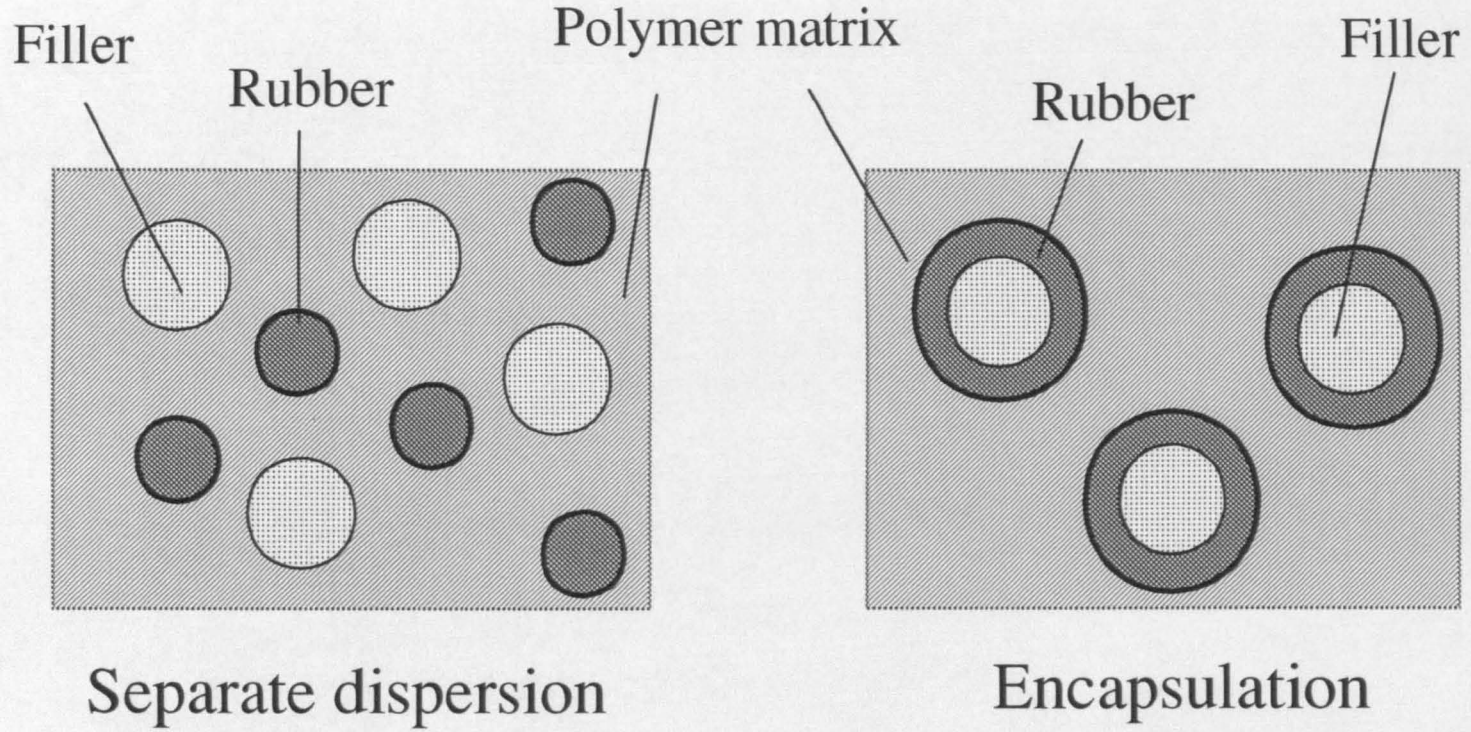

Figure 2.7 Phase structures of ternary-phase polymer composites

distribution, adhesion forces are small and shear forces separate the elastomer layer from the surface of large filler particles.

2.5.2 Mechanical Properties

The properties of the three-phase composites depend on many factors. These include type and characteristics of the components, processing techniques and conditions used, together with adhesion (or interaction) between the components.

Kosfeld et.al. [154-158] investigated the mechanical and morphological properties of three-phase polypropylene systems consisting of EPDM and various inorganic fillers such as kaolin, barium sulphate and zinc sulphide. The effect of different fillers which is strongly dependent on their particle size and shape, was studied. It was found that the composite consisting of a platelet-shaped filler (kaolin) has better mechanical properties than that with a grain (barium sulphate) or spherical-shaped filler [155]. Thus, the highest reinforcement was obtained in the binary systems of polypropylene filled with kaolin following by zinc sulphide and barium sulphate, respectively. However, this sequence is not the same for the three-phase systems. When EPDM was added, it brought about a change in the morphological structure which led to a change in the mechanical properties [156]. Evidence from SEM and IR studies [154,158] showed that except with the barium sulphate, there is an interface of bound polymer which can hardly be removed from the filler surface even after 96 hours of solvent treatment. The thickness of this bound polymer layer is estimated ranging from less than 1 nm to 12.5 nm.

Faulkner [152] investigated the system of PP/EPDM/mica. The Izod impact strength of these mica filled polypropylene composites was found to be significantly improved as the EPDM was incorporated, while only a modest reduction in flexural modulus was observed. In such system, dry blending was preferred over conventional single screw extrusion mixing. However, it was also mentioned that it may be possible to achieve better properties if mica is fed in further downstream from the EPDM feed zone.

Stamhuis [141] focused his attention on the balance of impact strength and rigidity of polypropylene which can be significantly improved by physical blending of the polypropylene with various fillers and elastomers. Unsaturated elastomers represented by styrene-butadiene-styrene (SBS) block copolymer, were found to be effective impact improvers in PP/elastomer/talc composites, whereas saturated elastomers such as EPDM gave rise to a high stiffness in such composites. This was attributed primarily to different

tendencies of the elastomers to coat the talc surfaces. Secondly, the quality of the elastomer as an impact modifier is also important. The modulus of the composite is found to be governed more by the amount of filler coating than the modulus of the free rubber [142]. Furthermore, it was reported that the small filler particles are coated more completely than the larger ones, resulting in the better properties [141].

2.5.3 Role of interfacial adhesion on the composite structures and properties

The interfacial adhesion between filler particles and polymer matrix is one of the most important factors controlling structures and properties of composites. The effect of interfacial adhesion on composite properties is proportional to the amount of the interphase, which depends on the size of the interface and on the strength of the interaction.

Scott et al. [160] found for the system of polyethylene/EPDM/filler that the presence of a rubbery layer around the filler particles changed the stress distribution around the filler particles. For rigid fillers in a polymer matrix with good interfacial adhesion, the stress concentration is at the pole of the particles where cracking will occur. For soft particles such as elastomer, the stress concentration is at the equator where cracking or crazing will develop. The presence of a rubbery layer around rigid fillers alters the stress concentration from the pole to the equator of the particles.

Stamhuis [143] reported that the balance of mechanical properties of polypropylene, as presented by the notched Izod impact strength and flexural modulus, can be significantly improved by application of short glass fibres instead of mineral fillers in elastomer modified polypropylene. The properties of such composites are strongly dependent on the adhesive forces at the fibre-matrix interface. Poor adhesion at the interface resulted in fracture by fibre-matrix debonding and relatively low impact strength. In contrast, high adhesion led to fracture not only by fibre-matrix debonding but also by crack propagation through the elastomer phase at the interface resulting in a good impact strength.

Modification of the interface can be achieved either by treating the filler surface using surface active agents or by incorporating functionalised materials.

Surface active agents are used to improve the wettability of fillers and help to increase the adhesion. Surface-active agents often used are low-molecular-mass additives that can

interact with fillers and polymer by ionic, van der Waals, or hydrogen bonding forces, while forming an oriented adsorption layer around the solid particles preventing the formation of filler agglomeration and improving the adhesion between the main components. Furthermore, surface-active agent should have low melting point but high polarity and mobility, thus, it can be the first to adsorb on the surface of the filler particles.

Functionalised materials are materials which contain both polar and non-polar groups on the polymeric chain. The polar group in the material will bond to polar substrates such as glass or metals; while the non-polar group will have a bond to non-polar material producing good adhesion throughout the system.

Marosi et.al.[150,151] focused their attention on the arrangement of the components and the modification of the interfacial layers between calcium carbonate ($CaCO_3$) and polypropylene matrix. Various models of filled polypropylene composites for different types of interfaces were investigated. Model C in *Figure 2.8* is the only case where a tough system was obtained. The basis of this system is the application of a surfactant and an elastomer to PP/$CaCO_3$ composites. The surfactant interacted with the filler surface and the elastomer formed a rather thick layer around the surfactant-coated filler particles resulting in a decrease in the concentration of local stress near to the particle surface.

The thickness of the interfacial layer depends on the concentration of elastomer. Increasing the elastomer content resulted in a thicker interface up to a certain critical value. Above this value the thickness of the interfacial layer stopped growing and the elastomer appeared as a separate phase dispersed in the polypropylene matrix. The value of this critical concentration is dependent on the characteristics of both polymeric matrix and elastomer such as polarity, the viscosity ratio between the two components.

Scott and co-workers [160-162] studied the composites of polyethylene/EPDM/filler. The fillers used were calcium carbonate ($CaCO_3$) and silicon dioxide (SiO_2). The fillers were treated with two different coupling agents : gamma-aminopropyltriethoxysilane (γ-APS) and gamma-methacryloxypropyltrimethoxysilane (γ-MPS). The rubbers used were ethylene-propylene-diene rubber (EPDM) and a maleic anhydride grafted EPDM (EPDM-MA). It was found that both PE/$CaCO_3$ and PE/SiO_2 systems exhibited particle-particle interaction effects. The use of silane coupling agents significantly reduced these interactions leading to an improvement in filler dispersion. By the incorporation of rubber to PE/filler systems, the impact strength was improved. EPDM-MA gave a greater improvement than EPDM. This was due to more filler-rubber interactions. The

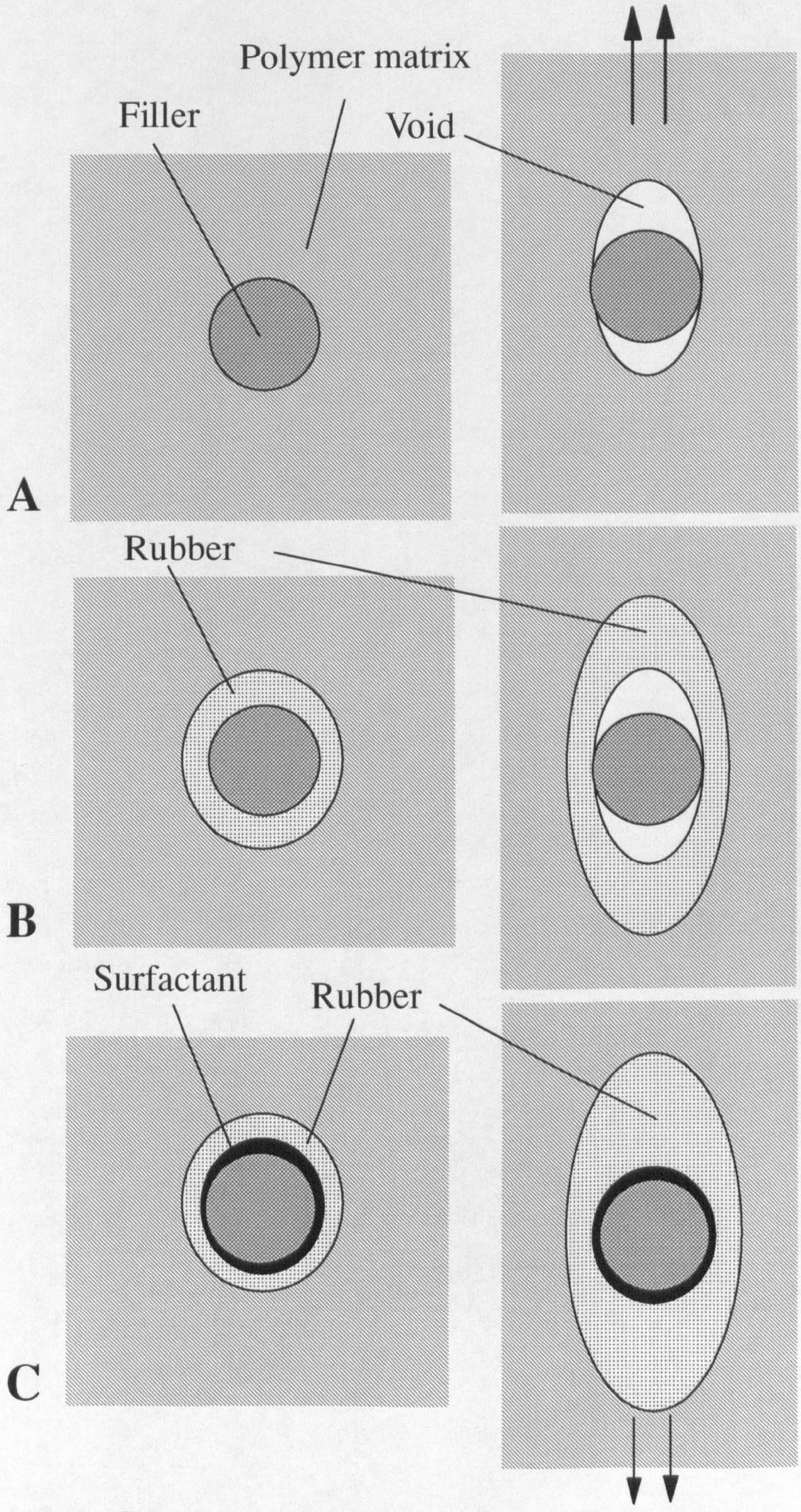

Figure 2.8 Failure process in multiphase composites

composite of PE/EPDM-MA/γ-APS treated filler provided the best impact strength. This was reported to be attributed to a chemical reaction between the amine functionality of the coupling agent and the maleic anhydride modification.

Kolarik et.al. [146] studied the relationship between the mechanical properties and phase structure of PP/EPR/$CaCO_3$ composites controlled by means of acid/base interaction. They found that the addition of a functionalised EPR into the three-phase composites led to an encapsulation structure. On the other hand, functionalised polypropylene which gave good adhesion between polypropylene and filler interface resulting in the separate dispersion structure. The former structure was found to give a higher impact strength because the incorporated rubber is extended by filler; while the latter composites yielded marked increase in the tensile yield stress and stress at break.

Similar phase structures were observed by Jancar and Dibenedetto [205] for ternary composites of PP/EPR/calcium carbonate and PP/EPR/magnesium hydroxide. Increasing the concentration of maleic-anhydride in the EPR phase caused encapsulation of filler resulting in composites of low modulus, while increasing the amount of maleic-anhydride in the matrix yielded separation of the rubber and filler leading to high modulus composites. Models for the prediction of the upper and lower bound responses of the elastic moduli were proposed. Their experimental results showed that upper and lower bound responses of the overall elastic moduli were achieved for perfect separation and perfect encapsulation, respectively. The dependency of EPR content on the upper bound response was found to be independent on the particle shape of fillers used, while the lower bound response for the relative elastic moduli was found significantly higher in the composite containing squared-plate particles such as magnesium hydroxide.

However, a more effective coating does not always lead to a better performance of the composites in terms of the flexural modulus and impact strength. Stamhuis [142] investigated the system of PP/elastomer/talc. Polar elastomers such as ethylene-vinyl acetate (EVA), nitrile rubber, acrylic rubber were used as the third component to produce a more complete coating of the filler surfaces. It was found [142] that enhanced filler coating was achieved, but the balance of properties was not improved. The impact strength of such composites was lower than that of similar blends with non-polar elastomers. It was reported to be attributed to (a) a high glass transition temperature of the polar components; (b) a poor dispersion of the elastomers in the polypropylene matrix; and (c) a reduced affinity of the elastomers for polypropylene. A similar observation was reported by Varga [163-164].

Varga [163-164] studied the filler dispersion in polypropylene/elastomer composites. The composites consisted of a polypropylene matrix, having a tendency to crystallise in the β-form; a polar and non-polar elastomer, represented by ethylene-vinyl acetate (EVA) and ethylene-propylene copolymer (EPR), respectively; and a talc filler possessing a strong α-nucleation effect. It was found that the dispersion of filler in the polymer phases (PP and elastomer) was determined mainly by the chemical character of the components, and only slightly by the changes in the phase viscosity ratio between the components or by the sequences of mixing. In these three-phase composites, filler particles were found to be encapsulated by elastomer. The presence of a polar elastomer resulted in a good wettability leading to a higher β-PP content, however, the final properties of these composites were poorer than those with a non-polar elastomer. This result was explained by the different morphology of the composites, such as the particle size of the dispersed polar elastomer (3-6 μm) which is significantly larger than that of the non-polar one (~1 μm), and by the higher glass transition temperature of the polar elastomer.

CHAPTER 3

EXPERIMENTAL PROCEDURE

3.1 INTRODUCTION

This chapter contains details of materials used throughout the course of this research, blend preparation and characterisation techniques. These techniques were chosen to give the greatest possibility for understanding the relationships between processing, structure and properties of multiphase polypropylene composites. Composite morphological structures were characterised using both direct and indirect methods. Direct observation of composite morphology was achieved by scanning electron microscopy. Image analysis was used to determine quantitative morphological information such as rubber particle size and size distribution. Dynamic mechanical analysis (DMA), differential scanning calorimetry (DSC), wide-angle X-ray diffractometry (WAXD) and fourier transform infrared spectroscopy (FTIR) were also used as indirect methods in determining the composite structures. Mechanical properties of the composites were investigated by tensile and impact measurements carried out at room temperature, while low temperature fracture toughness was undertaken using the J-integral technique.

3.2 MATERIALS

The three main materials used throughout this work were polypropylene homopolymer (PP) as a polymer matrix, ethylene-propylene rubber (EPR) as an impact modifier and glass beads as a filler.

3.2.1 Polypropylene

Two grades of polypropylene used were Novolen 1100HX and Novolen 1100L. Both are commercial extrusion grade polypropylene homopolymers having different melt flow rate and are supplied by BASF. Novolen 1100HX has a relatively lower melt flow rate or a higher in viscosity. Their properties were shown in *Table 3.1*.

3.2.2 Ethylene-propylene rubber

Ethylene-propylene rubber (EPR) was used in this work as an impact modifier to improve toughness of polypropylene at elevated and at low temperatures. EPR is a copolymer of ethylene and propylene made by solution polymerisation in the presence of a Ziegler-Natta catalyst. Three grades of EPR, namely Exellor PE805, Exellor PE808

and Exellor VA 1803 supplied by Exxon Chemical Co., were used throughout the work. Exellor PE805 and 808 are low and medium viscosity semicrystalline grades of EPR with a density of 870 kg/m^3 measured by ASTM D-792. Typical properties of Exellor PE805 and 808 are shown in *Table 3.2*. Exellor VA1803 is a low viscosity amorphous maleic-anhydride grafted ethylene-propylene rubber. It is supplied as white pellets coated with high density polyethylene powder. Typical properties of Exellor VA1803 are shown in *Table 3.3*.

Table 3.1 - Typical properties of polypropylenes used in the blends [185].

	Unit	ASTM method	Novolen 1100HX	Novolen 1100L
General				
Melt flow rate (at 230/2.16)	g/10 min	D-1238	1.8	5.0
Density	kg/m^3	D-792	907	908
Melting point	°C	D-3418	161	160
Physical				
Tensile strength	MPa	D-638	34	34
Elongation	%	D-638	>50	>50
Notched Izod impact strength, 23°C	kJ/m^2	D-256	3.5	3.0

Table 3.2 - Typical properties of Ethylene-Propylene rubber [186].

Grade	Ethylene (wt %)	Density (kg/m^3)	Mooney Viscosity ML (1+4) at 125°C	Melt flow rate (g/10 min)
Exellor PE805	75	890	35	5
Exellor PE808	75	890	46	3

Table 3.3 - Typical properties of Exellor VA 1803 [186].

Property	Test method	Unit	Value
Melt flow rate (230°C/10 kg)	ASTM D-1238	g/10 min	22
Density	ASTM D-792	kg/m^3	860
MA-content	FTIR	%	0.7
Glass transition temperature (Tg)	DSC	°C	-57

3.2.3 Glass beads

Glass beads or microspheres are spherical particles, typically less than 200 μm, which provide unique properties to plastics when used as filler. They differ from non-spherical fillers such as flakes, platelets, granules and fibres, in several important ways. At equivalent volume loadings, spheres have the smallest surface area in contact with the polymer matrix. Polymer viscosity increases slowly with glass bead loading, thus making high loadings possible with good flow properties.

Glass beads are isotropic, thus their properties are distributed uniformly over their spherical shape. As a result, the properties do not depend on the direction in which they are measured. In some polymer applications, this means that internal stresses during cure can be distributed evenly, thereby reducing the tendency toward cracking. During actual use, external stress is evenly distributed; hence the orientation of the fillers has no effect on failure. Because of the spherical shape of glass beads, the surface of its composite is smoother compared to those filled with fibrous or irregular-shaped fillers. Glass beads are typically made of a soda-lime glass similar in composition to A-glass. Its composition is shown below. This type is low melting , inert to chemicals, and inexpensive.

Composition of glass beads

SiO_2	72.5%
NaO	13.7%
CaO	9.8%

MgO	3.3%
Al_2O_3	0.4%
FeO,Fe_2O_3	0.2%
K_2O	0.1%

In order to achieve a better adhesion between polymer matrix and glass surface, glass beads are usually coated with coupling agents. One of the commercially used coupling agents is the organofunctional silane, represented by the following structural formula where R' represents a common organofunctional group bonded to the silicon atom by a short alkyl chain, and OR represents a readily hydrolysable group.

$$R'\text{--}Si\text{--}(OR)_3$$

Silane coupling agents react with the glass surface through these hydrolysable groups. Typically, two reactions involve in the formation of Si-O-Si covalent bonds between the glass surface and silane. First, hydrolysis of the silane to a silane triol must occur.

$$R'Si(OR)_3 \xrightarrow{H_2O} R'Si(OH)_3 + 3H_2O$$

This reaction can be catalysed by acids or bases. Then, reaction with the glass surface can occur.

$$R'Si(OH)_3 + \begin{array}{c}|\\ -Si-OH\\ |\end{array} \text{ (on surface)} \longrightarrow \begin{array}{c}|\\ R'\text{-}Si\text{-}O\text{-}Si\text{-}\\ |\end{array} \text{ (on surface)}$$

Throughout this work glass beads were chosen as the preferred filler due to their spherical shape and ease of dispersion, since mineral fillers such as calcium carbonate would cause complications in the interpretation of results due to the problem of particle shape and agglomeration of filler particles in the composite. Three grades of glass beads were used during this work, namely spheriglass 3000CPOO and 5000CPOO which are non surface-treated grades and 5000CPO3 grade where the surface has been treated with silane coupling agent. These glass beads were supplied by Croxton & Garry Ltd. Their typical properties are shown in *Table 3.4*.

Table 3.4 - Typical properties of glass beads [187].

Grade	nature	specific gravity ($\times 10^{-3}$ kg/m^3)	median dia. (micron)
3000 CPOO	uncoated	2.45-2.55	12-26
5000 CPOO	uncoated	2.45-2.55	3.5-7.0
5000 CPO3	silane surface coated	2.45-2.55	4.0-7.0

3.3 RHEOLOGICAL CHARACTERISATION

From literature resources on incompatible systems, the morphology of polymer blends is determined predominantly by the rheological factors of the components. Generally a high viscosity ratio results in a coarse morphology; while matching the viscosity results in a fine morphology [36,38,188].

To test this point for the PP/EPR blends, the rheology of individual raw materials and their blends were examined under the same conditions. This was achieved by using a Rosand Precision Capillary Rheometer. During testing, the molten material was forced from a reservoir through a capillary die under controlled conditions. The equipment was operated at 180, 190 and 200 °C by using a long die with ratio of length over diameter of 32:2 mm. After the barrel was charged and the temperature held at equilibrium for 5 min, the pressure drop over the die was measured using a 34.5 MPa (5000 psi) full scale pressure transducer in the shear range of 10 to 500 s^{-1}. The shear stress, shear rate and shear viscosity were then calculated using the following equations. The data reported as was calculated in the computer program. No corrections was applied.

$$\textbf{Shear stress (Pa)} = Pr / 2L = Fr / (2\pi R^2 L) \quad (3.1)$$

$$\textbf{Shear rate (s}^{-1}\textbf{)} = 4Q / \pi r^3 = 4V / \pi r^3 t \quad (3.2)$$

$$\textbf{Viscosity (Pa.s)} = P\pi r^4 / 8LQ = Fr^4 t / 8R^2 LV \quad (3.3)$$

Where: P = pressure by ram (Pa), F = force on ram (N), L = length of capillary, r = radius of capillary (m), R = radius of barrel (m), Q = flow rate (m^3/s), V = volume extended (m^3) and t = extension time (s).

3.4 BLEND PREPARATION AND COMPOUNDING PROCEDURES

Blends of various compositions were prepared by melt-mixing in a BTS 40 (Betol Machinery Ltd.) twin screw extruder. The BTS 40 machine is a modular intermeshing co-rotating twin screw-extruder. The initial machine was designed at Brunel University and was designated TS40-DVL. Details of the TS40 extruder have been reported by Hornsby [173]. The BTS 40 machine has facilities for interchangeable barrel and screw sections, thus permitting selection of the optimum screw configuration to suit the particular characteristics of the polymer or composite to be processed. This machine has found application in the preparation of heavily filled polymer composites for specific end-use requirements [173-177].

Throughout the work 40 mm diameter screws were used in a 21/1 mm length to diameter (L/D) barrel configuration. The screw flights and channels are closely-intermeshing trapezoidal non self-wiping type, which provide a strong positive conveying characteristics. The screw profile consists of a feed section, compression or melting zone, a decompression region with facilities for vacuum or atmospheric devolatisation, and a metering section (*Figure 3.1*). Screws are built up in a building block principle. The screw elements consist of different lengths and pitches and special kneading elements of various widths which are interchangeable. The screw elements and kneading blocks are secured on the shaft by keys. The screw elements are held on the shaft by the screw tip. Various modular screw sections and screw elements used in this work are shown in *Figure 3.2*. These elements were arranged on shafts to produce two different screw configurations, designated GM and SM, differing in the mixing shear intensity. The GM configuration (*Figure 3.3a*), providing a relatively low shear mixing, consists totally of right handed screw elements with a total length of 875 mm. It has two kneading disc blocks of 60 and 25 mm long located 200 and 570 mm, respectively along the length of the modular screw from the die. The SM screw configuration (*Figure 3.3b*) consists of right handed screw elements with three kneading disc blocks providing comparatively severe mixing. The three kneading disc blocks have 60, 80, and 65 mm long locating 80, 290 and 450 mm from the die, respectively. The modular screw assemblies and their details are presented in *Figures 3.3a-b.*

A number of different screw speeds and feed rates were used. Their details will be discussed in Chapter 6. Where possible, the temperature profiles along the extruder barrel were set constant in the range of 185° to 200°C from the feed zone to the die. However, due to the slight variation in the melting behaviour of various composites, die

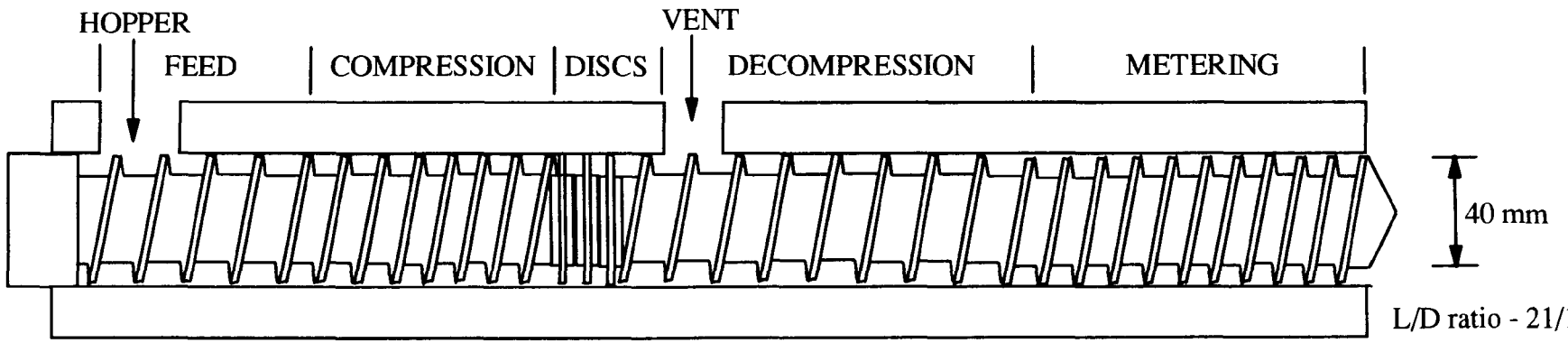

Figure 3.1 Schematic diagram showing standard screw configuration

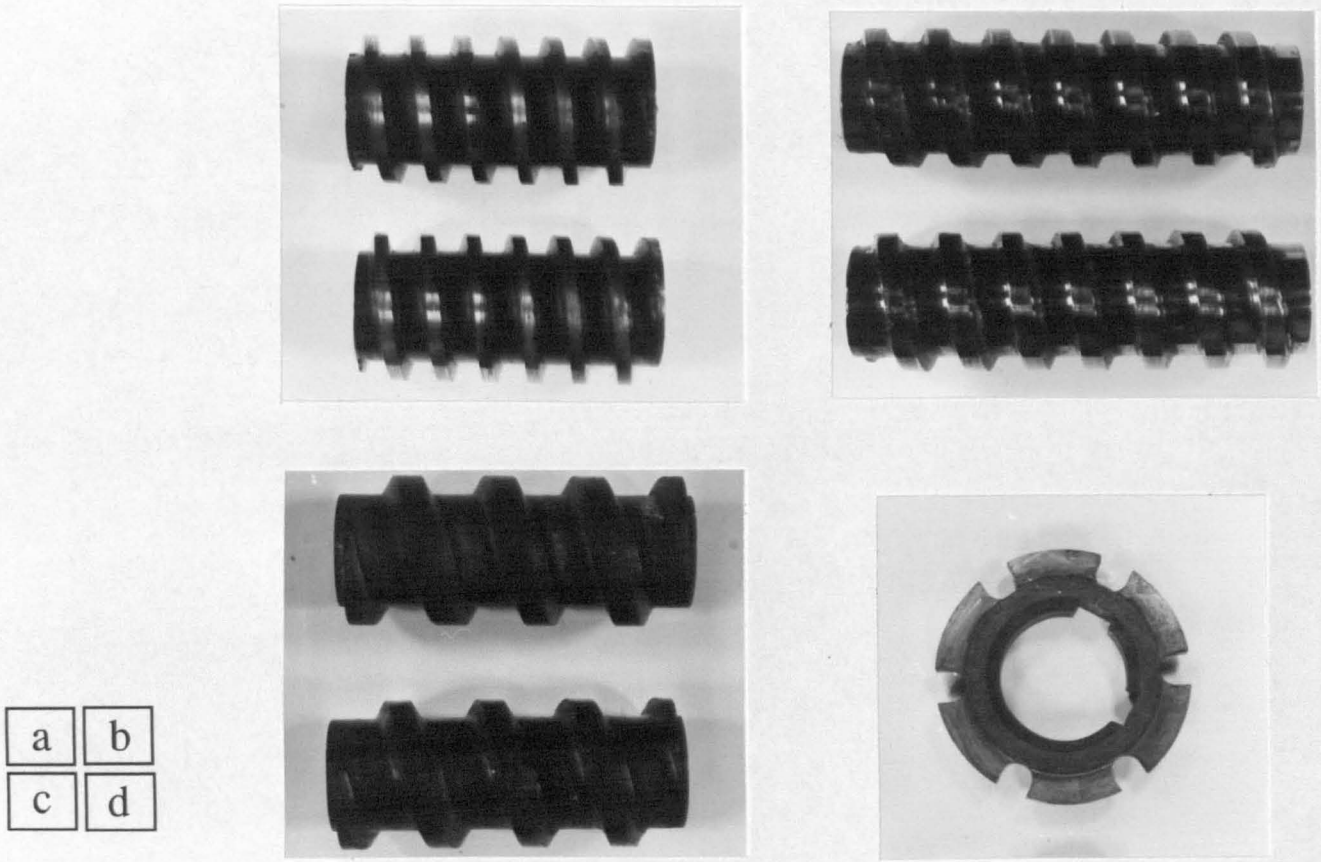

Figure 3.2 Various screw sections (a-c) and melting disk (d) used in this work.

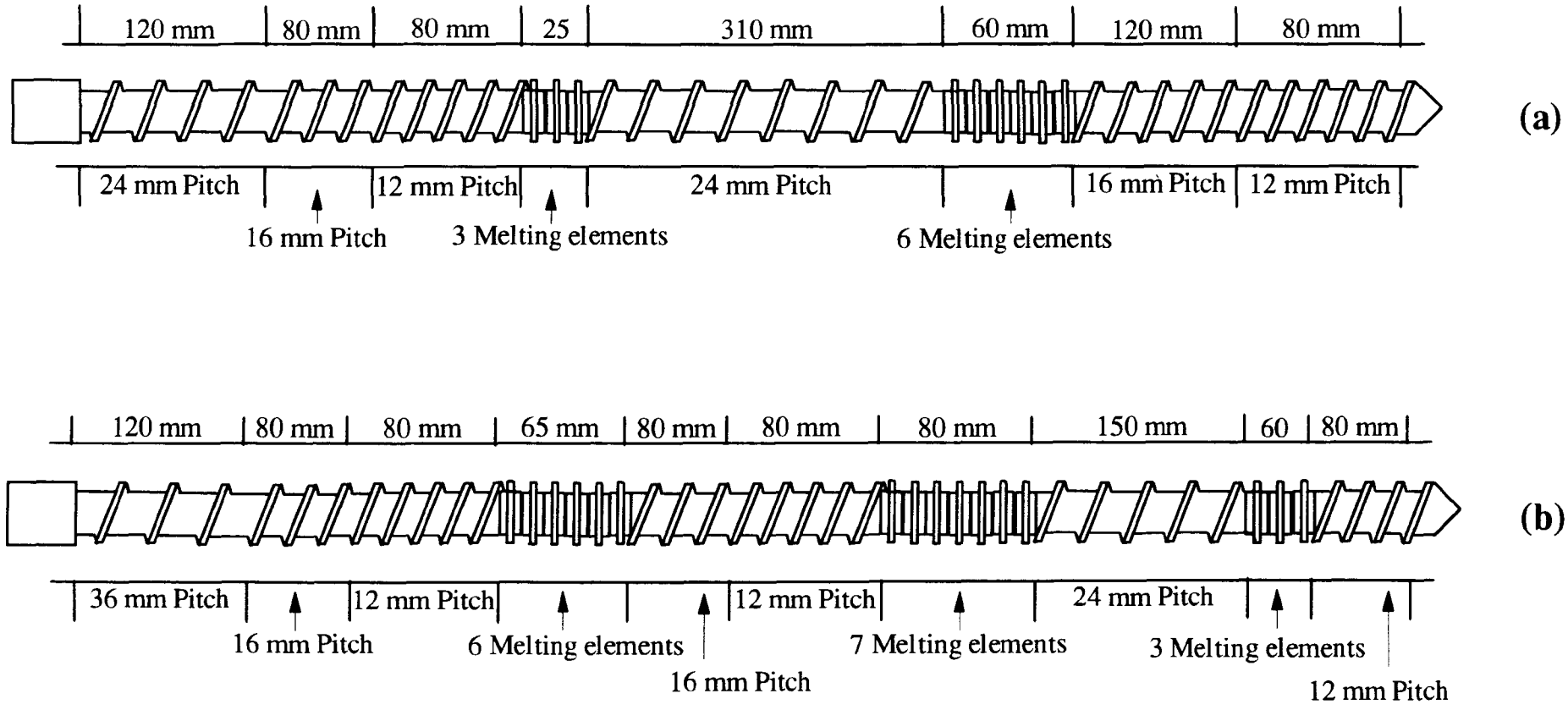

Figure 3.3 Dimensions of screw configurations used, (a) gentle screw profile and (b) severe screw profile.

temperature was adjusted (± 10°C) in order to control extrudate quality and to avoid the appearance of sharkskin which tend to increase water pick up from the cooling bath. Materials were dry-blended by hand for approximately 1 min (this was done in a plastic bag which was tumbled a number of times). The dry-blend was then fed into the extruder by a K-Tron twin screw volumetric feeder. The extrudate obtained was immediately quenched in water at 23°C and chopped in the pelletiser. For the comparison purposes, the unmodified polypropylene was also subjected to the same extrusion process in order to obtain a similar thermal history to that of the polypropylene component in the blends.

3.5 PREPARATION OF TEST SPECIMENS

From the compounds prepared earlier, test specimens for morphological and mechanical investigations were made by compression moulding. The objective of using compression moulding is to produce test specimens which are isotropic and have the same characteristics as the original compounds. In compression moulding process polymer materials are melted in a heated mould, pressure is then applied to the mould causing the melted materials to be squeezed out to take the shape of the mould. Unlike injection moulding process where polymer melt is forced from the barrel through a nozzle, sprue, runner system and gate into the mould cavity.

Injection moulding process leads to anisotropic specimens where the properties along and transverse to the flow directions are significantly different. During the process the injection machine also performs as a mixer whereby the rotation of the screw in the barrel causes the materials to move and mix again. This can lead to an alteration in the morphology and properties of the specimens from the original compounds. It has been reported [189] that injection moulded polypropylene yields a molecularly oriented nonspherulitic "skin" region and an unoriented "core". The morphological anisotropy in injection moulded polypropylene leads to a corresponding anisotropy in mechanical properties in both tensile and flexural modes [190-191] and also affects the tensile impact strength [192]. Similar effects were also observed in polypropylene-ethylene-propylene-diene polymer (PP-EPDM) blends [64]. In most cases, polypropylene forms the continuous matrix. Droplets of EPDM yield flattened ribbons elongated in the direction of the melt flow in the skin region and isotropic spherical inclusions in the centre "core" region [64]. However, when comparing PP-EPDM blends to neat polypropylene it exhibits fundamental differences in the orientation pattern. The orientation in PP/EPDM blends is significantly lower than that of polypropylene. The extent of orientation can be influenced by the melt temperature, injection speed and mould temperature [193].

In this work the mould used was a 23x23x0.2 cm flash-type (or picture-frame type) mould where a steel chase (a picture frame) is sandwiched between two thin steel plates. The composite granules were evenly spread over the mould surface. The mould was then placed in a preheated press and heated at 200°C for 8 min without any applied pressure. After this period a pressure of 40 tons was applied and kept constant for 5 min. In order to maintain the specimen properties the same as those of the extrudate obtained from the extruder, the mould was rapidly cooled (quench) to the room temperature. For rapid cooling two presses were used, one for heating and the other for cooling. After heating, the mould was transferred from the heating press (200°C) to the cooling press (23°C) as quickly as possible. The cooling process normally completed within 3 min. In order to prevent sticking of the materials to the mould surface and to ease flow during moulding, a thick Melinex (polyethylene terephthalate) film was used during the compression moulding. However, it should be noted that this film is not suitable if the moulding temperature is higher than 230 °C with moulding time longer than 1 hour since it tends to be degraded after this period of time.

3.6 DETERMINATION OF MECHANICAL PROPERTIES

3.6.1 Tensile testing

Tensile testing was carried out using an Instron Model 4206 tensile testing machine. The tensile dumb-bell specimens were cut from a 2 mm thick moulded sheet using an automatic hollow-die punching machine operated by compressed air. The hollow-die used is of ASTM D-638 Type IV (identical to BS 2782 Method 320 A). The prepared specimens were stored at room temperature for ten days prior to testing.

Testing was carried out in the tensile mode at 23°C at a speed of 50 mm/min and a load cell of 5 kN starting from a gauge length of 80 mm. The Young's modulus of each specimen was determined using an Instron strain gauge extensometer with a gauge length of 10 mm. Modulus, tensile yield strength, percentage elongation at yield and at break were recorded. A minimum of eight specimens were evaluated for each sample.

3.6.2 Instrumented falling weight impact testing

The falling weight impact test is a useful method of assessing the impact performance of plastics and composites. It can be used simply to characterise and compare the impact properties of different materials. By using high speed photographic [194], short pulse flash photographic [195] and grid techniques [195], crack development on the top or bottom surfaces of the specimen can be observed and toughness behaviour of the materials can also be monitored.

During impact testing, a free falling weight is released from a predetermined height to strike the specimen supported on a steel ring. The striker is instrumented with a force-transducer which provides a record of force-time throughout each impact event. The features of a force-time curve reflect the failure characteristics of the material. The result records the whole impact event from fracture initiation to final fracture. The total energy measured is therefore that required to initiate damage and propagate further damage until total destruction of the specimen or to allow the striker to penetrate the specimen.

The basic force-time curve record can be subsequently used to compute derived data such as force-deflection as shown in *Figure 3.4*.

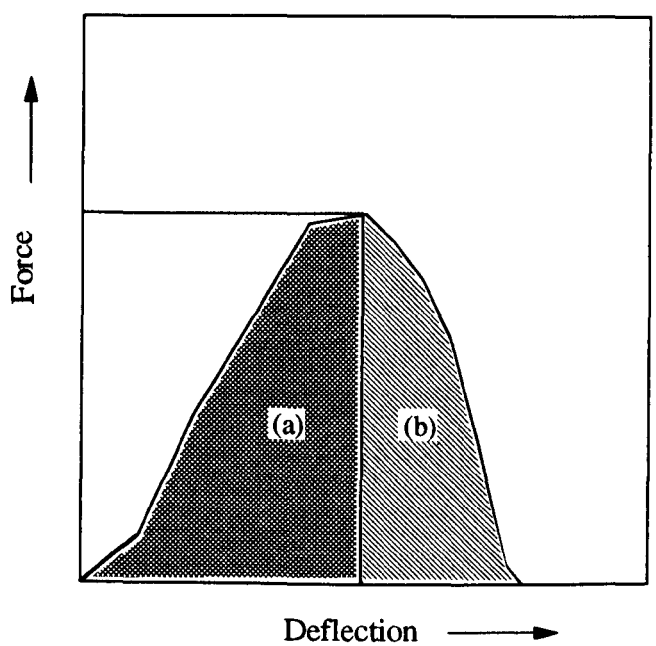

Figure 3.4 Typical load-deflection diagram of instrumented falling-weight impact test for a PP/R blend.

The first peak in the force-deflection curve corresponds to crack initiation, usually appearing on the bottom (tension) surface of the specimen- the surface opposite the one which is struck by the striker. Integration of the force-time curve up to the first peak (*area (a) of Figure 3.4*) will give the energy absorbed in initiation a crack. The second part of the curve (*area (b)*) corresponds to the crack propagation from the initial failure to the edge of the specimen. When the cracks reach the edge, complete fracture occurs and the force falls to zero. Therefore integration of the full force-deflection curve gives the total energy absorbed in initiation and propagation of the crack. The energy involved in propagating the crack can be calculated by subtracting the initiation energy from the fracture energy.

In impact testing various tup geometries may be used, for instance hemispherical or flat-headed tups. For tough materials, a flat-headed tup is recommended [196]. It is shown in *Figure 3.5* that a specimen tested using a hemispherical tup tends to wrap itself around the tup face, thus requiring deformation energy. At failure the specimen is stretched both under and around the surface of the tup. With a flat-headed tup it is only the material between the tup and the specimen support that is deformed so that the energy absorbed during failure is better defined [196]. *Figure 3.6* shows the failure mode of rubber modified polypropylene. It can be seen that the failure produced from a hemispherical tup is ductile and the deformation is large. The deformation develops gradually and there is no event to mark the peak force. The flat-headed tup produces a greater deformation speed than the hemispherical tup. This is attributed to the initial length of the surface to be deformed which is considerably less in the former case than the latter one where the specimen surface is stretched around the tup.

The falling weight impact testing was performed according to ASTM D-3209-78 using a Rosand Instrumented Impact Tester. Test specimens in the form of 70 x 70 x 2 mm thick moulded plates were laid flat and clamped on a steel ring having an internal diameter of 40 mm. A 5 kg striker was dropped on to the specimens from a constant height of 46 cm; corresponding to an impact velocity of 3 m s^{-1}. A flat-headed tup of 10 mm diameter was used.

After testing, a force transducer provides a record of force with time throughout each impact event. From a force against time curve, the deflection and absorbed energy were calculated. The total energy to break (failure energy) and the maximum force were recorded. Ten measurements were taken for each compound.

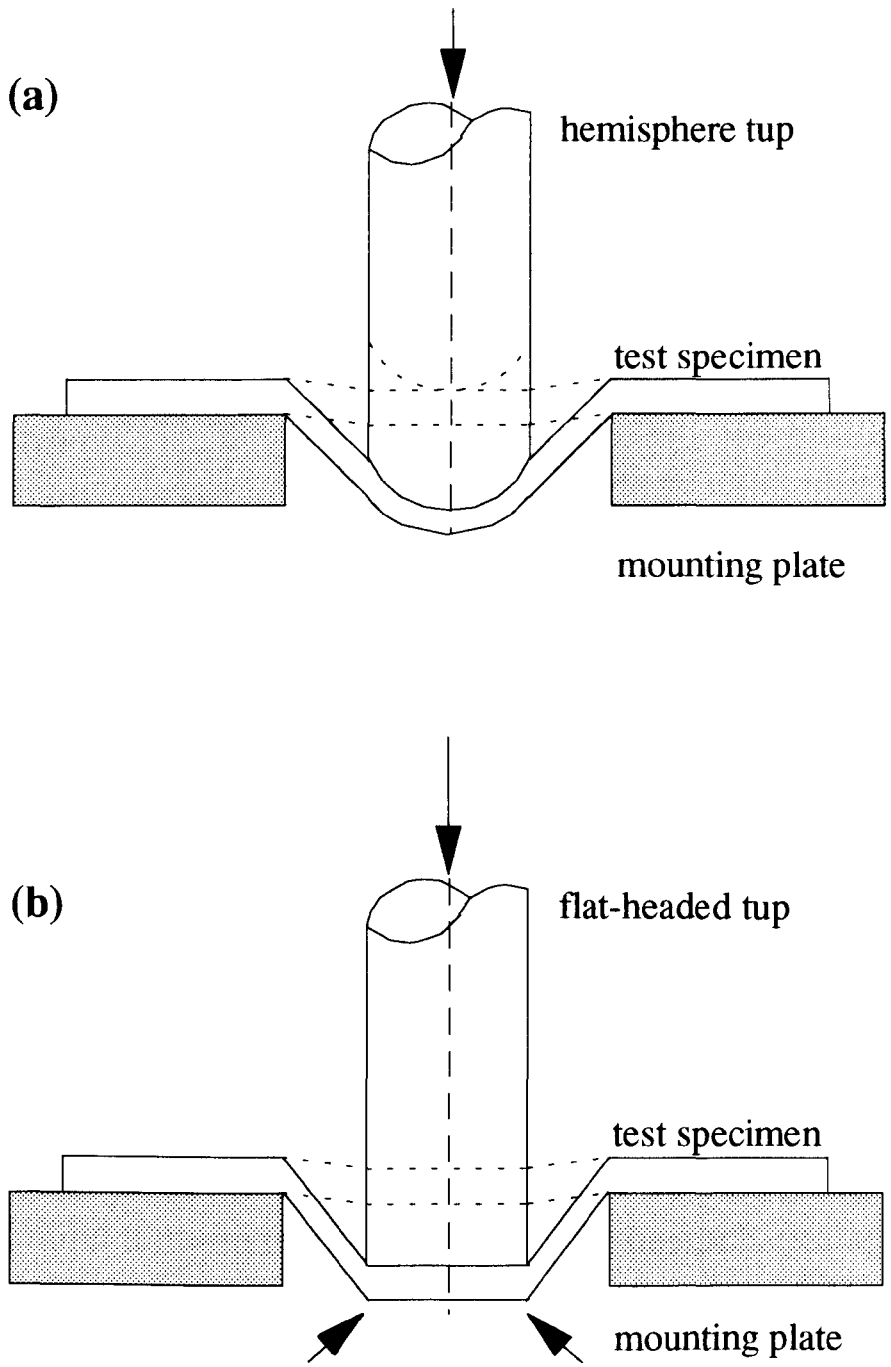

Figure 3.5 Specimens during the falling weight impact test using (a) hemisphere, and (b) flat-headed tups.

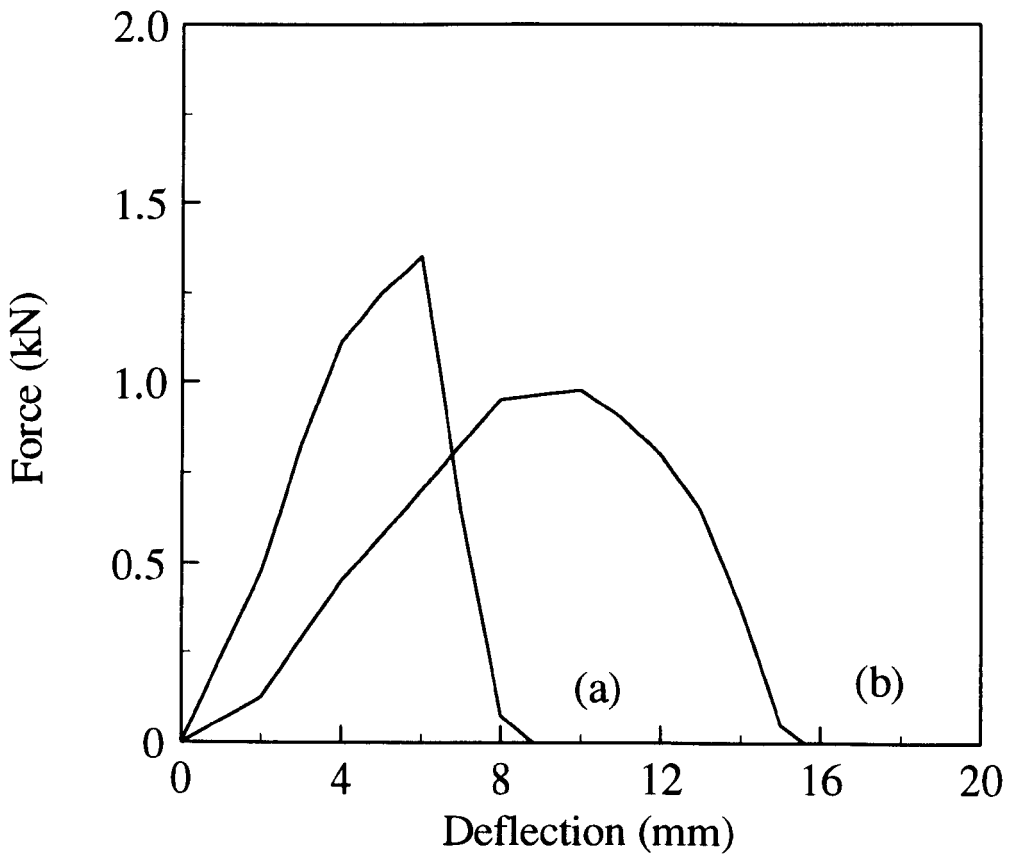

Figure 3.6 Force-deflection curves of a PP/R blend from the falling weight impact test with (a) flat-headed, and (b) hemispherical tup

3.6.3 Fracture toughness test based on J-integral method

3.6.3.1 Introduction

Fracture toughness is a property providing a measure of the material's resistance to crack propagation. The criterion of fracture toughness for polymers has been extensively investigated because of design and safety of engineering components and structures. One of the most practically used criteria for brittle and ductile fracture is based on the J-integral concept.

In the ASTM standard E813-81 for the J-integral characterisation, the crack initiation point is estimated using the so-called "blunting line". This procedure has been recently used to described the criteria for the onset of crack growth in many ductile materials [74-80]. However, the crack blunting line phenomenon is highly complicated and the validity of such an approach is still questionable [77, 79]. There is considerable interest in the application of this method to multiphase polymer composites where either or both rubber and filler are incorporated in a polypropylene matrix. The objectives of this investigation are twofold. Firstly, to analyse whether the fracture toughness of polypropylene and its composites can be determined using the J-integral method based on the crack blunting line concept and secondly, to understand the mechanism and development of a failure occurred in such composites. A significant amount of preliminary work was undertaken to establish optimum specimen geometry, testing conditions and interpretation of results. Detail of preliminary work is also included in this section.

3.6.3.2 The J-Integral Test Method

Because a standard for J-integral testing of polymers currently does not exist, the J-integral method used here was that proposed by Rice [70]. This concept later was developed by Begley and Landes [197], and standardised by the ASTM for metal testing [101].

The starting point of Rice's considerations was the assumption of elastic material behaviour. This implies that stresses can be derived from a potential, strain energy density, which is a unique function of stresses or strains. On that basis it was not only shown that J is path independent, but also equivalent to the energy release rate G in linear elastic fracture mechanics (LEFM) analysis.

Begley and Landes [197] used J as a fracture criterion parameter and proposed a multi-specimen procedure to measure the material fracture toughness. The J determined by this method is based on the following equation:

$$J = (-1/B)\,(dU/da) \qquad (3.4)$$

where : B is the specimen thickness, a is the initial crack length and U is the energy given by the area under the load-deflection curve. Employing eq. 3.4, J can be evaluated from the load-deflection records of specimens which differ only in initial crack length. However, it is not an easy task to obtain a reliable value of dU/da at a constant deflection when the material exhibits a non-linear locus line.

Kim and Joe [198-200] recently introduced a method to evaluate the critical J-integral value, using the locus of the crack initiation points on load-displacement curves. This locus method partitions the fracture energy along the locus line based on an energy rate interpretation. J_c of highly deformable materials such as a thermoplastic elastomer like Santoprene was reported [198-200] to be determined by this method without restricting the ratio of initial crack length to the specimen width (a/W).

However, this method enables J_c to be evaluated only if the crack initiation point can be detected during the test. Thus, this can present considerable problems in some materials especially in opaque materials.

A method for determining crack initiation point has been proposed by the ASTM standard [201] using several specimens and a form of resistance curve (R-curve). A set of identical specimens are each loaded to different deflections, all less than that to give total failure (break). For each specimen, the J value is calculated from the energy up to that deflection. Then the J values are plotted against the crack growth length (Δa) and extrapolated to $\Delta a = 0$. However, in tough materials there is an additional complication in that crack will blunt prior to initiation. To find a true initiation point, the ASTM test standard [101] outlines a graphical process using the so-called " blunting line " given by the following expression :

$$J = 2\sigma_y \Delta a \qquad (3.5)$$

where :σ_y is the yield stress and Δa is the apparent crack growth. In this expression, the apparent crack growth (as measured on the fracture surface) is assumed to be equal to one-half of the crack tip opening displacement.

The crack initiation energy (J_c), according to this method, can thus be obtained by the intersection of the crack blunting line and the R curve as shown in *Figure 3.7*. For fracture to be characterised by this method, a specimen must meet certain size requirements in order to achieve a plane-strain stress state along the crack front. According to the ASTM standard E813 -81 [101], a size criteria required is as follows :

$$\mathbf{B, a, (W-a) \geq 25 (J_c/\sigma_y)} \qquad \mathbf{(3.6)}$$

where : B and W are the specimen thickness and width, respectively. a is the original crack length and σ_y is the yield stress of the material.

J_c obtained from this method can be directly related to the K_c for linear elastic behaviour via the relationship :

$$\mathbf{K_c^2 = E J_c / (1-P^2)} \qquad \mathbf{(3.7)}$$

where : P is Poisson' s ratio and E is Young's modulus so that J_c is equal to G_c in the LEFM case.

Another important parameter describing material's ability to resist crack propagation is "tearing modulus" (T_m). Rivin and Thomas [202] introduced the tearing energy concept based on fracture mechanics to characterise the rupture of cross-linked rubbers. Oh [203] devised a single specimen test method to measure tearing energy by calculating the J_c value of a nicked rubber strip. Although Oh's method requires only one specimen, the calculation of the J-integral involves tedious measurement of strain energy distribution along the edges of the specimen. Paris [204] introduced the concept of tearing instability through a non-dimensional parameter called tearing modulus, defined as

$$\mathbf{T_m = (E/\sigma_y^2) [dJ/d(\Delta a)]} \qquad \mathbf{(3.8)}$$

where : dJ / d(Δa) or the tearing resistance is the slope of R-curve and E is the modulus of elasticity.

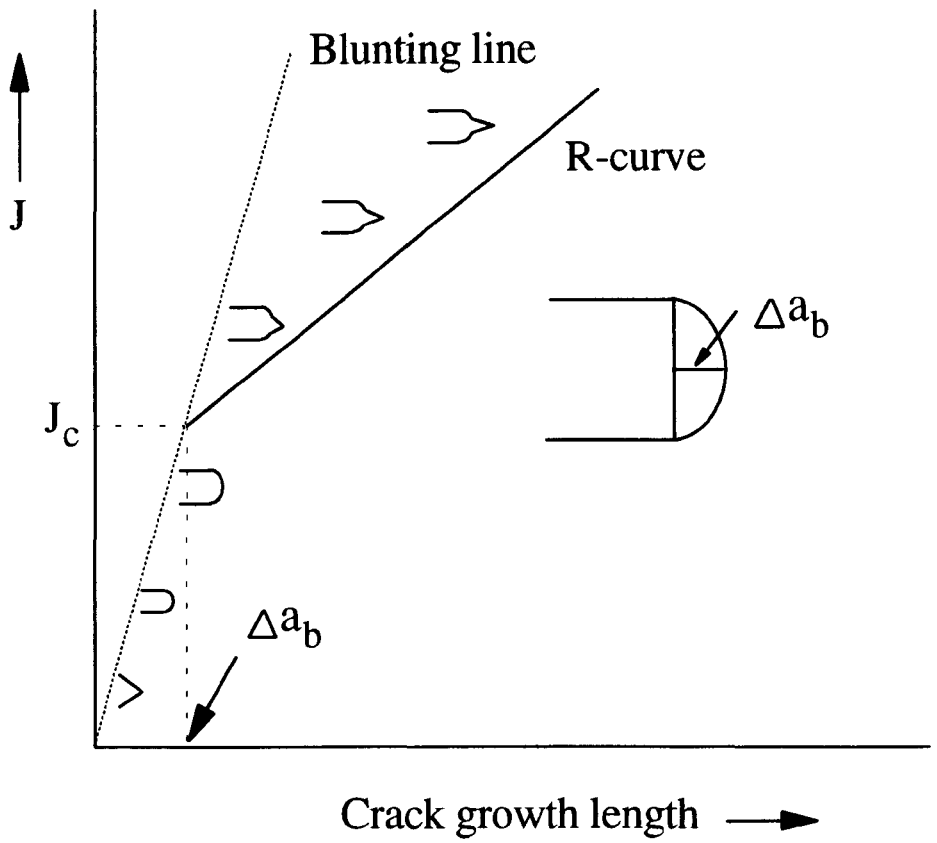

Figure 3.7 Schematic representation of the R-curve and the crack tip blunting component of crack growth

3.6.3.3 Preliminary work on experimental technique evaluation

(i) Test specimens

The first problem encountered in the present investigation was that of selecting suitable specimen geometry. According to the ASTM standard E813 -81 [101], J-integral test specimens used must meet the certain size requirement ($B \geq 25\ [J_c/\sigma_y]$). Following this equation, the specimen thickness may be specified only if the J_c value of the material can be estimated beforehand. Based on the published work on similar materials, J_c of 1.1 kJ/m^2 [76] and 2.8 kJ/m^2 or 2.9 kgf cm/cm^2 [84] were reported for polypropylene homopolymer while J_c of 15.5 kJ/m^2 was for polypropylene copolymer [74]. This means that the suitable sample thickness for the investigated materials (neat and modified polypropylene) may be in the range of 1 to 12 mm.

Six millimetre thick specimens were then prepared by compression moulding. The test was carried out according to the ASTM E813 -81 using an Instron testing machine. The testing was performed in a three-point bending mode at room temperature and at a testing rate of 1 mm/min. A series of identical specimens was loaded to the different predetermined displacements and then unloaded. Typical load-displacement curves for PP and PP/R (70/30) samples are shown in *Figure 3.8*. Due to the load control conditions, unstable ductile cracking of polypropylene occurred at or near the load maximum indicated by the arrows in *Figure 3.9*. The values of J at each point of loading were calculated from the area under its load-displacement curve. The length of crack growth zone was measured under an optical microscope using a micrometer eyepiece. Details of experimental procedures will be reviewed in the following section.

The calculated J values were then plotted as a function of crack growth length, Δa, as shown in *Figures 3.10a and b*. The J_c value was taken from the value of J at the intersection between R-curve and the blunting line calculated using eq. 3.5. The J_c value of 2.19 kJ/m^2 was observed for a PP sample while that of only 1.33 kJ/m^2 was found for a PP/R (70/30) sample.

Although, in this experiment the J_c values of PP and PP/R samples can be determined by using this conventional blunting line technique. However, the J_c value obtained from a PP/R sample seems to be underestimated and quite possibly incorrect. Reason for this testing failure might possibly be due to the unsuitable specimen size.

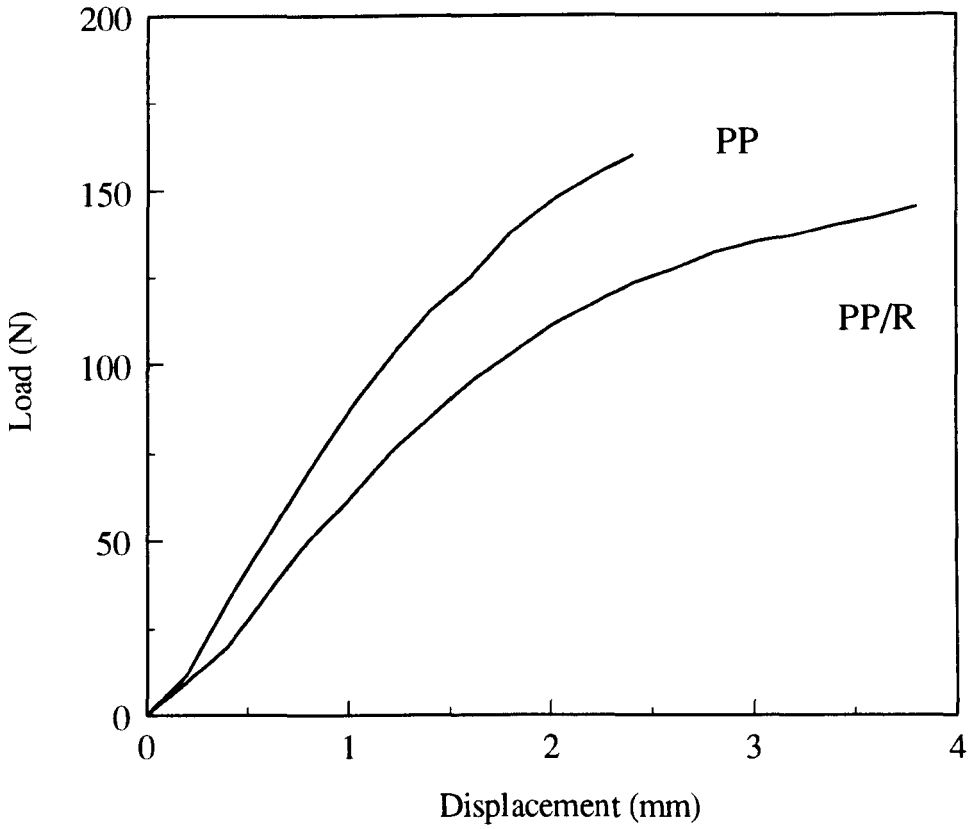

Figure 3.8 Typical load-displacement curves of PP and PP/R at 23 °C.

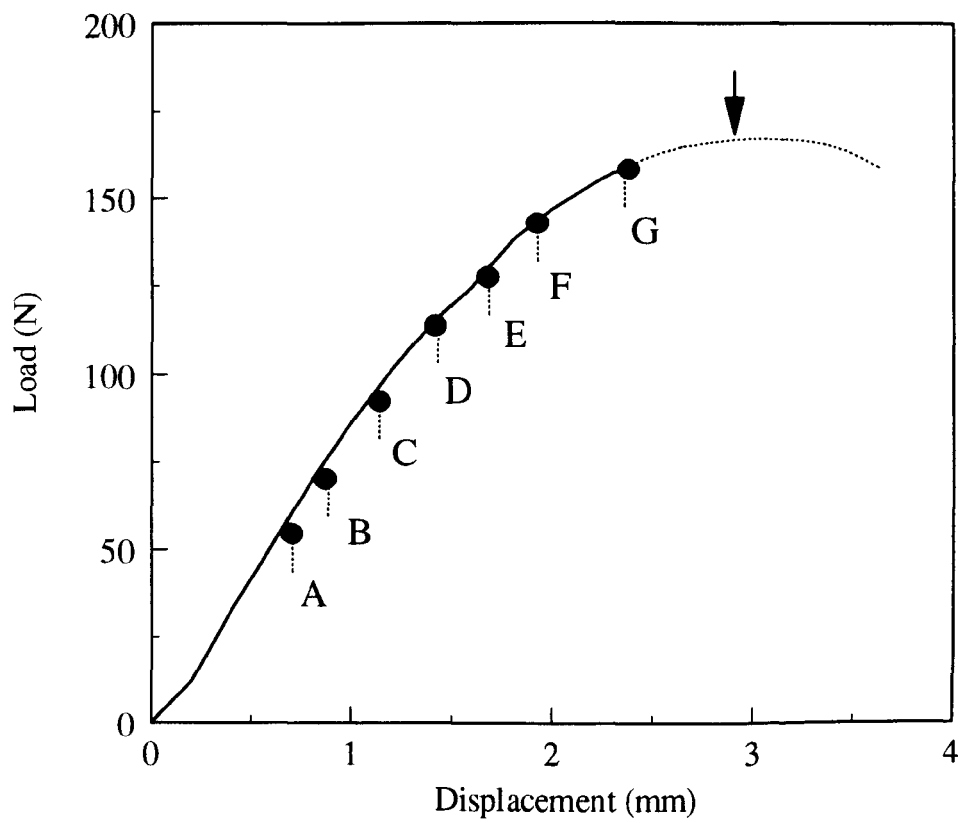

Figure 3.9 Typical load-displacement curve of PP at 23 °C. The arrow indicates the onset of instability.

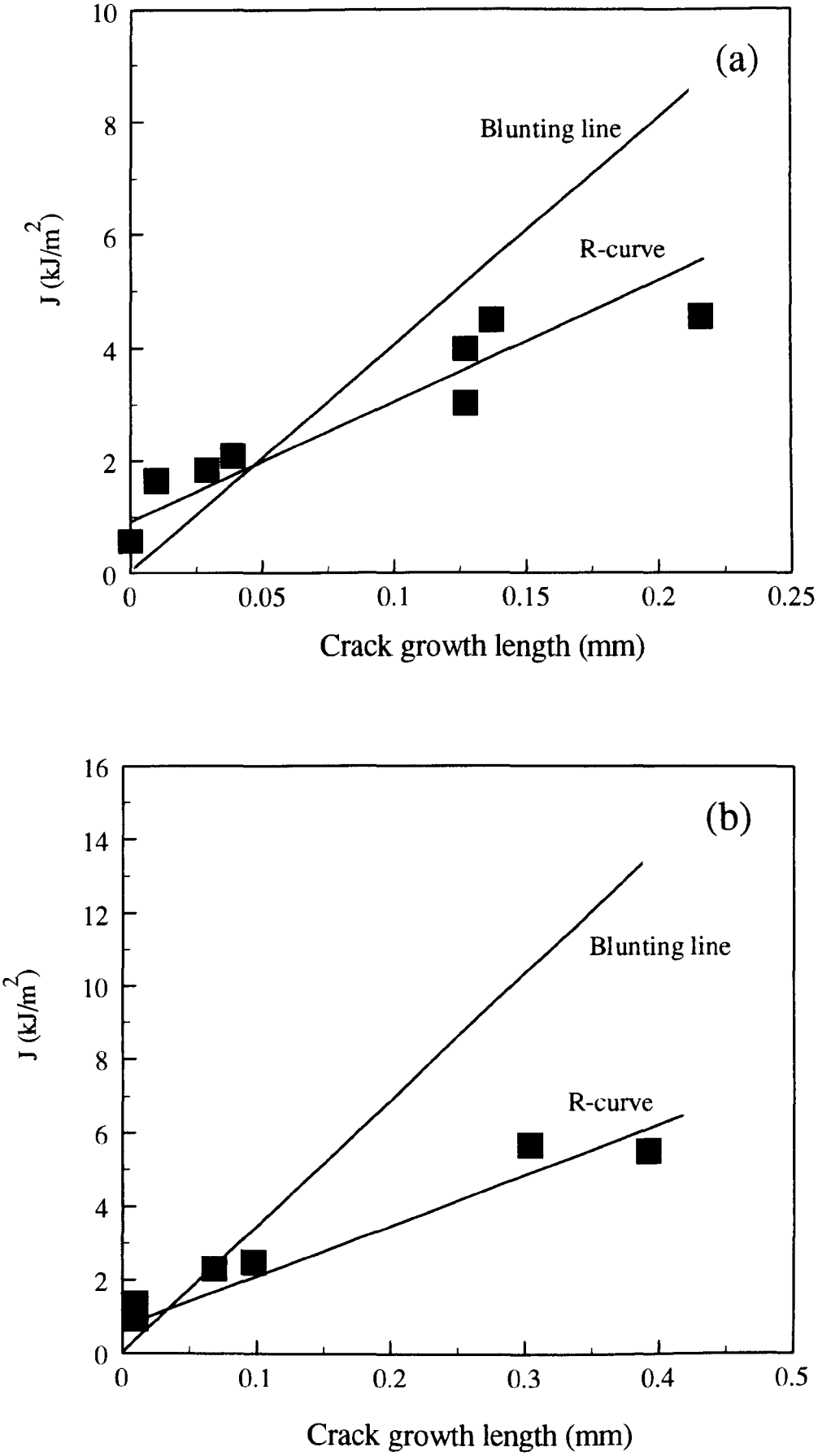

Figure 3.10 Plot of J against crack growth length for (a) PP and (b) PP/R samples at 23 °C. The specimens are of 6 mm thick.

Thus, specimens of 12 mm thick were then prepared and tested under the same testing conditions as mentioned above. The preparation of 12 mm thick compression moulded specimens will be discussed in the next section. *Figures 3.11a and b* show the plots of J against crack growth length of 12 mm thick PP and PP/R samples. The J_c value of 2.27 kJ/m^2 was observed for a PP sample and the J_c value of 1.86 kJ/m^2 for a PP/R sample. The J_c value of a PP/R sample was, once again, lower than that of an unmodified PP sample. A similar observation was recently reported by Ha et.al. [84] in which a J_c value of PP/EPDM (50/50) blend was found lower than that of pure PP. In their study the J_c value was determined using the locus line method, developed by Kim and Joe [198-200].

Narisawa [83] investigated the fracture toughness of polyethylene and polypropylene using the conventional blunting line method. The specimens of 10 mm thick were loaded in three-point bend test at a bending rate of 1 mm/min. He found the difficulty in obtaining the values of J_c for both polyethylene and polypropylene from the blunting lines.

The use of blunting line technique in this study worked well with a PP homopolymer, however, failed to specify properly the J_c value of a rubber modified polypropylene (PP/R). The reason still remained an open question. Continuing the investigation by experiments on thicker specimens did not seem a good idea. Since preparation of defect-free specimens thicker than 12 mm by compression moulding, is extremely difficult. Effort was then focused on the testing conditions used.

(ii) Testing conditions

J-integral testing was also performed at low temperature in addition to room temperature. The reasons for this were firstly to verify that toughness of polypropylene, especially at the temperature below its glass transition (0-6 °C) can be enhanced by the incorporation of EPR and secondly to increase the yield stress of the materials and hence more closely approach plain strain conditions.

The low temperature testing was performed at -20°C and at a bending rate of 1 mm/min. Detail of low temperature testing procedure will be discussed in the next section. Specimens used were of 12 mm thick. Typical load-displacement curves at -20°C for PP and PP/R are shown in *Figure 3.12*. The plots of J values against crack growth length of PP and PP/EPR samples are shown in *Figures 3.13a and b*, respectively.

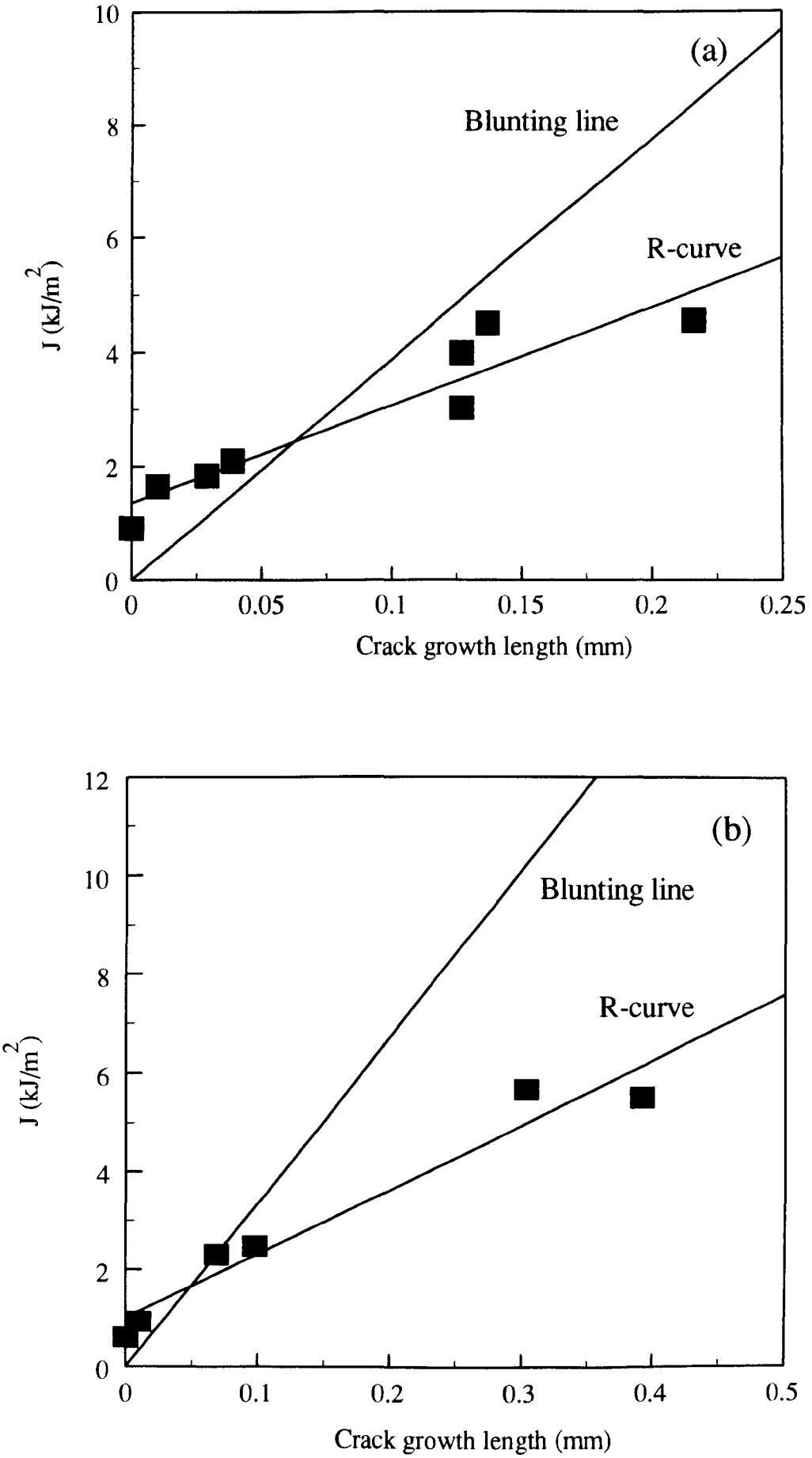

Figure 3.11 Plot of J against crack growth length for (a) PP and (b) PP/R sample at 23 °C. The specimens are of 12 mm thick.

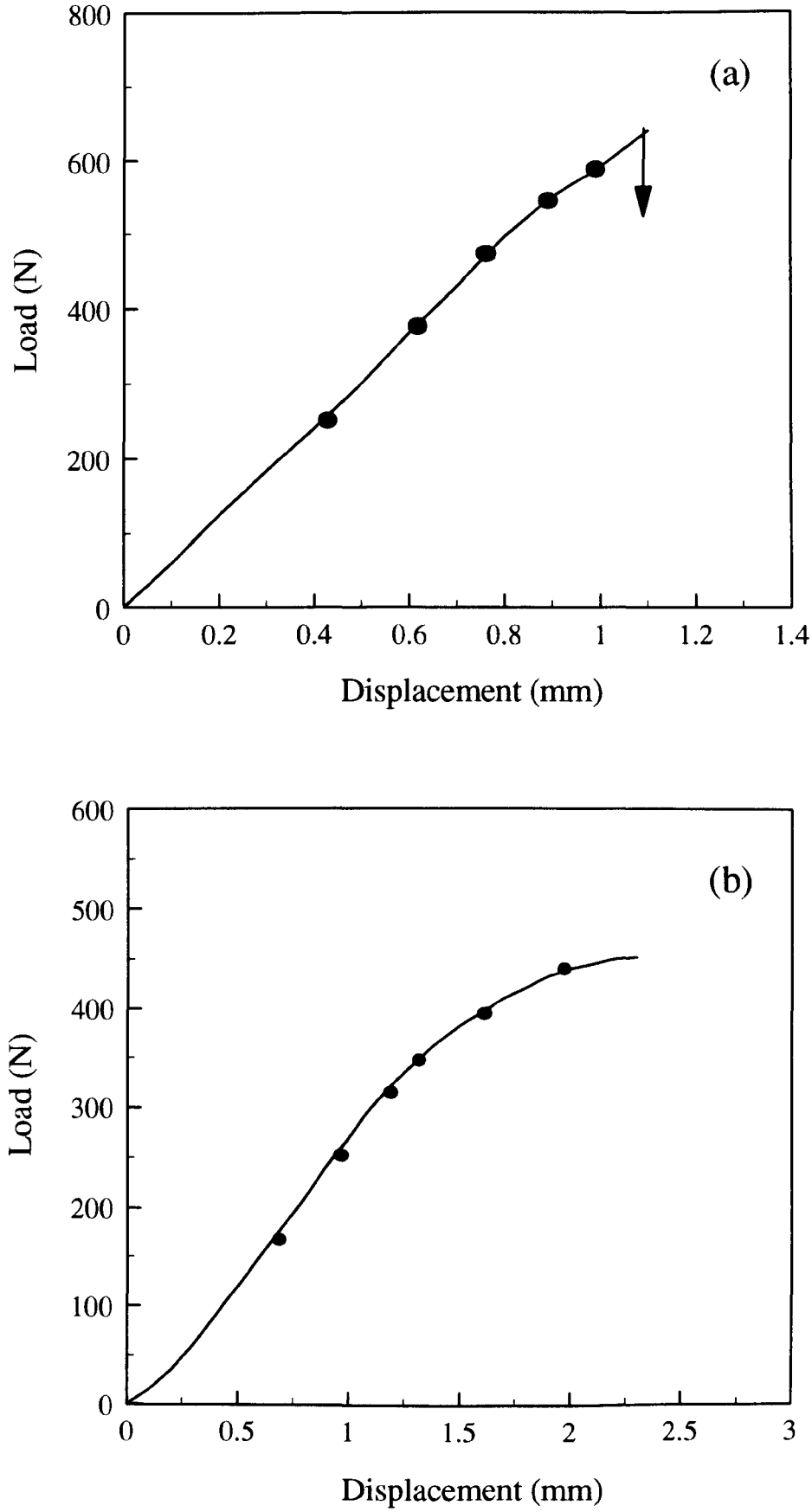

Figure 3.12 Typical load-displacement curves of (a) PP and (b) PP/R samples at -20 °C.

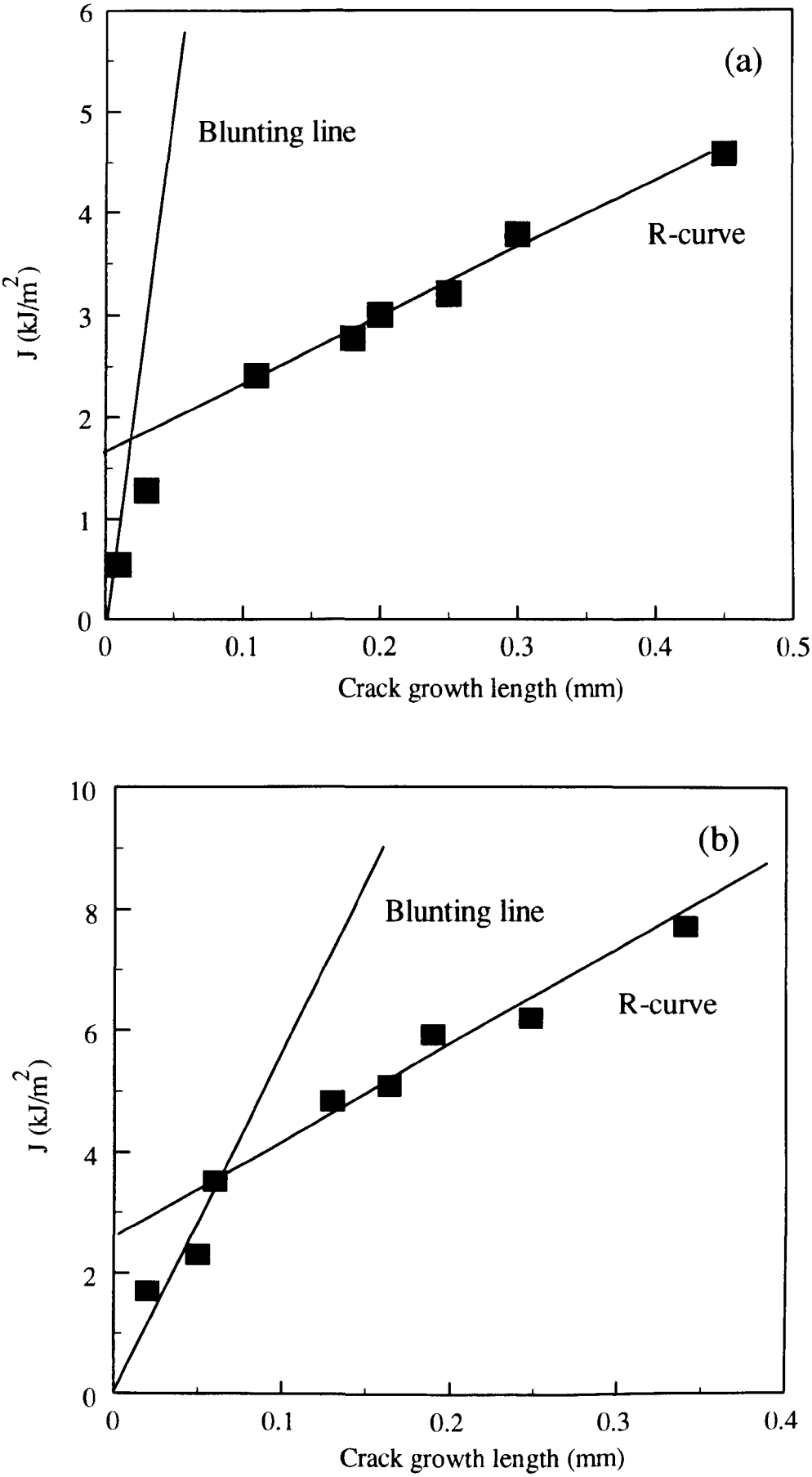

Figure 3.13 Plot of J against crack growth length for (a) PP and (b) PP/R sample at -20 °C. The specimens are of 12 mm thick.

The J_C value of 1.75 and 3.48 kJ/m^2 was observed in PP and PP/R samples, respectively. Thus, it can be concluded that the incorporation of EPR increased the toughness at low (-20°C) temperature of PP as can be seen in terms of the J_C value.

(iii) Crack growth length determination

A difficulty in determining crack growth lengths (Δa) has been found in the three-phase composites. *Figures 3.14a-c* shows the optical micrographs of side views of a PP/R/G (70/15/15) tested sample. The sample was tested at -20°C. It can be seen from *Figure 3.14* that subcritical crack growth initiated at the crack tip and propagated within the damage zone. With further loading (*see Figure 3.14b*), both damage zone extension and subcritical crack growth continue. With neat PP samples, however, (*see Figure 3.14c*) the crack occurred ahead of the precrack tip which was very sharp, greatly facilitating determination of crack growth length.

Several papers have been published in which J_C was determined from the intersection between R-curve and blunting line from the plot of J values against crack growth lengths. In no case was there a theoretical justification that was supported by substantial experimental evidence given for the use of the crack blunting line. In the present study the blunting line concept gave a wrongly estimated result in the J-integral test for a PP/R blend at room temperature and was unsuitable for testing a PP/R/G composite at -20°C. There are several reasons that might explain why the crack blunting line concept is not appropriate for ternary phase composites.

The first reason is the problem of crack growth length measurement. Crack growth length observed in a PP/R sample was very small. Measurement of such small cracks (sometimes on the order of microns) is very difficult either from the specimen surfaces or fracture surfaces unless the differences between crack growth zone and damage zone can be clearly identified. In case of a PP/R/G sample the measurement of crack growth length was impossible since the deformation area composed of many fine deformation bands in which many microcracks are involved as shown in *Figure 3.14*.

The second reason relates to the crack blunting line concept. This model assumes a semicircular crack blunting shape ahead the notch tip caused by simple plastic deformation and yielding. However, in three-phase composites the crack tip does not appear to be blunted, but instead develops a rather complex damage zone composed of a

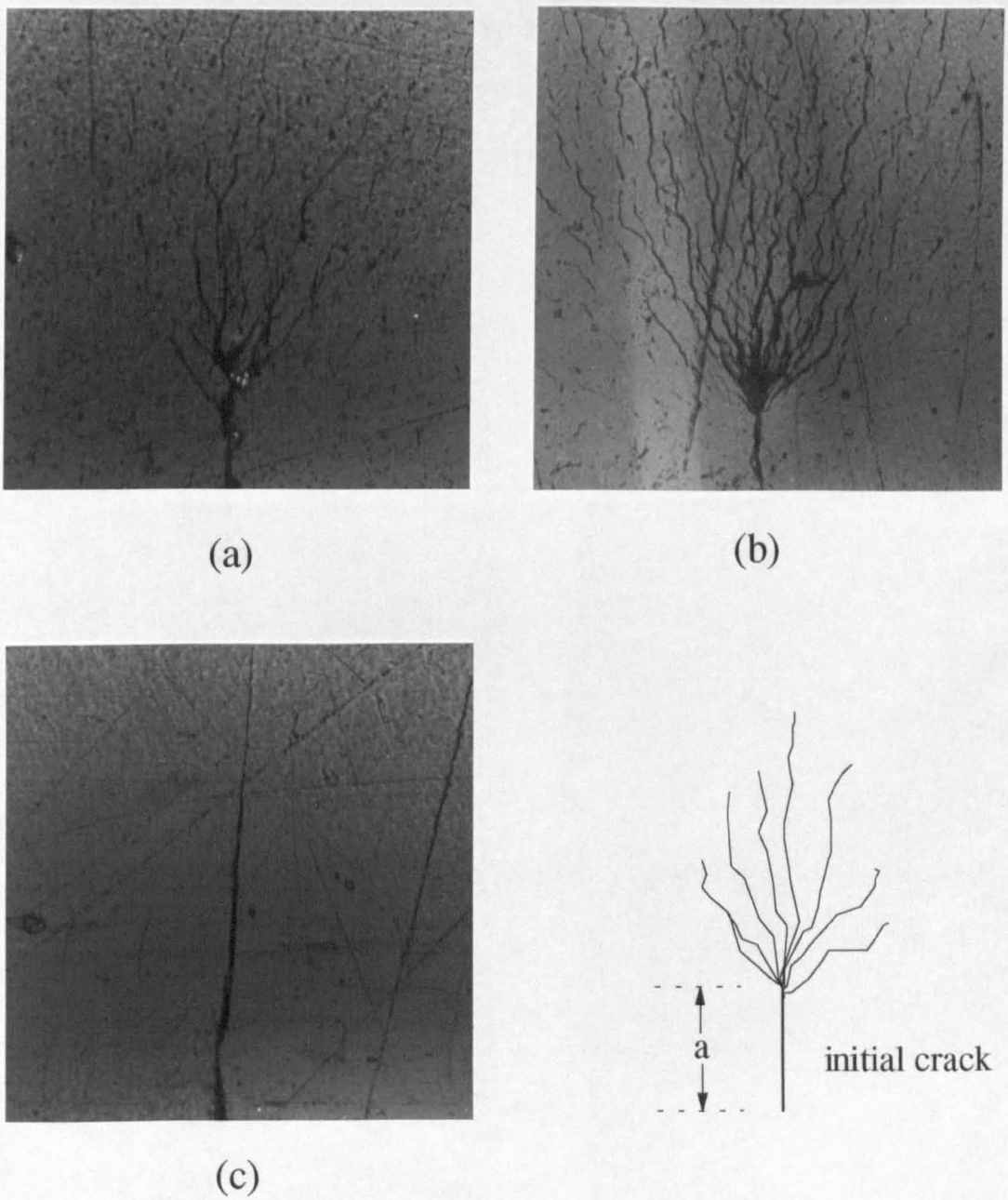

Figure 3.14 Optical micrographs of cracks observed on the surfaces of PP/R/G (a, b) and PP (c) samples : where the mark "a" shows the initial crack by a razor blade.

combination of local shear yielding, crazing and void formation. The fracture surfaces and toughening mechanisms in these composites will be discussed in detail later.

In tough materials where the crack growth length is very small and composed of many microcracks, the determination of crack length is sometimes impossible. During the test, stress-whitening was observed ahead the initial notch when the load was applied above a certain level. The higher the load, the longer the whitening region. Some researchers [78, 80] have used the length of the whitening zone, instead of crack growth zone in the evaluation of J_C.

In this study, the J-integral results obtained from the conventional crack growth length method were compared to those determined from the stress-whitening method. A set of identical PP/R specimens was tested at -20°C at a bending rate of 1 mm/min.

Figure 3.15 shows a typical load-displacement curve of a PP/R sample, in which the specimens were loaded and then unloaded at points *a* to *d*. J-integral values were calculated using the procedure outlined previously. These calculated J-values were then plotted against the crack growth length (Δa). A typical plot of J-integral values as a function of crack growth length, is shown earlier in *Figure 3.13b* where the J_c value of 3.48 kJ/m^2 was observed by this method.

For the stress-whitening region method the length of the whitening zone was measured both from the surface of specimens and from observation of the fracture surfaces. *Figure 3.15a to d* are the photographs of the stress-whitening regions observed on the surface of PP/R specimens taken from the surfaces of the original 12 mm thick specimens. The observed stress whitening zone is less defined at lower loading (*Figure 3.15a*), with the zone domain becoming increasingly well defined at later stages where deformation is higher (*Figure 3.15b to d*).

The fracture surfaces for stress-whitening zone measurement were prepared by freezing the tested specimens in liquid nitrogen before breaking using an Instron testing machine. The photograph of a cryogenic fracture surface of PP/R specimens is shown in *Figure 3.16*. Where the boundary line between the initial notch by a razor blade and the stress-whitening zones was clearly defined. The stress-whitening zone observed at the centre of the specimen is longer than that observed at the edge (surface) as demonstrated in *Figure 3.16*. The length of stress-whitening was measured at the longest part of the whitening zone (between lines B and C in *Figure 3.16*).

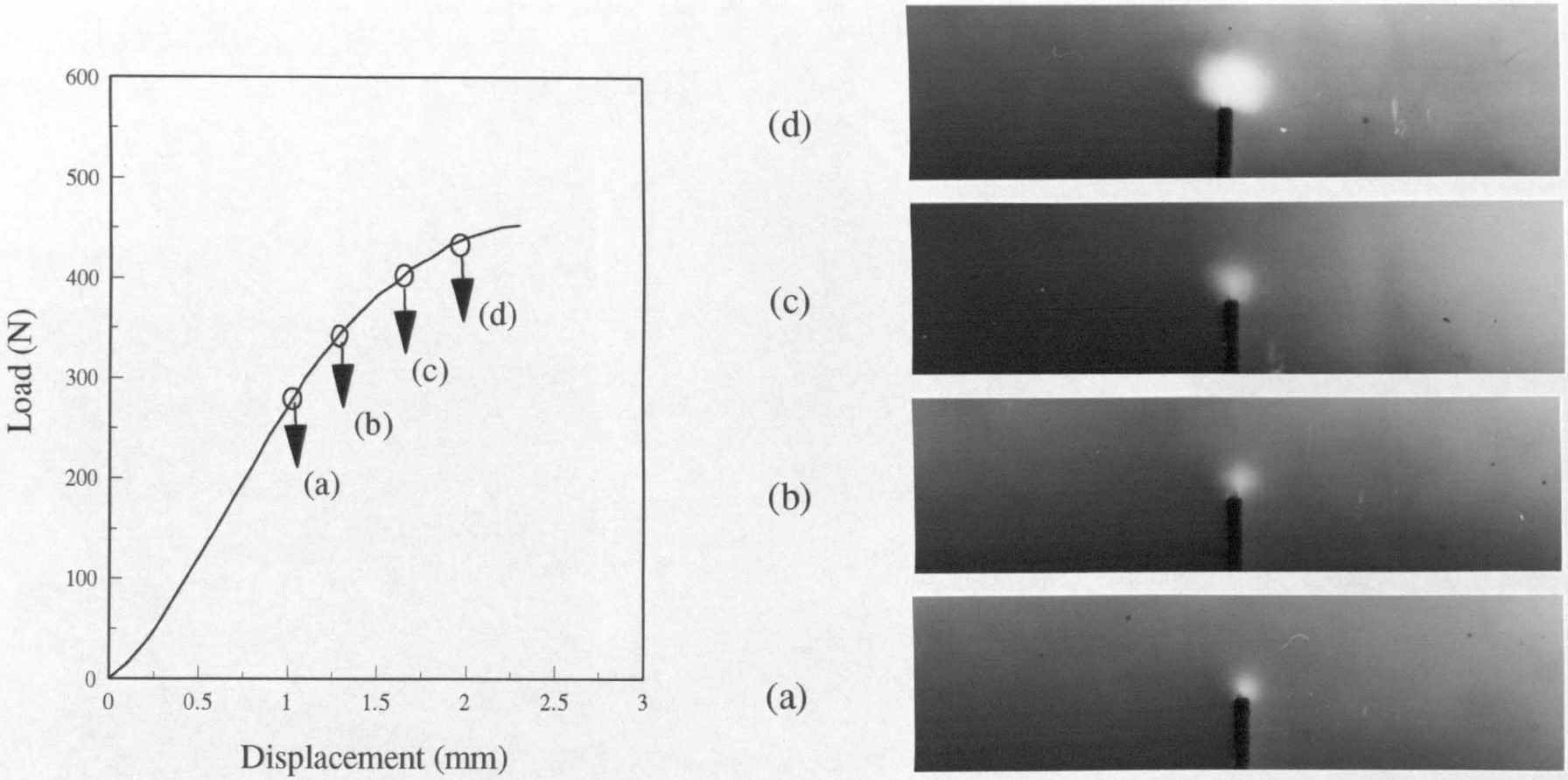

Figure 3.15 The photographs of surfaces of PP/R specimens showing stress-whitening zone development (a-d) at various stages of loading

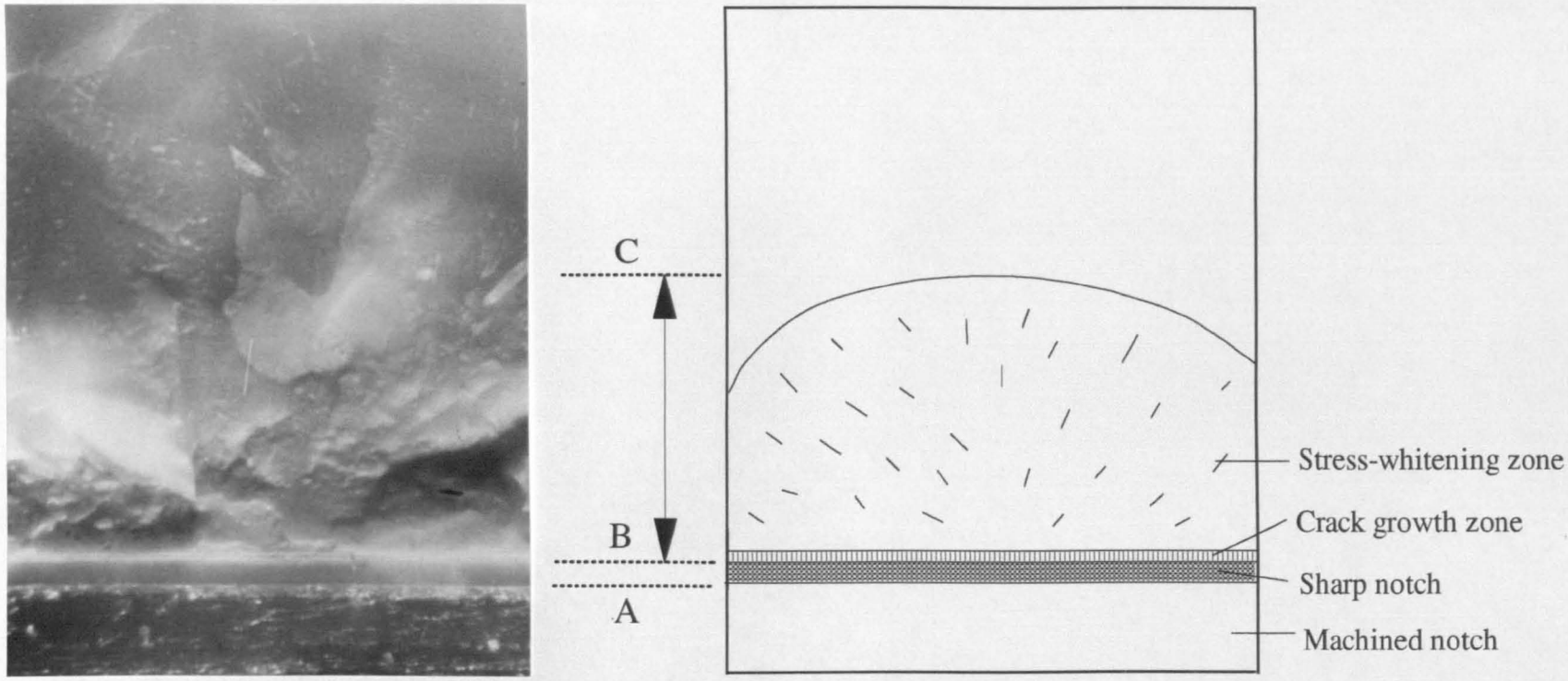

Figure 3.16 Cryogenic fracture surface of a PP/R specimen showing stress-whitening zone

Figure 3.17 shows the plot of the stress-whitening zone length (Δl) measured at the centre of the specimen against the crack growth length (Δa) for a PP/R (70/30) sample. The slope is higher at the early stages of deformation but later becomes lower, as shown in *Figure 3.17.* The intersection between these two lines is related to the crack initiation point.

Figure 3.18 shows the plot of J-integral values as a function of the length of stress-whitening zone (Δl). The resistance curves were composed of two lines of different slopes, since the length of stress-whitening zone ahead the initial notch tip is composed of the growing crack and the crack damage zone. In the lower J-value case, the energy input is only for the creation of crazes so that the stress-whitening zone increased rapidly with J-value. After the onset of crack growth, a part of energy was consumed by crack growth so that the stress-whitening zone extension was retarded. The intersection of these two lines may be regarded as the onset of crack growth. From *Figure 3.18* the J_c value of 3.22 kJ/m^2 was observed for a PP/R sample by this method comparison to that of 3.48 kJ/m^2 from the conventional crack growth length method.

From these preliminary procedures, the method used throughout the project was decided.

3.6.3.4 Experimental procedure

(i) Specimen preparation

Test specimens for fracture toughness tests were prepared by compression moulding. The mould used was a picture-frame type mould with dimensions of 170 mm by 200 mm with a thickness of 12 mm. The composite granules were evenly spread over the mould surface. The mould was heated at 210°C without any applied pressure for half an hour or until the granules were melted. In moulding of thick specimens, the moulding time should be long enough to allow heat transfer evenly through the mould. However, in order to avoid a chance of degradation during a long heating period, the temperature was reduced to 190°C after half an hour at 210°C. The mould was then kept at 190°C for another half an hour. After approximately one hour of melting, a pressure of 25 tons was applied and kept constant for 5 min. The mould was then cooled down to room temperature within 7 min. In compression moulding, sticking of materials to the mould surface might occur. To prevent this problem and also to ease flow during moulding, Melinex (PET) film, or mould release agent could be used. In this work, a mould release agent was found to be

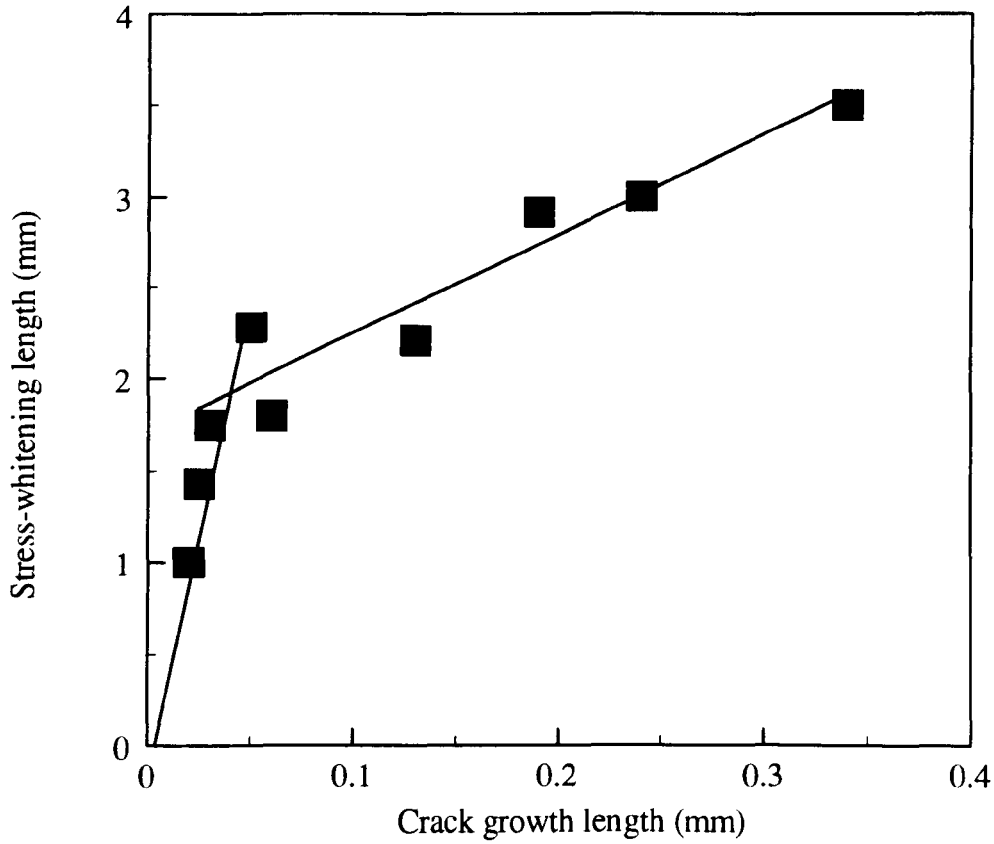

Figure 3.17 Plot of stress-whitening length against crack growth length for PP/R at -20 °C

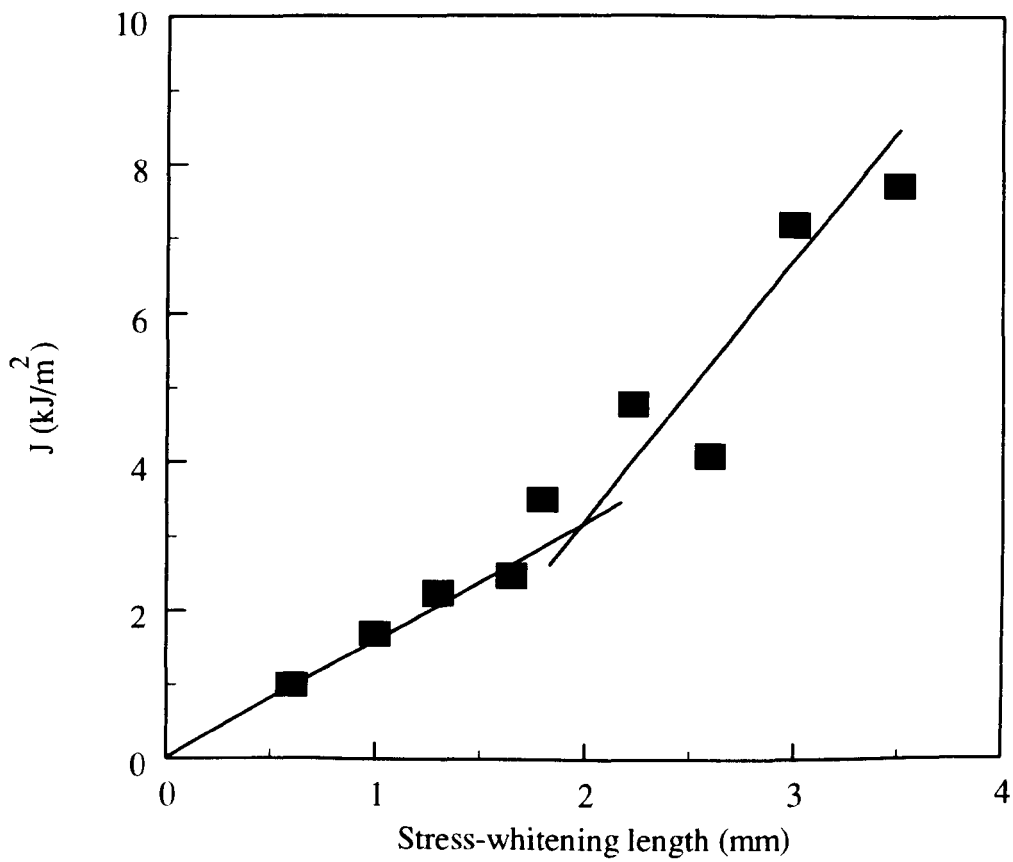

Figure 3.18 Plot of J against stress-whitening length for PP/R at -20 °C

more suitable due to its low cost, also after a long period of moulding time a PET film tends to degrade and stick to the mould surface. Owing to these reason, a mould release agent (non-silicone type) was applied to the mould surface prior to moulding. However, it has to be mentioned here that after each moulding the release agent should be removed and the mould surface need to be cleaned thoroughly with acetone.

Rectangular bar specimens of 24x108x12 mm were cut from a 12 mm thick compression-moulded sheet using a band saw. Specimen geometry and dimensions used are shown in *Figure 3.19*. However, in compression moulding of such thick samples shrinkage at the centre of the moulding is unavoidable. To be sure that all specimens are identical in dimensions, the rectangular bars were ground and polished down to 500 μm. The single-edge initial notch of 13 mm was then created by a saw cut and then sharpened with a fresh razor blade. The razor blade was discarded after every four samples to ensure consistency in the size and sharpness of the crack. This initial notch including the crack made by band saw and by razor blade, was then measured under a microscope using a micrometer eyepiece..

(ii) J-integral Testing

The J-integral testing was undertaken using the multiple specimen R-curve method according to ASTM E813-81 [101] carried out at room temperature (23°C) and at low temperature (-20°C). The three-point bend test was performed using an Instron tensometer Model 1195 at a bending rate of 1 mm/min with a span of 96 mm. In case of low temperature testing, the temperature chamber was equipped to the Instron machine. Liquid nitrogen was fed into the chamber controlling the temperature by a thermostat. The low temperature testing equipment is shown in *Figure 3.20*.

In testing, a series of identical specimens were loaded to different predetermined deflections and then unloaded. The load-displacement curve was recorded. The area under the curve, and hence the energy absorbed up to this point was calculated by cutting out and weighing the load-deflection curve. *Figure 3.21* shows an example of load-deflection curve and the measured area for determining J value.

After testing, the length of crack growth zone was measured using the optical microscope at 100 times magnification. *Figure 3.22* shows an example of photographs and their schematic representations of crack growth length determination. In samples where the determination of crack growth length is impossible since the crack is very

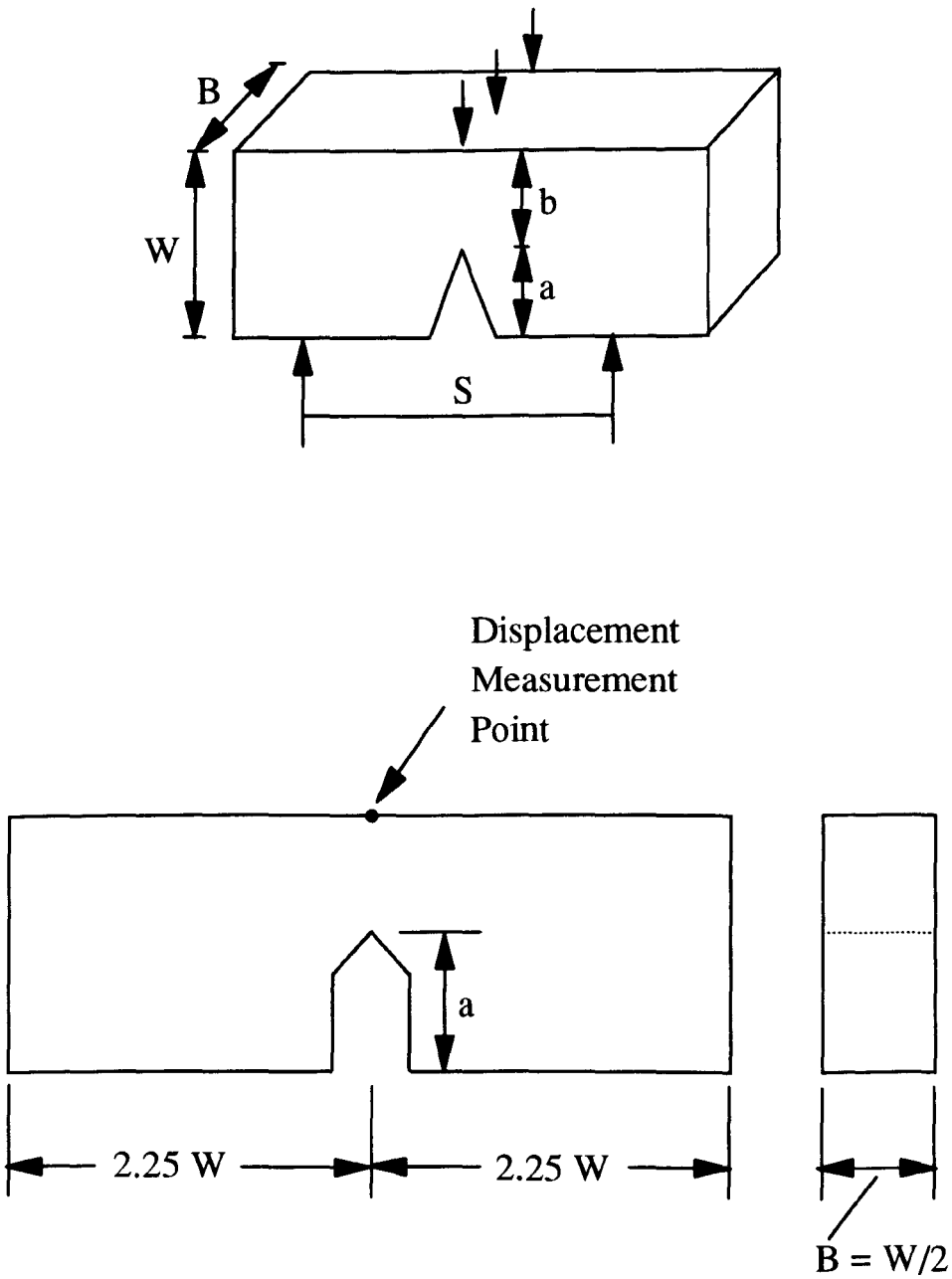

Figure 3.19 Typical bend specimen configuration for J-integral test
a is the initial crack length, *b* is the ligament length
B is the specimen thickness and *W* is the specimen width

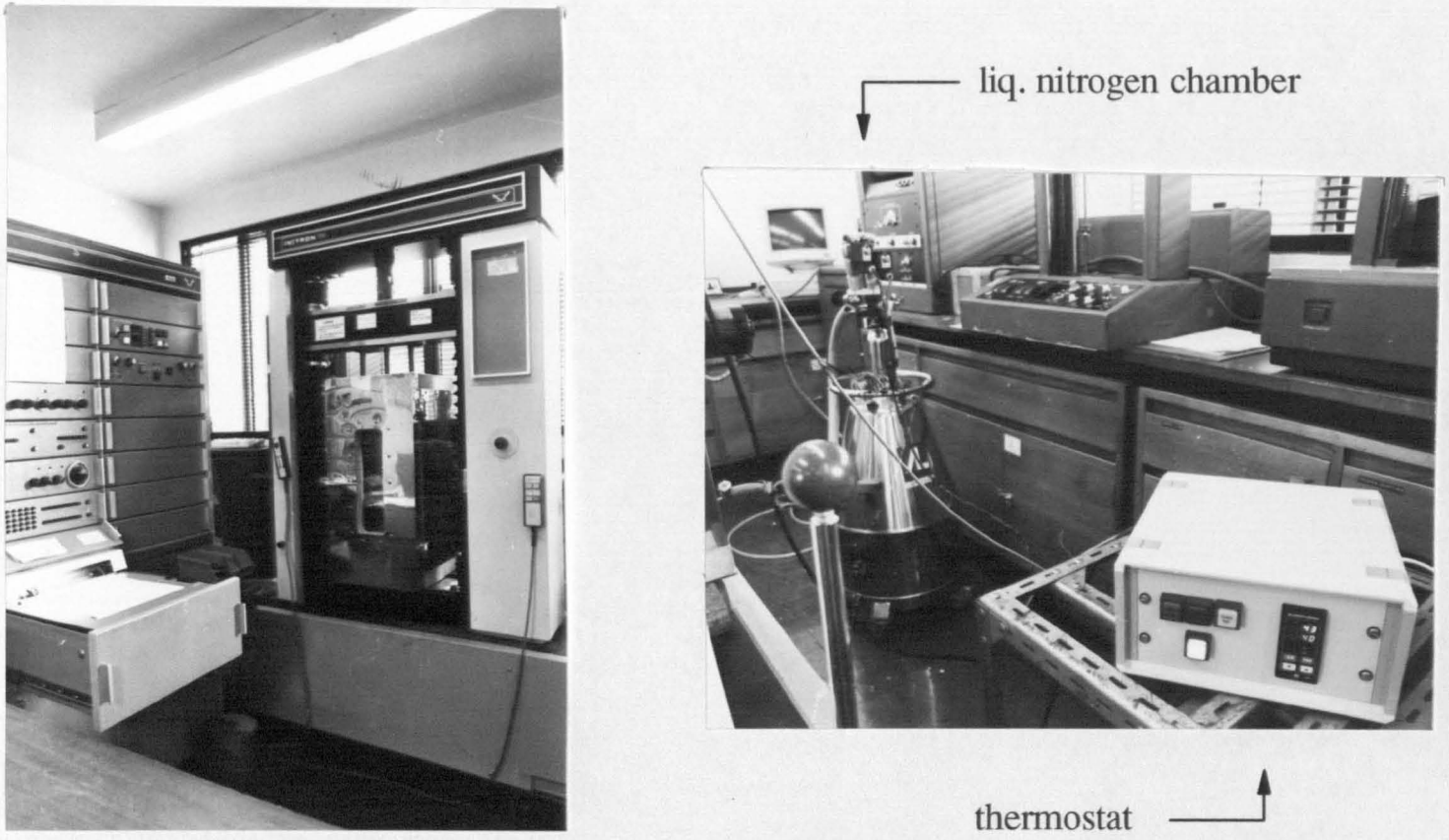

Figure 3.20 The Instron machine equipped with the temperature chamber for low temperature fracture toughness testing

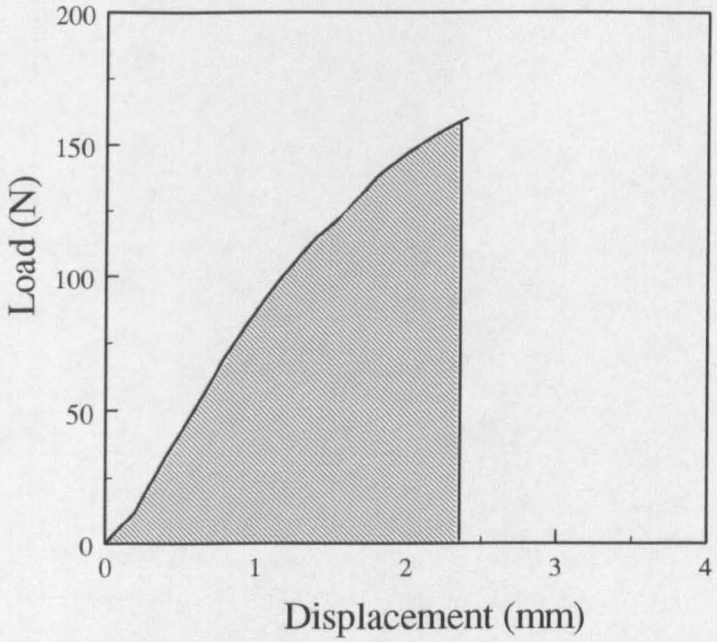

Figure 3.21 Conventional method for determining J value

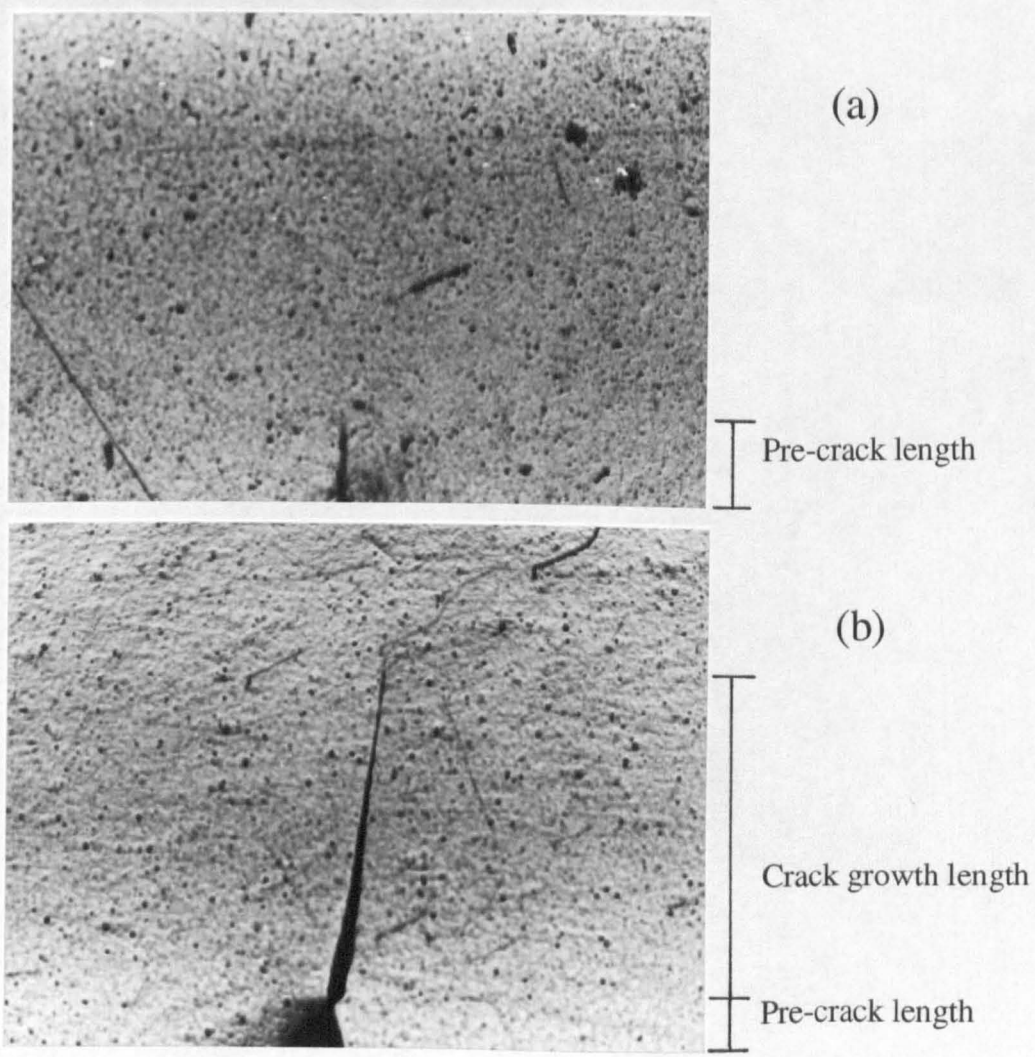

Figure 3.22 An example of photographs shows (a) pre-crack at the state of the unloading time and (b) is the state in which the small crack of the length of 0.12 mm initiated at the pre-crack tip

small and composed of many microcracks, the stress-whitening length was measured. The fracture surfaces for stress-whitening zone measurement were prepared by freezing the tested specimens in liquid nitrogen before breaking using an Instron testing machine. An example of a cryogenic fracture surface of PP/R specimens for stress-whitening zone measurement was shown earlier in *Figure 3.16*. The length of stress-whitening was measured at the longest part of the whitening zone (between line B and C in figure 3.16).

A minimum of ten specimens were tested for each material. The specimens were kept at 23 °C for 10 days prior to testing in order to allow the residual stress, which might generate during the specimen preparation stage, to be released. In order to avoid any scratches or marks on the specimen surfaces which can lead to a confusion in determining a crack growth length after test, care must be taken in storing the specimens.

According to ASTM E813-81 [101] the J-integral value for a three-point bend specimen with S/W = 4 is given in the following equation :

$$J = 2U / B(W-a) \qquad (3.9)$$

Where U is the input energy of the specimen which is the area under load-displacement curve. B and W are the specimen thickness and width, respectively. *a* is the notch length up to the end of pre-crack. By this conventional method, the J value at the onset of crack growth, J_c, is determined by the intersection of the R-curve and the blunting line calculated using the following equation :

$$J = 2 \sigma_y \Delta a \qquad (3.10)$$

Where σ_y is the tensile yield stress and Δa is the crack growth length. In the determination of tensile yield stress value, the test was performed according to ASTM D638 using the same test conditions as used in the J-integral test. In the stress-whitening zone method, the R-curve composes of two lines of different slopes. J_c is determined as the intersection of these two lines (the crack blunting and the crack growth lines). The difference between this method and the conventional method is that the blunting line comes from experimental data, while in the conventional method the bunting line is calculated from Eq. 3.10.

(iii) Microscopy

The mechanism of failure in the composites was investigated on fracture surfaces using scanning electron microscopy. Fracture surfaces were prepared by freezing the tested specimens in liquid nitrogen then breaking using the Instron testing machine operating at 50 mm/min. To obtain a good fracture surface, great care must be taken not to leave the sample far long in liquid nitrogen since the fracture directions of such brittle material tend to be random instead of one fracture through the centre of the sample. Also, the sample needs to be carefully positioned in the machine. The sample notch and the machine loading point has to be in the same vertical position. The fracture surfaces prepared, were gold-coated on a sputter coater and viewed on a Cambridge S250 scanning electron microscope. The acceleration voltage was set at 20 KV and the tilt angle of 30 degrees.

3.7 STRUCTURAL ANALYSIS

3.7.1 Dynamic Mechanical Analysis

Dynamic Mechanical Analysis (DMA) is generally used to characterise the dynamic mechanical properties of polymers. It can also be used as a complementary method for determining blend compatibilisation, phase separation or structural changes, in conjunction with microscopy techniques.

In a dynamic mechanical test, a controlled oscillatory strain is applied to the material and the resulting stress developed in the sample is measured. Since polymers are viscoelastic materials which display both elastic and viscous types of behaviour, the resulting stress response can be separated into two components : an elastic stress which is in phase with the strain, and a viscous stress which is 90°C out of phase with the strain. The elastic and viscous stresses are related to material properties through the ratio of stress and strain, the modulus. The ratio of the elastic stress to strain is the storage modulus (E') and the ratio of the viscous stress to strain is the loss modulus (E''). The ratio of the loss modulus to the storage modulus is the tangent of the phase shift δ between the stress and strain (tan δ).

DMA measures the storage modulus (E'), loss modulus (E'') and damping or loss factor (tan δ), as a function of temperature. It is sensitive to molecular motions therefore it is used to study transitions in materials. The most conspicuous of the transition

characteristics of amorphous and semicrystalline polymers is the glass transition temperature (T_g) which can be characterised in DMA by a peak in the loss modulus and a decrease in the storage modulus. In addition to T_g, the lower temperature transitions involving motions of side chains and imperfections can also be observed by DMA [205].

A dynamic mechanical instrument Rheometric Solids Analyser RSA II was used for measuring the dynamic mechanical properties of the composites as a function of temperature ranging from -100 to 100 °C. Testing was carried out in three-point bending mode using a frequency of 6.28 rad.s $^{-1}$ (Hz) according to ASTM D 5023 -89. The storage and loss modulus as well as damping or tan δ were measured every 2.5 °C with increasing temperature. The test specimens used were 10×48×2 mm rectangular bars, cut from the compression-moulded sheets. At least two specimens for each composite were tested to ensure reproducibility of test results.

3.7.2 Wide Angle X-ray Diffraction

X-ray diffraction is one of the oldest and most widely used techniques available for the study of polymer structures. A beam of X rays incident to a material is partly absorbed and partly scattered, and the rest is transmitted unmodified. The scattering of X-rays occurs as a result of interaction with electrons in the material. The X rays scattered from different electrons interfere with each other and produce a diffraction pattern that varies with scattering angle. The relationship between scattering angle and its intensity can be written in the form of the Bragg relation :

$$\mathbf{d = \lambda / (2 \sin \theta)} \qquad \mathbf{(3.11)}$$

where d is the interplanar distance between crystallographic planes that gives rise to the scattered intensity at 2θ. The variation of the scattered and diffracted intensity with angle provides information on the electron density distribution, and hence the atomic positions, within the material.

X-ray diffraction techniques are usually categorised into wide-angle X-ray diffraction (WAXD) and small-angle X-ray scattering (SAXS). In WAXD, the smallest 2θ angle at which intensity can be measured conveniently is about 6°, leading to information on structural features smaller than about 1 nm, such as the structure and orientation of crystals, whereas SAXS allows detection of structural features on a scale of 1-1000 nm such as the size and regularity lamella packing in crystals.

It has been reported that isotactic polypropylene can crystallise in different polymeric forms such as monoclinic (α), hexagonal (β) and triclinic (γ) [2]. The structure depends on many factors such as thermal treatment of the samples, molecular weight and degree of isotacticity. The incorporation of either impact modifiers or fillers may lead to an alteration of these polymeric structures. In this work, wide-angle X-ray diffraction (WAXD) was used to study any changes in the polypropylene structure within the various composites.

Wide-angle X-ray diffraction measurement was performed using a Philips X-ray generator equipped with a microprocessor controlled recorder unit. Radial scans of intensity versus diffraction angle (2θ) were recorded over the range of diffraction angles from 12° to 24° using nickel filtered CuK_{α} radiation. The samples used were in the form of 13×13×2 mm thick plates cut from compression-moulded sheets. The samples were rotated around a fixed axis during the test with an operating voltage of 36 kV and a filament current of 26 mA.

3.7.3 Differential Scanning Calorimetry

Differential Scanning Calorimetry (DSC) is a technique in which the difference in energy input into a substance and a reference material is measured as a function of temperature. The results are recorded as a DSC curve or thermogram.

A heating (melting) thermogram of a DSC scan can provide information about the onset of melting (the beginning of an endothermic peak) and the melting temperature which (theoretically) is the highest temperature at which crystallites can exist. Above this temperature the polymer melts. These values can be used to define the melting range of the polymer. The area under the melting peak is the heat required to melt a specific mass of polymer and is called the heat of fusion which is directly related to the polymer's crystallinity. A higher value of the heat of fusion suggests a higher degree of crystallinity.

A cooling (crystallisation) thermogram, on the other hand, provides information about the crystallisation behaviour of polymers. The onset of the cooling peak relates to the nucleation process while the difference between the onset and the peak temperature of crystallisation (T_c-$T_{c\ onset}$) infers the rate of crystallisation. A decrease in this difference is generally attributed to an increase in the rate of crystallisation.

The crystallinity of semicrystalline polymers is very sensitive to their thermal history. This can be overcome by subjecting the sample to a 3-stage heat-cool-heat cycle in a thermal analyser. The first stage (stage 1) involves heating the material above its melting point in order to erase any previous thermal history. The cooling stage (stage 2) then imparts a known thermal history allowing samples produced, using various processing conditions, to be compared using the results obtained from the second heating stage (stage 3).

In this investigation, representative samples of the blends prepared were analysed on a Perkin-Elmer DSC-7 differential scanning calorimeter using a thermal cycling (heat-cool-heat) technique. Since the sample size in conjunction with the scanning rate can affect the quality of DSC results, slower scanning rates improve the peak resolution while faster rates improve the usable sensitivity. Throughout the analysis, samples of 7±1 mg were held in closed aluminium pans under a nitrogen environment and scan at a constant rate of 10°C/min.

During the first cycle samples were heated from 30°C to 210°C at a scan rate 10°C/min. Temperature was then maintained at 210°C for 10 min before cooling down to 30°C at the same rate and then heated up again to 210°C using the same condition as the first heating run. To ensure a high accuracy, the temperature/area scale was first calibrated using indium (T_m 156.60°C, ΔH_m 28.45 J/g) as a reference material.

3.7.4 Fourier Transform Infrared Spectroscopy

Fourier transform infrared (FTIR) spectroscopy is one of the most widely used methods for characterising the molecular structure of polymers. When infrared radiation is passed through a polymer sample, some of the frequencies are absorbed while other are transmitted through the sample without being absorbed. Plot of percent absorbance or transmittance against frequency of radiation is an "infrared spectrum". It is fundamental to the analysis of infrared spectra to understand the principles that give rise to the absorption bands, in particular, their position and relative intensity. The absorption of infrared radiation is dependent upon the molecular vibration association with a dipole moment. The intensity of the vibration is proportional to the square of the change in dipole moment. The simplest types of vibration are stretching and bending of chemical bonds. Each absorption corresponds to a specific type of deformation of a particular

bond (or bonds) and is characteristic of that bond deformation with frequency not greatly affected by the other atoms present in the molecule. Thus, comparison of the positions of absorption in the IR spectrum with the characteristic absorption regions, leads to identification of the bonds and functional groups present in polymer. In this study FTIR was used in monitoring interactions which might occur in the ternary phase polypropylene composites, through the appearance or loss of an absorption of particular bands.

For the purpose of infrared spectroscopy, polymers in the form of thin films are essential. The preparation of thin films may be by solvent casting, cold or hot pressing, extrusion and by microtomy. In this work thin films of approximately 15 μm thick were prepared by hot pressing. All of the infrared data was recorded using a Nicolet 710 fourier transform IR spectrometer which is equipped with a data processing computer. To determine the spectral absorption, the background interferogram was measured and subtracted. Once the background was scanned using an empty sample holder card, the instrument need no longer be adjusted. The spectrum was then accumulated and averaged over 200 scans. In order to obtain spectra of the highest quality, the spectrometer was purged with dry air to remove bands associated with water and CO_2 in the air.

3.8 MICROSCOPIC ANALYSIS

3.8.1 Light microscopy

The light (optical) microscopy has found extensive use in the study of the microstructure of polymers, as it is relatively simple and cheap. The resolving power of light microscope is wave-limited by the wavelength of light to around 0.2 μm. To observe structures below this size, other techniques such as electron microscopy are required.

The examination of polypropylene spherulitic structures (type and shape) in various composites was undertaken using polarised-light microscopy. Spherulitic structure of polymers can be observed when a thin section is examined between cross-polars. In this study, the thin sections were prepared using a sledge microtome. Due to the low glass transition temperatures, PP and PP/R blend samples were sectioned using a cold-stage microtome. Since the heat built-up during cutting action at the room temperature leads to unacceptable knife markings and great damage of the sections.

The cold-stage microtomy technique involved building-up a platform of ice on a single layer of paper tissue which is placed on top of the cold surface. The sample was then placed on top of this layer and encapsulated in more ice using water added via a micro-pipette. A semiconductor device having the DC supply controlled a platform temperature via a water switch. The power is automatically shut off when the flow of water stops. The samples were cut using a traditional steel microtome knife. Great care should be taken when dressing and sectioning samples. When dressing the sample the feed mechanism should not be advanced by more than 10 μm. The great forces involved in cutting thicker slices may distort the sample or even dislodge it from its ice-bed. The section for light microscope should not be thicker than 6 μm. The cut section was then allowed to dry before being mounted. Extreme care was taken when removing the section from the knife blade. A fine, soft haired brush was used to minimise curling of the section. The section was then placed between the coverslip and glass-slide. A small drop of mounting liquid was used. The thin section was then viewed under a Reichert polarised light microscope.

Some difficulty was encountered in sectioning glass-bead filled composites. Due to the rigidity of glass beads, the knife blade was easily distorted and blunted. Also the edge became irregular producing unacceptable marks on the surface.

3.8.2 Scanning electron microscopy

The advantages of scanning electron microscopy (SEM) are good depth of field, good resolution and easy specimen preparation. Throughout the work, SEM was used to evaluate the morphological structure of various polypropylene composites. The investigation are toward three goals, (i) to understand fracture and deformation processes occurred in the composites, (ii) to investigate phase structure in the composites including dispersion and distribution of particulate additives, and (iii) to evaluate PP spherulitic structures in the composites especially in the filled composites where sectioning of thin specimens for optical microscopic observation was unachievable.

(i) Fracture surface morphology

The fractured surfaces of failed specimens from tensile, impact and J-integral tests were examined. From the fracture or markings observed on the surface, the origin of fracture and deformation process that occurred in the composites were analysed since the

scattering of visible light can be observed if the deformations involved changing in the refractive index of the material, such as the creation of voids, crazes, or even shear bands with very high shear orientation.

(ii) Phase structure evaluation

Due to a similarity in density and chemical elements of component materials, most polymer blends have a poor contrast between phases. To enhance this contrast an etching technique was introduced. By using suitable etching agents or solvents, one phase (usually a dispersed phase) can be removed from another phase (a matrix phase) leaving holes which are an imprint of the dispersed phase.

- Sample preparation techniques

For electron microscopically examination of polymer samples, the following techniques may be used, namely examination of free surfaces, thin sections, or fractured surfaces. The examination of free surfaces is simple, however, the morphology of the free surface may not be the same as that in the interior of the sample. Preparation of thin section of polymers by microtomy is not easy and the transformation from the original morphology during sectioning may not be fully excluded. Fractured surfaces can reveal the microstructure only if the crack propagates through well-defined interfaces and the shape of the second (dispersed) phase is easily recognisable.

In this study, cryogenic fracture was found to be the most suitable technique for the preparation of the polypropylene composites investigated, since sectioning samples by microtomy, both at room temperature and in the cold stage condition, produced distorted surfaces. *Figures 3.23a and b* shows the phase structures of a PP/R blend sample prepared by microtomy (a) at room temperature, and (b) at low temperature (on ice). To enhance the contrast between phases, the rubber particles were removed from the polypropylene matrix, the location of holes showed where the rubber phase had been while the remaining structure was that of the polypropylene matrix. The surfaces prepared by this technique were clearly seen to be distorted by the cutting action resulting in a change in shape of the rubber particles. The problem of cutting this sample was due to the low glass-transition of EPR in the composites. At the cutting temperature rubber is very soft and can be easily damaged by the shear generated during cutting. In comparison, the cryogenic fracture surface of the same PP/R blend showed spherical EPR particles dispersed in the polypropylene matrix as shown in *Figure 3.23c*.

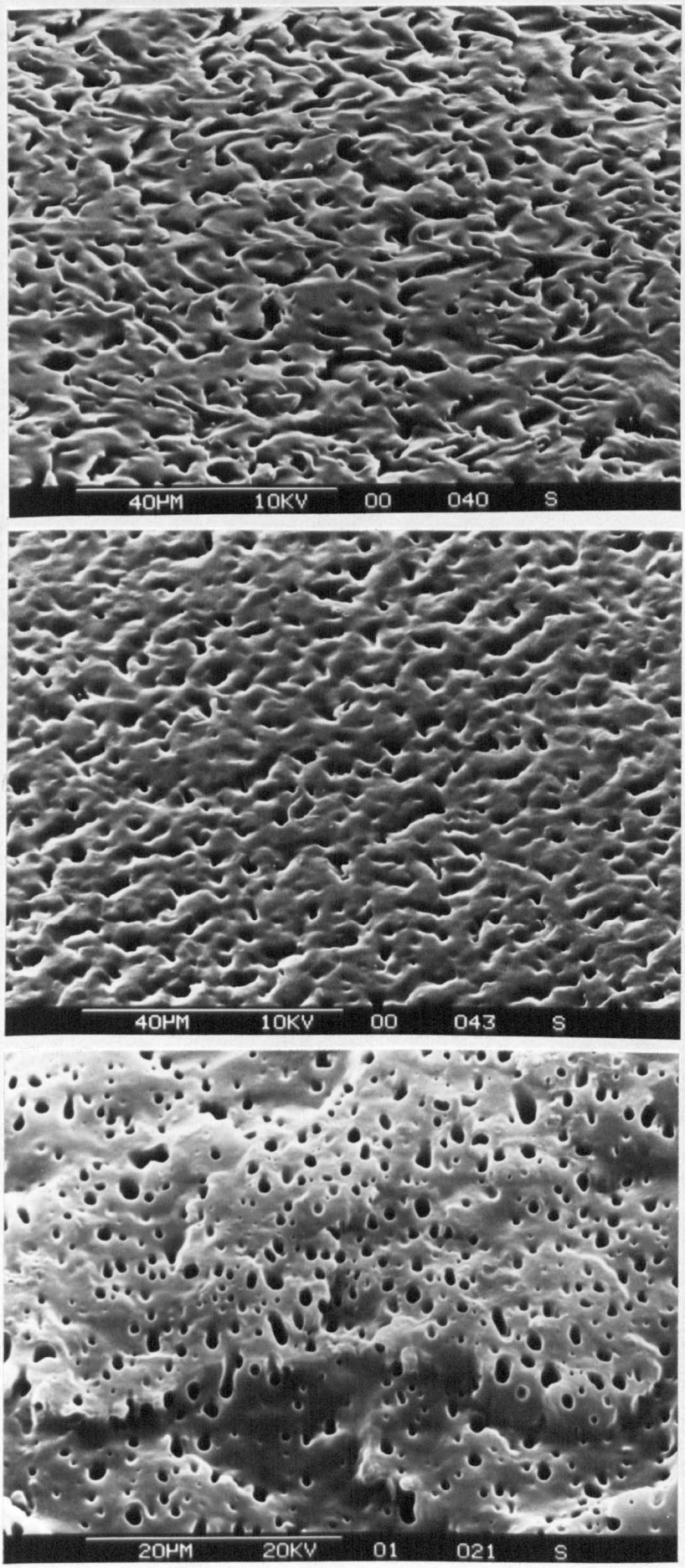

(a)

(b)

(c)

Figure 3.23 Phase structures of a PP1R2 (70/30) sample prepared by (a) microtomy at room temperature (b) microtomy on ice and (c) cryogenic fracture.

-Etching agents and conditions

(a) etching agents for phase structure evaluation

To reveal phase structure of polypropylene composites, chemical etching was used to remove the EPR particles from the polypropylene matrix and thus improve contrast between phases. Two etching agents commonly used for etching EPR were examined i.e. xylene and heptane. For studying phase structure in PP/EPR blends, D'Orazio and co-workers [36] used boiling xylene vapour to extract the EPR phase from the PP matrix, while in a similar blend Greco et.al.,[37] removed the EPR phase by using heptane.

In this study, cryogenic fracture surfaces of PP/R blend samples were etched either with xylene or heptane using variations in etching time. The effect of the etching agents as well as the optimum etching time were also examined on a neat polypropylene sample.

Figure 3.23c shows the SEM micrographs of a PP/R blend sample prepared by cryogenic fracture and etched with hot xylene vapour for 3 sec. Phase structure of a PP/R blend was clearly revealed since the EPR particles were removed from the polypropylene matrix, dark circular holes were shown on the micrograph. To verify that the holes observed on the micrograph are imprints of the EPR particles, an unmodified polypropylene sample was subjected to the same etching procedure. *Figures 3.24a to d* show effect of etching time on the morphological structure of an unmodified polypropylene sample. Some parts of the sample were shown being etched out after 3 sec of exposure to hot xylene vapour. After 30 sec of etching the structure believed to be the spherulitic structure of polypropylene was clearly seen as shown in *Figure 3.24d.* The effect of heptane on the morphological structure of an unmodified polypropylene is shown in *Figures 3.25a to d.* At etching times of up to 5 seconds, the surface topography of polypropylene was unchanged. From this investigation, heptane was thus selected to be an etching agent for phase structure investigation of polypropylene composites. Detail of sample preparation for phase structure evaluation was as follows.

Selected samples were firstly kept at liquid nitrogen temperature for 3 min before fracture. Fractured samples were exposed to hot heptane vapour for 3 sec and then washed with fresh heptane to stop the etching procedure and also to remove EPR inclusions from the surface. Samples were then mounted on a stub using adhesive. Conductive paint was used to ensure that any static charges were earthed (as far as

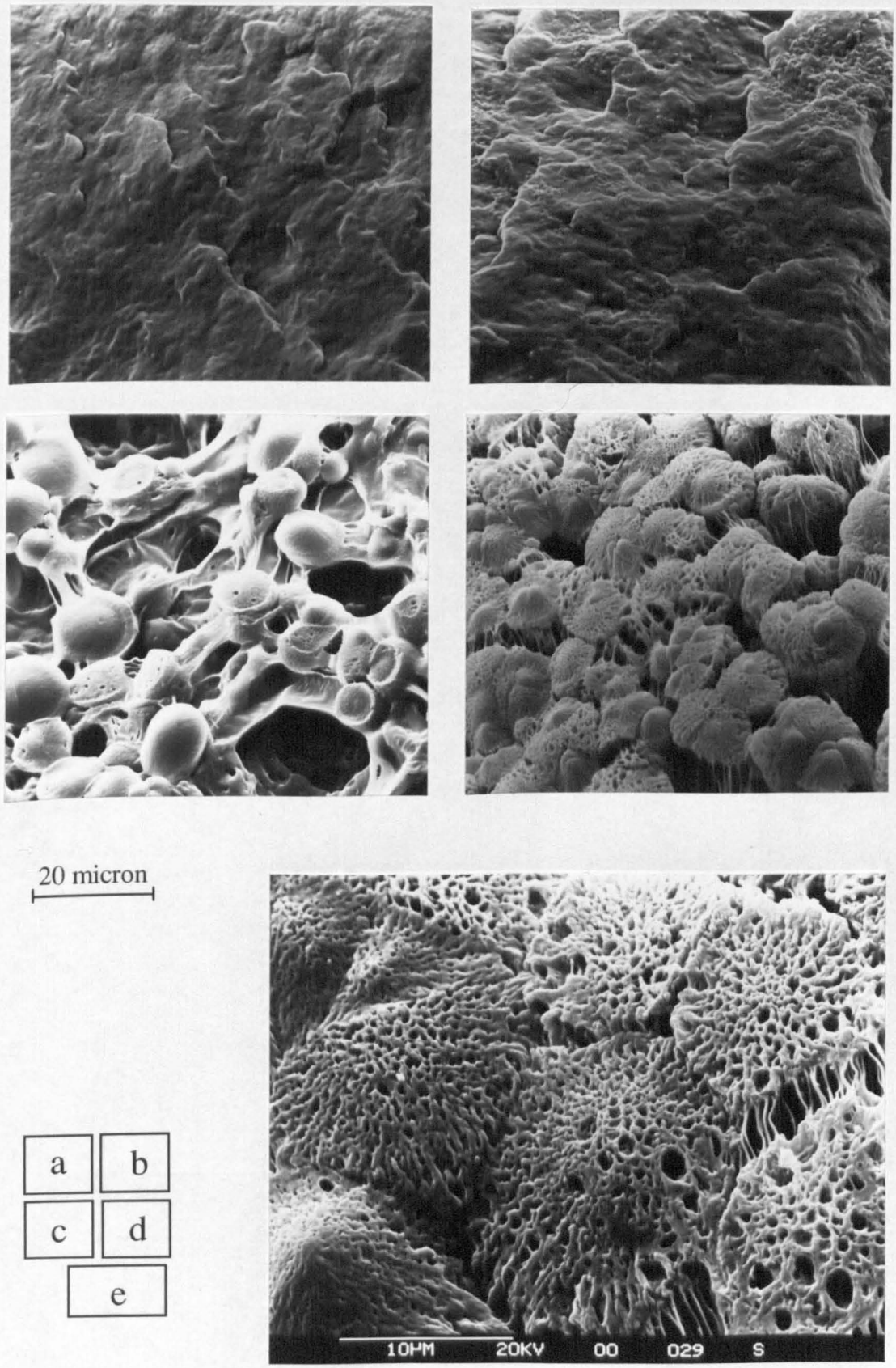

Figure 3.24 SEM micrographs of PP fractured surfaces after exposing to hot xylene vapour for (a) 1 sec, (b) 3 sec, (c) 10 sec, (d) 30 sec, and (e) higher magnification of (d).

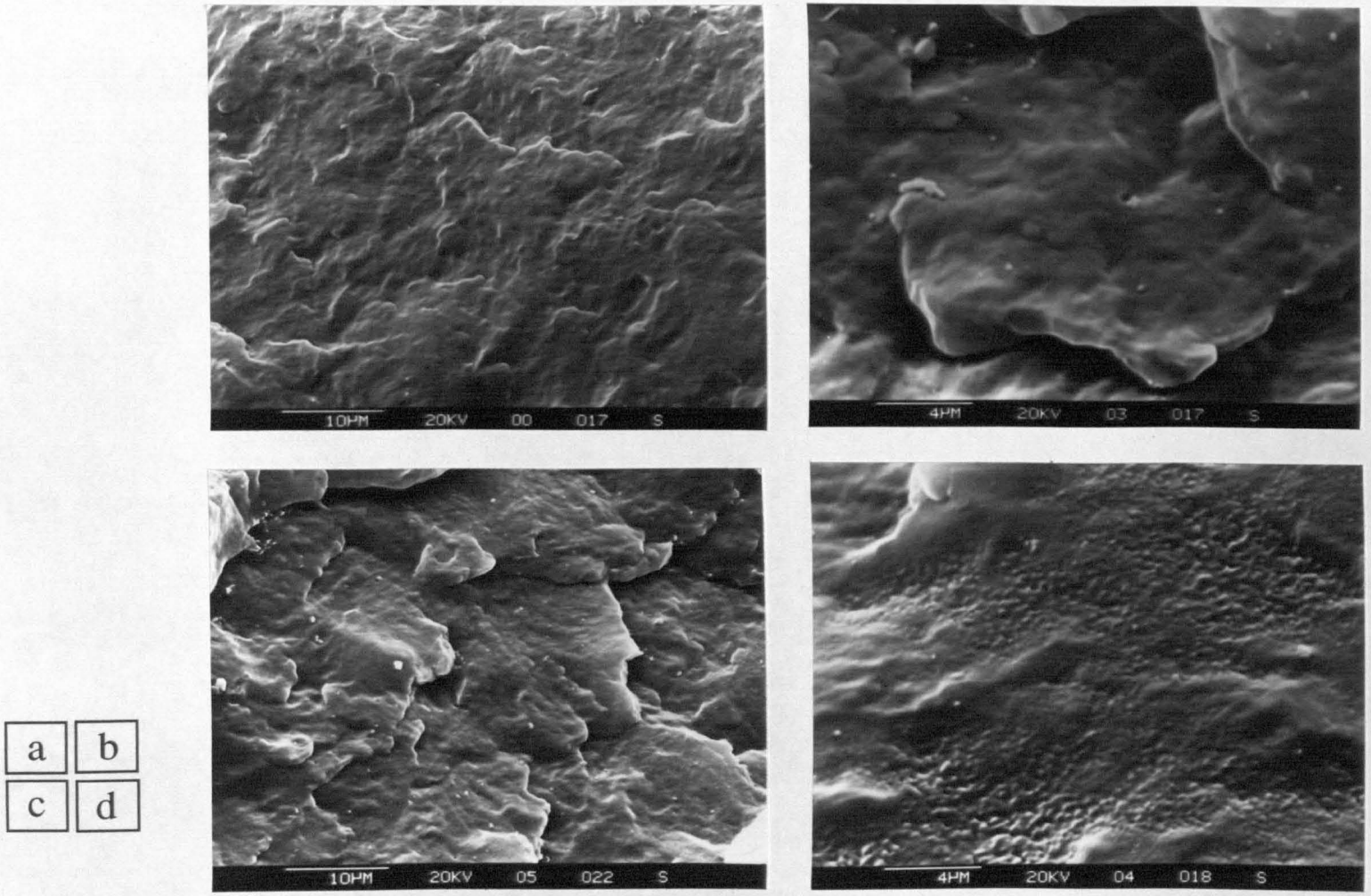

a b
c d

Figure 3.25 SEM micrographs of PP fractured surfaces after exposing to hot heptane vapour for (a) 1 sec, (b) 3 sec, (c) 5 sec and (d) 10 sec.

possible). All samples were sputter-coated with gold-palladium alloy before viewing under the scanning electron microscope - Cambridge S-250 Stereoscan.

(iii) Polypropylene spherulitic structure evaluation

The aim of this part of work was to investigate the complex spherulitic structure of polypropylene in the PP composite samples containing rubber and/or glass beads. Although the optical microscopic observations, in conjunction with diffraction techniques, has been widely used to reveal PP spherulitic structures; they are based on observations performed on thin specimen (~5μm) which were obtained either by casting samples between glass plates, or by microtoming the material. However, these techniques were found unsuitable for analysis the structure of the investigated composites since the spherulites in such composites are very small. Also, it is hardly possible to prepare a thin section which is in a good condition for the optical microscopic observations since both highly rigid phase (glass beads) and soft phase (EPR) are included in the system.

Scanning electron microscope is a particularly well suited instrument, especially since specific etching agents have been developed which are capable for revealing the spherulitic structures of crystalline polymers. Many chemical etching agents have been used, e.g. solution of chromic acid in aqueous sulphuric acid (CrO_3/H_2SO_4) [37,207], fuming nitric acid [208]. *Figures 3.26a-b* show the spherulitic and lamella structure of an unmodified polypropylene. The samples were etched with CrO_3/H_2SO_4 saturated solution at 80 °C for 60 min.

For selective etching of polyolefins, the reagents based on potassium permanganate or permanganic etchants first introduced by Olley et.al. [209], are widely used. The chemistry of reaction is oxidative but it has not been studied in detail. The way in which permanganic etching achieve its effects is thus somewhat complex, but it is known that the permanganic etchant preferentially etches the amorphous part of the polymer in the spherulites, in such a way that the lamellae then became more visible [210]. Many researchers [211-213] have used this etchant in the study on spherulitic structure of polyolefins. However, the composition of the etchant as well as the etching conditions may vary for each system.

Aboulfaraj et.al. [211] studied the monoclinic and hexagonal phases in bulk polypropylene samples from direct SEM observations of etched surfaces. In their work,

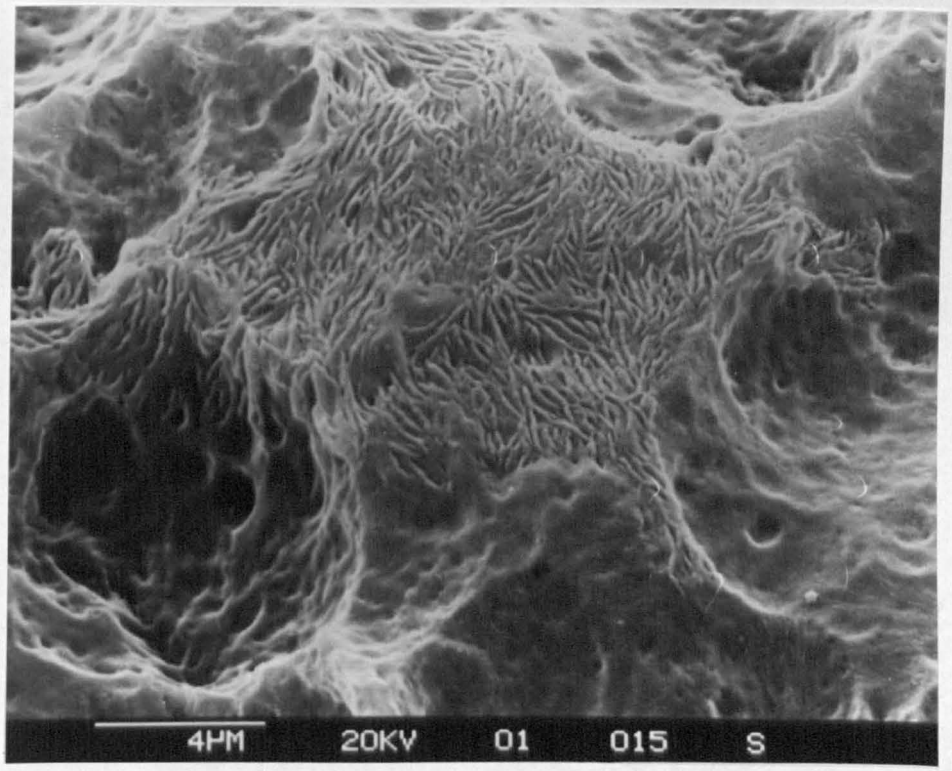

(a)

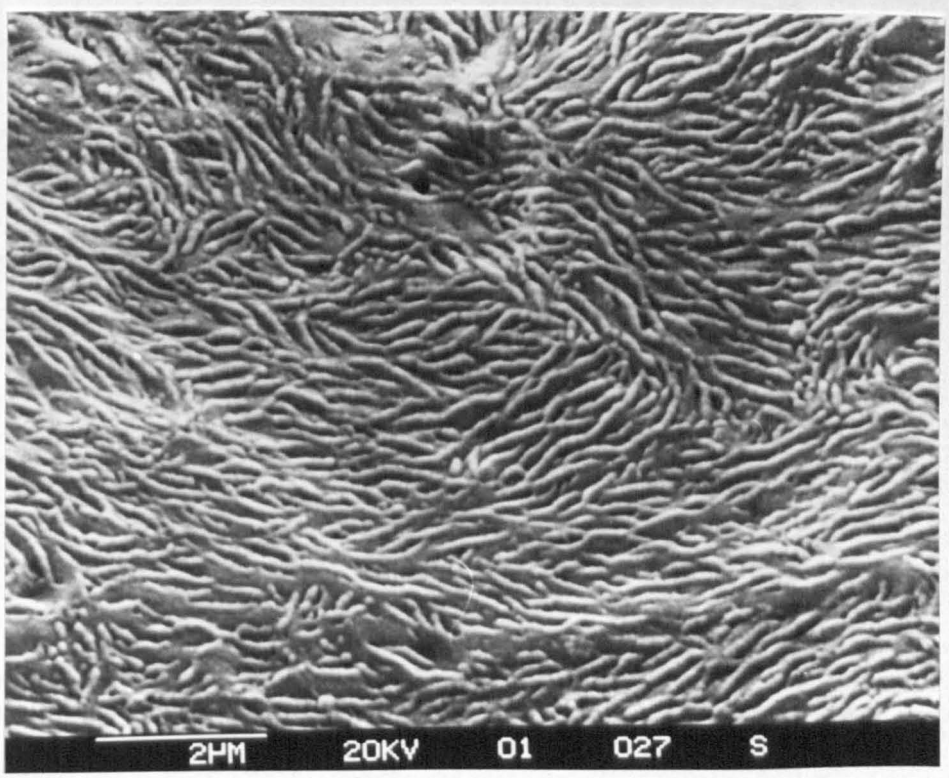

(b)

Figure 3.26 Polypropylene compression-moulded surfaces after etching with Cr_2O_3/ H_2SO_4 for 60 min showing (a) spherulitic structure and (b) higher magnification of (a) revealing lamellae within the spherulite.

1.3 wt% potassium permanganate ($KMnO_4$) in a mixture of 32.9 wt% concentrated phosphoric acid (H_3PO_4) and 65.8 wt% concentrated sulphuric acid (H_2SO_4) was used. The samples were etched for 18 hrs. before investigation.

Basset [210,212] also used the etching solution based on $KMnO_4$ in a mixture of conc.H_2SO_4 and H_3PO_4 in revealing the lamellae structures of polyethylene. This etching agent was reported [210] to be more delicate reagent than that first introduced [209]. The phosphoric acid slows the etching rate. Therefore this method produces very crisp detail and avoids the production of artefacts encountered with the samples etched with solutions of sulphuric acid alone.

Rybnikar [213] studied the kinetics of isothermal etching of polypropylene samples using the solution of $KMnO_4$ in H_2SO_4 or in H_3PO_4 with various amount of potassium permanganate. He found that both solutions have different mechanisms in etching polypropylene. With $KMnO_4$ in H_3PO_4 the etching is more uniform without excessive forming of artefacts, in contradiction to $KMnO_4$ in H_2SO_4 solution. By increasing the etching time and temperature and $KMnO_4$ concentration, the amount of over-etched regions and artefacts increases, especially with $KMnO_4$ in H_2SO_4 solution.

- Etching procedure

The etching solution used in this work was 1 %w/v solution of potassium permanganate in a 2:1 mixture of concentrated sulphuric : orthophosphoric acids. The solution was prepared by adding fine powders of potassium permanganate ($KMnO_4$) slowly into the acid in a conical flask with rapid agitation. The flask is stopped once all the permanganate has been added and shaken occasionally until all crystals of potassium permanganate have been dissolved giving a dark green solution. The time taken to dissolve potassium permanganate may be up to one hour. For rapid agitation a PTFE covered magnetic stirrer is not recommended [214], since it may be stained by the solution. There have been reports [214-215] that certain mixtures of permanganate and sulphuric acid produce unstable manganese heptoxide which is explosive but thoroughly strict adherence to the above procedure no difficulties are encountered. The active species in this solution is believed to be O_3MnOSO_3H [216].

A sample of 4×4×2 mm cut from a 2 mm thick compression moulded sheet was used. The surface was rinsed with water and acetone prior to etching. The prepared surfaces either from cryogenic fracture, grinding and polishing, or microtoming, were found

unsuitable for the spherulitic structure study of the investigated composites. Cryogenic fracture resulted in an uneven fractured surface. The structure after etching was difficult to identify due to its roughness surface. Flattening the surface by grinding and polishing although worked well with filled composites. It was unsuitable for the composites involving soft dispersed phase such as EPR since mechanical damage on the surface was unavoidable.

The selected sample was placed in 5 cm^3 of the permanganic etching solution in a test tube and left at room temperature for 10 hrs. After etching is completed, the solution was decanted and the sample was washed in a mixture of hydrogen peroxide and aqueous sulphuric acid in order to remove manganese dioxide. This cleaning solution was prepared by adding the hydrogen peroxide in the proportion of 1 cm^3 in 25 cm^3 of 2:7 aqueous sulphuric acid (2 volumes of sulphuric acid to 7 volumes of water). In order to prevent the sample affected by the heat of this solution, the cleansing solution was precooled before use. The sample was then soaked in distilled water and washed in acetone before being allowed to dry.

The sample was then sputtered with gold-palladium alloy prior to viewing under the Cambridge S-250 Stereoscan microscope.

3.8.2 Image analysis

Image analysis is a technique widely used to characterise and quantify the relative size of features in blends and composites. Such analysis is aimed at establishing correlations between processing, physical or mechanical properties and morphological characteristics of the materials. Image analysis included a number of sequential steps : (i) sampling the specimen from the material investigated, (ii) specimen preparation, (iii) image acquisition, (iv) image processing and image editing, (v) selection of objects, (vi) measurement, (vii) statistical analysis, and (viii) interpretation.

In this work an automatic image analyser (an Optomax IV image analyser) was used to examine the particle size and size distribution of the dispersed rubber phase in the composites prepared from various compositions and conditions. Steps of automatic image analysis is shown in *Figure 3.27*. The equipment consists of camera and associated hardware of the image analyser which is interfaced to a computer and printer. The camera views micrographs and the image is then memorised in grey tone levels. The particle sizing is carried out by shading the particles and comparing the area shaded to

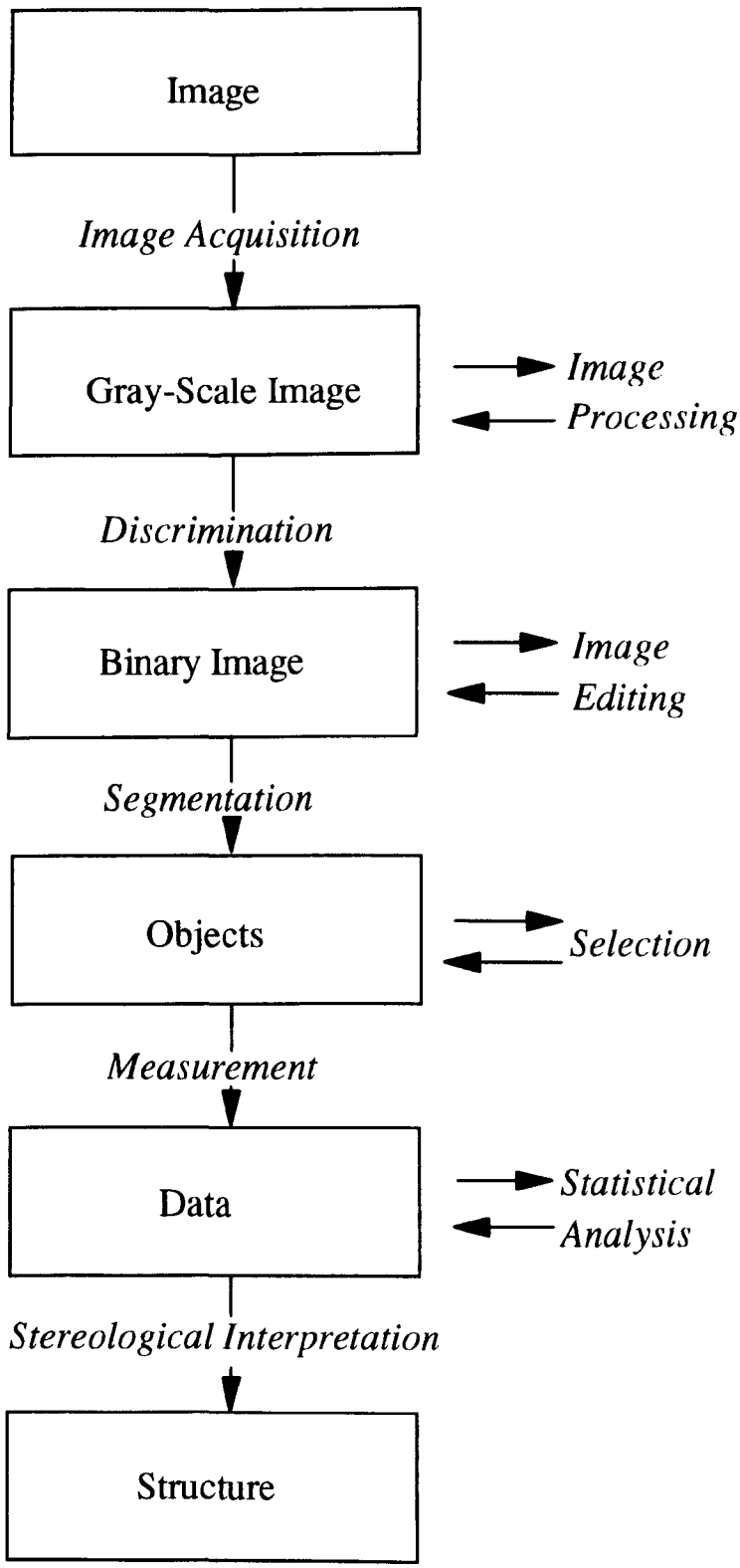

Figure 3.27 Steps of automatic image analysis

the total measured area under examination. In order to transform the two dimensional data to three dimensions, certain assumptions and corrections are required. The Schwartz-Saltykov analysis [217] was applied to account for the probabilities of cutting through particles at different levels other than at their centre (diameter), whilst transforming the data into the number of particles per unit volume (N_V). The equation for the analysis is as follows:

$$N_{V(j)} = 1/\Delta \left[\alpha_i N_{a(i)} - \alpha_{i+1} N_{a(i+1)} - \alpha_{i+2} N_{a(i+2)} - \ldots\ldots\ldots - \alpha_k N_{a(k)} \right] \quad (3.12)$$

where :
N_V and N_a are the number of particles per unit volume and unit area, respectively.
i and j are the size group of sections, vary from 1 to k.
k is the total number of groups.
α is a coefficient relating N_V to N_a
Δ is the ratio of the diameter of the largest particle to k.

Since it is impracticable to size all the particles in the samples, a statistical count must be considered. To obtain a statistically accurate count, as many particles (fields) as possible may be counted. It is advisable [218] to examine at least 100 fields of view and avoid to size more than six particles in any field. The number of particles to be sized to achieve a given accuracy is given by :

$$\sigma(M_q) = M_q / \sqrt{n_d} \quad (3.13)$$

where :
$\sigma(M_q)$ = standard deviation expressed as a percentage of the total by weight,
M_q = percentage by weight in the given size range,
n_d = number of particles counted in the size range.
In this work approximately 1000 particles from fifteen different areas were counted per analysis.

To obtain accurate particle sizing with this technique, it is necessary to have a very good contrast between the particles and the background. This was achieved through the development of contrast during printing the micrographs by using a special grade printing paper (Agfa Rapidtone P1-3) to enhance the contrast difference.

Although the image analyser used has an automatic operation, the grey level processing such as shading corrections, filtering or smoothing to remove the effects of uneven

illumination, can be performed manually. However, to reduce this time-consuming stage during the analysis, the unwanted dark areas on the micrographs (which might be due to an uneven of the fracture surface or due to the cavitation of glass bead particles) were painted with a correction fluid to ensure that only rubber phase was detected by the analyser.

CHAPTER 4

STRUCTURE AND PROPERTIES OF PP/EPR BLENDS

4.1 INTRODUCTION

Polypropylene homopolymer (PP), while having a number of valuable properties, has inadequate low-temperature impact resistance. A number of reports indicated that the impact strength of polypropylene can be favourably influenced by physical blending with various elastomers. One of the most commonly used is ethylene-propylene rubber (EPR). The mechanical properties of PP/EPR blends as well as their morphology, although, have been investigated to some extent, the contradictory results still remain to be verified especially the effect of EPR on the molecular structures of polypropylene in the blends. Also, the toughening mechanisms in such blends were studied only to a limited extent.

The aim of this part of work is to investigate how EPR influences the morphology and mechanical properties of the blends. The morphological studies concern mode and state of dispersion of rubber particles in the blends, the changes in PP supermolecular structure and also the effect of EPR on crystallisation behaviour of PP phase in the blends. Particular attention has been directed to studying the correlation between structures and properties as well as factors affecting them, e.g. viscosity ratio between phases. An attempt to understand the toughening mechanisms of PP/EPR blends in response to a variation in rubber particle sizes is also accomplished. The understanding gained from this work will provide background knowledge to facilitate interpretation of more complex three-phase composites which will be considered later.

4.2 BLEND PREPARATION AND TESTING

In this work two grades of polypropylene homopolymer and two grades of ethylene-propylene rubber were investigated. Some important characteristics of these materials are summarised in *Table 4.1*.

Blends of 70/30 %v PP/EPR were prepared by melt-mixing in a BTS-40 co-rotating twin-screw extruder, operating at a speed of 100 rpm with a feed rate of 16 kg/hr and the barrel temperature of 200°C. The screw used throughout this work was that designated earlier as the "GM screw profile". Details of the screw profile and extruder used were described earlier in Chapter 3.

Table 4.1

Material characteristics, glass transition (T_g) and melting temperature (T_m) of isotactic polypropylenes (PP) and ethylene-propylene copolymers (EPR)

Materials	Trade name	MFI (g/10min)	Mooney viscosity ML(1+4)	T_g (°C)	T_m (°C)	Code
Isotactic polypropylene	Novolen 1100HX	1.8	-	6	163	PP1
	Novolen 1100L	5.0	-	6	162	PP2
Ethylene-propylene random copolymer	Exellor PE805	-	35 [a]	-33	55	R1
	Exellor PE808	-	46 [a]	-33	55	R2

[a] measured at 125°C

Samples for morphological and mechanical testing were prepared by compression-moulding. The morphological structure of the blends was studied by optical and scanning electron microscopy on etched surfaces. Melting and crystallisation behaviours of polypropylene in the blends were determined by DSC and XRD. A Rheometric Solids Analyser RSA II was used for dynamic mechanical analysis. Tensile and falling weight impact measurements were carried out at room temperature (23°C) according to standard test methods. These techniques and testing procedures were discussed in detail in Chapter 3.

4.3 RESULTS AND DISCUSSION

4.3.1 Structural Studies of PP/EPR blends

The structures of PP/EPR blends were studied by SEM, DMA, DSC and WAXD in order to investigate the phase morphology of the blends and to understand the effect of EPR on the microstructure and crystallisation behaviour of polypropylene in the blends.

4.3.1.1 Phase morphology : mode and state of dispersion of rubber particles in the polypropylene matrix

(i) Dynamic mechanical analysis studies

Dynamic mechanical analysis (DMA) measures dynamic storage modulus (E'), loss modulus (E") and loss factor (tan δ) as a function of temperature. E' is related to the storage energy and is used to indicate the inherent stiffness of a material. E" is associated with the dissipation of energy as heat when the material is deformed and tan δ is the ratio of energy dissipated per cycle to the maximum potential energy stored during a cycle.

Figures 4.1 and 4.2 show the temperature dependence of E' and E" moduli and tan δ at 1 Hz. of two grades of polypropylene used. In the temperature range from -100° to 100°C polypropylene may show three dynamic mechanical relaxations (α, β and γ relaxations). The dominant relaxation on the DMA spectra for PP is the β-relaxation which is generally recognised to be the glass-rubber relaxation of amorphous phase in PP. This main relaxation can be observed in the region where the E' curve has an inflection point and the E" and tan δ curves go through a maximum. But the maxima peak in the E" curve is much less intense than the corresponding one in the tan δ curve. *Figure 4.2* shows the β-relaxation peak of PP at about 6°C corresponding to its glass transition

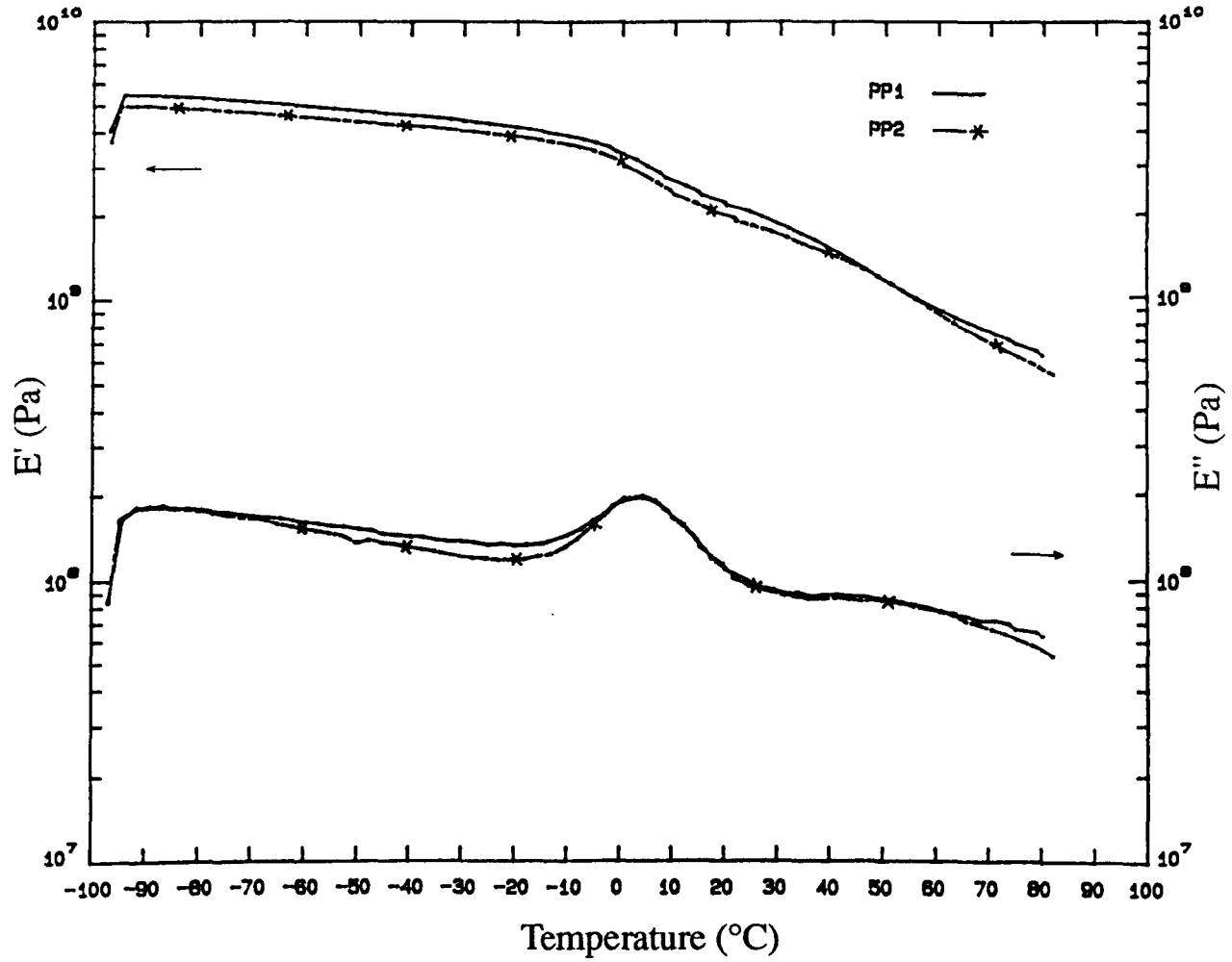

Figure 4.1 Temperature dependence of storage modulus (E') and loss modulus (E'') at 1 Hz. for PP1 and PP2

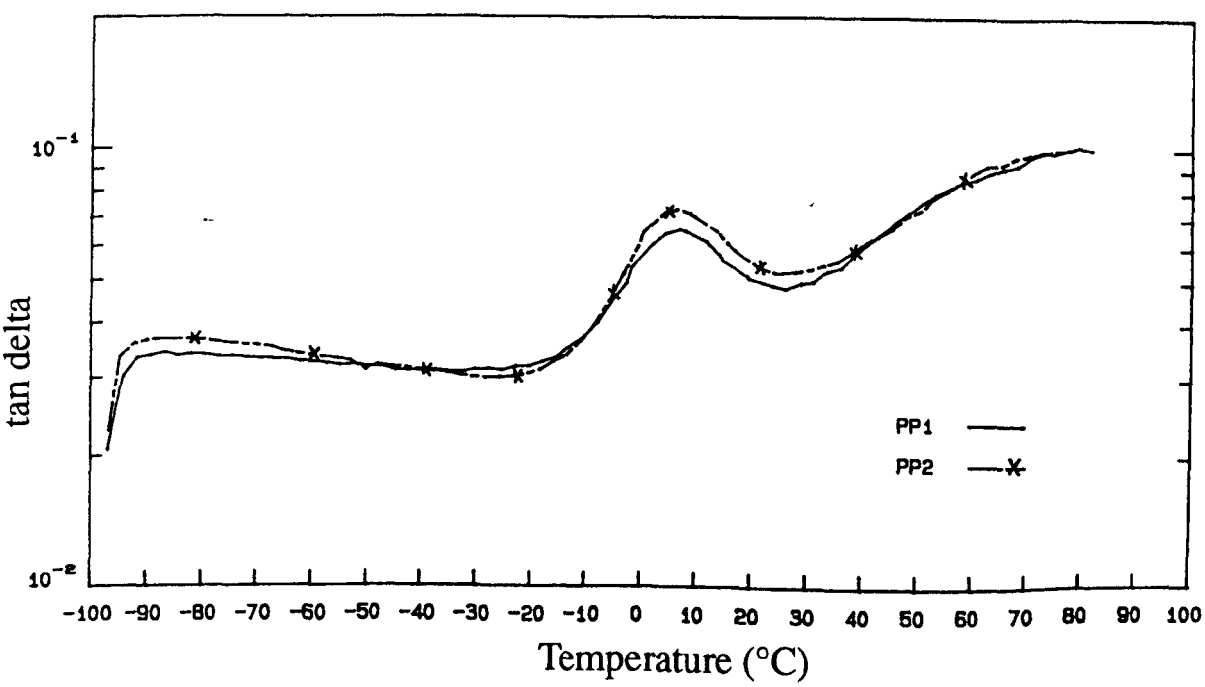

Figure 4.2 Temperature dependence of loss factor (tan delta) at 1 Hz. for PP1 and PP2

temperature (T_g), while the less intensive and broader peak at around -90°C is associated with the γ-relaxation which is attributed to the motion of short chain segments in amorphous regions rather than involving the motion of more complex morphological units of PP [221]. Inamura et.al. [222] also observed the weak peak which is associated with the crystalline regions of PP at about 70-100°C, however, the properties of this relaxation was strongly dependent on the crystal morphology. It can be seen from *Figure 4.1* that the two grades of polypropylene used have distinguishable features in their relaxation behaviour. PP1 (Novolen 1100HX) shows higher stiffness (on the E' curve) than PP2 (Novolen 1100L), while they both have the same glass transition process (T_g at about 6-8°C). Dynamic mechanical data for the two grades of EPR used is shown in *Figure 4.3*. Both grades of EPR show the same glass-transition peak temperature at around -33 °C.

Figures 4.4 to 4.7 show dynamic mechanical data for PP/EPR blends and again include the storage and loss moduli (E' and E") and the loss factor (tan δ) as a function of temperature. Incorporation of EPR causes a decrease in the storage modulus (E') values in the blends as indicated by the curve in *Figures 4.4 and 4.6* . The decrease in the E' values seems to be more pronounced with R1 (Exellor 805) than R2 (Exellor 808) in the PP1 system. From the tan δ curve two well-defined peaks were observed at -43° and 6°C corresponding to the glass transition temperatures of EPR and PP, respectively. The observation of two T_g peaks (at -43 and 6°C) on the tan δ curve indicated that in this system, PP and EPR are incompatible, since the T_g values in partially compatible blends are expected to shift towards each other [223]. The location of PP glass transition temperature observed in the blend (at 6°C) remains unaffected by the presence of EPR. However, the glass transition temperature of EPR shifted to a lower temperature from -33°C in neat EPR as shown in *Figure 4.3*, to -43°C in the blend as shown in *Figure 4.5*. A depression in glass transition temperature of EPR has also been observed in several systems [43, 224]. This phenomenon is due to a higher in thermal expansion coefficient of EPR than the PP matrix. The cooling of the blend resulted in a negative hydrostatic pressure on the rubber particles. The thermal stress generated in the blend then caused a decrease in EPR glass transition temperature.

(ii) Phase morphology of PP/EPR blends by SEM observations

To clarify the nature of phase separation of PP and EPR in the mixtures, selected PP/EPR blends were investigated by SEM. A micrograph of a cryogenic fracture surface of the PP1R1 blend sample is shown in *Figure 4.8 (a)*. To better elucidate the phase

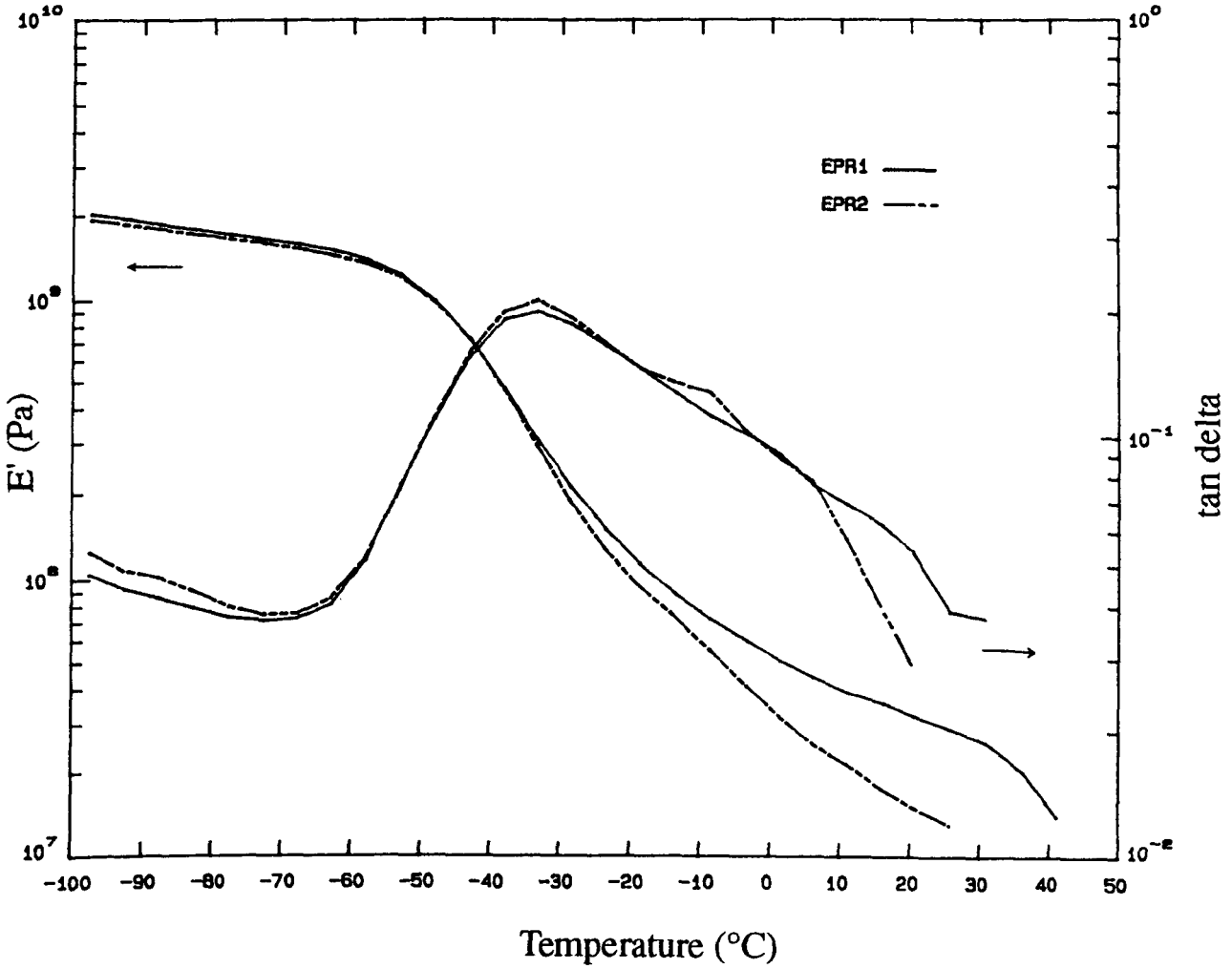

Figure 4.3 Temperature dependence of storage modulus (E') and loss factor (tan delta) at 1 Hz. for EPR1 and EPR2

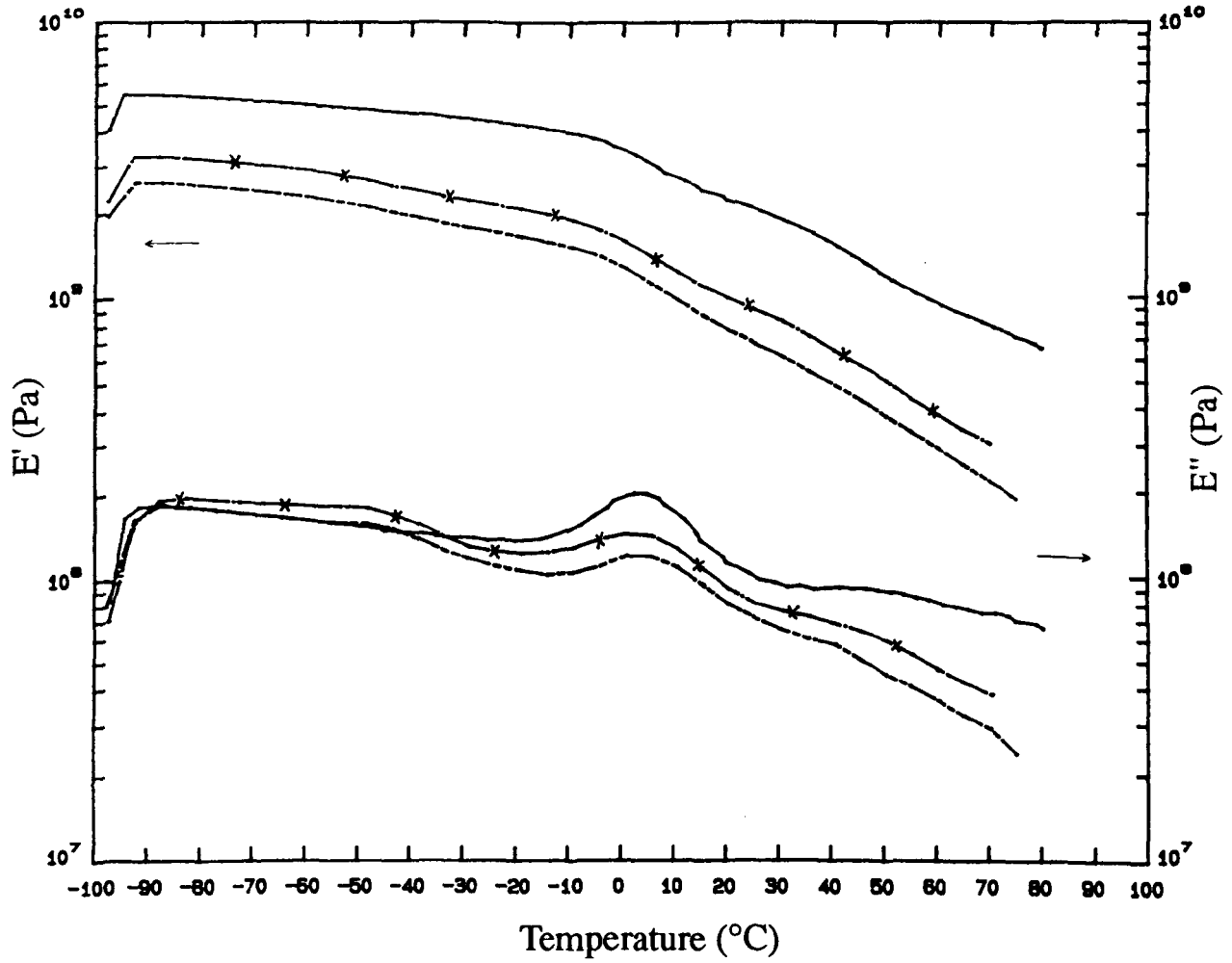

Figure 4.4 Temperature dependence of storage modulus (E') and loss modulus (E'') at 1 Hz. for PP1, PP1R1 and PP1R2

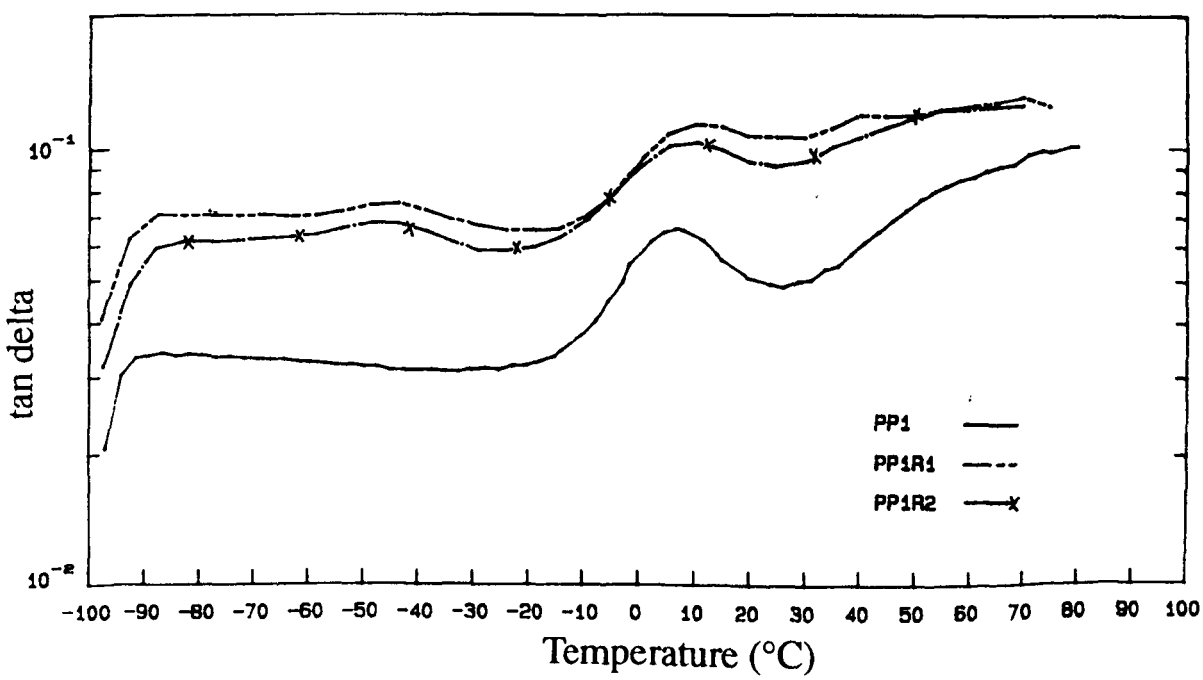

Figure 4.5 Temperature dependence of loss factor (tan delta) at 1 Hz. for PP1, PP1R1 and PP1R2

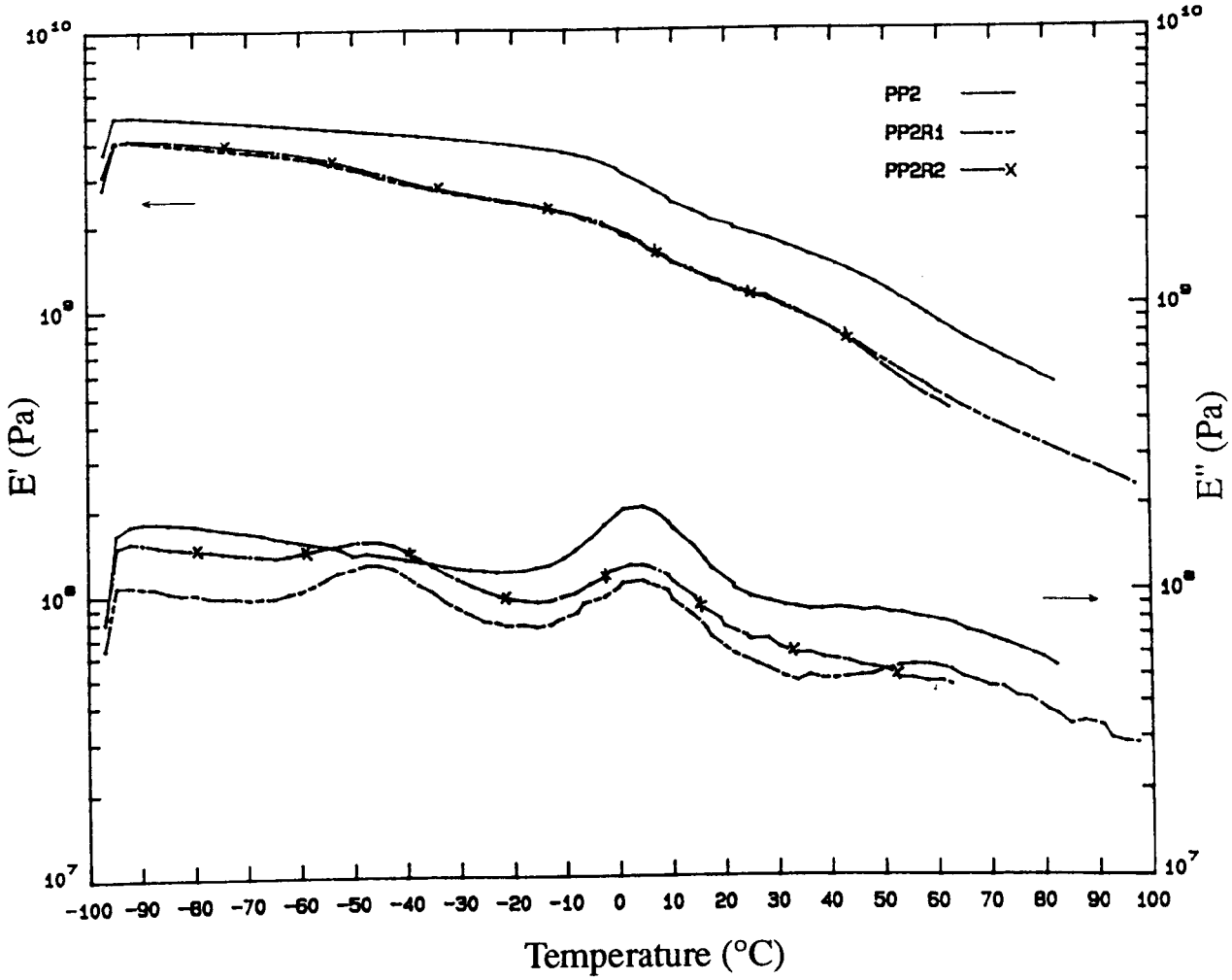

Figure 4.6 Temperature dependence of storage modulus (E') and loss modulus (E'') at 1 Hz. for PP2, PP2R1 and PP2R2

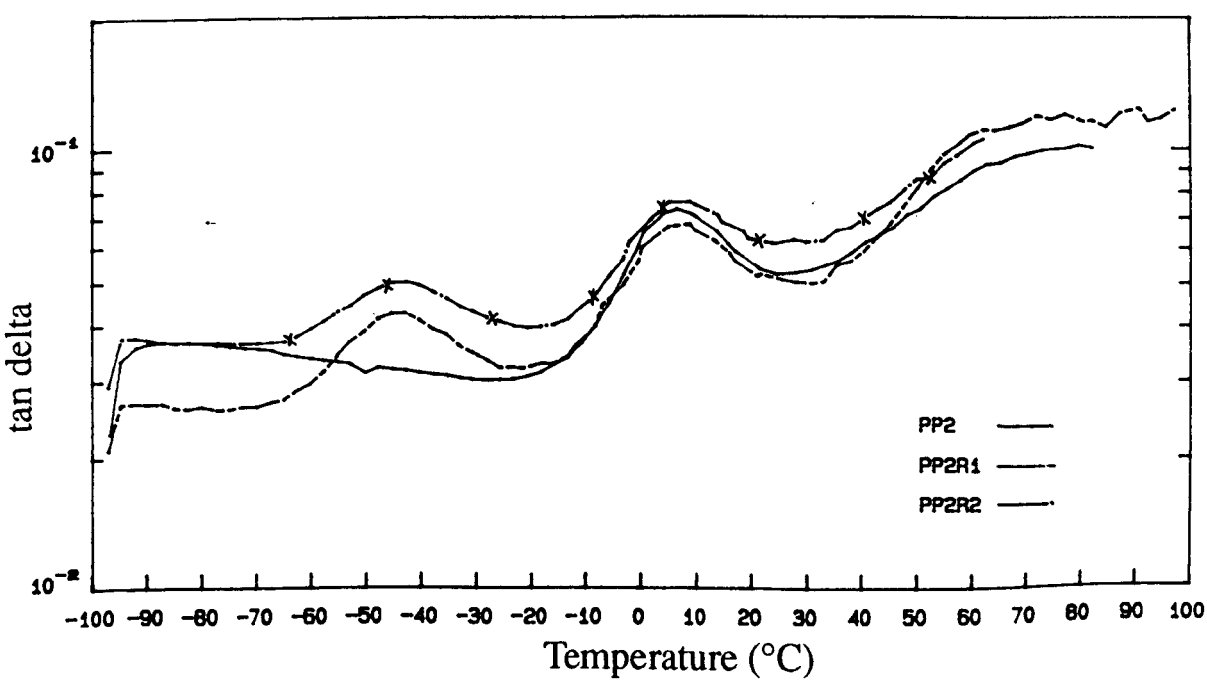

Figure 4.7 Temperature dependence of loss factor (tan delta) at 1 Hz. for PP2, PP2R1 and PP2R2

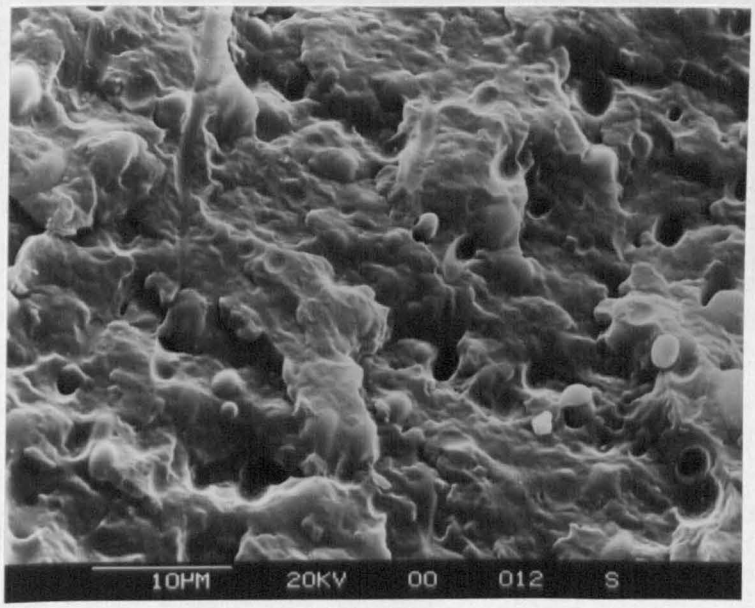

Figure 4.8 *a* Scanning electron micrograph of a cryogenic fracture surface of a PP1R1 (70/30) sample

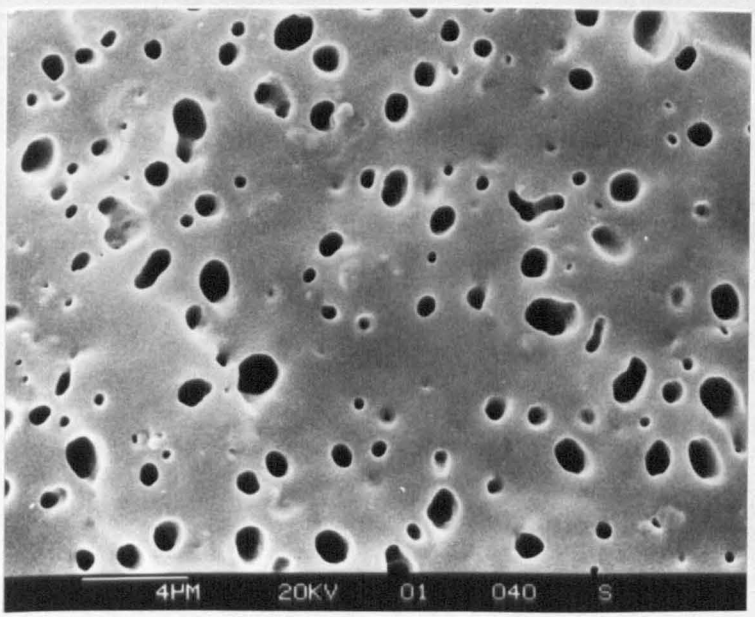

Figure 4.8 *b* Scanning electron micrograph of a cryogenic fracture surface of a PP1R1 (70/30) sample after exposing to heptane vapour for 3 sec. Dark circular holes shown on the micrograph are imprints of the EPR particles.

structure developed in such a blend, the fracture surfaces have been etched with boiling heptane vapour for 3 sec to remove EPR particles. The etching procedure has been reviewed earlier in Chapter 3. A two-phase system was observed in *Figure 4.8 (b)* where the spherical EPR particles were randomly dispersed in a continuous PP matrix. As EPR had been removed from the PP matrix by heptane, dark circular holes which are imprints of the EPR particles are shown on the micrograph. A similar observation was also found in the PP2 blend systems.

4.3.1.2 Spherulitic structure of polypropylene in the blends

Throughout the project, all PP blends prepared have been quenched rapidly after the blending process from the melt into a water bath at room temperature. Under these conditions, three possible crystalline structures may be formed in PP [225]. The thermodynamically stable and most common α-modification consists of i-PP chains in the 3_1 helical conformation packed in a monoclinic unit cell. The metastable hexagonal β-form has 3_1 helical chains arranged in groups of the same helical handedness (left or right). The intermediate structure which is known as "smectic state" consists of 3_1 helices but the disorder exists in the packing of the chains perpendicular to their axes. The formation of these crystalline structures are dependent upon many factors. The incorporation of additives to polypropylene has been reported to cause an alteration of these structures. In this part of work, effect of EPR on the spherulitic structures of polypropylene in the blends is reported.

(i) Optical microscopy observations

Optical micrographs, taken with crossed polars, of thin sections microtomed from 2 mm thick compression-moulded sheets of PP1 and PP1R1 samples, are shown in *Figures 4.9 and 4.10*, respectively. As expected, the unmodified polypropylene crystallised in a microspherulitic superstructure (see *Figure 4.9*). The structure is primarily composed of the positive birefringence type I modification, representing the stable monoclinic α-form spherulites.

With the incorporation of EPR, the spherulite size of PP phase in the blends changed markedly (see *Figure 4.10*). The average spherulite diameter of a blend sample was about two-thirds that of the unmodified PP. The changing in spherulite size has also observed in other PP composites containing impact modifiers such as EPDM and SBR

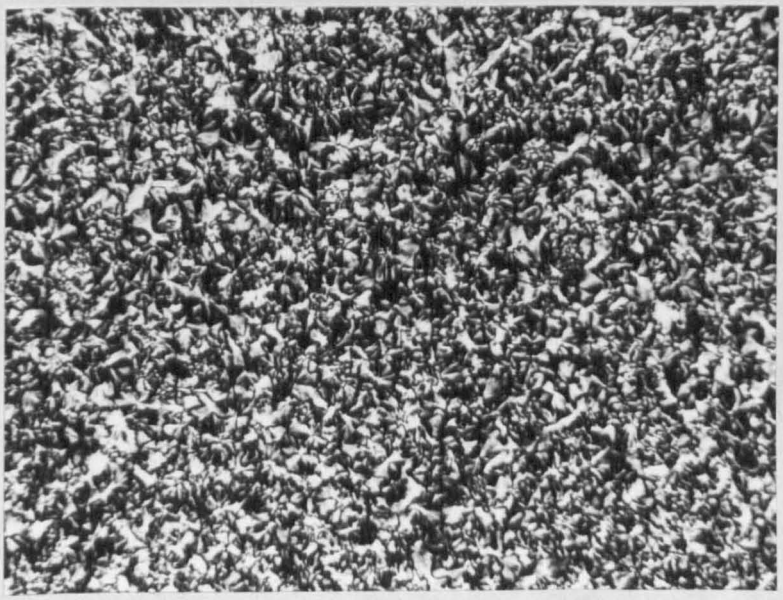

Figure 4.9 Optical micrograph of PP1 sample shows polypropylene α - monoclinic spherulites

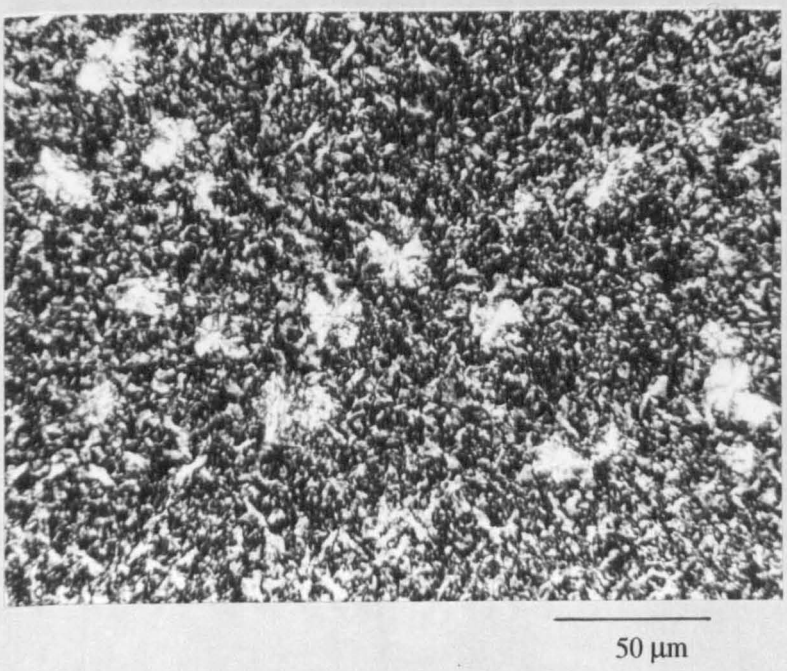

Figure 4.10 Optical micrograph of PP1R1 sample shows the promotion of polypropylene β - hexagonal spherulites by the addition of ethylene-propylene rubber

[58]. Not only the size of spherulites but also the spherulitic morphology changed by addition of the EPR phase. As seen in *Figures 4.9 and 5.2*, unmodified PP showed a regular structure with a relatively ordered spherulitic texture. Addition of EPR (see *Figure 4.10*) resulted in a less regular spherulitic structure with less sharp spherulite boundaries. Furthermore, EPR in the blend tends to promote the hexagonal β-type spherulites appearing sporadically and stand out clearly (bright area) in great contrast to the darker type I matrix. Generally, in samples containing both α and β modifications, β-spherulites are usually larger than α-spherulites. This is attributed to the higher growth rate of β-spherulites [20]. This observation is in agreement with the work by Pukanszky et.al. [30] on PP/EPDM blends. However, some references in the literature indicated, contrary to this finding, that by the incorporation of EPR [26, 37] or EPDM [43, 64] the amount of β-PP decreased.

(ii) Wide angle X-ray diffraction (WAXD) studies

The wide angle X-ray diffraction (WAXD) diffractograms for unmodified polypropylenes and their blends are shown in *Figures 4.11 and 4.12*, where the intensity in arbitrary units is plotted against the diffraction angle 2θ. In the given range of scattering angle, polypropylene shows four maxima at 2θ of 14.0, 16.9, 18.5, 21.0 and 21.8° corresponding to the (110), (040), (130) and overlapping (131), (041) and (111) reflections which are characteristic of the monoclinic α-phase [226].

With the incorporation of EPR, the position of these reflections in the blends remained unchanged. Although the evidence from the optical microscopic study shows the promotion of β-spherulites by addition of EPR, no reflection at 2θ ~16°C, which corresponding to the (300) diffraction peak of the hexagonal β-phase [6], was observed. This may be due to the amount of β-spherulites in the blends being too small to be detected by this method. No significant difference could be detected between the effects of R1 and R2 in both PP systems.

(iii) Differential scanning calorimetry (DSC) studies

Effect of EPR on the crystallisation behaviour of polypropylene was investigated by DSC using a thermal (heat-cool-heat) cycle. The first heating stage involves heating the material above its melting point to erase any previous thermal history. The cooling stage,

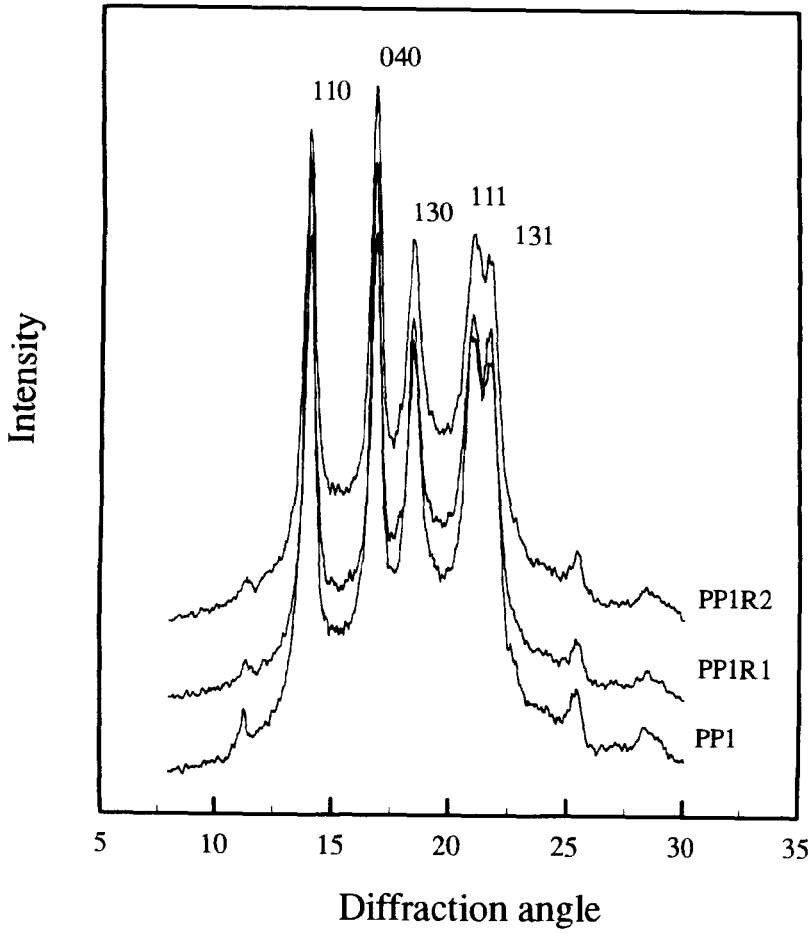

Figure 4.11 WAXD patterns of PP1, PP1R1 and PP1R2

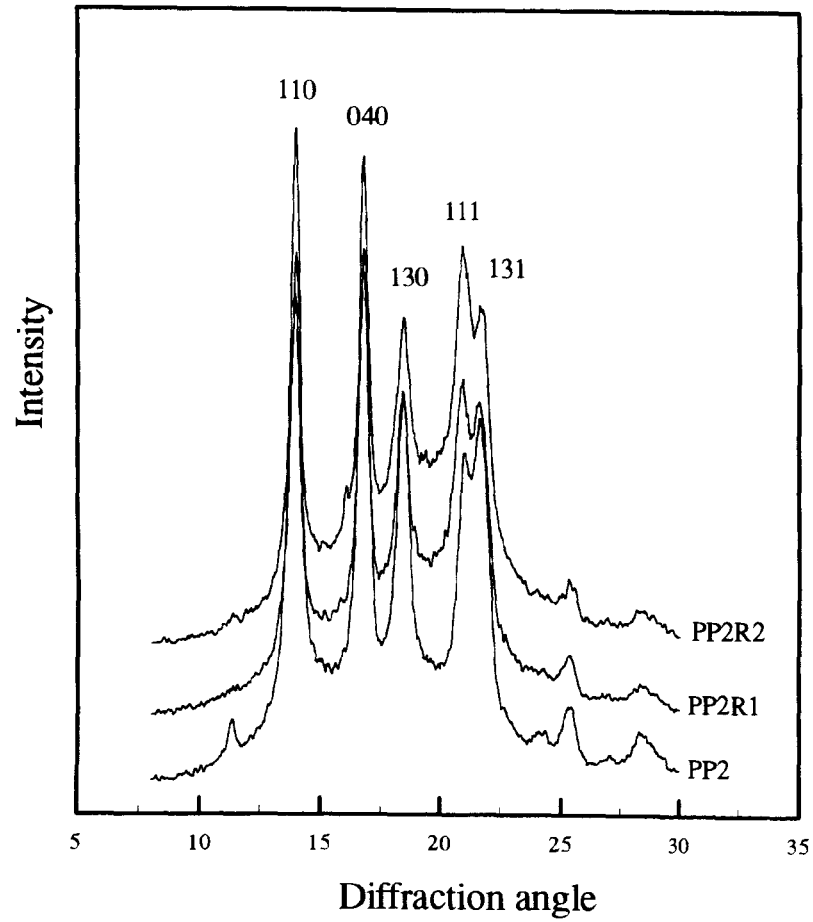

Figure 4.12 WAXD patterns of PP2, PP2R1 and PP2R2

then imparts a known thermal history allowing various samples to be compared using the results obtained from the second heating cycle.

Crystallisation behaviour of PP in the blends

The term "crystallisation" includes the formation of a stable nucleus or "nucleation step" and the addition of the other chains to the nucleus or "growth step". During the cooling cycle in the DSC scan crystallisation exotherms were observed. *Figures 4.13 and 4.14* show the crystallisation exotherms of unmodified PPs and PP/EPR blends in the temperature range from 60° to 160°C. These exotherms were characterised by determining :

- the crystallisation temperature (T_c) which is determined from the peak temperature of the exotherm and is related to the perfection of crystals in the material. A high T_c normally referred a rather perfect crystals with wide and thick lamella.
- the temperature of onset of crystallisation ($T_{c\ onset}$) which is the starting temperature of crystallisation and is determined from the temperature where the thermogram initially departs from the baseline on the high temperature side of the exotherm.
- the difference between T_c and $T_{c\ onset}$ (T_1) which is related to the rate of crystallisation. A decrease in this value is attributed to an increase in the rate of crystallisation.
- the heat of crystallisation (ΔH_c) which is determined from the area under the exotherm.

As shown in *Table 4.2*, with the addition of EPR the crystallisation peak of the blends shifted to lower temperatures, e.g. from 109.5°C in the PP1 sample to 108.2°C in the PP1R1 blend. This, consequently leads to an increase in the degree of undercooling (T_2) defined as the difference between the melting and cooling peak temperatures. It was noted from the polarised light microscopic studies that the superstructure of PP was changed by the incorporation of EPR, resulting in the formation of smaller spherulites. As a theoretical interpretation for the size reduction of spherulites with increasing the undercooling, the thermodynamic barrier of nucleation is proportional to ΔT^{-2} while that of growth is linear with ΔT^{-1} [24]. In other words, the rate of nucleation increases at a considerably greater extent than that of growth nuclei when the temperature decreases.

Both DSC and microscopy techniques seem consistently to point out a reduction in spherulite size in the blends. Dao [227] observed that the average spherulite diameter

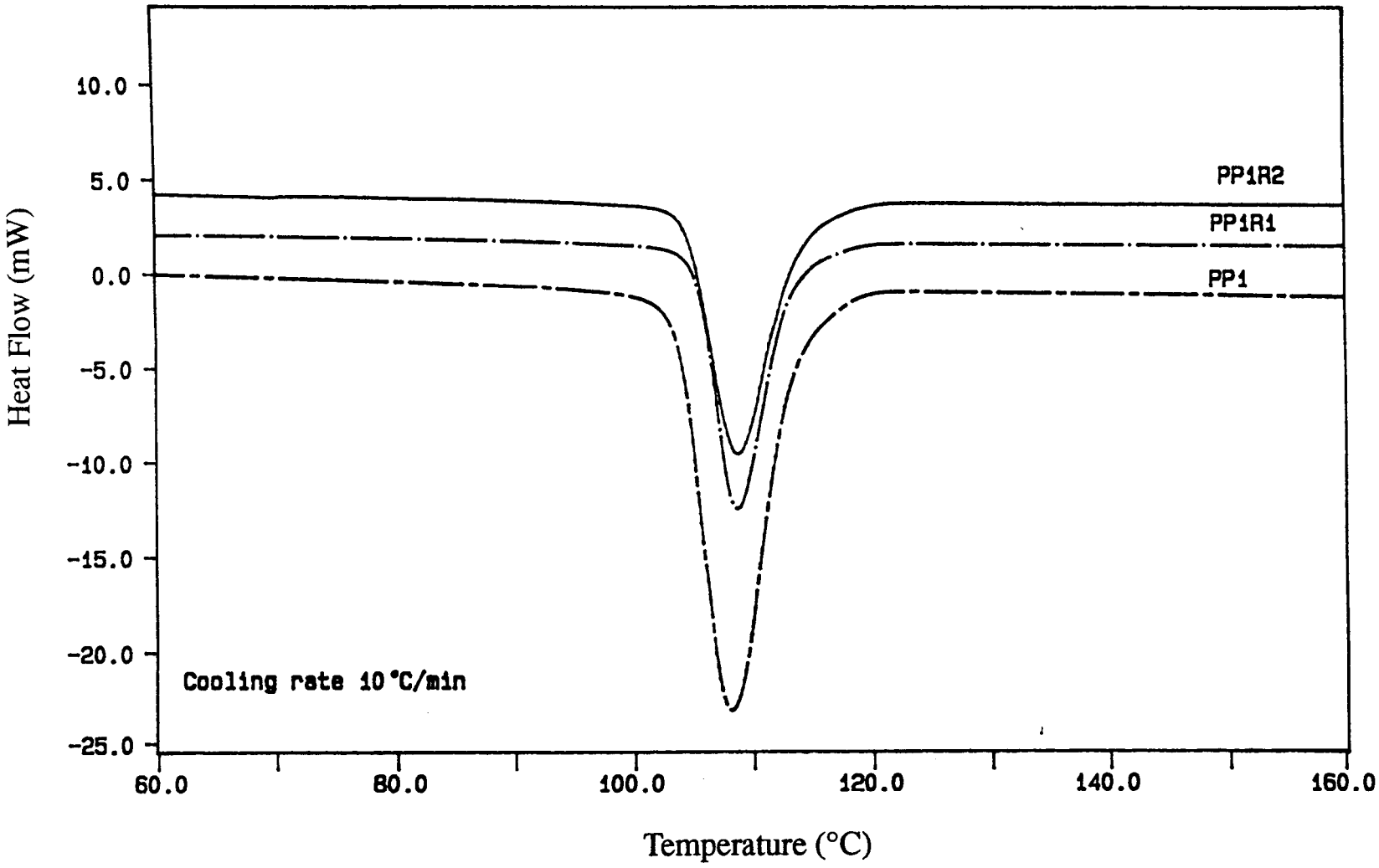

Figure 4.13 Crystallisation exotherms of PP1, PP1R1 and PP1R2

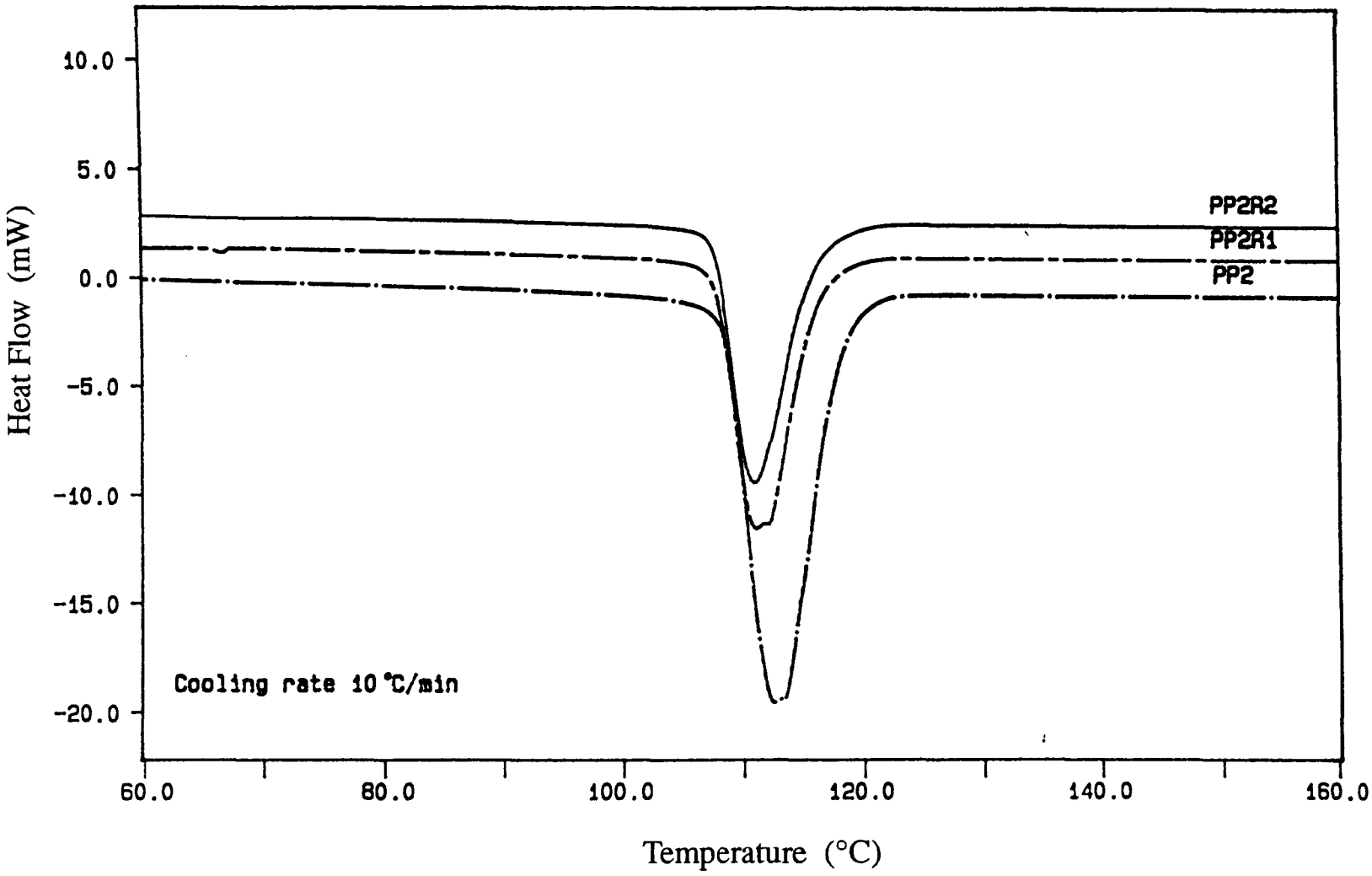

Figure 4.14 Crystallisation exotherms of PP2, PP2R1 and PP2R2

Table 4.2

The temperature of onset of crystallisation ($T_{c\ onset}$), crystallisation temperature (T_c), heat of crystallisation (ΔH_c), melting temperature (T_m), percentage crystallinity, difference between $T_{c\ onset}$ and T_c (T_1) and degree of undercooling (T_2) of unmodified PPs and PP/EPR (70/30) blends

Sample	$T_{c\ onset}$ (°C)	T_c (°C)	ΔH_c (J/g)	T_m (°C)	Crystallinity (%)		T_1 (°C)	T_2 (°C)
					experiment	recal. [a]		
PP1	114.6	109.5	95.1	163.3	49.0	49.0	5.1	53.8
PP1R1	113.5	108.2	66.1	162.8	34.5	34.3	5.3	54.6
PP1R2	113.4	108.4	65.3	162.5	34.4	34.3	5.0	54.1
PP2	118.3	112.6	96.4	162.2	49.3	49.3	5.7	49.6
PP2R1	116.4	111.2	66.1	161.4	34.3	34.5	5.2	50.2
PP2R2	116.2	111.1	62.7	161.0	33.5	34.5	5.1	49.9

[a] Recalculated percentage crystallinity based on the weight % of polypropylene in the composites.

decreased from 50 μm for an unmodified polypropylene to 20 μm for polypropylene blends containing 20% EPDM.

A decrease in T_c peak in the blend not only implies a reduction in spherulite size but also a reduced thickness of crystalline lamellae. According to the kinetic theory of crystallisation, lamella thickness tends to increase with increasing T_c [24]. Hence at a high T_c wide and thick lamellae are formed, since the chain mobility is quite high and the crystallisation times are long enough to allow the development of larger and more perfect crystals.

Similarly $T_{c\ onset}$ and ΔH_c also decreased in all blends. A decrease in $T_{c\ onset}$ in the blends clearly indicates that the incorporation of EPR in PP resulted in delayed nucleation. The observed decrease in ΔH_c values was a result of the presence of rubber which acted as a diluent in the blends. However, no change in ΔH_c was observed compared to an unmodified PP, after subtracting the volume percent of EPR in the blends and recalculating ΔH_c only on the volume percent of PP component. These results thus indicated that the propylene-ethylene segments of EPR do not co-crystallise with PP. If such a crystallisation had taken place then ΔH_c in the blends would have become higher.

Melting behaviour of the crystalline phase in the blends

The DSC thermograms recorded during the second heating cycle of unmodified polypropylenes and their blends are shown in *Figures 4.15 and 4.16*. The melting temperature (T_m), heat of fusion (ΔH_m) were determined from the peak temperature and the area under the endothermic peak in a DSC scan, respectively. The percentage of crystallinity of the composites was calculated from the obtained heat of fusion values (ΔH_m) by using the relationship:

$$\% \text{ crystallinity} = \Delta H_m / \Delta H_o \times 100$$

A value of ΔH_0 of 189 J/g for 100% PP [228] was used for the calculation. In this context, it is worth mentioning that the crystallinity value obtained from the endotherm peak resulted only from the crystalline PP phase in the blends. Although both grades of EPR used in this work are reported to be semicrystalline polymers, EPR shows no peak in the second heating thermogram of a DSC scan. For the comparison purposes, the recalculated crystallinity based on the weight % of PP in the composites is included.

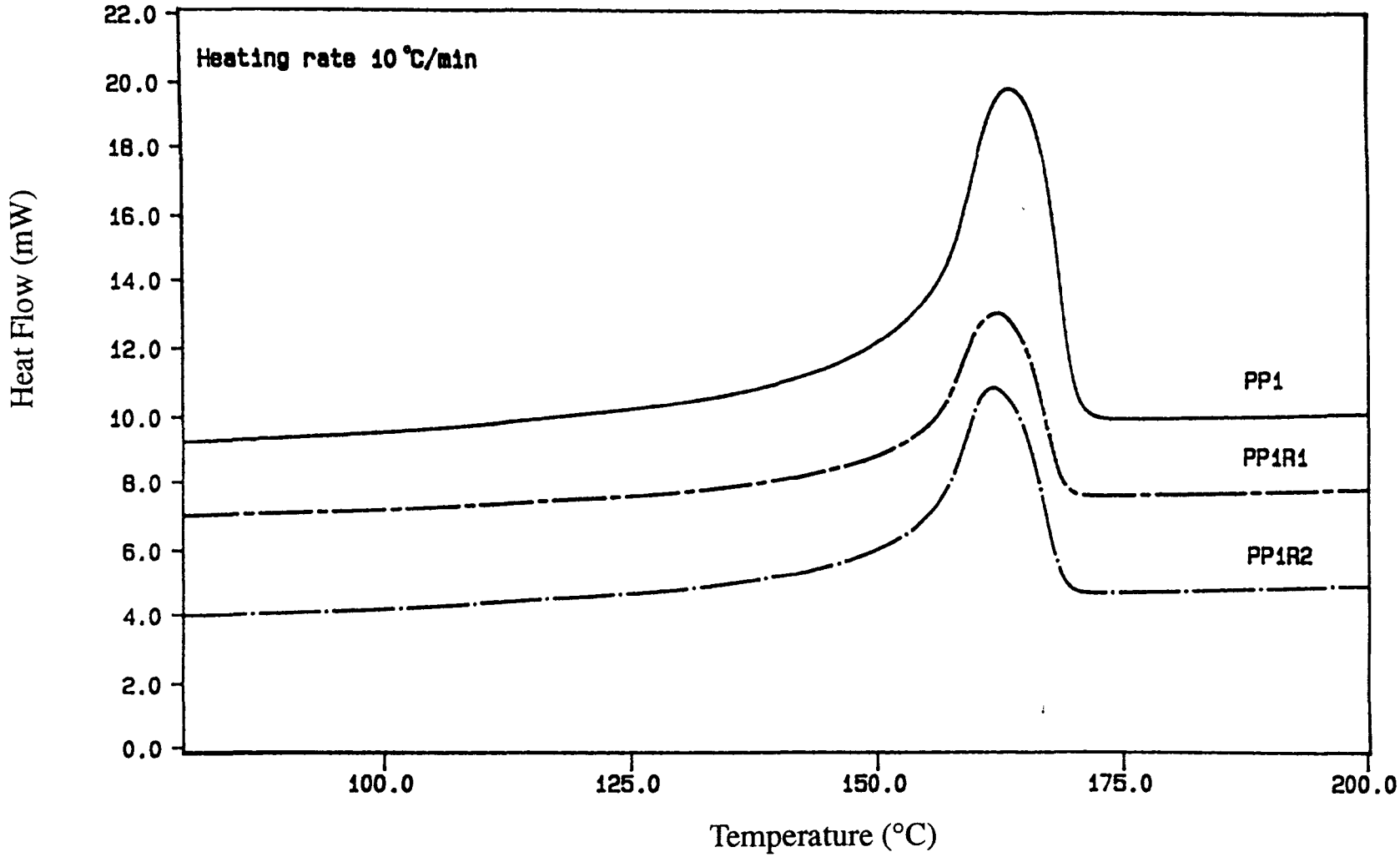

Figure 4.15 Melting endotherms of PP1, PP1R1 and PP1R2 recorded during the second heating cycle

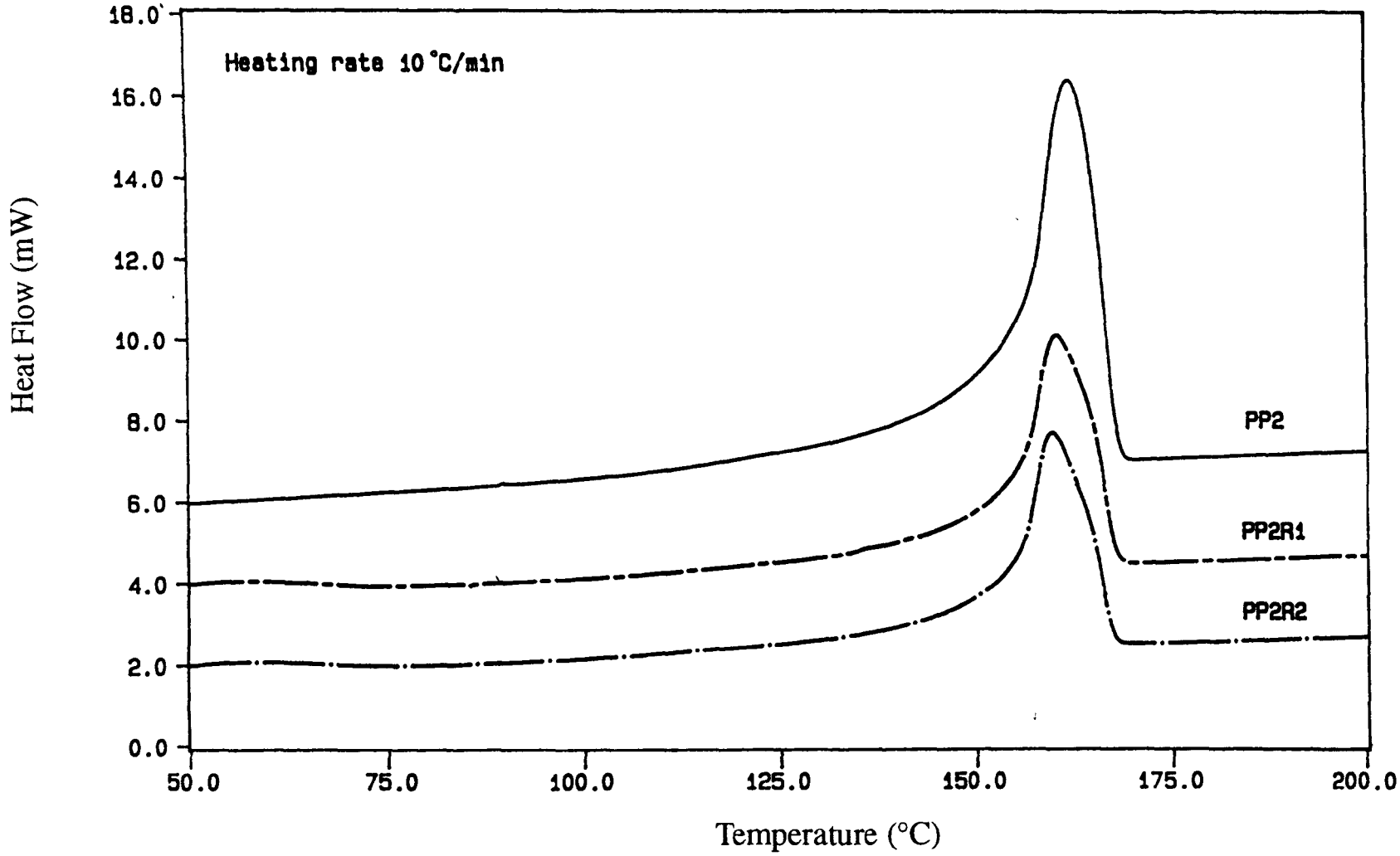

Figure 4.16 Melting endotherms of PP2, PP2R1 and PP2R2 recorded during the second heating cycle

Generally, all commercial grades of EPR which contain above 40 mol% ethylene can develop crystallinity below ambient temperature if annealed for several hours [229]. Full development of crystallinity may take weeks. The crystallinity observed is that of polyethylene (PE) orthorhombic cell. At ca 40% ethylene the melting point of PE is suppressed by comonomer content to the T_g. Below this ethylene content, the polymers remain amorphous at all temperatures [229]. Both EPR grades used in this work contain 55 wt% ethylene content. After annealing for 8 hrs at 140°C, EPR shows an endothermic peak upon heating at around 55°C as shown in *Figure 4.17.*

From *Figures 4.15 and 4.16,* a single peak characteristic of the melting of α-PP, was clearly seen at about 163°C in a PP1 sample and 162°C in a PP2 sample. No evidence of the EPR melting peak at around 55°C was observed. By annealing the PP/EPR blend sample for 8 hrs at 140°C, two endothermic peaks at 55°C and 162°C were revealed, corresponding to the melting peak of EPR and PP, respectively (see *Figure 4.18c*). Comparison with the annealed blend sample in *Figure 4.18c*, the sample cut from the compression moulded sheet also shows a little shoulder at 55°C (see *Figure 4.18 d*) belonging to EPR. However this peak disappears in the second heating run, where only a significant melting peak was observed at 163°C attributed to PP (see *Figure 4.18 e*).

Although it has been noted earlier that the introduction of EPR phase seems to promote the formation of β-type spherulites. However, the β-PP peak was not observed in the blend samples under the DSC test conditions. By annealing the samples at 140°C for 8 hr however, a β-PP peak in the blend can be identified. *Figures 4.18c and 4.18e* are the DSC thermograms of an annealed PP1R1 sample recorded during the first and second heating cycles, respectively. The thermogram recorded from the annealed sample at the first heating cycle (*Figure 4.18c*) shows a small β peak at about 148°C [17] appearing as a shoulder on the α endotherm. This shoulder subsequently disappears from the α endotherm in the second heating cycle (*Figure 4.18e*). To clarify that the small β peak observed in the blend sample after annealing was due to the effect of EPR in the blends, an unmodified polypropylene sample was also subjected to the same annealing conditions. After annealing for 8 hrs at 140°C, a PP1 sample shows only a tiny shoulder on the α endothermic peak (see *Figure 4.18b*). This observation confirmed the state that EPR promotes the formation of β-spherulites. However, under the DSC test conditions only a very small number of the β-spherulites may form and hence the β peak was not detected.

It was concluded from the light microscopy results that with the addition of EPR the average spherulite size of PP also decreased. As a consequence, by the presence of

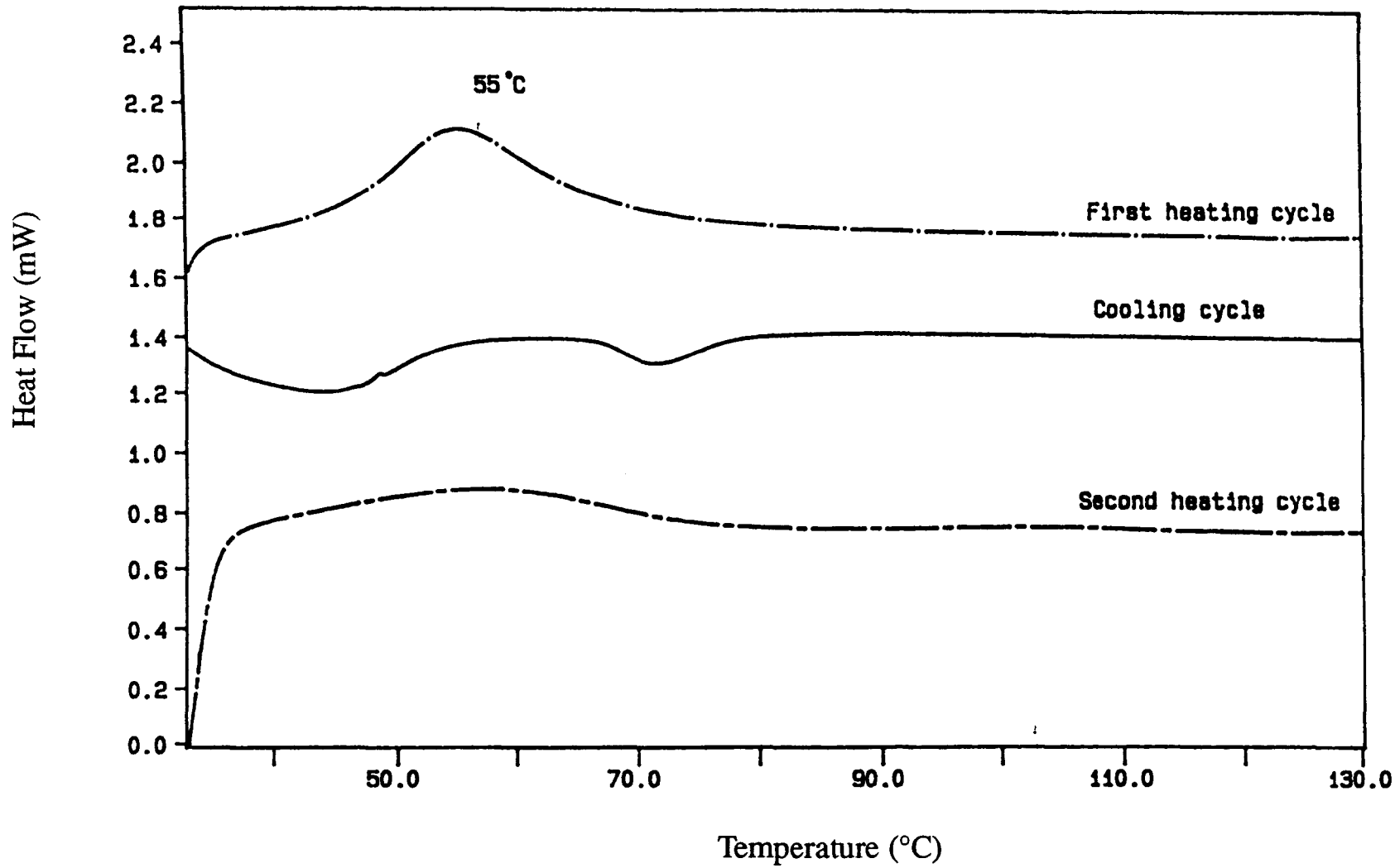

Figure 4.17 Melting and cooling thermograms of an annealed EPR. An endothermic peak at around 55 °C can be revealed after annealing EPR at 140 °C for 8 hr.

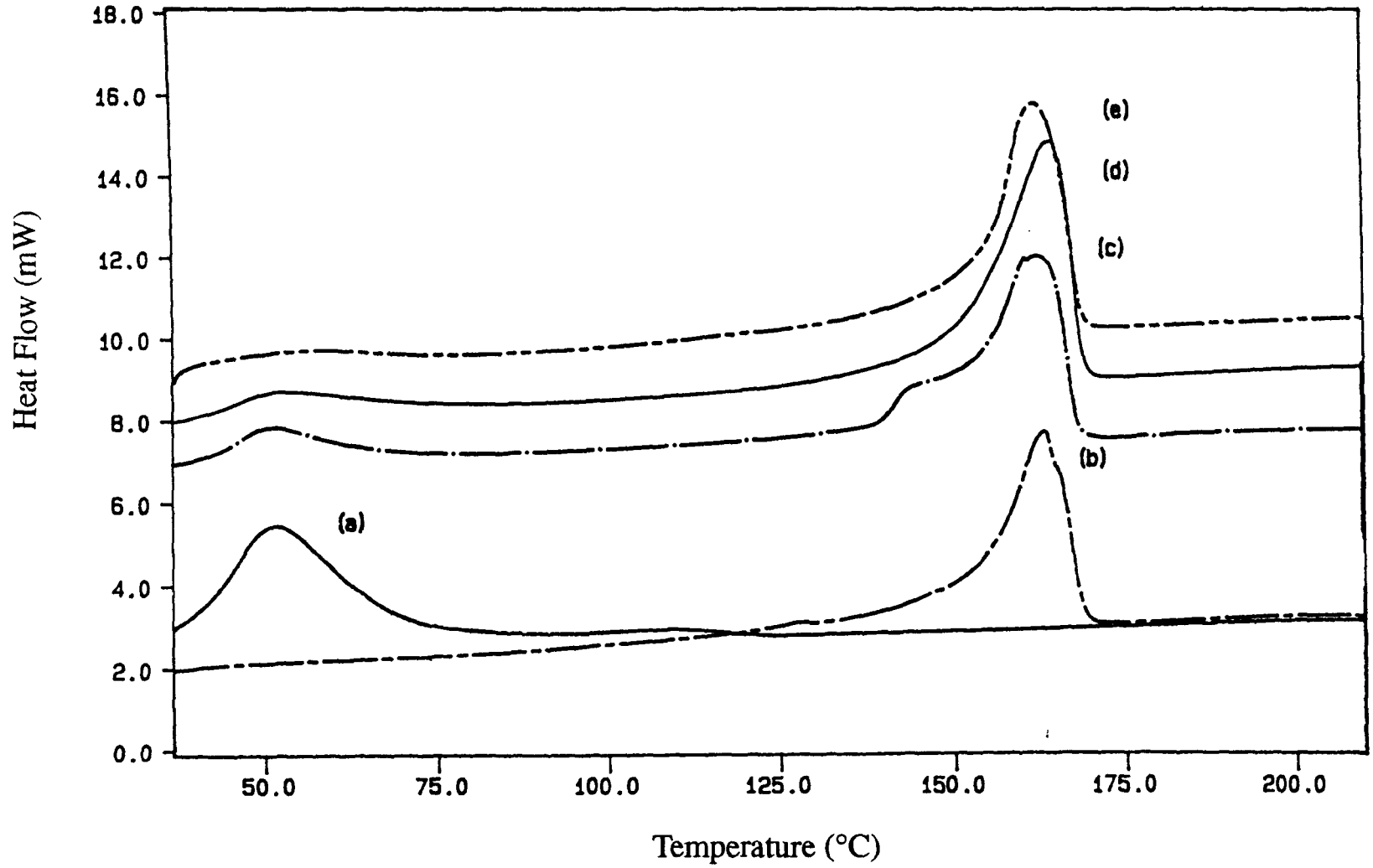

Figure 4.18 Effect of annealing on the course of melting endotherms of *(a)* R1,*(b)* PP1 and *(c)* PP1R1 samples compare to *(d)* an unannealed PP1R1 sample and *(e)* the change in the PP1R1 endotherm under the second heating cycle

smaller spherulites which have lower heat capacity, the melting peak of the blend should shift to lower temperature. DSC results verify this assumption (see *Table 4.2* p.87). The observed crystallinity also decreased for all blends with respect to an unmodified PP sample. However, this reduction in crystallinity is due to the substitution of 30% of PP by EPR. There was no influence of EPR on the percentage crystallinity in PP.

4.3.2 Effect of EPR on the mechanical properties of the blends

4.3.2.1 Tensile properties of the PP/EPR blends

Tensile properties of the blends depend on many factors. One of the most important of these being the characteristics of components in the blends. In this study, two grades of polypropylene with differences in melt viscosity, were investigated. As shown in *Table 4.3* PP1 which has a lower melt flow index (MFI = 1.8 g/10 min), inferring higher viscosity and molecular weight, shows a better tensile strength and elongation at yield, but has slightly lower Young's modulus than PP2 (MFI = 5 g/10 min). This result is in agreement with the work of Ogawa [230] on the effect of molecular weight on mechanical properties of polypropylene. He observed an increase in tensile strength and elongation as molecular weight increased while modulus was found to decrease with it.

Incorporation of 30% EPR into PP improves ductility in the blends, accompanying by a decrease in both tensile modulus and strength values. Danesi and Porter [47] reported a yield stress of 24 MPa (2.4×10^2 kg/cm^2) and a modulus of 0.82 GPa (8.2×10^3 kg/cm^2) in a (70/30) PP/EPDM blend. Similar data were observed in the present study e.g. a yield stress of 24 MPa and a modulus of 1.16 GPa were observed in a PP1R1 sample, despite the fact that these two studies involved slightly different materials and compounding conditions.

A decrease in tensile modulus and strength can be firstly explained by the substitution of PP by EPR, which is a low modulus material, and secondly by the morphological changes due to EPR incorporation. The earlier findings from DSC and optical microscopic studies show that addition of EPR into PP leads to an increase in the degree of undercooling. Thus the blend structure is characterised by the presence of small PP spherulites interconnected by a large fraction of tie molecules. When the external load is applied these tie molecules give more local transfer leading to ductile mechanical properties. Way et.al. [231] observed that the tensile yield strength of PP first increased

Table 4.3 Young's modulus, tensile yield stress and elongation at yield at 23 °C for unmodified PPs and PP/EPR blends

Sample	Composition (PP/EPR in vol%)	Young's modulus (GPa)	Yield stress (MPa)	Elongation at yield (%)
PP1	100/0	1.78 (0.03)[a]	33.44 (0.74)	5.47 (0.27)
PP1R1	70/30	1.16 (0.03)	24.24 (2.83)	4.94 (0.56)
PP1R2	70/30	1.13 (0.01)	23.41 (3.00)	5.19 (0.31)
PP2	100/0	1.80 (0.03)	31.97 (0.56)	5.06 (0.25)
PP2R1	70/30	1.19 (0.04)	20.76 (0.89)	4.87 (0.53)
PP2R2	70/30	1.12 (0.05)	19.13 (0.53)	5.15 (0.24)

[a] Standard deviations in parentheses, means from eight specimens.

with increasing the average spherulite diameter (reaching a maximum at about 60 μm) and then decreased thereafter.

Comparing the effect of R1 and R2 on tensile properties of the blends, R1 seems to provide slightly better tensile properties than R2. The observed difference in modulus of the two blends can be explained using Kerner's theory for the modulus of composites containing spherical inclusion [114]. According to this theory, the modulus of the composite, at a given matrix modulus and volume fraction of spheres, increases as the modulus of the included spheres increases. From the DMA study, R1 shows a higher modulus than R2 at all test temperatures (-100 to 100 °C) and the modulus of a PP1R1 sample was consequently higher than that of a PP1R2 sample.

4.3.2.2 Falling weight impact properties of the PP/EPR blends

Falling weight impact testing of PP/EPR blends was undertaken at 23 °C using a Rosand Instrumented Impact Tester. The testing procedure has been described in Chapter 3. After each impact event, force-deflection curve was recorded and these parameters were determined.

a) The first peak in the force-deflection curve is taken to relate to crack initiation. The average force at this point can be converted to a strength at crack initiation (σ_I) [232] using the following equation :

$$\sigma_I = 2.5F / t^2 \qquad (4.1)$$

where F is the initiation force and t is the thickness of specimen

b) Integration of the force-deflection curve up to the first peak will give the energy to initiate crack formation.

c) Integration of the full force-deflection curve gives the total energy absorbed in both initiation and propagation of the crack.

Results from the impact tests are shown in *Table 4.4*, from which the following conclusions can be drawn.

(1) Toughness characteristics in terms of crack initiation, propagation and total fracture appear to be improved by the incorporation of EPR into PP.

(2) Initiation, propagation and fracture energy in the blends increase more noticeably using R2 than R1, for both PP1 and PP2 systems.

Table 4.4 Falling weight impact results for unmodified PPs and PP/EPR blends at 23 °C

Sample	Initiation properties			Fracture properties		Propagation energy (J)
	Strength at initiation σ_I ,(MN/m^2)	Deflection (mm)	Energy (J)	Deflection (mm)	Energy (J)	
PP1	812.5	4.40	2.82	7.38	3.64	0.82
PP1R1	682.1	6.73	3.99	12.02	5.94	1.95
PP1R2	765.9	6.94	4.65	12.06	6.82	2.17
PP2	528.7	3.67	1.46	6.69	1.91	0.45
PP2R1	533.8	5.57	2.29	8.13	2.84	0.55
PP2R2	548.8	6.46	2.83	9.42	3.45	0.62

It was also observed that the rise in impact strength in PP/EPR blends was accompanied by stress-whitening. Stress whitening is a phenomenon where the region becomes white in appearance attributed to the formation of microvoids around the rubber particles during absorption of stress energy. *Figures 4.19 b and c* show force-deflection curves and crack patterns of PP/EPR blends. These samples failed by the development of stress whitening in a central area of 40 mm which is related to the diameter of specimen support ring. The observation of stress whitening area was also reported by Jones et.al. [194] using a high-speed photographic record during deformation of specimen. They found that a pronounced white spot develops on the under side of the specimen. This spot starts just after the maximum peak force observed (point a in *Figure 4.19 b*) and becomes more concentrated around the striker. At point b, the striker eventually penetrates the specimen flicking off a thin cap of drawn material. Friction between the hole and the striker then maintain a small force after failure. In contrast to PP/R blends, an unmodified PP sample shows more a cracking mode (*Figure 4.19 a*). Post-test broken specimen shows both radial and circumferential crackings with slightly whitening area appearing at edges. The energy to failure in an unmodified polypropylene is mainly on that required to initiate a crack. The energy to propagation a crack across a specimen is insignificant and contributes little to the material impact strength.

4.3.3 Toughening mechanisms in the PP/EPR blends

Various theories have been proposed to explain the toughening of polymers with a dispersed rubbery phase. However, rubber toughening mechanisms in tough-semicrystalline polymers have been studied only to a limit extent. The present investigation was aimed at obtaining an understanding on the toughening mechanisms in the PP/EPR blends.

4.3.3.1 Structure-property relationships

With the incorporation of EPR into PP, the improvement in impact strength of the blends was observed as shown in *Table 4.4*. This improvement can be explained either by the influence of rubber on the deformation mechanisms in the blends, or by the alteration of blend microstructures due to rubber addition.

In order to evaluate the mechanism of rubber toughening in the PP/R blends, the ductile fracture surfaces obtained from a specimen under the J-integral test, were examined. In

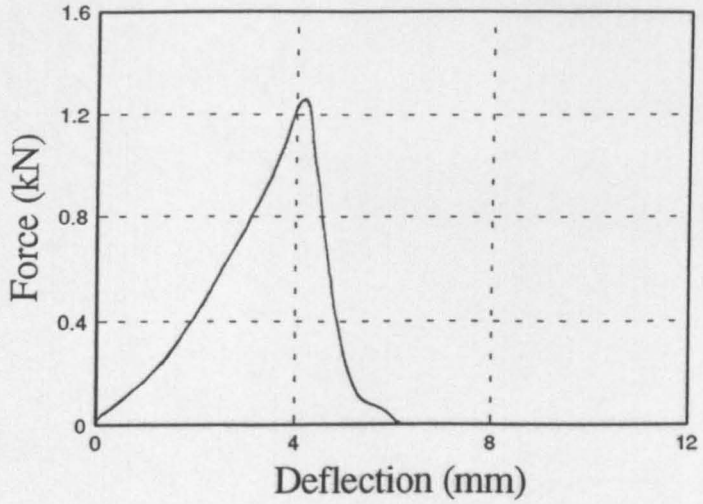

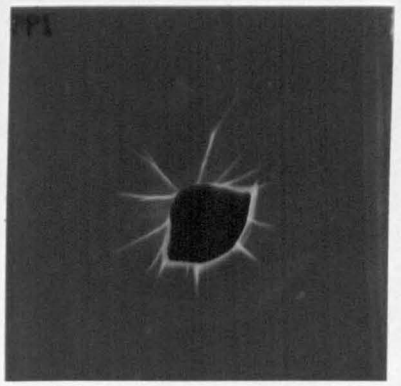

(a)

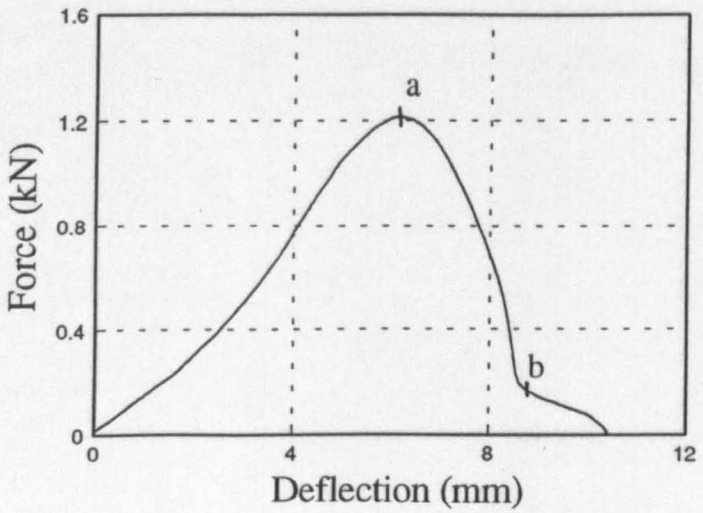

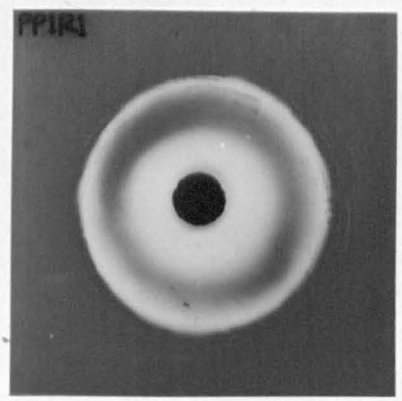

(b)

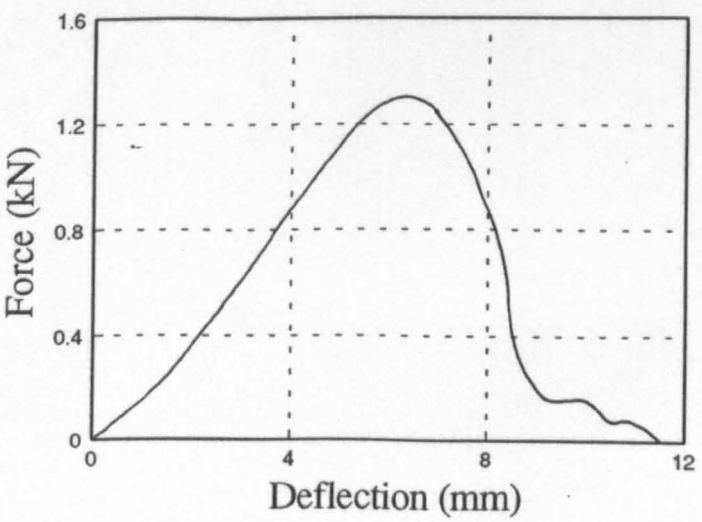

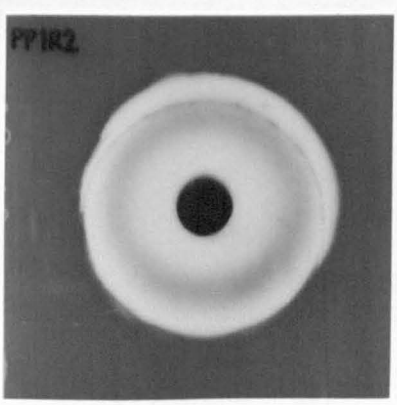

(c)

Figure 4.19 *a* -Impact force-deflection curves and post-test specimens of (a) PP1, (b) PP1R1 and (c) PP1R2

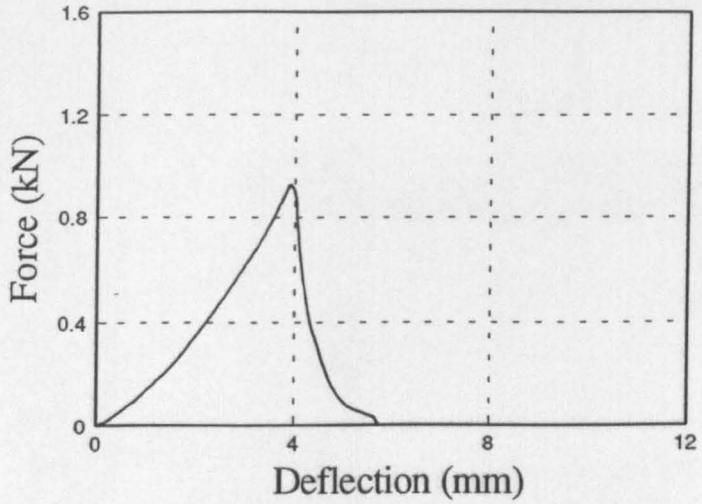

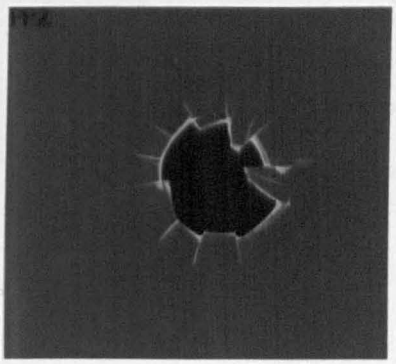

(a)

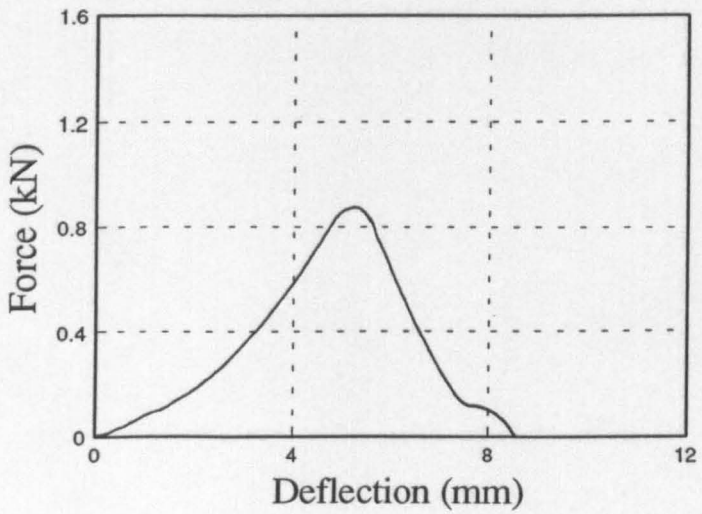

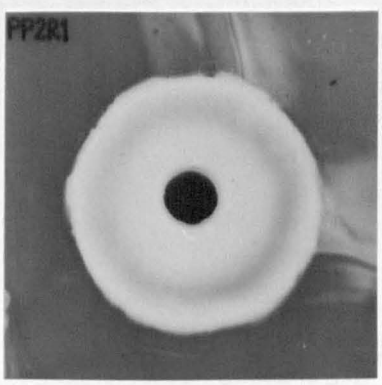

(b)

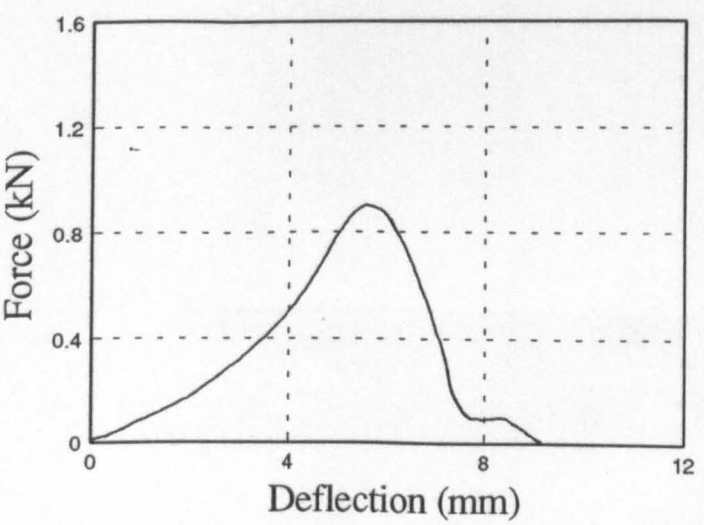

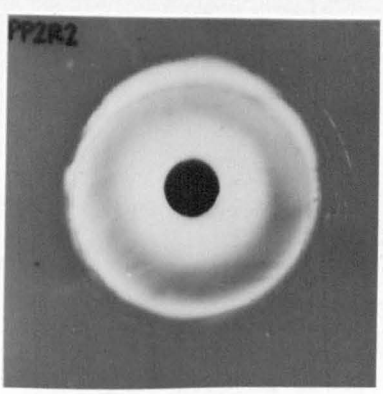

(c)

Figure 4.19 *b* -Impact force-deflection curves and post-test specimens of (a) PP2, (b) PP2R1 and (c) PP2R2

the J-integral testing, a notched specimen was loaded at the rate of 1 mm/min to a predetermined deflection that was less than that to give total failure. The specimen was then fractured at liquid nitrogen temperature to reveal the ductile fracture caused by load during the J-integral test. The significance of the present analysis is based upon the assumption that the state of the deformation specimen after ductile fracture is not altered by the following cryogenic fracture. This type of testing involves a considerable investment in time and effort, but on the other hand provides a much better basis for discussions of structure-property relationships than can be provided simply by the falling weight impact fracture surfaces.

Figures 4.20a to d reveal ductile fracture surfaces of a PP1R2 sample. The fractograph shows general cavitation and the absence of rubber particles (*Figure 4.20a*). The intensity of cavitation is really remarkable in the area where stress-whitening was observed on the fracture surface (*Figure 4.20b*). Voids can be observed with diameters a few times greater than the original rubber particle diameter (~ 1 μm). The huge dimension of some voids might be caused , at least partly, by coalescence between neighbouring cavities. Some voids also highly stretch and elongate along the draw direction (*Figure 4.20c*). In the area ahead a notched tip where the force is maximum, similar cavitation phenomena in association with extensive plastic deformation was observed (*Figure 4.20d*).

From these observations, the following conclusions can be drawn. In the present study, cavitation around the rubber particles and shear yielding of polypropylene matrix are primary important toughening mechanisms during the ductile fracture of the PP/R blends. The EPR particles initiate voiding either internally or at the rubber-matrix boundaries (*Figure 4.20a*). The voids then elongate as the specimen extends (*Figure 4.20c*). The number of voids increases with strain and they eventually become interconnected, producing polypropylene fibrils stretched parallel to the draw direction (*Figure 4.20d*). Finally, the fibrils begin to break and fracture of the whole specimen follows.

For similar PP systems, however, Jang [233] claimed that both shear yielding and crazing can occur in rubber-modified polypropylenes, depending on the temperature and speed of testing. A shear yielding-to-crazing transition can be induced either by decreasing the temperature, or by increasing the strain rate.

The combination between cavitation and shear yielding as toughening mechanisms in the PP/R blends agrees quite well with the toughening mechanisms in rubber modified nylon 6 observed by Borggreve et.al. [234] and by Wu [94], also in toughened nylon 6,6 by

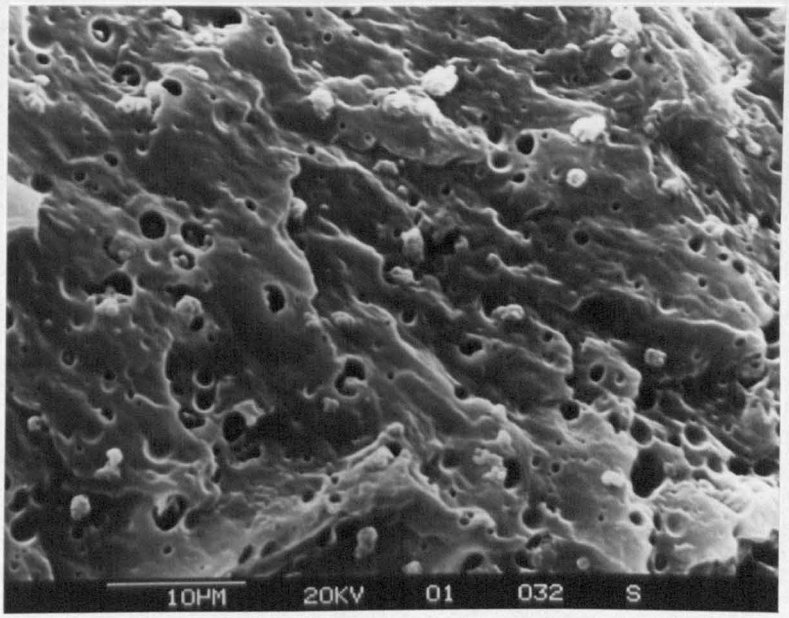

(a)

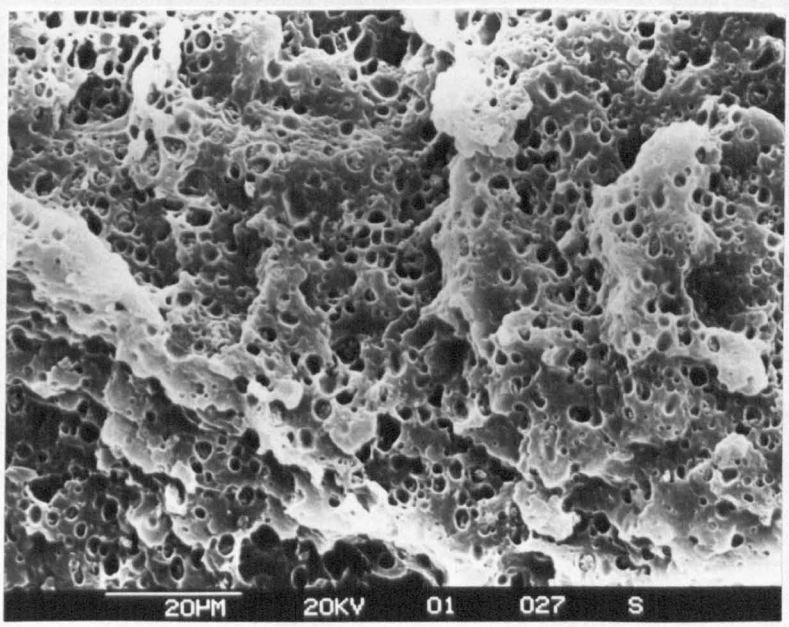

(b)

Figure 4.20 Ductile fracture surfaces of a PP1R2 sample showing *(a)* cavitation and void formation , and *(b)* more cavitation intensity in a stress-whitening area.

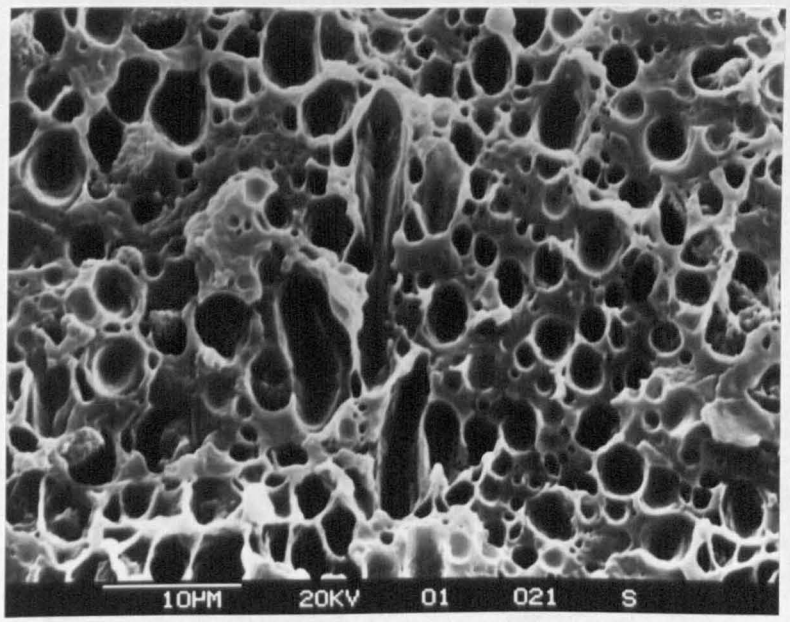

(c)

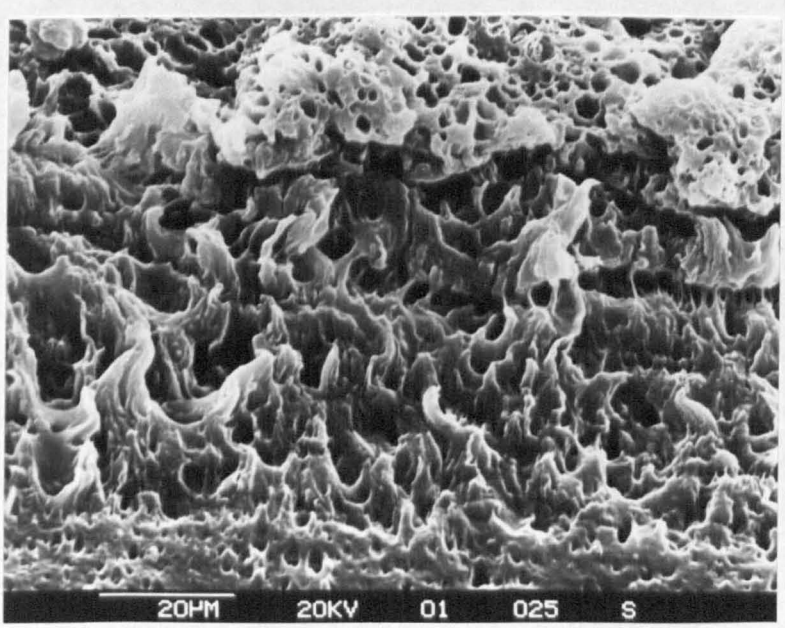

(d)

(cont.)

Figure 4.20 Ductile fracture surfaces of a PP1R2 sample showing *(c)* elongated voids in the stress-whitening area, and *(d)* PP deformation in the form of shear yielding along the draw direction, in the area ahead a notched tip.

6 observed by Borggreve et.al. [234] and by Wu [94], also in toughened nylon 6,6 by Ramsteiner and Heckmann [235] and by Bucknall et.al. [236]. None of these authors observed crazing. The observed extensive cavitation in the present study also strengthens Wu's theory [94] considering that optimum performance is achieved when the rubber particles are sufficiently close to enable stress fields of neighbouring particles overlap, since a strong interaction between the stress fields surrounding neighbouring particles promotes the growth of cavitation fronts and of shear yielding inside the continuous polypropylene matrix.

The improvement in impact strength and toughness of the blends , as mentioned earlier, could be due to an alteration of blend microstructure influenced by rubber. From the DSC studies, with the incorporation of EPR into PP, a decrease in $T_{c\ onset}$ was observed. Hutley and Darlington [129, 130] observed a correlation between $T_{c\ onset}$ and impact strength of calcium carbonate filled polypropylene composites. A high $T_{c\ onset}$ was observed in the composite of poor impact strength. The present results on the PP/EPR blends agree with their finding.

Addition of EPR also resulted in a less regular spherulitic texture with less sharp spherulite boundaries. Not only the spherulitic structure but also the size of the spherulites was changed markedly by the incorporation of the EPR phase. The dependence of fracture resistance of polypropylenes on spherulite size has been reported by Friedrich [237]. Reduction in spherulite size by rubbery phase was reported to be partially responsible for property modification.

Also, of note was the observation that the EPR particles are randomly dispersed in the polypropylene matrix (*Figure 4.8b*). The SEM investigation of $KMnO_4$ etched surfaces reveal that these EPR particles are mainly engulfed by the growth of PP spherulites (*Figure 4.21a*). Only small amounts were observed at the spherulite boundaries (*Figure 4.21b*). Such a random dispersion is believed to be more effective in inhibiting or retarding the subcritical growth of microcracks, since cracks were observed to propagate through the spherulites, not preferentially along spherulite boundaries [90].

4.3.3.2 Rubber particle size effects in rubber toughening of polypropylene

(i) Particle size analysis

The evidence from SEM studies on etched surfaces showed the presence of spherical EPR particles dispersed in the continuous polypropylene matrix. The SEM micrographs

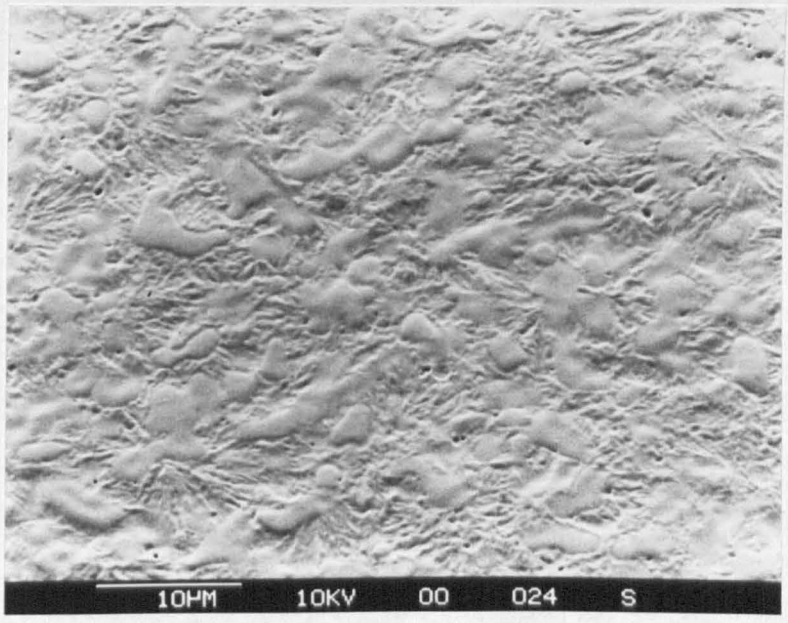

(a)

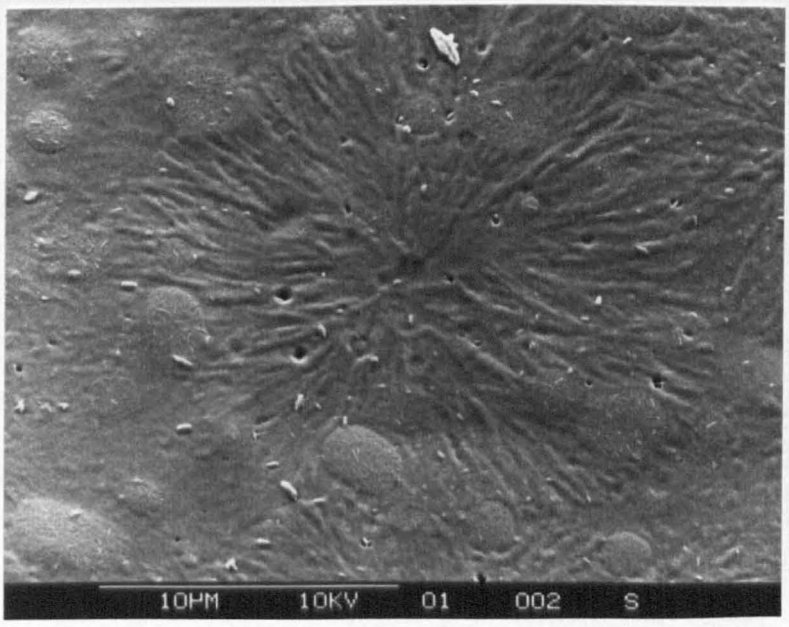

(b)

Figure 4.21 SEM micrographs of $KMnO_4$ etched PP1R2 sample revealing *(a)* randomly dispersion of EPR particles in the growth PP spherulites, and *(b)* small amounts of EPR particles at the spherulite boundaries.

were scanned with an image analyser to determine the EPR particle size. Approximately one thousand particles were measured for each sample using the image analysis technique described in Chapter 3.

Table 4.5 shows a number-average diameter of EPR particles in various blends prepared. EPR particles are slightly smaller in a PP1R2 sample than those in a PP1R1 sample. A similar observation was also found in the PP2 system where R2 provided smaller particles than R1. The difference in rubber particle size in these blends can be explained in terms of differences in melt viscosity and viscosity ratio in the blends.

Table 4.5 -Falling weight impact fail energy, the temperature onset of crystallisation ($T_{c\ onset}$) and average particle size of EPR in the blends

Sample	Impact fail energy (J)	Tc onset (°C)	EPR particle size (μm)
PP1	3.64	114.6	-
PP1R1	5.94	113.5	1.04
PP1R2	6.82	113.4	0.82
PP2	1.91	118.3	-
PP2R1	2.84	116.4	1.05
PP2R2	3.45	116.2	0.86

In this study, the melt viscosity of the two grades of polypropylene and ethylene-propylene rubber were examined using a capillary rheometer under controlled conditions. Variation of viscosity with shear rate at 200°C for PP and EPR materials is shown in *Figure 4.22*. Similar behaviour was observed at 190 and 180°C (*Figures 4.23 and 4.24*). At any given temperature, viscosity decreased with increasing shear rate. Both of polypropylenes used in this work have a lower melt viscosity than that of EPRs. No crossover between PP and EPR curves occurs at any of the test temperatures used (200,190 and 180°C). PP1 has higher viscosity than PP2 at all test temperatures and shear rates. In case of EPR, at the lower shear rate (below 10^2 1/s) R1 has a lower melt viscosity than R2. However at the higher shear rate (above 10^2 1/s which is similar to shear generated by the extruder) the viscosity of R2 becomes lower.

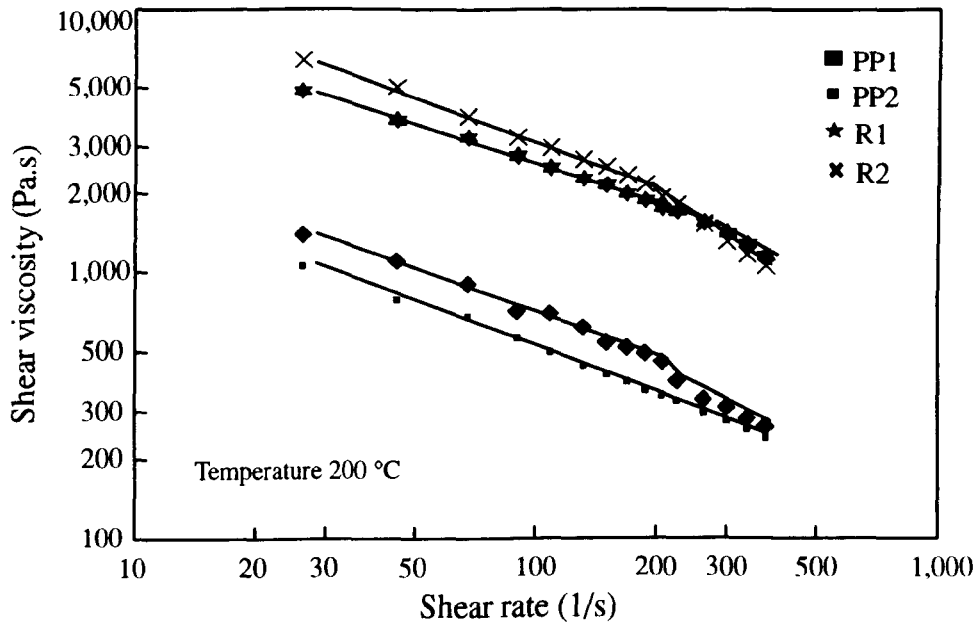

4.22

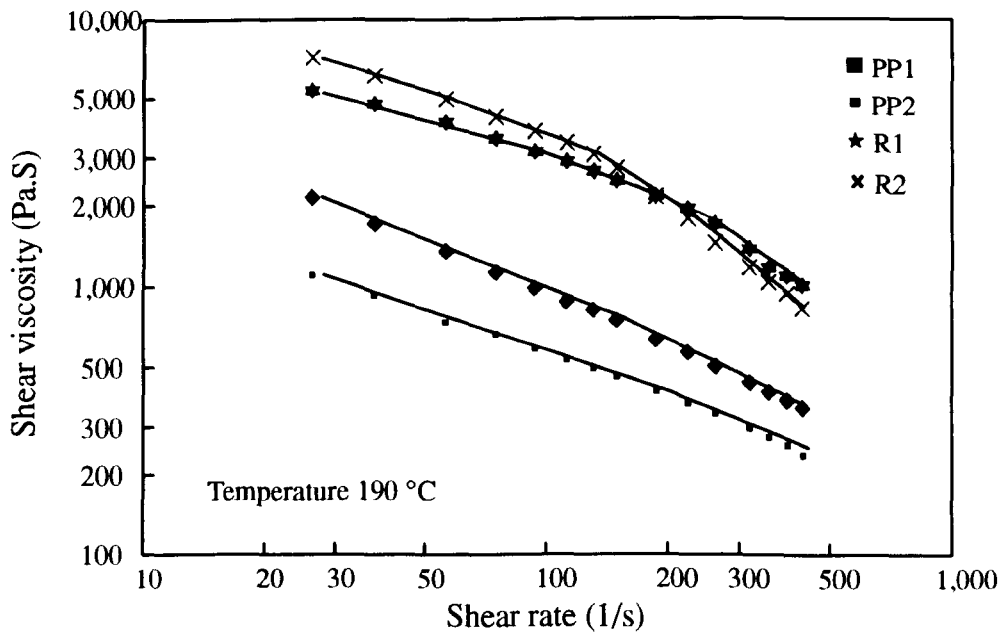

4.23

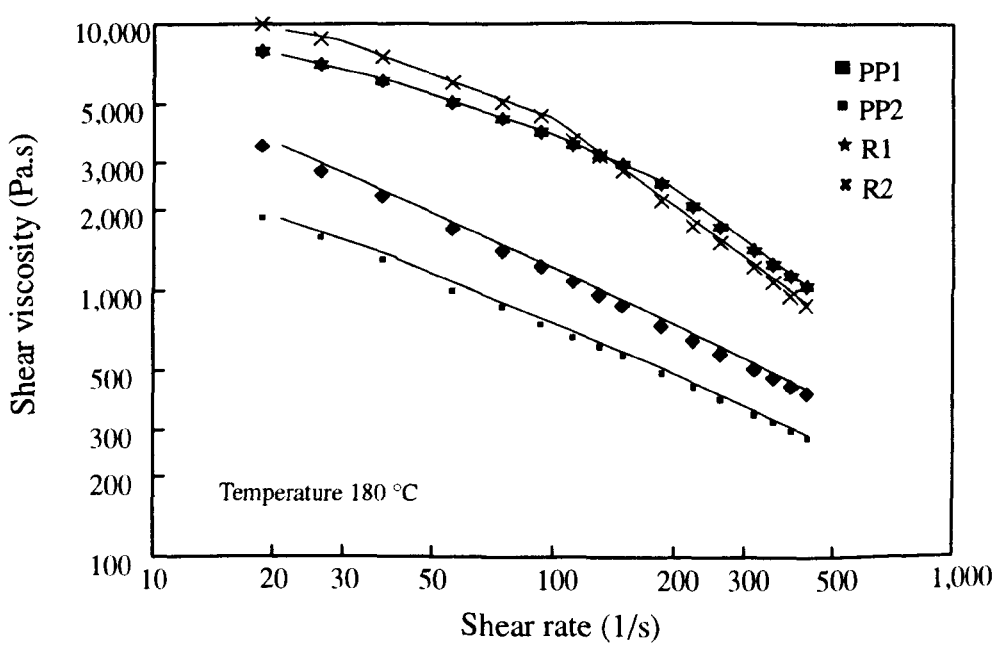

4.24

Figures 4.22-4.24 Shear viscosity as a function of shear rate of raw materials at 200, 190 and 180 °C.

It can be seen that for a given PP matrix, the rubber particle size decreased with decreasing its viscosity, e.g. in the PP1 system a lower melt viscosity R2 provides smaller particles than R1. This finding is in agreement with the work by Fortelny [65] where the efficiency of collisions of particles in the minor component was found to increase with a decrease in its melt viscosity, leading to a decrease in the particle size. Comparison between PP1 and PP2 systems, rubber particles in PP1 blends are smaller than those in PP2 blends.

From these results, it can be concluded that a rise in the viscosity of the polymer matrix leads to a decrease in rubber particle size while a rise in the viscosity of the minor phase causes an increase in particle size. Since both PP and EPR are considered viscoelastic, factors affecting particle size can be quantitatively described using Flumerfelts's equation [238].

$$D = K (\Omega / \tau) (\eta_d / \eta_c)^{\beta-1} \qquad (4.2)$$

where : D is critical drop break-up diameter

τ is shear stress

η_d and η_c are viscosity of continuous and dispersed phase, respectively

K and β are constants

Ω is interfacial tension

That relationship, which was derived from dimensional analysis of viscoelastic fluids under shear stress [239], implies that the particle size of the dispersed phase is proportional to the viscosity of the dispersed phase, and inversely proportional to the viscosity of the matrix phase. The present results are in agreement with this relationship.

(ii) Particle size effects in rubber toughening of polypropylene

In the present study, two grades of EPR with differences in melt viscosity were investigated. Both grades were found to be good impact modifiers for polypropylenes. However, R2 performs better than R1 in both PP1 and PP2 systems, as shown earlier in *Table 4.4*. The higher efficiency in toughening of polypropylene by R2 can be explained in terms of the rubber particle size effect. It has been reported for PP/EPDM blends that the phase morphology of small rubber particle size is more effective than with large particle size in toughening polypropylene [90]. The present results agree with this

statement. Speri and Patrick [31] similarly observed that impact strength of PP/EPDM blends was increased as the rubber particle size reduced. The mean rubber diameter of 0.3 μm appeared to be adequate. Dao [227] also reported that the rubber particle size of approximately 0.4 μm is favourable in PP/EPDM blends.

From the work of Jang [90] on rubber modified polypropylenes, it has been reported that $D \approx 0.5$ μm is the critical rubber particle size below which the particle could not nucleate crazes in polypropylenes. It has been suggested that the loss of craze nucleation efficiency of small particles were due to the small size of the stress concentration region being insufficient to accommodate the formation of craze with its characteristic structure.

In this investigation cavitation and shear yielding are the important mechanisms in toughening of polypropylenes. By comparison between R1 and R2, at fixed concentration (30%) R2 having smaller particles should provide extensive numbers of rubber particles in the blends and hence more sites for cavitation and less interparticular distances. These reasons may account for the better impact strength in the blends containing smaller rubber particles.

CHAPTER 5

STRUCTURE AND PROPERTIES OF GLASS BEAD FILLED POLYPROPYLENE

5.1 INTRODUCTION

The original purpose of adding fillers to polymers was primarily one of cost reduction. However, in recent years fillers are increasingly being utilised to fulfil some functional roles such as enhancing stiffness of polymers. Of all the fillers used for polypropylene, the bulk consists mainly of inorganic fillers such as talc and calcium carbonate. The influence of various inorganic fillers on the mechanical properties of polypropylene has been extensively studied [102]. Although a large number of theoretical equations have been proposed to explain and predict the mechanical properties of filled composites, there is no unifying theory allowing for a general prediction since there are many factors controlling the composite properties. Important parameters are, for example, particle size and shape, filler concentration and dispersion [102].

In this study, glass beads were chosen as the preferred filler for polypropylene due to their spherical shape and ease of dispersion. This is due mainly to the fact that mineral fillers such as calcium carbonate would lead to complications in the interpretation of result, especially in the three-phase composites, due to the problems of particle shape and possible agglomeration. This chapter describes the effect of glass beads on the microstructure and mechanical properties of polypropylene composites. The influence of bead particle size and composition were also considered. Various theoretical models were used to analyse the mechanical data. Greatest emphasis has been given to the relationships between the microstructure and properties of the filled composites.

5.2 COMPOUNDING AND CHARACTERISATION

Two grades of polypropylene homopolymer with differences in melt viscosity, were investigated. They are PP 1100HX and PP 1100L, having melt flow rates of 1.8 and 5.0 g/10 min, respectively. Two grades of glass beads used were 3000 CPOO and 5000 CPOO. Both grades are non-coated spherical glass, having different particle sizes. The 3000 CPOO grade has particle sizes in the range of 12-26 μm while 5000 CPOO has particles between 3.5 and 7.0 μm.

All composites were prepared in a BTS-40 co-rotating twin-screw extruder by melt-mixing polypropylene with various concentrations of glass beads. The extruder was operated at a screw speed of 100 rpm with a feed rate of 14 kg/hr and the barrel

temperature of 200 °C. The screw profile used was that designated as the "SM profile" described previously in Chapter 3 -section 3.4.

Samples for mechanical testing were prepared by compression-moulding. All prepared composites were dried for 12 hr at 90 °C in a vacuum oven prior to moulding, in order to remove water which might be on the extrudate surfaces. Tensile and falling weight impact measurements were conducted at room temperature (23°C) according to standard test methods mentioned earlier in Chapter 3. The composite morphology was studied using scanning electron microscopy (SEM). The effect of glass beads on nucleation and crystallisation behaviour of polypropylene was investigated using differential scanning calorimetry (DSC). A Rheometric Solids Analyser RSA II was used in determining molecular mobility of polypropylene in the filled composites. All techniques and testing procedures used were described in detail in Chapter 3.

5.3 RESULTS AND DISCUSSION

5.3.1 Microscopic studies

5.3.1.1 Characterising the dispersion in glass bead filled composites

The optimal use properties of filled composites cannot be achieved without a satisfactory dispersion of fillers in the polymer matrix. In this study the dispersion of glass beads in polypropylene composites was evaluated using SEM. *Figure 5.1* shows a cryogenic fractured surface of a polypropylene composite filled with 30 %vol of glass beads. The spherical glass bead particles were observed dispersed evenly in the matrix without evidence of agglomeration. The bead surfaces appear very smooth and clean.

5.3.1.2 Characterising the micromorphology of glass beads filled composites

The typical morphology of polypropylene homopolymer used throughout this study is a microspherulitic structure. *Figure 5.2* shows an optical micrograph, taken with crossed polars, of thin sections of an unfilled polypropylene sample where large spherulites were produced. The addition of glass beads into polypropylene caused greater formation of spherulites, as shown by a much more spherulites of smaller size in the filled specimen (see *Figure 5.3*).

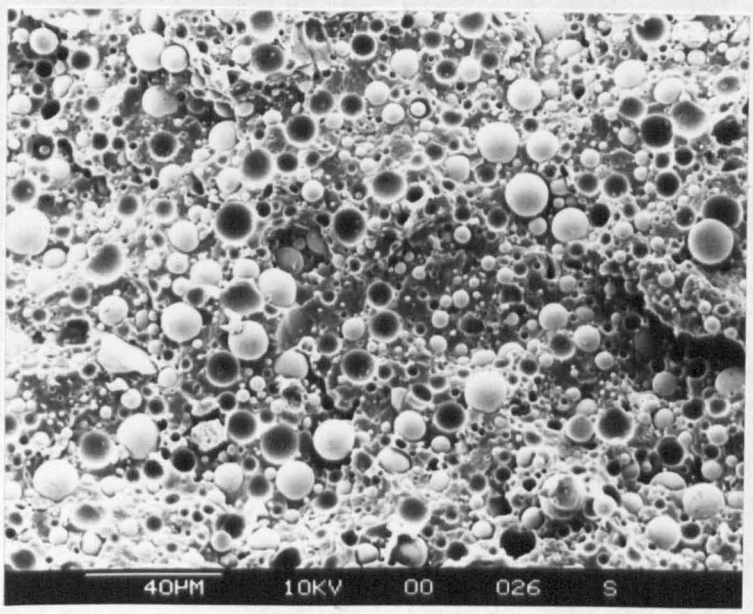

Figure 5.1 Cryogenic fractured surface of a PP composite filled with 30 %vol of glass beads shows the dispersion of glass beads in the matrix.

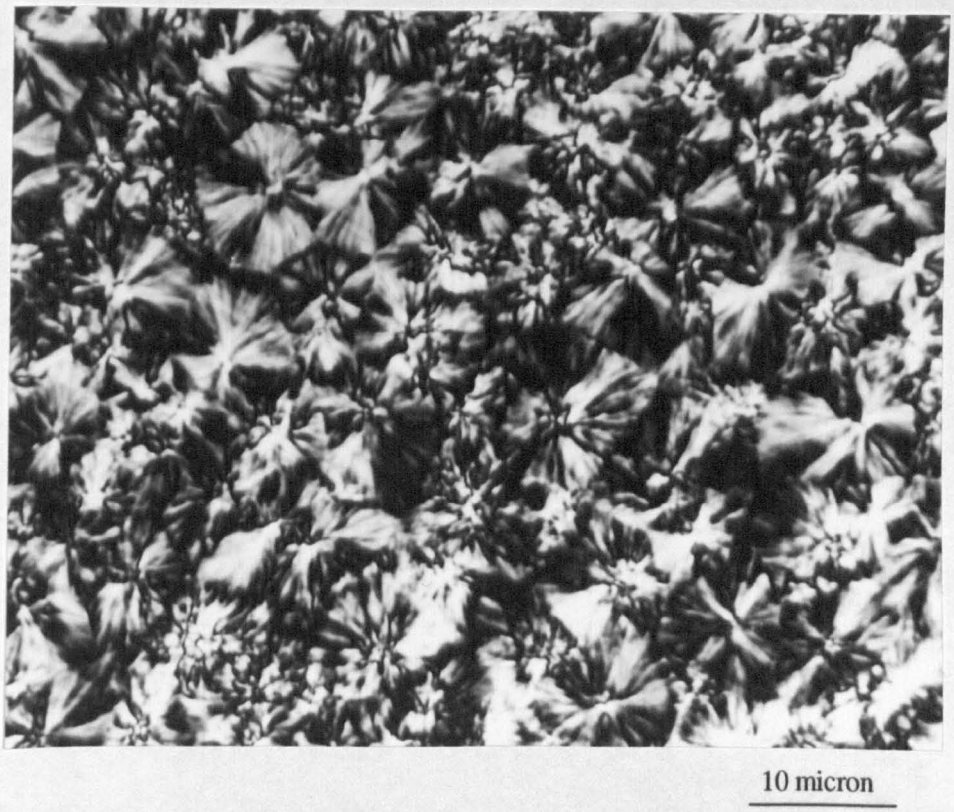

Figure 5.2 Optical micrograph of an unfilled polypropylene sample shows large PP spherulites.

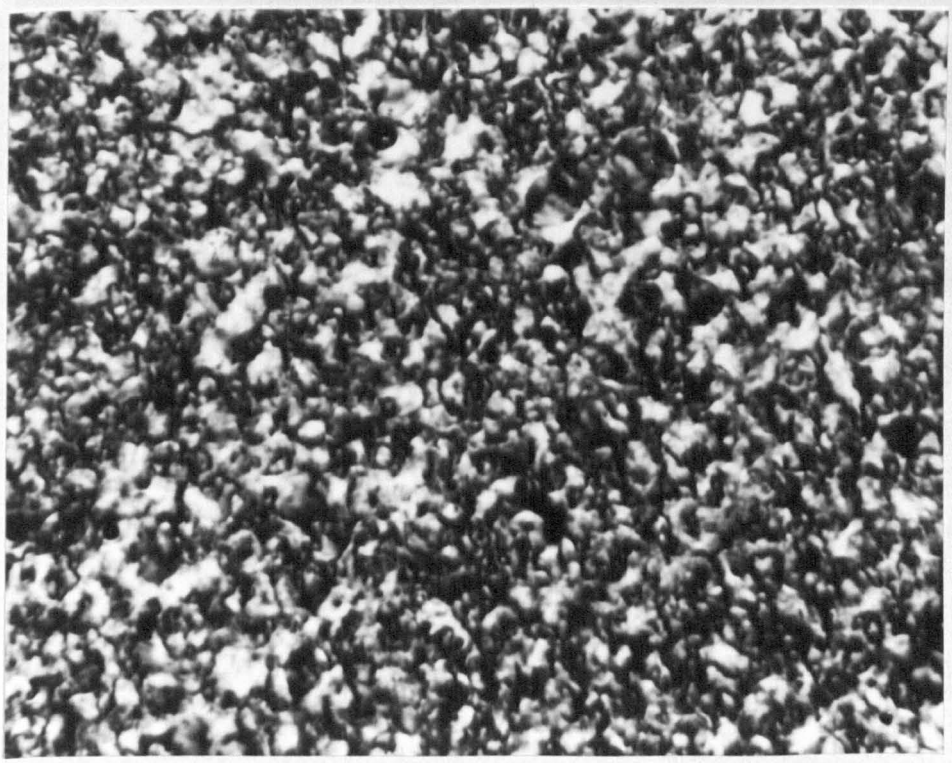

Figure 5.3 Optical micrograph of a PP composite filled with 20 %vol of glass beads shows smaller PP spherulites (compare to figure 5.2).

Due to the small spherulite size of polypropylene in the filled composites and high rigidity of the glass bead, the technique of microtomy and optical microscopy of thin sections as shown earlier is not beneficial in revealing the micromorphology of such filled composites. This, and the ability to resolve lamella morphology, makes the technique of permanganic etching [209-214] especially attractive for study microstructure in this composite system.

To reveal the spherulitic structure of polypropylene in glass bead filled composites, the compression-moulded surfaces were etched with a solution of 1 %wt potassium permanganate in concentrated sulphuric acid. The details of the etching procedure were reported earlier in Chapter 3 -section 3.8. From the preliminary evaluation of the effect of etching time on the morphology of PP/G composites, the results show that in the case of an unfilled polypropylene sample, hardly anything could be etched out even after being left for 3 hr in a permanganic solution, whereas in the filled sample the polypropylene spherulites can be revealed after 1 hr of etching. This indicated changes in the polypropylene crystalline phase after glass beads are being incorporated. Shown here in *Figure 5.4a* is a SEM micrograph of an unfilled polypropylene sample after being etched for 10 hr, showing large distinct spherulites with a diameter up to 15 μm. Comparison to an unfilled polypropylene, a glass bead filled sample (*Figure 5.4b*) shows a less regular spherulitic structure with less sharp spherulite boundaries. Also, the spherulite size of polypropylene in the filled composites was smaller than that in an unfilled polypropylene. A similar observation on the effect of fillers on spherulite size of polymers has been reported by many researchers [131, 241]. The glass bead particles were found to be engulfed by the growth of crystalline polypropylene rather than being forced outward to the spherulite boundaries, as observed in silicon dioxide filled polypropylene composites [256].

5.3.2 DSC Studies

5.3.2.1 Crystallisation and melting behaviour of polypropylene in the filled composites

The crystallisation and melting processes in the filled composites were studied by differential scanning calorimetry (DSC), according to the thermal treatment (heat-cool-heat cycle) mentioned previously in chapter 3 -section 3.7.

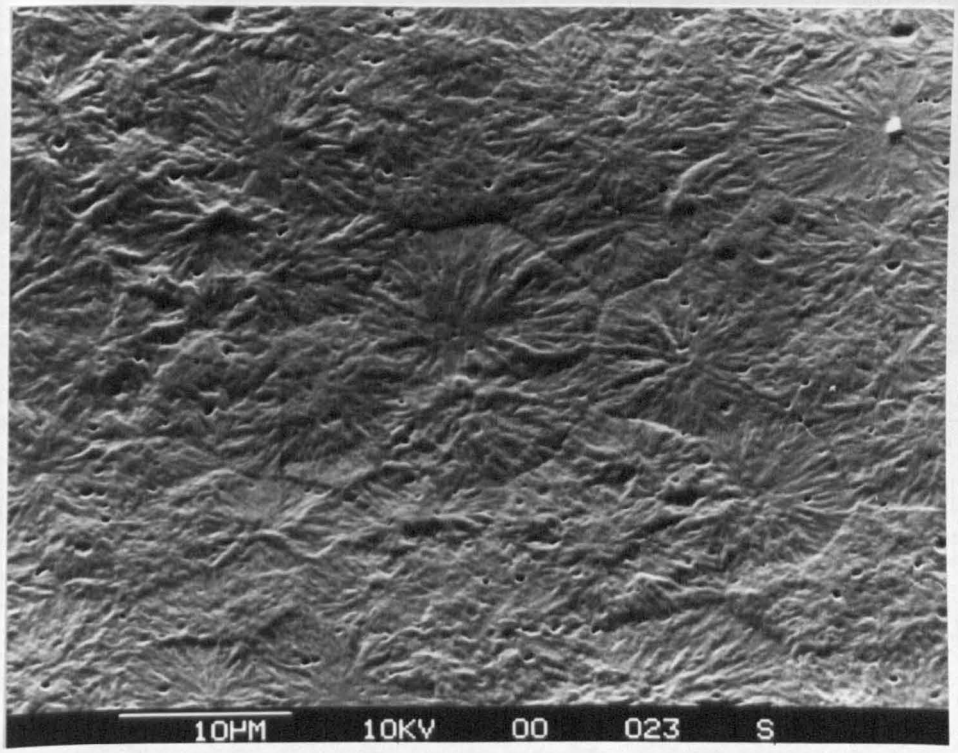

(a)

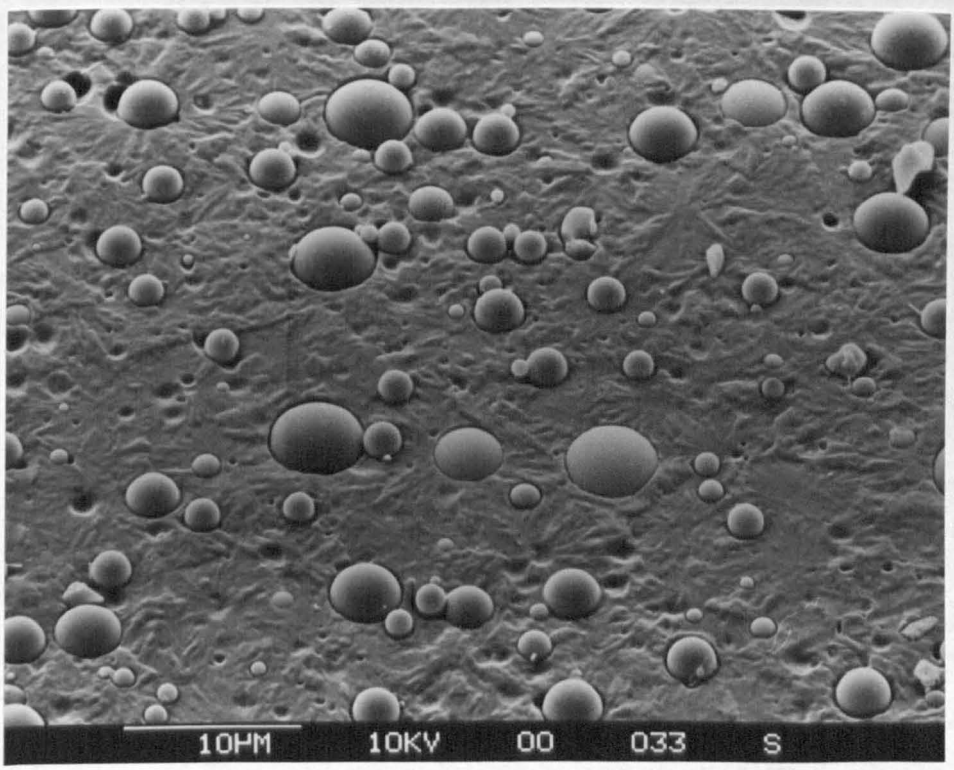

(b)

Figure 5.4 Scanning electron micrograph of fractured and etched surfaces of *(a)* an unfilled polypropylene after 10 hours of etching with a permanganic solution and *(b)* a 30 vol% glass bead filled polypropylene sample after 4 hours of etching.

Table 5.1 summarises the DSC results of an unfilled polypropylene (PP) and polypropylene composites filled with various concentrations of glass beads (PP/G). The incorporation of glass beads to polypropylene led to an increase in both $T_{c\ onset}$ and T_c values. As the concentration of glass bead increased, $T_{c\ onset}$ and T_c of polypropylene increased as shown in *Figure 5.5*. Greatest effect of the increasing in $T_{c\ onset}$ and T_c values was observed at the concentrations of glass bead up to 10 %vol. With further increasing the levels of glass beads (from 10 to 30 %vol) $T_{c\ onset}$ and T_c values still increased but less sharply. An increase in $T_{c\ onset}$ clearly indicated that the crystallisation started earlier in the filled composites than in an unfilled polypropylene. In other words, glass beads in this system act as nucleating agents promoting the crystallisation process. The nucleating effect of fillers on polypropylene crystallisation has been reported by a number of researchers [129-131]. The incorporation of glass beads also resulted in a decrease of T_1, defined as the difference between $T_{c\ onset}$ and T_c. T_1 is a parameter related to rate of crystallisation. A decrease in T_1 values implies an increase in the rate of crystallisation. However, to ensure that glass beads act as nucleating agents which increase the crystallisation rate in the filled composites, an isothermal experiment was performed, with results shown in the following section (5.3.2.2).

Figure 5.6a shows the effect of glass beads on the melting temperature of polypropylene in the composites. As the glass bead content in the composite increased, the melting temperature was found to decrease systematically. Apart from the melting temperature, degree of undercooling (T_2) was also reduced. This reduction in T_m and T_2 values implies that smaller spherulites are presented in the filled composites. Since by the presence of these small spherulites, having a lower heat capacity, the filled samples consequently show a lower melting temperature than the unfilled sample.

The observed crystallinity in the filled composites was also found to decrease compared to the unfilled polypropylene. As the concentration of glass beads increased, the composite crystallinity decreased monotonically as shown in *Figure 5.6b*. The reduction in the composite crystallinity was due to the substitution of PP by glass beads. No significant change in percentage crystallinity was found compared to PP when subtracting the wt.% of glass beads and recalculating percentage crystallinity only on the wt.% of PP in the composite.

Comparison of the two bead sizes examined shows no difference in the effect on the crystallisation behaviour of polypropylene phase in the filled composites as presented in *Table 5.2*.

Table 5.1

The temperature of onset of crystallisation ($T_{c\ onset}$), crystallisation temperature (T_c), heat of crystallisation (ΔH_c), melting temperature (T_m), percentage crystallinity, the difference between $T_{c\ onset}$ and T_c (T_1) and degree of undercooling (T_2) of an unfilled PP and glass bead filled PP (PP/G) composites

Composition of PP/G		$T_{c\ onset}$	T_c	ΔH_c	T_m	Crystallinity (%)		T_1	T_2
(by vol)	(by wt)	(°C)	(°C)	(J/g)	(°C)	exper.[a]	recal.[b]	(°C)	(°C)
100/0	100/0	113.8	108.1	95.1	163.8	48.5	48.5	5.7	55.7
90/10	76/24	117.3	113.0	79.5	162.1	40.6	37.1	4.3	49.1
80/20	59/41	117.7	113.5	58.9	161.2	29.9	28.7	4.2	47.7
70/30	46/54	118.3	114.2	44.2	160.5	22.2	22.1	4.1	46.3

[a] Percentage crystallinity obtained from the experiments.

[b] Recalculated percentage crystallinity based on the weight % of polypropylene in the composites.

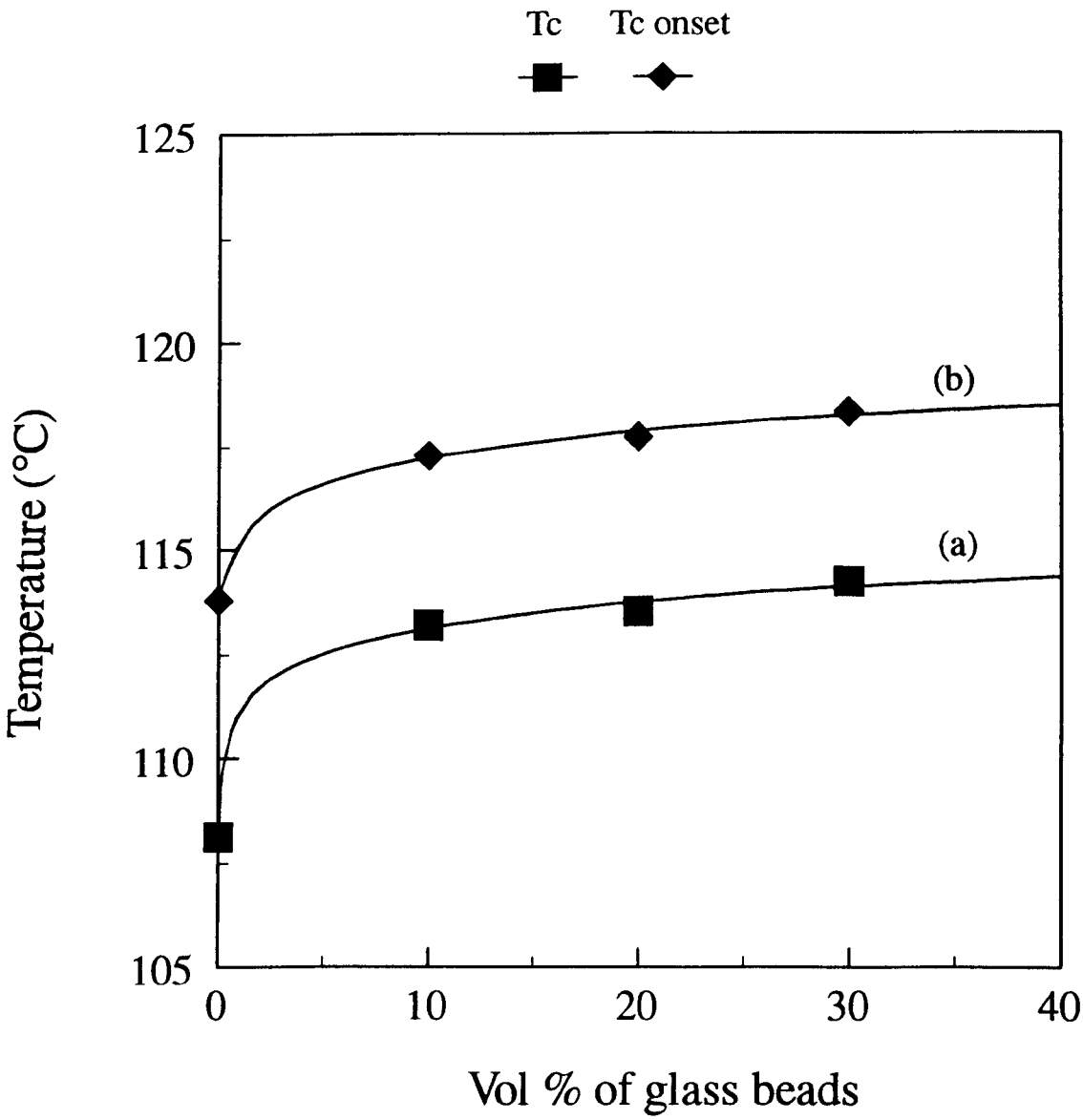

Figure 5.5 Dependence of the crystallisation temperature *Tc* (a) and the temperature onset of crystallisation *Tc onset* (b) on glass bead content

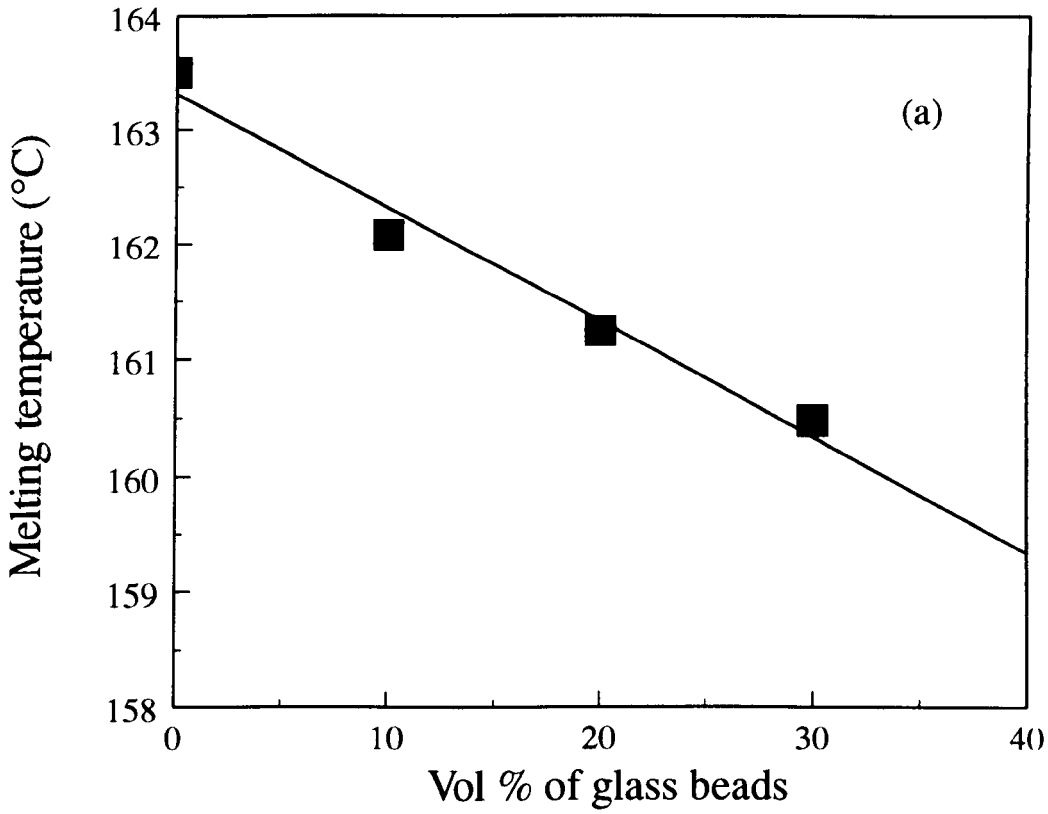

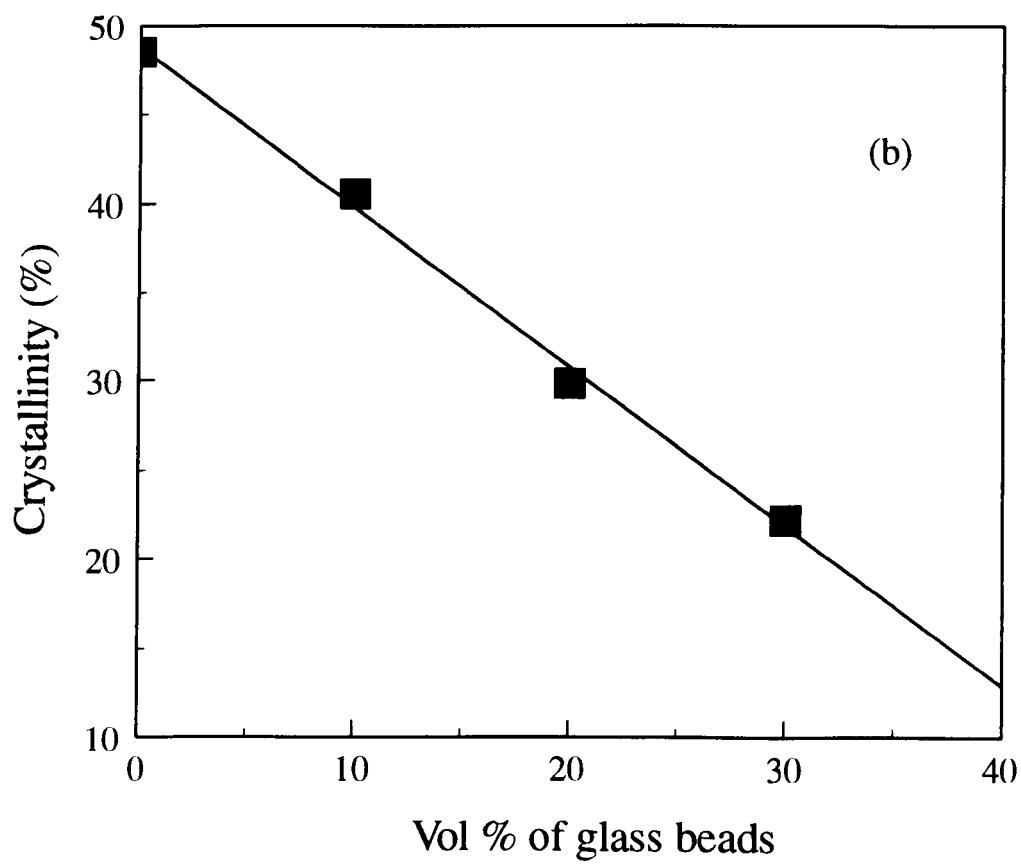

Figure 5.6 Dependence of the melting temperature *Tm* (a) and the crystallinity (b) on glass bead content

Table 5.2

Effect of glass bead size on the temperature of onset of crystallisation ($T_{c\ onset}$), crystallisation temperature (T_c), melting temperature (T_m), percentage crystallinity, the difference between $T_{c\ onset}$ and T_c (T_1) and degree of undercooling (T_2) in 60/40 % by weight PP/G composites

Sample	$T_{c\ onset}$ (°C)	T_c (°C)	T_m (°C)	Crystallinity (%)		T_1 (°C)	T_2 (°C)
				exper.[e]	recal[f]		
PP1[a]	114.6	109.2	163.3	48.9	48.9	5.4	54.1
PP1G1[c]	117.9	113.9	161.4	30.9	29.3	4.0	47.5
PP1G2[d]	117.9	113.7	160.9	31.2	29.3	4.2	47.2
PP2[b]	118.9	113.9	162.2	49.2	49.2	5.0	48.3
PP2G1	119.8	115.3	161.3	29.7	29.5	4.5	46.3
PP2G2	119.9	115.5	160.5	31.4	29.5	4.4	45.0

[a] Polypropylene Homopolymer Grade PP 1100HX, MFI 1.8 g/10min
[b] Polypropylene Homopolymer Grade PP 1100L, MFI 5.0 g/10min
[c] Spherical Glass Grade 3000CPOO, bead size 12.0-26.0 micron
[d] Spherical Glass Grade 5000CPOO, bead size 3.5-7.0 micron

[e] Percentage crystallinity obtained from the experiments.
[f] Recalculated percentage crystallinity based on the weight % of polypropylene in the composites.

5.3.2.2 Determination of crystallisation rate by DSC kinetic studies

The kinetics of isothermal crystallisation from the melt of glass bead filled composites was studied by differential scanning calorimetry, using the following procedure. The sample was heated to 200°C at 40°C/min and held at this temperature for 10 min, before being cooled to the controlled crystallisation temperatures ranging from 124° to 130°C.

The heat (dH/dt) evolved during the isothermal crystallisation was recorded as a function of time t, and the weight fraction X_t of material crystallised after time t was determined using the following relation :

$$X_t = \int_0^t (dH/dt)\,dt \Big/ \int_0^\infty (dH/dt)\,dt \qquad (5.1)$$

where the first integral is the crystallisation heat evolved at time t, and the second integral is the total crystallisation heat for $t = \infty$. In other words, $X_t = A_t/A$, where A_t is the area of exotherm on the curve from $t = 0$ to t, and A is the total area of the crystallisation exotherm.

From each crystallisation experiment the half-crystallisation time, t_{50}, was determined. t_{50} is the time taken by the sample to reach 50% crystallinity. *Figure 5.7* shows the half time of crystallisation (t_{50}) as a function of crystallisation temperature (T_c), for polypropylene composites of various glass bead contents. The values of t_{50} for a given T_c decrease with an increase of glass bead content, meaning that polypropylene composites with relatively high glass bead content take a shorter time to crystallise. This fact is in agreement with equation 5.2 that links the overall kinetic rate constant K_n with the spherulite growth rate G and the nucleation density N [242].

$$K_n = [4\pi\rho_c / 3\rho_a (1-\lambda_\infty)]\,[G^3N] \qquad (5.2)$$

with

$$K_n = \ln 2 / t_{50}^n$$

where : ρ_a and ρ_c are the density of amorphous and crystalline phases, respectively, λ_∞ is the overall crystallinity at time $t = \infty$ and n is an Avrami exponent. As the density of nucleation increases with an increase of glass bead content, whereas the variation of G is practically negligible, the values of t_{50} decrease (K_n increases) with an increase in glass bead content.

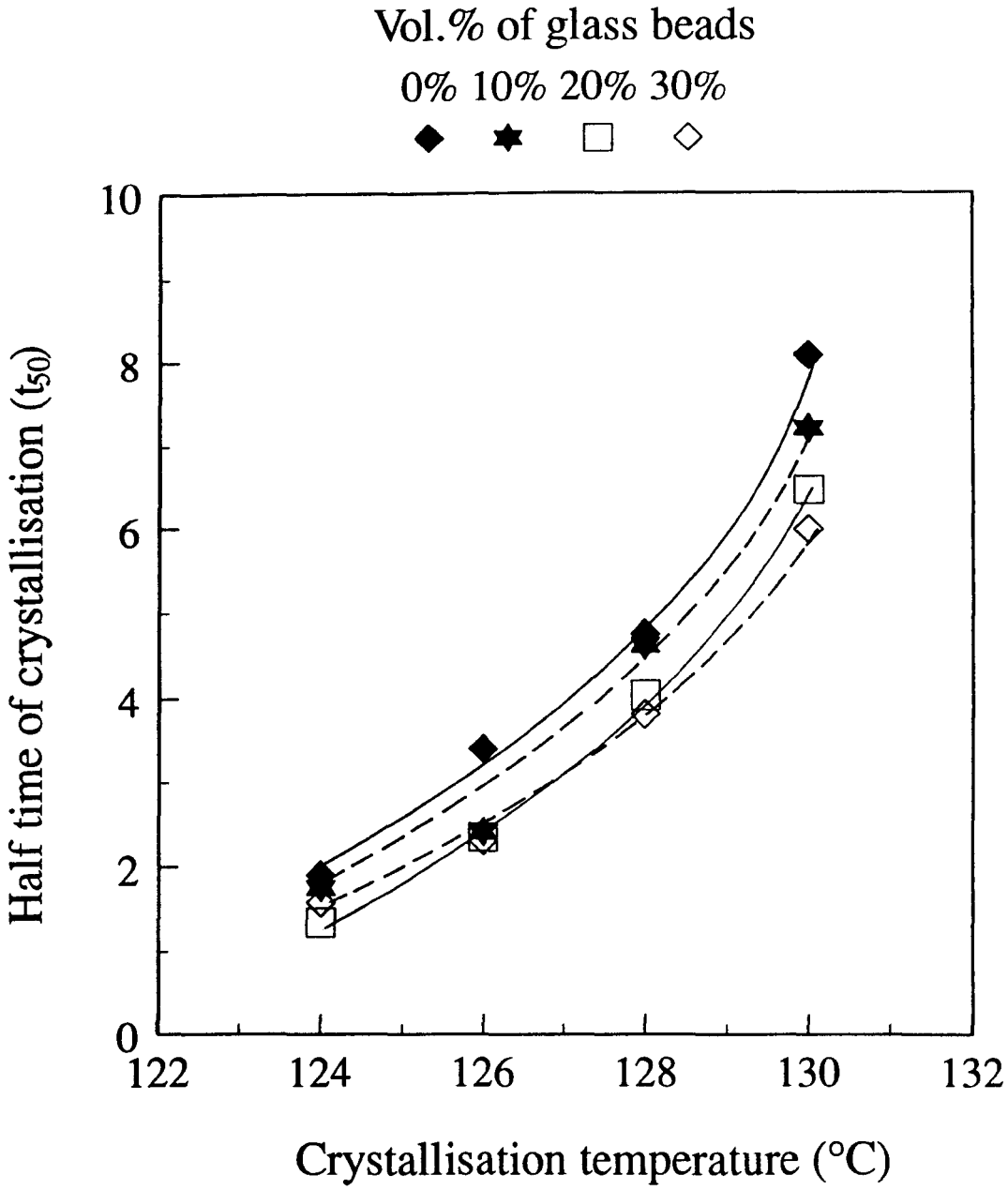

Figure 5.7 The half time of crystallisation as a function of crystallisation temperature

In *Figure 5.8* the quantity log[-log ($1-X_t$)] is related to log t, for unfilled PP and a PP/glass bead (70/30) composite. The plot shows a linear relationship for all samples and T_c investigated, indicating that the kinetics of bulk crystallisation follow the Avrami equation [243] :

$$\mathbf{1-X_t = exp\ (-K_n t^n)} \qquad \mathbf{(5.3)}$$

where X_t is the weight fraction of crystallisable material crystallised at time *t*, K_n is the overall kinetic rate constant including the parameters of the nucleus formation and crystal growth processes, and *n* is the Avrami exponent depending on type of nucleus and the growth geometry of the crystals. With spherulite (three-dimensional) crystallisation from the melt, generally $3 \leq n \leq 4$, with two dimensional crystallisation $2 \leq n \leq 3$, while with one-dimensional crystal growth $1 \leq n \leq 2$ [242]. Values of K_n and *n* may be calculated from the intercept and the slope, respectively, of the linear plot of log[-log($1-X_t$)] against log *t*. However, it is often difficult to estimate *n* from such plots because its values can vary with time. Significant deviations from the Avrami expression can be found. From the plot of *Figure 5.8* the *n* values for glass bead filled composites vary from 2.01 to 2.22. The values between 2.2 and 2.5 were reported in low and high-yield polypropylenes [247], whereas the values between 1.8 and 2.9 for glass-fibre reinforced polypropylenes [248]. The origin of the differences in *n* value is not completely clear. Non-integral values of *n* have been reported to be due variously to secondary crystallisation [258-259], a mixed nucleation mode [260] and changes in the radial density of crystallisation units [261].

Hoshino et.al. [244], studying the kinetics of isothermal crystallisation of polypropylene, have shown that their results could be interpreted on the basis of a two stage model of crystallisation characterised by a primary crystallisation with $n = 3.9$ and a secondary crystallisation with $n = 1.8$.

Secondary crystallisation is a nucleation process taking place on a pre-existing crystal surface. This process is similar to a primary crystallisation but differs somewhat because less new surface per unit volume of crystal is created than in the primary case [245]. According to literature [242, 246], the process of secondary crystallisation may result from the crystallisation of a more difficult crystallisable component and/or from an increase in the perfection of the existing crystallites following an annealing at T_c.

From these DSC results and from the earlier findings in SEM studies, it can be concluded that the incorporation of glass bead into polypropylene results in an alteration of the

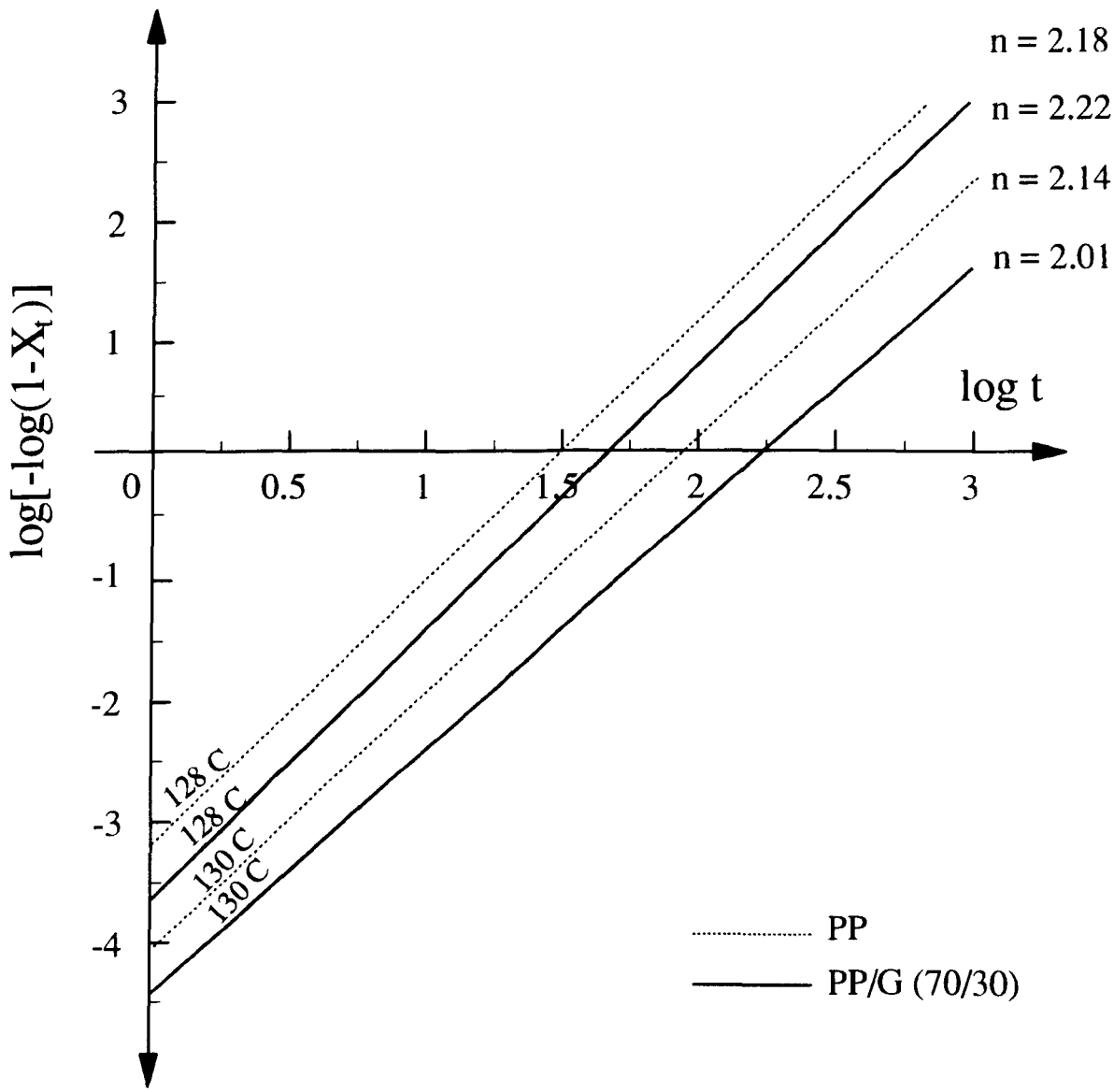

Figure 5.8 Avrami plot for unfilled and glass-bead filled polypropylenes crystallising from the melt at different indicated temperatures. The data points have been left off for clarity. The "n" value is slope of the graph.

crystallisation rate in the filled composites. Glass beads influence the rate of crystallisation of polypropylene by acting as nucleating agents, promoting the formation of crystal nuclei. If it is assumed that all nucleation occurring at time *t* develops at a rate equal to that in the unfilled polymer and the crystallisation stops when the leading edges of adjacent spherulites touch each other. Therefore, an increase in the number of nuclei by the presence of filler will lead to a decline in polypropylene spherulite size. This trend was similar to that observed in polypropylene composites filled with calcium carbonate [131] and titanium dioxide [241].

5.3.3 Influence of glass beads on the molecular mobility of polypropylene

Dynamic mechanical data of glass bead filled polypropylene composites at 1 Hz are shown in *Figures 5.9* to *5.12*. These include the storage (E') and loss (E") moduli and the damping (tan δ) as a function of temperature. *Figure 5.9* shows that the incorporation of glass beads resulted in an increase in E' and E" moduli of PP at all test temperatures. This observation indicated that glass beads enable the composites both to store more energy elastically and to dissipate more mechanical energy. As the concentration of glass bead increased, E' and E" values increased accordingly. The observed increase in E' and E" moduli can be explained by the reinforcing effect of a relatively rigid inclusion in the composites. No difference in E' values was observed in the composites prepared by using different size of glass beads as shown in *Figure 5.11*. However, glass beads with finer particle size (G2) seems to provide a composite of higher E" moduli than the coarser one (G1) in both PP1 and PP2 systems. This means the composite with finer beads can dissipate more energy than that with coarser beads. The changes in E" and tan δ values were reported to be proportional to the surface area of the filler [108]. Thus these changes should become more apparent with increasing filler concentration, or as the size of filler particles decreases since the effect should be due to changes in the polymer which becomes adsorbed onto the filler. Our results precisely prove this remark. The E" values were observed increasing as the glass bead concentration increased (*Figure 5.9*) and as the glass bead size decreased (*Figure 5.11*).

Figure 5.10 shows the tan δ peaks of PP composites containing 0-30 %vol glass beads, as a function of temperature. The glass transition temperature of polypropylene, defined as the temperature at the tan δ peak maxima, was clearly seen at about 6°C. This temperature changed neither with the volume fraction of glass bead nor its particle size (*Figure 5.10 and 5.12*). This indicated that glass bead has no effect on the mobility of

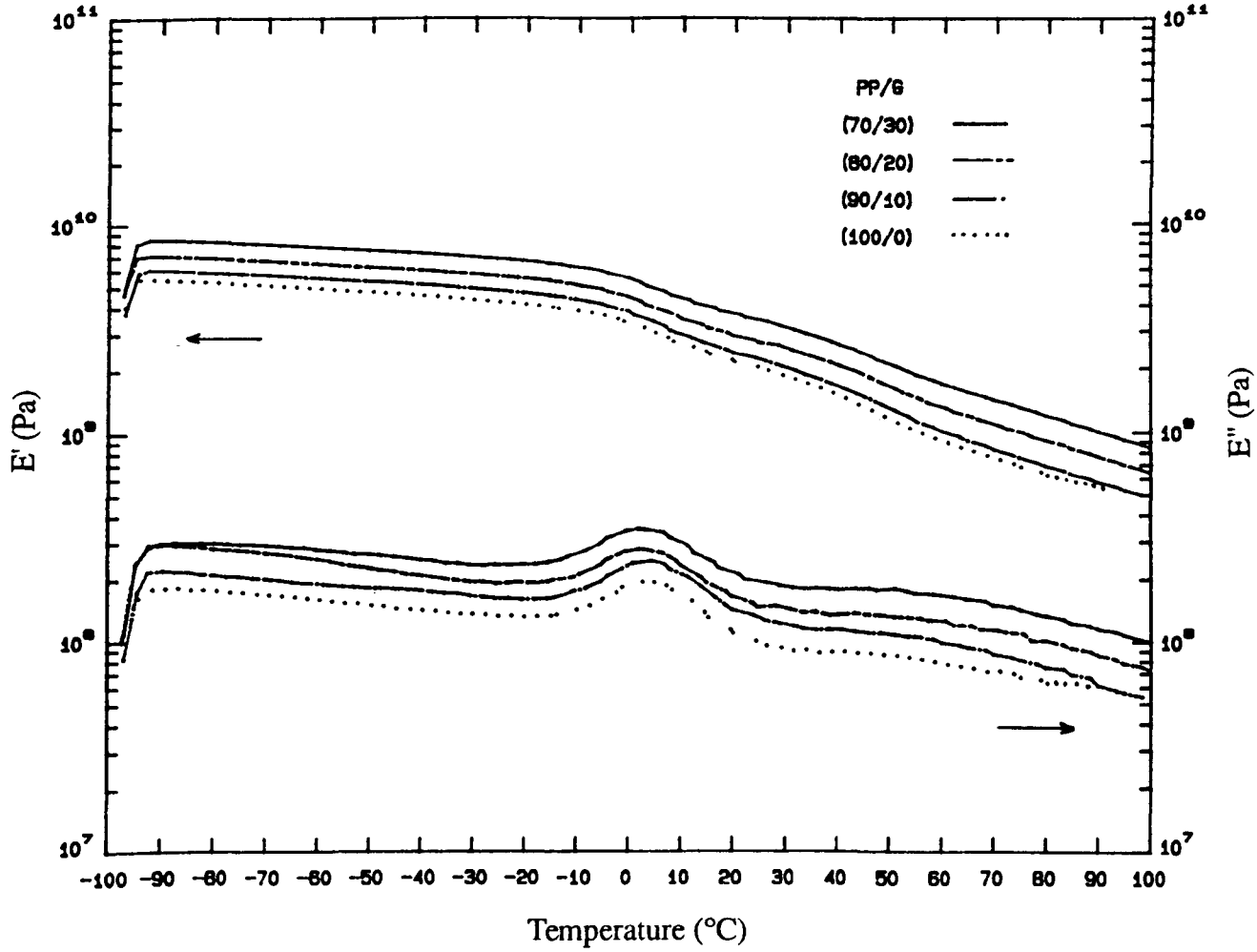

Figure 5.9 Effect of glass bead content on the storage (E') and loss modulus (E") of polypropylene

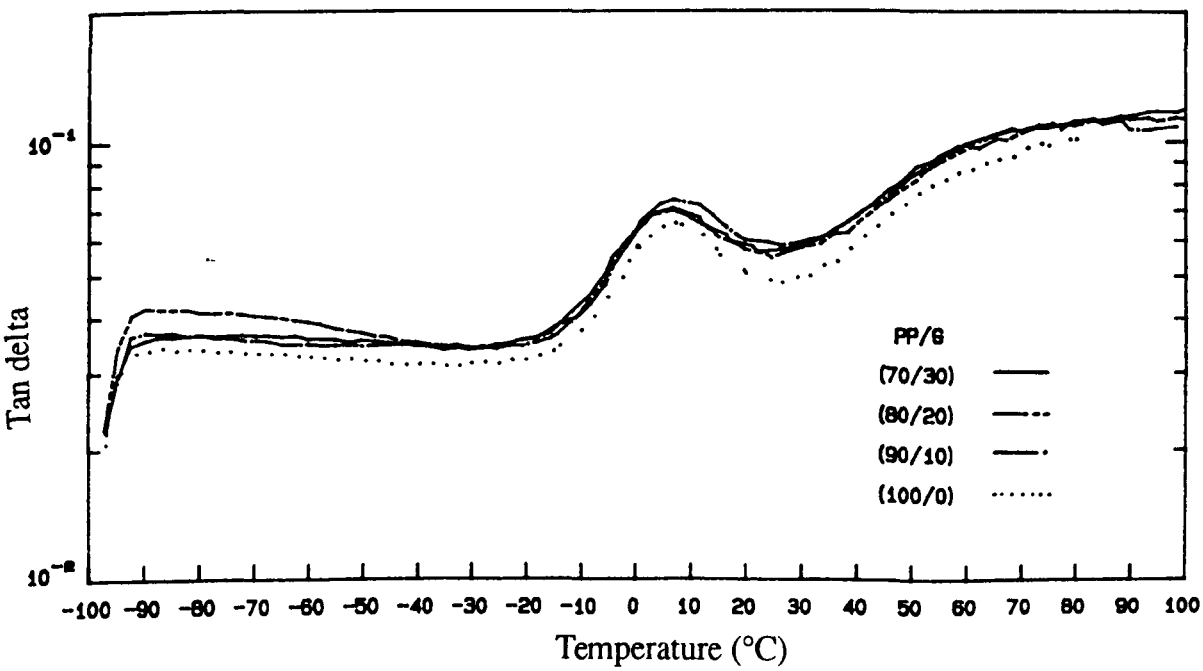

Figure 5.10 Effect of glass bead content on damping (tan delta) of polypropylene

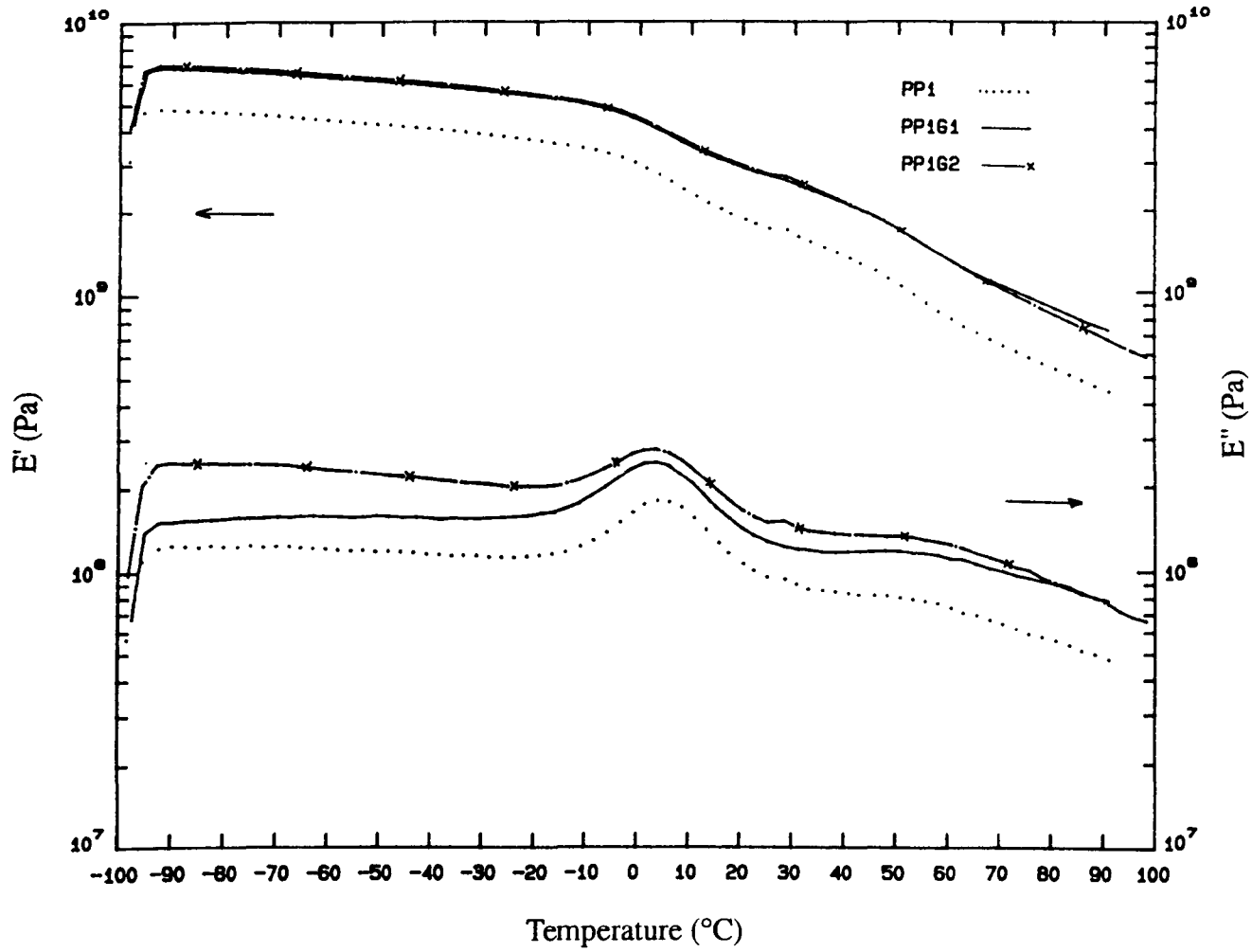

Figure 5.11 Effect of glass bead particle size on the storage (E') and loss modulus (E") of polypropylene

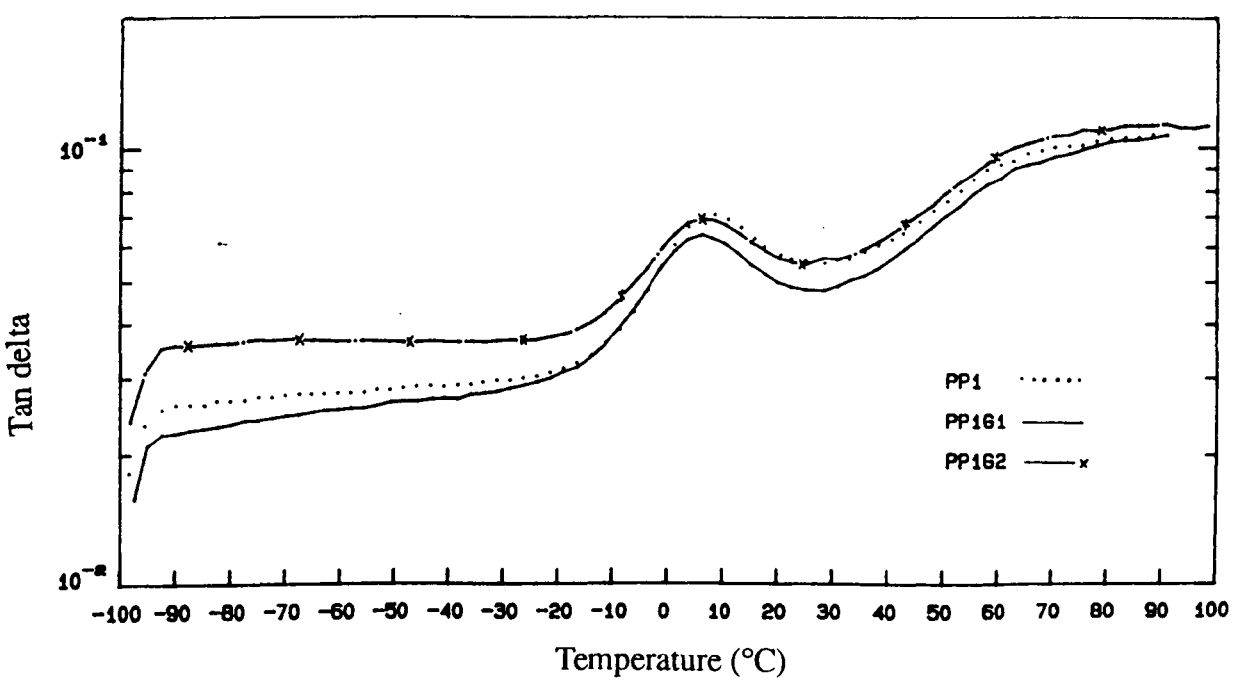

Figure 5.12 Effect of glass bead particle size on damping (tan delta) of polypropylene

polypropylene in the composites inferring a poor adhesion between glass beads and a polypropylene matrix. Similar results were also observed by Jancar [134] for calcium carbonate and magnesium hydroxide filled polypropylene composites.

Figure 5.10 shows the maxima in the damping curves to all occur at the same temperature. Generally fillers often decrease the damping as expressed by E"/E'; in which case the damping can be approximated by [108] :

$$E''/E' = (E''/E')_1 \phi_1 + (E''/E')_2 \phi_2 \qquad (5.4)$$

The damping of most rigid fillers is very low compared to that of the polymer, so $(E''/E')_2$ is nearly zero and can be neglected. However, in the composites examined in this study, the presence of filler increased damping. This can probably be attributed to the introduction of new damping mechanisms which are not present in the pure polymer [108]. These include : filler-polymer friction where there is essentially no adhesion at the interface, or excess damping in the polymer near the interface because of induced thermal stresses or changes in polymer conformation or morphology [108].

5.3.4 Mechanical properties of glass bead filled polypropylene composites

Frequently, the properties of polymers are modified by incorporating fillers. Properties of filled polymers were reported to be determined by a number of factors, for example filler particle size and size distribution, shape, content and interaction between filler and polymer matrix. In this part of work, some of these parameters (particle size and content of filler) were studied.

5.3.4.1 The dependence of tensile properties on glass bead content

Typical stress-strain curves for polypropylene filled with various concentrations of glass beads at 23°C and at strain rate of 50 mm/min are shown in *Figure 5.13*. Summaries of tensile results are given in *Table 5.3*. Data for unfilled polypropylene are included for comparison. In each case about 8 samples were tested, the mean values and standard deviations are given.

As seen in *Figure 5.13* at a certain applied stress level, the curves of all examined filled composites exhibit a distinct deviation of the linear elastic behaviour at about 13 MPa. This stress level was found to be practically independent of glass bead concentration, at

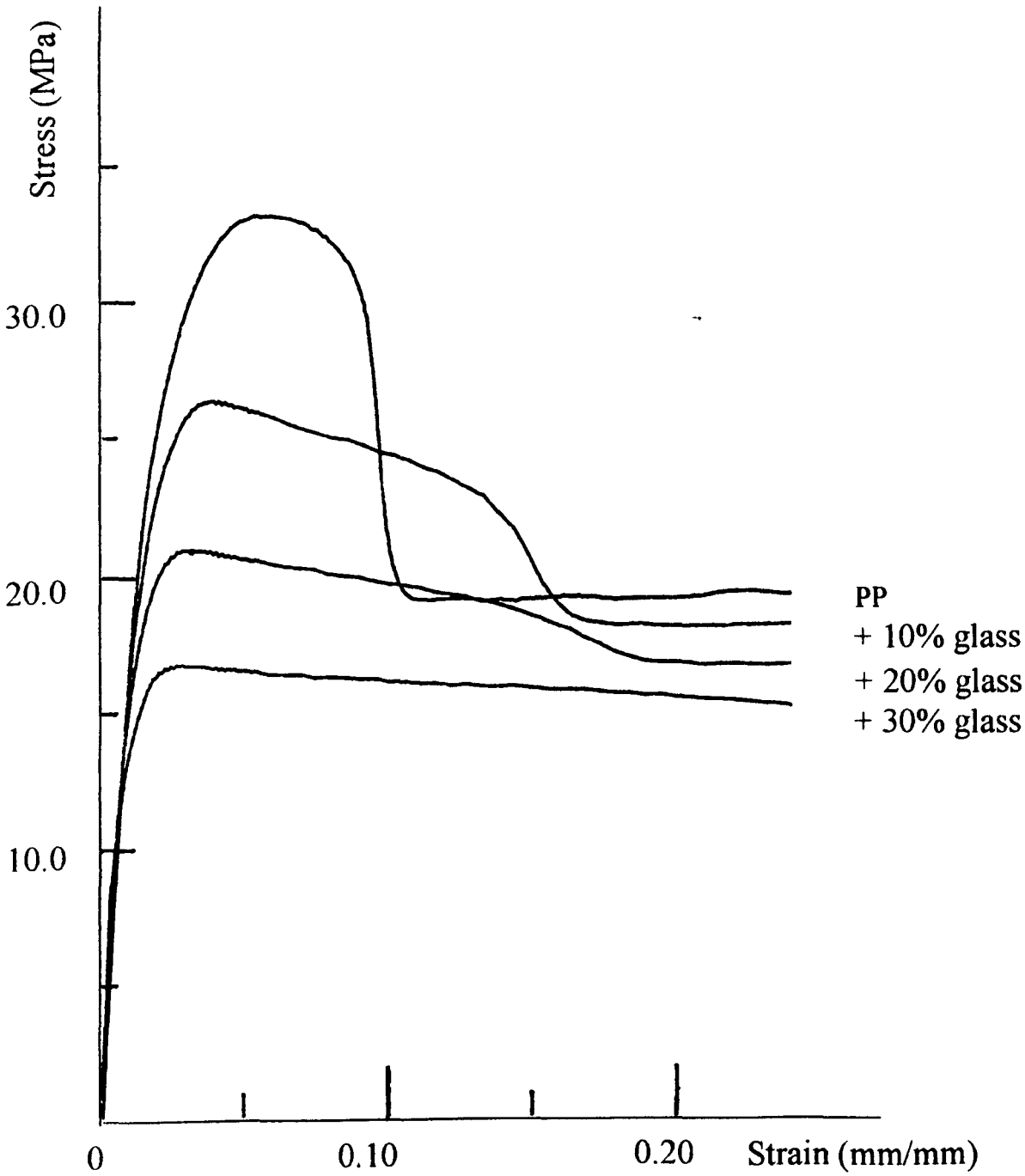

Figure 5.13 Typical stress-strain curve for polypropylene filled with various contents of glass-beads

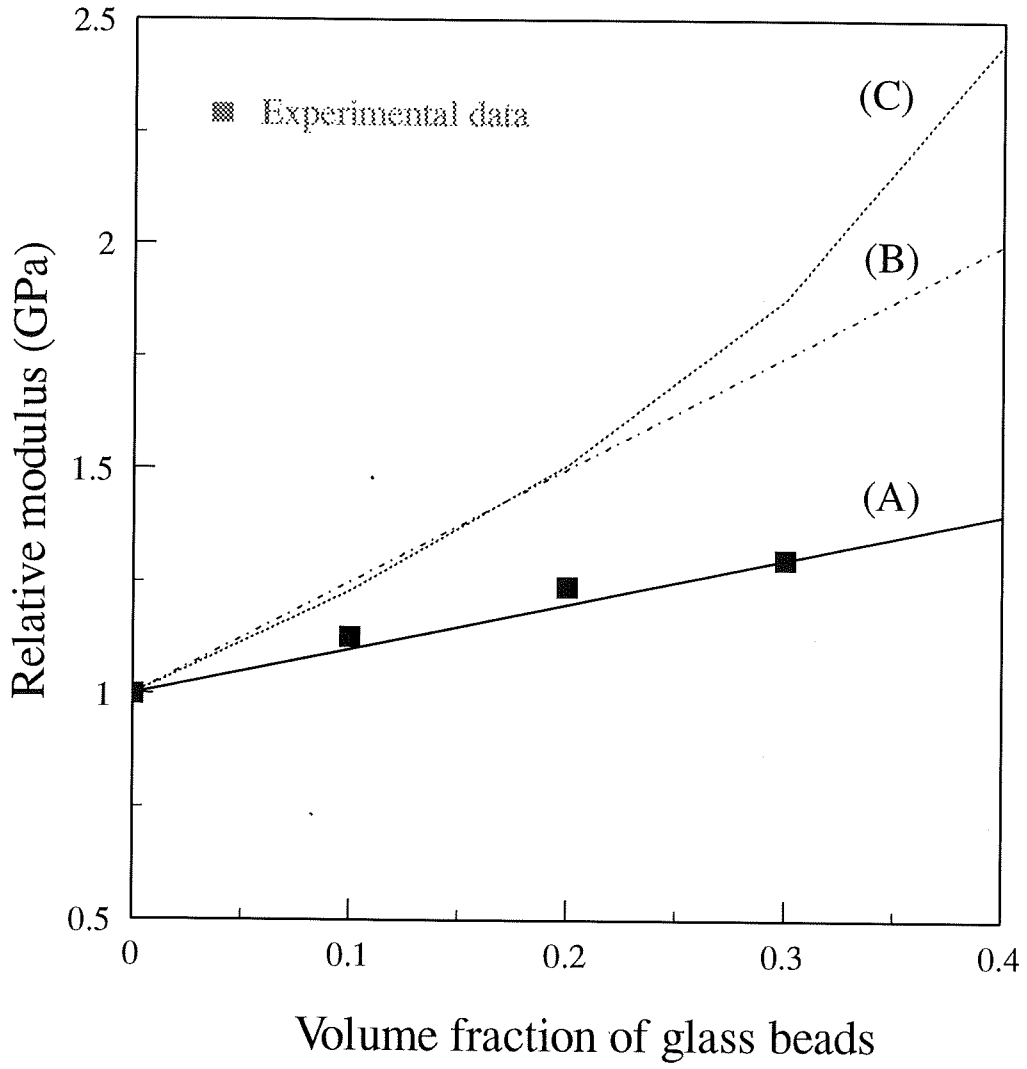

Figure 5.14 Comparison of experimental data with theoretical predictions for composition dependence of relative tensile modulus of glass bead filled polypropylene composites, where **curve A** represents Einstein's eq.(eq.5.5), **curve B** shows the modified Einstein's eq. (eq.5.6) and **curve C** is from Kerner's eq. (eq.5.7).

Table 5.3

Tensile yield strength, tensile modulus, elongation at break and falling weight impact fail energy at 23°C of various glass bead filled polypropylene composites

Composition PP/G (by vol.)	Yield strength (MPa)	Modulus (GPa)	Elongation at break (%)	Impact fail energy (J)
100/0	33.24 (0.30)[a]	1.72 (0.06)	146.9 (12.1)	3.64 (0.13)
90/10	25.78 (0.63)	1.95 (0.08)	11.7 (7.9)	1.85 (0.15)
80/20	20.72 (0.23)	2.20 (0.09)	27.76 (8.7)	1.83 (0.07)
70/30	16.57 (0.30)	2.23 (0.10)	33.34 (8.3)	1.60 (0.17)

[a] Standard deviations in parentheses, means from eight specimens.

least up to 30 % of volume. A similar observation was reported by Dekkers and Heikens [249] for glass bead filled polystyrene composites, where the critical stress level at which the curves deviated from the linear elastic behaviour was found to be lower for poor adhering beads compared with excellent adhering ones : for poor adhesion the deviation begins at about 13 MPa and for excellent adhesion at about 20 MPa.

In comparison to glass bead filled composites, unfilled polypropylene shows yielding as seen in *Figure 5.13*. Addition of glass beads into polypropylene caused a reduction in both yield and necking stresses. A similar observation also observed in glass bead filled ABS systems [254]. As the concentration of glass beads increased the reduction became pronounced. This observation was contradictory to that observed in calcium carbonate filled polypropylene composites [250]. Generally, fillers often introduce yield points in the stress-strain curves [108]. The yield phenomenon in filled composites may be due to a crazing effect or to a dewetting effect in which the adhesion between the filler and matrix phases is destroyed. However, in the present system under discussion, at high stresses the unfilled polypropylene shows a well-defined yielding but the composite filled with high concentration of glass beads (30 %vol) passes through a broad maximum with little change in stress level. After this region of zero slope is attained, the sample continued to elongate with no further change in appearance and no necking.

The incorporation of glass beads increased the modulus of the composites, as measured from the initial slope of the stress-strain curves. As the concentration of glass beads increased, the composite modulus increased accordingly. The variation of relative tensile modulus (E_c/E_m) with volume fraction of glass beads is shown in *Figure 5.14*. The raw data of composite properties are summarised in *Table 5.3*.

The modulus data were compared with some theoretical predictive models for two phase composites. Curve A of *Figure 5.14* is the plot of Einstein's equation for the filled composites without adhesion [108,252,253]

$$E_c/E_m = 1 + \Phi_f \qquad (5.5)$$

where E_c and E_m are modulus of the composite and matrix, respectively. Φ_f is the filler volume fraction. Curve B represents the modified Einstein's equation for the system with some adhesion between rigid spheres and the polymer matrix [111].

$$E_c/E_m = 1 + 2.5\,\Phi_f \qquad (5.6)$$

Curve C exhibits the plot of Kerner's equation [114] expressed by

$$E_c/E_m = 1 + \{15\,(1-\upsilon_m) / (8-10\Phi_f)\}\,\{\Phi_f / (1-\Phi_f)\} \quad (5.7)$$

where υ_m is Poisson's ratio of polypropylene. In this work υ_m of 0.27 [148] was used for the calculation.

As shown in *Figure 5.14* the data for glass bead filled polypropylene fits conveniently with Einstein's model without adhesion (eq. 5.5). The agreement between the experimental results and the no adhesion model seems quite expected since there is no chemical interaction between glass beads and polypropylene in this system.

The yield strength of these composites was also found to decrease as the concentration of glass bead increased as shown in *Figure 5.15* and *Table 5.3*. This reduction in yield strength is simply a reflection of the decreased cross-sectional area of the polymer bearing the load. To analyse the dependence of composition on the composite strength, some of the most commonly used theoretical predictive models, were undertaken. An estimate of the lower bound response for tensile strength proposed by Nielsen [108] is shown in eq. 5.8 where the filled composite strength (σ_c) can be calculated by

$$\sigma_c = \sigma_m (1- \phi) S \quad (5.8)$$

where σ_m is the tensile strength of the matrix and ϕ is the volume fraction of filler in the composites. The parameter *S* was introduced to account for the weakness in the structure brought about by a discontinuity in stress transfer and the generation of stress concentration at the filler-polymer interface. The maximum value of *S* is unity for " no stress concentration effect". The lower the *S* value, the greater the stress concentration or poorer the adhesion.

Equation 5.9 was introduced by Nicolais and Nicodemo [117]. The strength of filled composite was expressed by :

$$\sigma_c = \sigma_m (1- a\phi^b) \quad (5.9)$$

where *a* and *b* are constants. The value of *a* is related to the stress concentration or the quality of adhesion between the matrix and filler and *b* is related to the geometry of the filler. For spherical fillers with no adhesion, uniformly distributed, *a* becomes 1.21. For the case of some adhesion, *a* becomes smaller than 1.21. The constant *b* is equal to 1 if

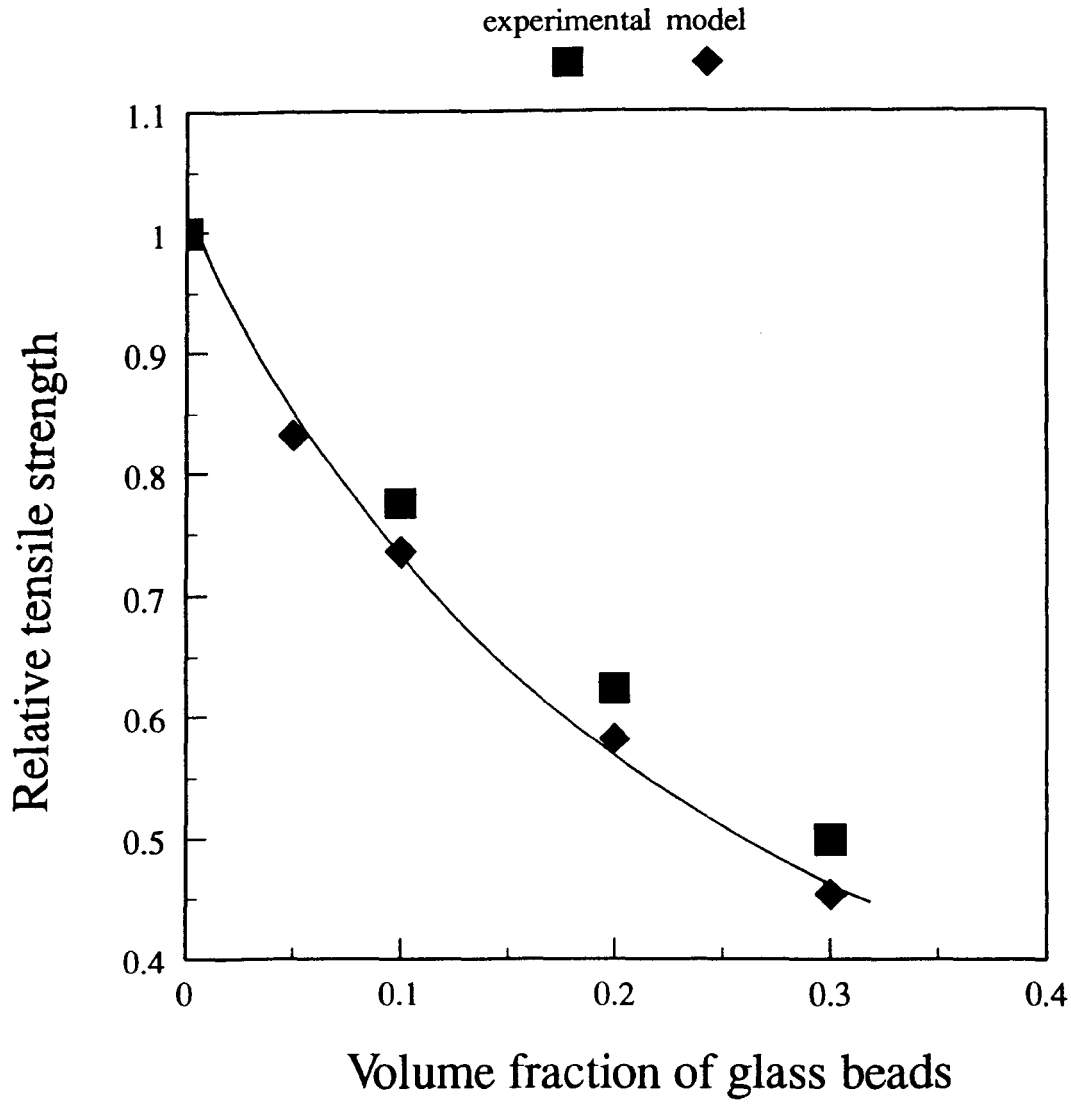

Figure 5.15 Comparison of experimental data with theoretical prediction using Nicolais's model (eq.5.10) for glass bead filled polypropylene composites

the material fails by planar fracture and 2/3 if it fails by random fracture. Thus eq. 5.9 can be modified as

$$\sigma_c = \sigma_m (1 - 1.21\phi^{2/3}) \qquad (5.10)$$

Using suitable values of S and a at each individual concentration, some degree of agreement can be obtained between tensile strength data and the theoretical models by both Nielsen [108] and Nicolais and Nicodemo [117]. *Table 5.4* summarised the calculated values of stress concentration parameters, S from eq. 5.8 and a from eq. 5.9 in glass bead filled polypropylene composites.

Table 5.4 Values of stress concentration parameters, S (from eq.5.8) and a (from eq.5.9) in various PP/G composites

Glass beads (vol%)	σ_c/σ_m	S	a
0	1	1	1
10	0.78	0.86	1.03
20	0.62	0.78	1.09
30	0.50	0.71	1.11
Mean value	-	0.78	1.08

It can be seen that calculated stress concentration values are less than one according to Neilsen's model (eq. 5.8) and greater than one according to Nicolais-Nicodemo's model (eq. 5.9). Both results indicate a weakness or poor adhesion between filler and polymer matrix. However, the a values calculated from eq. 5.9 were less than 1.21 indicating stress transfer between filler and polypropylene is present in this system. A close fit with experimental results was obtained using eq 5.9 by letting a = 1.08 and b = 2/3.

Comparison of the experimental data to relative tensile strength values calculated from eq. 5.10 are presented in *Figure 5.15*. These results also confirmed that there is some stress transfer between polypropylene and glass beads since the experimental data points lie above the lower bound curve calculated using eq. 5.10. The same observation was reported by Faulkner for a similar system [255].

The ultimate elongation of the filled composites was also found to decrease as glass beads were added, as shown in *Table 5.4*. This is expected since all the elongation in the filled composites arises from the polymer matrix if the filler is rigid [108]. However, in contrast to theoretical predictions, as the glass bead concentration increased (from 10 to 30 %vol) the ultimate elongation of glass bead filled polypropylenes was found to increase slightly. This phenomenon has been observed earlier by Nicolais et.al. [254] where the ultimate elongation of ABS/glass bead system increased with the concentration of glass beads.

The increase in elongation of the filled composites may be explained if one can assume that fillers introduce craze and perhaps at the same time act as stoppers to crack growth [108]. It is known that the rubber phase can act as a stress concentrator to initiate crazes and assist in the terminating process. A similar process may also occur in this system. The stress concentration effect in the filled composites can be seen by a stress-whitening all along the specimen. *Figure 5.16* shows a picture of tested specimens, with and without glass beads, after fracture. The sample shows a stress-whitening over the whole gauge length while the unfilled one does not.

5.3.4.2 The dependence of tensile properties on bead particle size

Several models and equations have been developed to describe the Young's modulus of filled composites. These all consider that the elastic moduli of a composite material does not depend on the particle size of filler, but only on the volume fraction of filler. Unexpectedly, however, experiments generally show an increase in composite modulus as the filler particle size decreases. Experimental results from this study are in agreement with this statement.

The modulus of various glass bead filled polypropylenes is shown in *Table 5.5*. It can be seen that the Young's modulus of the filled composites tend to be higher with decreasing bead size, i.e. composites with finer bead particles (PP1G2) have a slightly higher modulus than the composite containing coarser particles (PP1G1). Apart from Young's modulus, strength of the composites also increased as the bead size decreased.

Several possible reasons for this discrepancy between theory and experiment have been reported by Nielsen [108], including changes in the surface area and particle agglomeration. However, the explanation for the glass bead system can be derived as

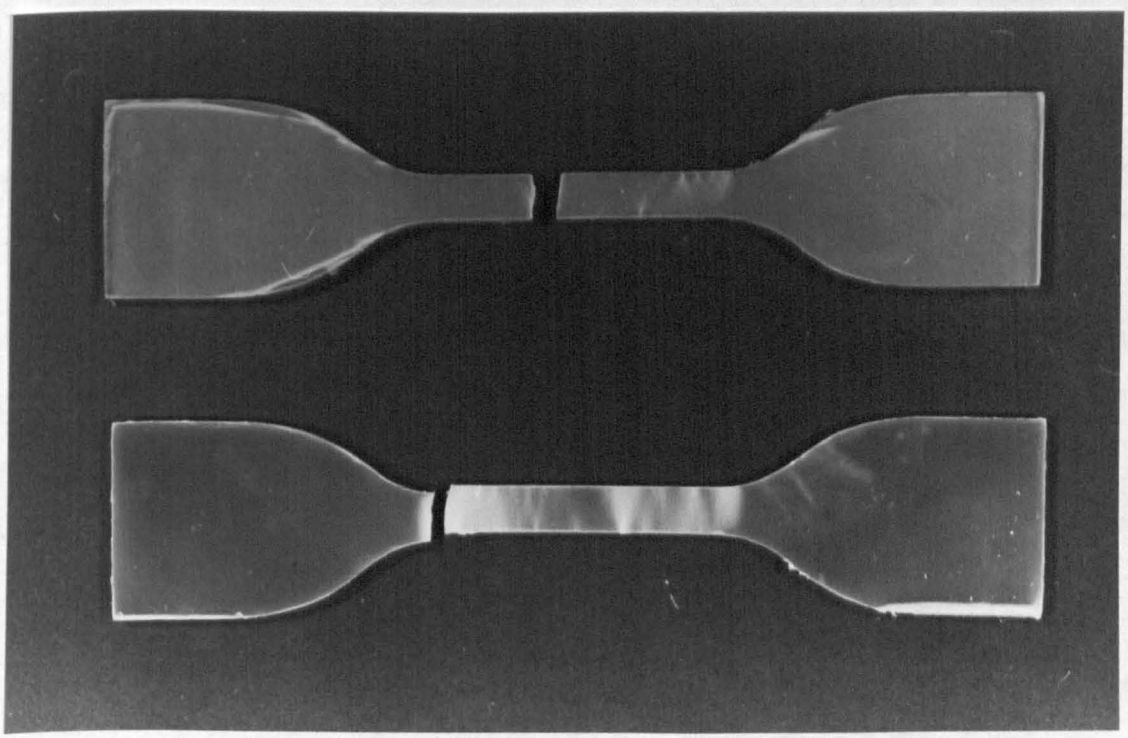

Figure 5.16 Tensile tested-specimens of (a) unfilled and (b) polypropylene filled with 20 %vol glass beads

Table 5.5

Tensile yield strength, tensile modulus and falling weight impact fail energy at 23°C of various glass bead filled polypropylene composites

Sample	Yield strength (MPa)	Modulus (GPa)	Impact fail energy (J)
PP1[a]	33.24 (0.30)	1.78 (0.03)	3.64 (0.11)
PP1G1[c]	21.31 (0.45)	2.04 (0.04)	1.31 (0.22)
PP1G2[d]	22.95 (0.42)	2.11 (0.03)	1.91 (0.18)
PP2[b]	31.97 (0.56)	1.80 (0.03)	1.91 (0.09)
PP2G1	21.02 (0.41)	2.17 (0.01)	1.10 (0.21)
PP2G2	21.46 (0.38)	2.21 (0.05)	1.45 (0.07)

[a] Polypropylene Homopolymer Grade PP 1100HX, MFI 1.8 g/10min
[b] Polypropylene Homopolymer Grade PP 1100L, MFI 5.0 g/10min
[c] Spherical Glass Grade 3000CPOO, bead size 12.0-26.0 micron
[d] Spherical Glass Grade 5000CPOO, bead size 3.5-7.0 micron

follows : (i). As the bead size decreases, surface area of the particle increases. Thus, if the polymer is changed in some manner at the interface, as by adsorption, the composite properties should change in relation with particle size due to the change in surface area. (ii). The filler particles can act, as in the case of crystalline materials, as a nuclei for the crystallisation process and are therefore surrounded by a layer of polymer with an increased modulus. As the particle size decreases the filler surface area increases, therefore greater nucleation occurs in the crystallisation process leading to an increase in a number of higher modulus layers in the composite.

5.3.4.3 Effect of glass beads on impact properties of polypropylene composites

Falling weight impact fail energy of polypropylene composites filled with various concentrations of glass beads is given in *Table 5.3* (p.106). By the incorporation of 10 %vol of glass beads the impact strength reduced drastically from 3.64 J in an unfilled polypropylene to 1.85 J in a (90/10) PP/G composite. With further increase the glass beads contents (from 10 to 30 % vol), no significant difference in the impact strength was observed. The relative impact strength values (I_c/I_p) of various glass bead filled composites are presented in *Figure 5.17*, as a function of glass bead contents. The reduction in composite toughness when filler is incorporated, is as expected. However, as pointed out theoretically the particle size and nature or dispersion of filler, has little influence on this phenomenon. In the present study, the greater reduction in impact strength was observed in the polypropylene composites of coarser bead size. As shown earlier in *Table 5.5*, the composites with glass beads code G1 show a lower impact energy than those with glass beads G2, for both PP1 and PP2 systems.

(i) Fracture mechanisms in glass bead filled composites

Fracture processes in glass bead filled polypropylene composites were investigated by considering the progress of a crack through the composite material. In polymers, two basic deformation mechanisms can be distinguished : crazing and shear yielding. In heterogeneous polymer systems, an addition mechanism of dewetting is frequently observed. Polypropylene deforms almost exclusively by shear yielding [54]. Extensive dewetting takes place in its filled composites as shown in *Figure 5.18*. Experimental results demonstrate that the crack travels through the polypropylene matrix and, instead of going through glass bead particles (*Figure 5.19a*), the crack path deviates to travel along the interfaces between polypropylene and glass bead particles (*Figure 5.18 and*

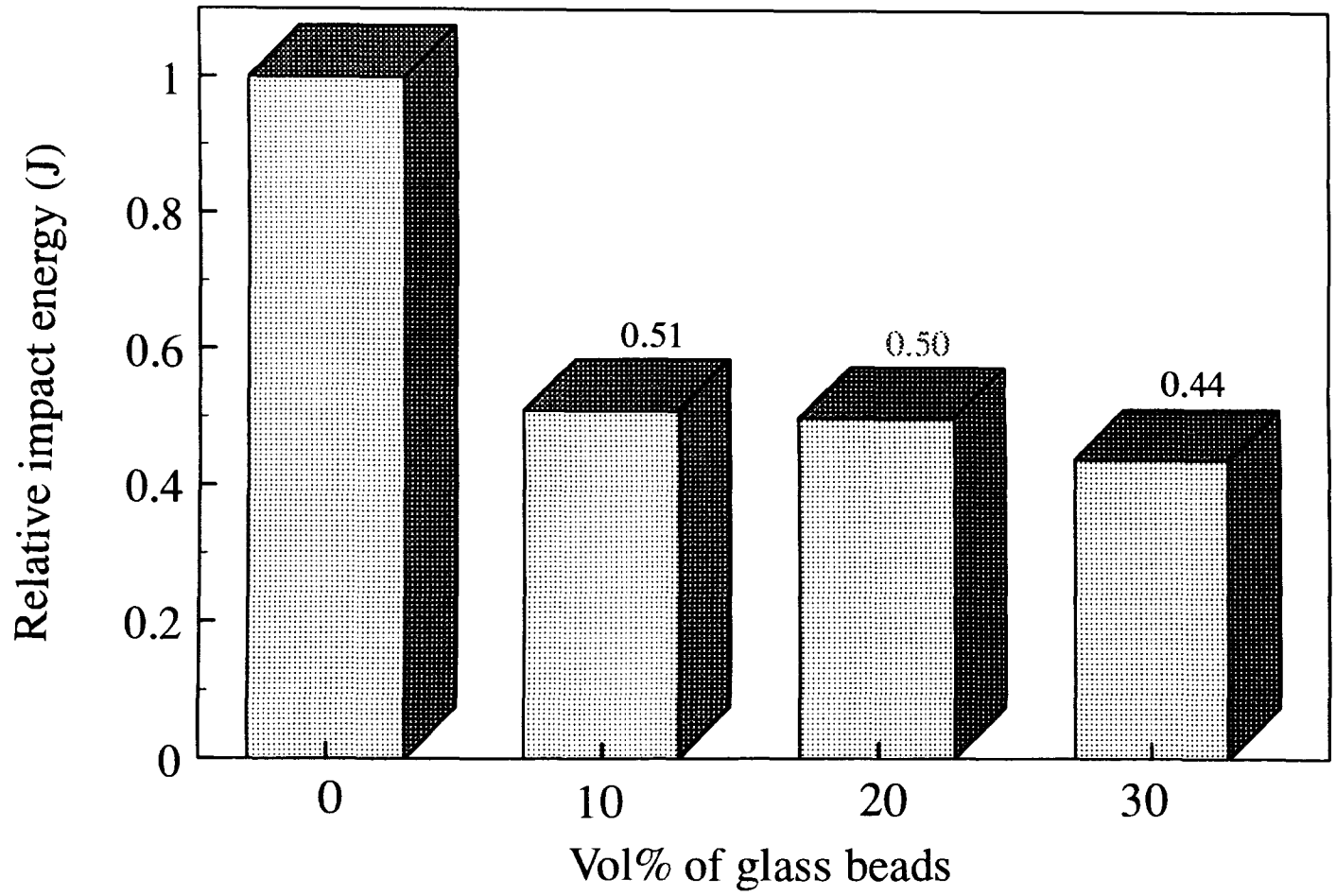

Figure 5.17 Relative impact fail energy of PP/G as a function of glass bead content

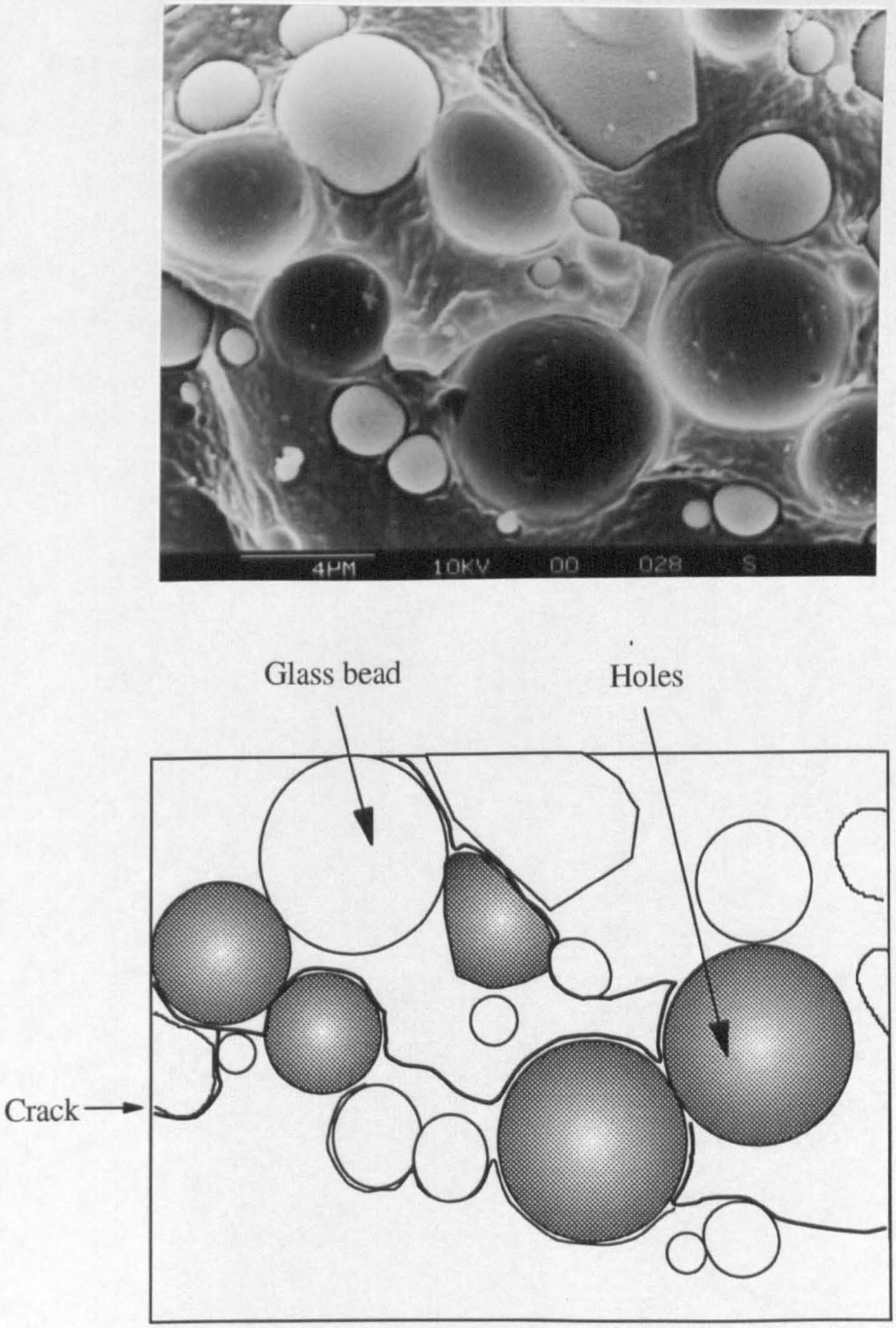

Figure 5.18 Fractured surface of a polypropylene composite filled with 20 %vol of glass beads showing the crack path and dewetting of glass bead particles. The dark holes are where glass particles have been torn out.

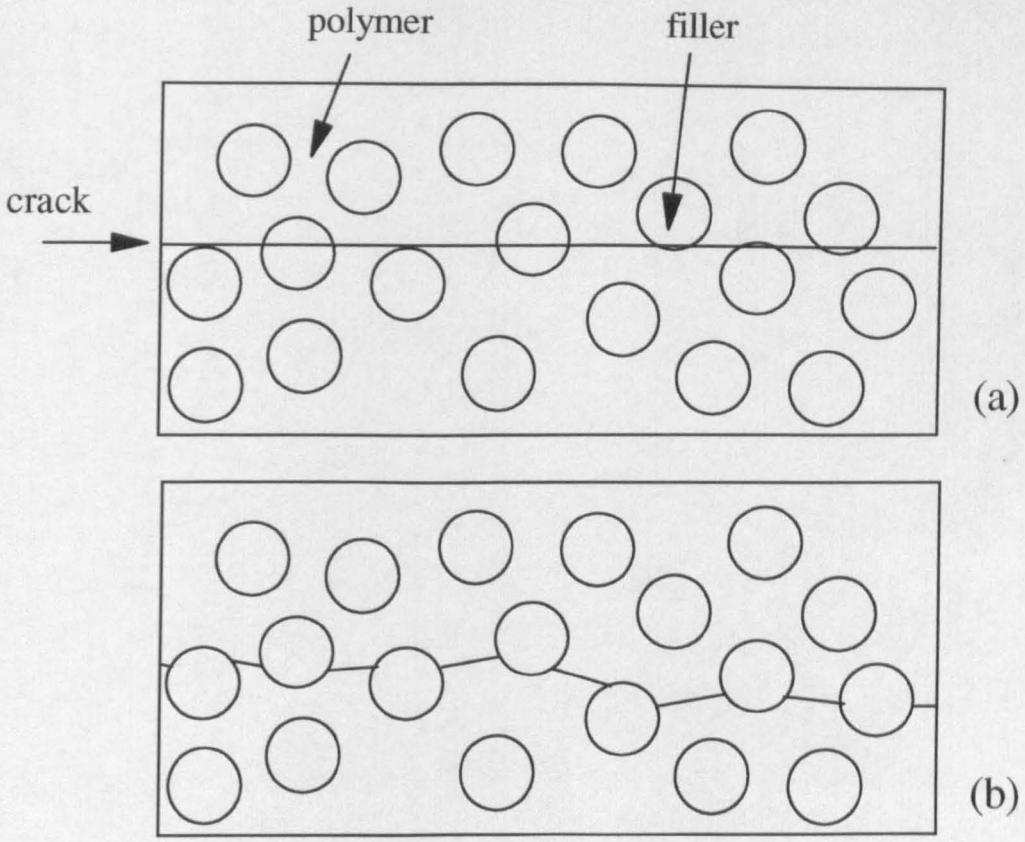

Figure 5.19 Two models of the crack path in a filled polymer *(a)* plane crack and *(b)* devious crack

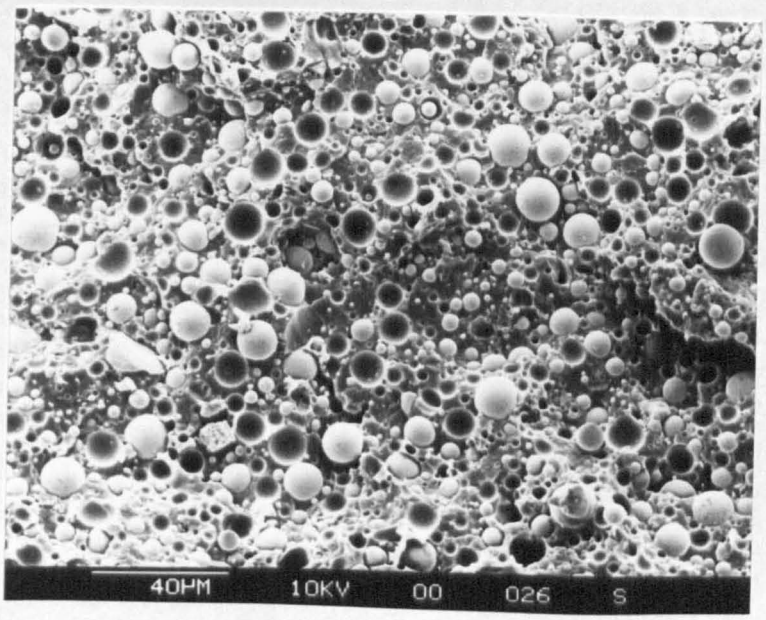

Figure 5.20 Fractured surface of a polypropylene composite filled with 20 %vol of glass beads showing a number of filler particles on the fractured surface.

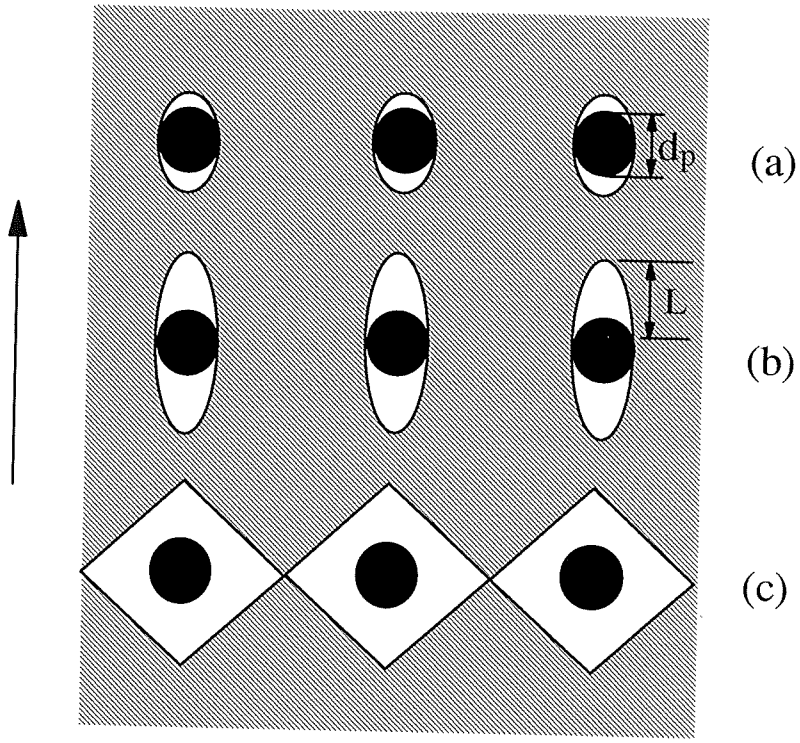

Figure 5.21 Schematic of crack formation around hard particles in a ductile matrix. *dp* is the particle diameter and *L* is the length of dimples around particles.

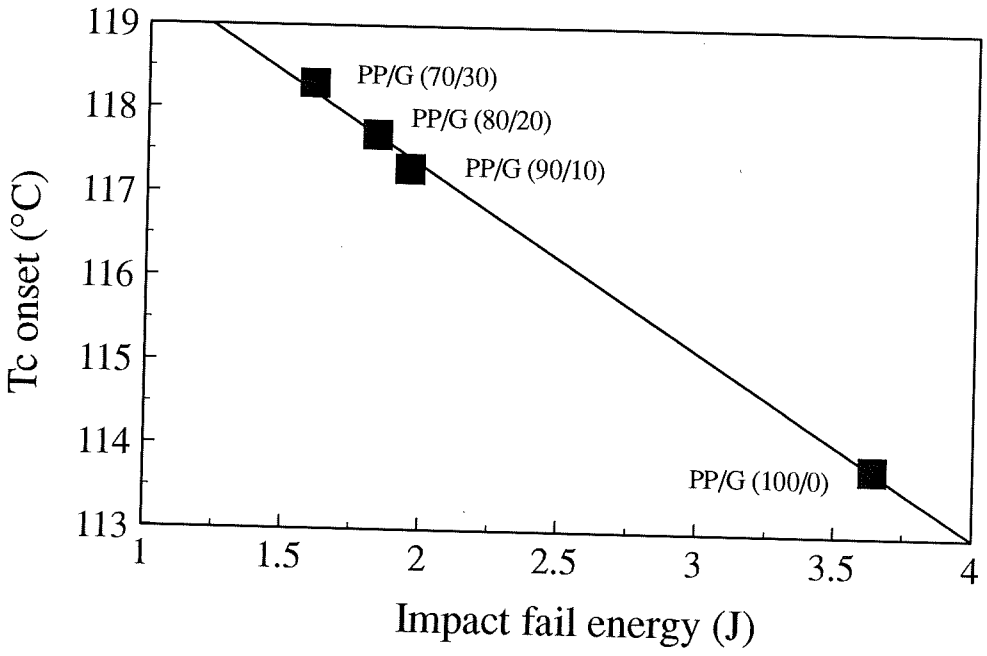

Figure 5.22 Relationship of the temperature onset of crystallisation *Tc onset* and impact fail energy of PP/G composites

5.19b). Evidence from the SEM micrograph of *Figure 5.20*, shows much more glass bead particles on the crack surfaces than the volume fraction of glass beads would suggest.

The observed mechanisms are very similar to those observed in soft metallic alloys containing hard particles [262]. They are schematically represent in *Figure 5.21*. Due to the very poor bonding between filler and matrix, the polymer detaches easily from the filler particles and creates a series of voids on both sides of the particles, perpendicular to the applied stress. Only a small amount of plastic strain is needed for this first step of damage in the composite (*Figure 5.21a*). With further strain, the voids grow and form dimple-like holes around the particles (*Figure 5.21b*). Their individual length L corresponds to the diameter of the particles, d_p. After these processes additional strain is needed to deform the rest of the matrix until the holes coalesce leading to failure of the composites (*Figure 5.21c*).

(ii) Relationship of nucleation, crystallisation and microstructure to impact strength

It has been suggested that fillers can modify the mechanical characteristics of a polymer in two ways [107]. Firstly, the properties of the particle themselves (size, shape, modulus) have a direct effect while, secondly the presence of filler particles can lead to changes in micromorphology which may give rise to differences in observed bulk properties.

Hutley and Darlington [129-130] have observed a correlation between the temperature onset of crystallisation ($T_{c\ onset}$) and impact strength in calcium carbonate filled polypropylenes, cooled from the melt. High $T_{c\ onset}$ was observed in composites with poor impact properties. This correlation was confirmed by Paynter et.al. [263]. The explanation for this has been suggested to be due to the formation of larger spherulites in the filled composites, since at higher temperature (high $T_{c\ onset}$) crystal growth can proceed more rapidly, resulting in larger spherulites. Large spherulites are believed to be conducive to poor crack propagation resistance [264].

Results from the DSC and impact studies of glass bead filled polypropylene composites also confirmed the observation of Hutley [129-130]. The relationship between $T_{c\ onset}$ and impact properties of the filled composites is shown in *Figure 5.22*. Generally, a filler with good nucleating properties would give a high $T_{c\ onset}$ and a large number of nuclei per unit volume. This would imply a fine spherulitic morphology and, hence, by analogy

with unfilled polymer, good impact strength [264]. However, this simple argument cannot be correct because it predicts an opposite trend to the results observed.

Although high $T_{c\ onset}$ are observed for composites of poor impact strength, it does not necessarily mean that glass beads, also other fillers, affects the impact strength of the composites through their effect on the crystallisation process. The reasons for the observation are not altogether clear at present. Also, in the present study no different effect between glass bead sizes was observed, on the crystallisation behaviour of polypropylene in the composites, but the impact test results show the greater reduction in impact properties in the composites of larger bead size. Thus, if the previous argument is truly correct, effect of bead size on the impact properties should not be observed.

CHAPTER 6

STRUCTURE AND PROPERTIES OF TERNARY PHASE POLYPROPYLENE COMPOSITES

: Effect of processing variables and formation

6.1 INTRODUCTION

From the preliminary investigations of rubber-modified polypropylene and glass bead filled polypropylene composites described earlier in chapters 4 and 5, respectively, the addition of ethylene-propylene rubber (EPR) to a polypropylene (PP) matrix was found to enhance the impact strength but reduce the modulus of the composite. On the other hand, incorporation with glass beads (G) increased the composite modulus but also resulted in increased brittleness.

Hence it was considered that incorporation of both EPR and glass beads into the polypropylene could result in an improvement of both impact strength and composite modulus. Multiphase systems consisting of a polymer matrix, rubber and filler are expected to exhibit quite complex behaviour, not only from the effect of each component itself, but filler-matrix, filler-rubber, and rubber-matrix interface and/or interphases may also be involved. The morphology of these composites is also complicated. Many different morphologies may be imagined. One possibility is the structure where the filler and rubber existed as separate, non-interacting particles within the matrix. Another morphology might involve filler particles encapsulated by the rubber inside the matrix.

Few publications have considered three-phase systems. Most work has focused on the properties of three-phase of PP, EPDM and various mineral fillers. Stamhuis [141-143] investigated the impact strength and flexural modulus in the PP/EPDM blends filled with talc and short glass fibres. Pukanszky et.al. [144-145] discussed calcium carbonate filled and toughened polypropylene systems. Fernando [73] described the fatigue mechanism at break in rubber modified polypropylenes containing calcium carbonate, calcium sulphate and mica.

The achievable properties of three-phase composites depend, on the one hand, on the characteristics and properties of the individual components and their proportion in the composite. On the other hand, however, the blending process also plays a critical role in determining the mixing uniformity, appearance and quality of the composites. During mixing, dispersive and distributive processes take place [265]. Dispersive mixing usually refers to the break-up of agglomerates of solid particles in the matrix. This is achieved through shear and tensile deformations. In distributive mixing, the actual particle size does not change; instead, the particles are distributed in the matrix reducing the non-uniformity.

In this investigation, the ternary phase composites of polypropylene, ethylene-propylene rubber and glass beads (PP/R/G) were studied. The main objective was to investigate the morphological structures and properties of these complex three-phase composites as well as their changes owing to the following variables :

(i) Processing variables including screw configuration, screw speed, feed rate and the sequence in which each component was mixed in the extruder.

(ii) Composite formulation (rubber and filler content in the composites)

6.2 EXPERIMENTAL

6.2.1 Selection of Materials

The materials used in this study are given in *Table 6.1*. Details of their properties have been reported earlier in chapter 3.

Table 6.1 - Raw materials used in this study

Code	Material	Grade	Supplier
PP	Polypropylene homopolymer	Novolen 1100HX	BASF
R	Ethylene-propylene rubber	Exellor PE808	Exxon
G	Uncoated glass beads	Spherical 5000CPOO	Croxton & Garry

The selection of these materials was justified by the results of the preliminary work on the two-phase systems of PP/EPR and PP/Glass beads (as reported earlier in chapter 4 and chapter 5, respectively). In chapter 4, the influence of EPR on the morphology and properties of polypropylene was discussed. Two grades of polypropylene homopolymer and two grades of ethylene-propylene rubbers differing in melt viscosity, were investigated. The experimental results showed that the blends containing PP1 (a high viscosity polypropylene grade 1100HX) and EPR2 (a low viscosity EPR grade Exellor PE808) provided a better balance of tensile and impact properties than the others. In chapter 5 the two-phase system comprising polypropylene filled with glass beads, was considered. The addition of glass beads to polypropylene led to a significant enhancement in composite modulus. Glass beads with finer particles (grade 5000CPOO) has a more profound effect than the coarser grade in terms of modulus improvement. From these preliminary experimental results, the suitable materials were thus selected.

6.2.2 Compounding

All compounding was carried out on an intermeshing co-rotating twin screw extruder (BTS-40 Betol Machinery Ltd.). Extrusion variables investigated include screw configurations, screw speeds and feed rates, as well as the mixing sequences of the components in the extruder.

The investigation started with the effect of screw configuration on the composite properties. Two screw profiles, designated *GM* and *SM*, were used in this study (see *Figures 6.1 a-b*). GM stands for "gentle mixing" while SM is for "severe mixing". Both configurations contained right-handed screw elements and had a total length of 875 mm with a diameter of 40 mm (L/D ratio of 21/1). They differed in the contents of kneading disc blocks and their locations along the modular screw. Screw GM included two kneading disc blocks of 60 and 25 mm long located 200 and 570 mm, respectively along the length of the molecular screw from the die. The SM screw configuration consisted of three kneading disc blocks providing comparatively more intensive mixing. The three kneading blocks were 60, 80 and 65 mm long and were located 80, 290 and 450 mm from the die, respectively. The modular screw assemblies and their details are presented in chapter 3 section 3.4.

A number of different screw speeds and feed rates were used as shown in *Table 6.2*. In this part of work, all composites were processed using a severe screw profile "SM" and the composition of PP/R/G was kept constant at 60/20/20 (%wt) or 69/23/8 (%vol).

Table 6.2 - Screw speeds and feed rates used

Code	Composition of PP/R/G	Screw Speed (rpm)	Feed rate (kg/hr)	Power consumption (amp)	Processing conditions
S100F11		100	11	9	: barrel temperatures (feeder→die)
S100F19	60/20/20	100	19	12	185, 190, 190, 200, 200 °C
S100F28	(%w)	100	28	16	: severe screw profile "SM"
	or				
S170F11	69/23/8	170	11	6	
S170F19	(%vol)	170	19	10	
S170F28		170	28	14	

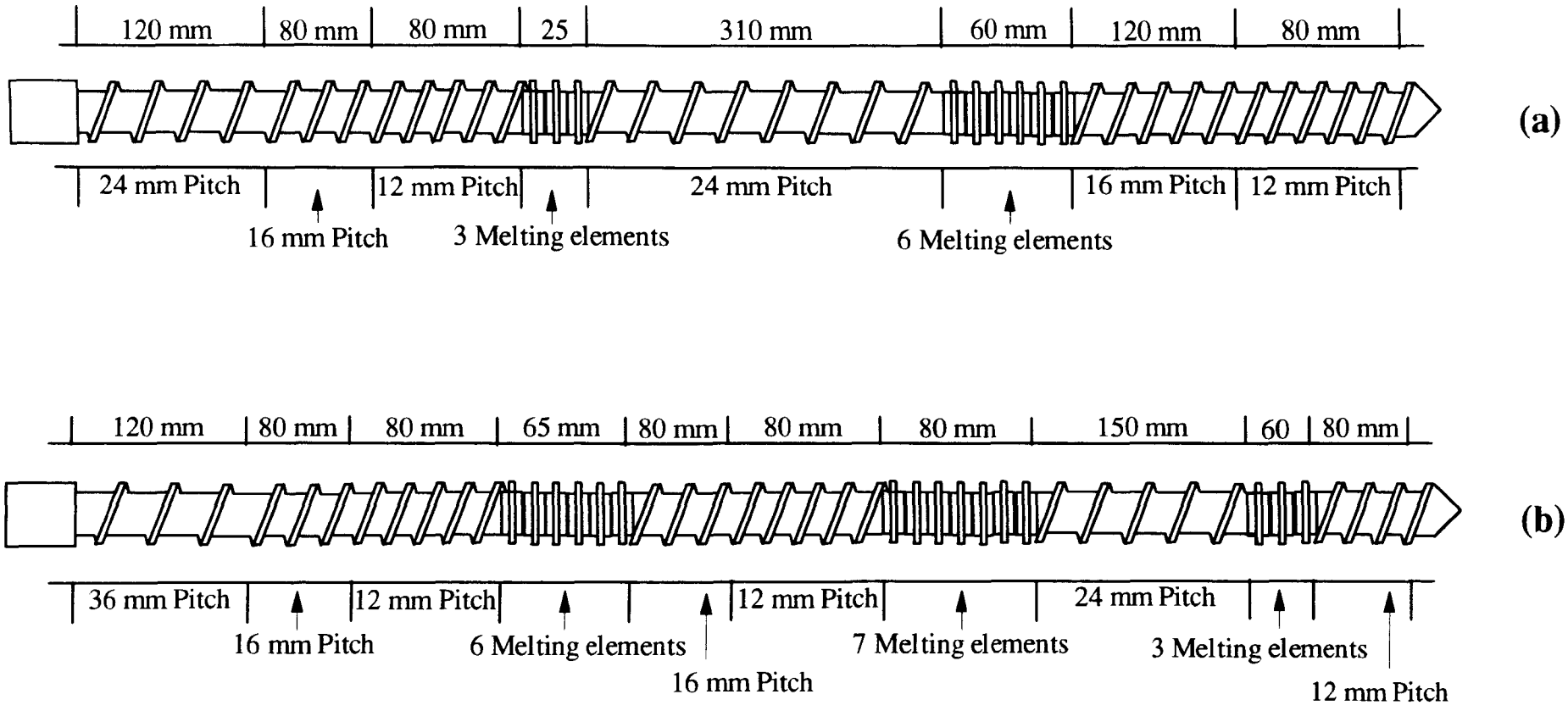

Figure 6.1 Two screw profiles used in the study (a) *GM* profile for gentle mixing and (b) *SM* profile for severe mixing.

Apart from the extrusion variables mentioned above, the sequence in which the components (PP, EPR or glass bead) were mixed in the extruder was also investigated. *Table 6.3* shows the five mixing sequences considered.

Table 6.3 - Sequences of mixing investigated

Code	Material	Composition	Processing conditions
TC1	PP+R+G	60/20/20	: barrel temperatures (feeder→die)
TC2	PP+R+G (II)	(%w)	185, 190, 190, 200, 200 °C
TC3	(PP+R)+G	or	: severe screw profile "SM"
TC4	(PP+G)+R	69/23/8	: screw speed 170 rpm
TC5	(R+G)+PP	(%vol.)	: feed rate 19 kg/hr

TC1 *(PP+R+G)* is a single pass compounding in which all the three components were fed into the extruder and mixed at the same time.

TC2 *(PP+R+G II)* is a reprocessing of TC1 where the TC1 extrudates were passed through the extruder for a second time.

TC3 *((PP+R)+G)* , in this compounding approach, PP was firstly blended with EPR in the extruder. The extrudate was granulated, then glass beads were added and they were all fed into the extruder and mixed for a second time.

TC4 *((PP+G)+R)* is the composite where PP was mixed with glass beads first and the rubber was then added into the filled polypropylene composites and mixed for a second time.

TC5 *((R+G)+PP)* is the composite in which the rubber and glass beads were mixed prior to being added in the extruder for a second pass with polypropylene.

6.2.3 Testing

The composites prepared earlier were characterised using mechanical measurements and by morphological studies. *Figure 6.2* represents schematic of experimental procedure adopted. Samples for mechanical testing were prepared by compression moulding. The conditions used and sample preparation procedure were reported in detail in chapter 3-

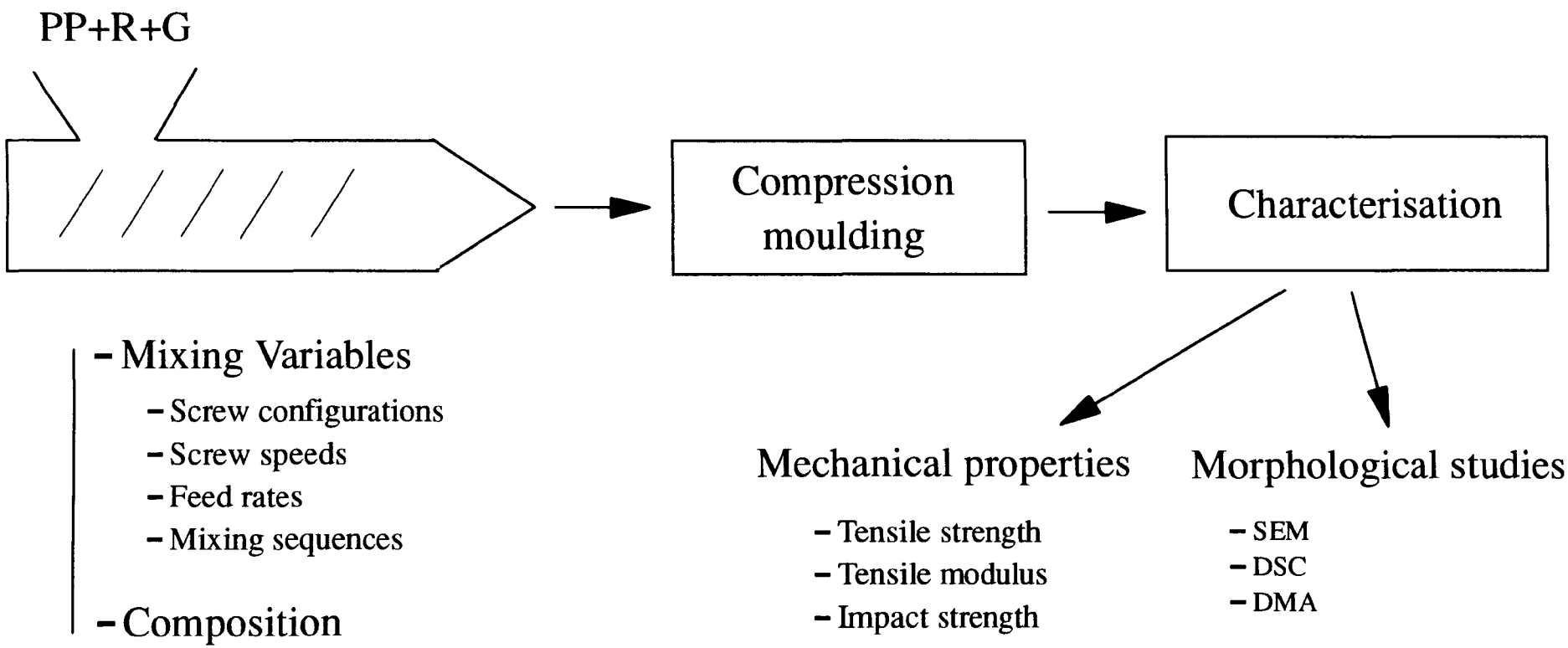

Figure 6.2 Schematic of experimental procedure adopted

section 3.5. The tensile and impact properties were determined at room temperature (23 °C) according to the ASTM standard test methods. Morphology of the composites was characterised by both direct and indirect methods. Direct observation was undertaken by scanning electron microscopy. To obtain quantitative information, some samples were analysed using an image analysis to determine the mean rubber particle size in the composites. Dynamic mechanical analysis (DMA) and differential scanning calorimetry (DSC) were used as indirect methods in determining the morphological structures of the composites. Details of all testing procedures have been described in chapter 3.

6.3 RESULTS AND DISCUSSION

6.3.1 Preliminary Evaluation of the Three-Phase PP/R/G Composites

6.3.1.1 Phase structure of the PP/R/G composites

In the three-phase composites containing a polymer matrix, filler and elastomer, two phase structures can take place [141-162] i.e. separate dispersion and encapsulation of filler by elastomer. In the PP/EPDM/$CaCO_3$ systems Kolarik et.al. [144] observed an encapsulation of the filler particles by EPDM, while a separate dispersion of filler and EPDM was found when a surface treated $CaCO_3$ was used [146]. In this study, phase structures of the investigated PP/R/G composites were studied by SEM, DMA and DSC.

(i) Direct observations by SEM

Phase structure of the PP/R/G composites was studied by SEM of fracture surfaces produced at liquid nitrogen temperature. To improve the contrast between EPR and the polypropylene matrix, the EPR particles were removed from the fracture surfaces by etching with boiling heptane vapour for 3 seconds. The etching procedure was described in detail in Chapter 3-section 3.8.1. *Figure 6.4* shows the SEM micrograph of a fractured and etched surface of PP/R/G composite. As the EPR particles were removed by etching, dark circular holes were seen on the micrograph. To verify that the holes observed in the composites are the imprints of the EPR particles, an unmodified polypropylene sample was also subjected to the same etching conditions. As seen in *Figure 6.3* nothing was etched out from an unmodified polypropylene sample after 3 seconds of etching time. In other word heptane has no effect on etching polypropylene, at least under the conditions used (3 second exposure to boiling heptane vapour).

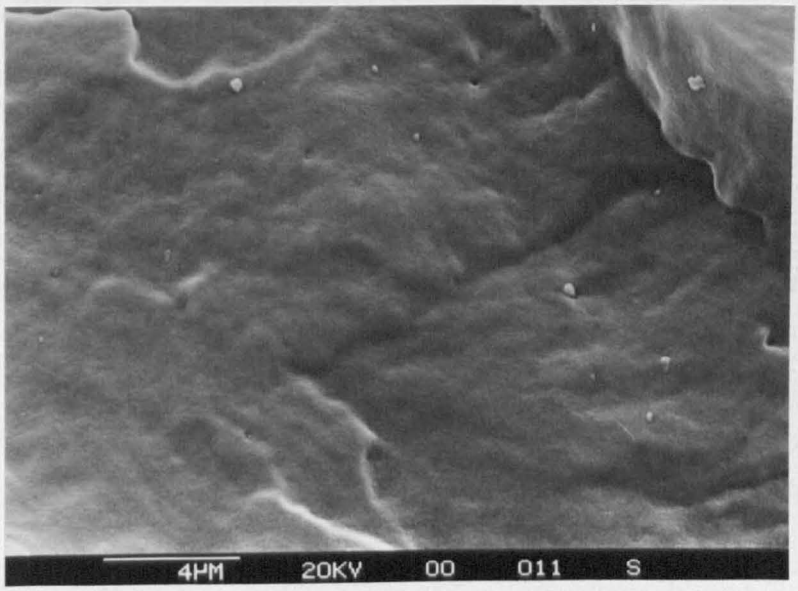

6.3

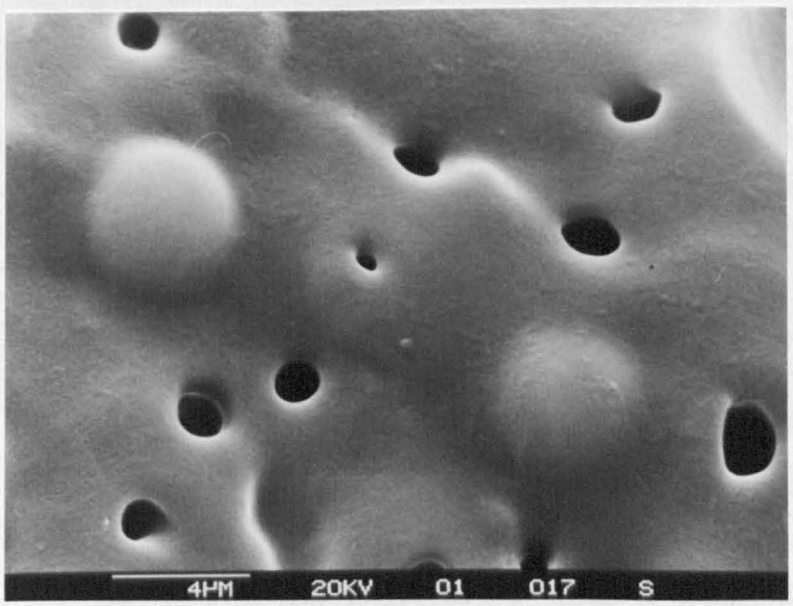

6.4

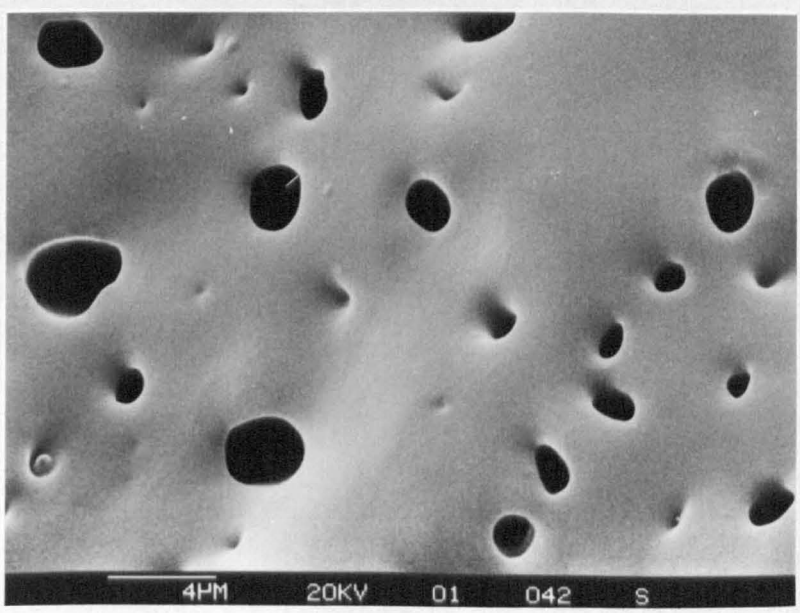

6.5

Figures 6.3 to 6.5 SEM micrographs of cryogenic fractured and etched surfaces of an unmodified polypropylene (6.3), three-phase PP/R/G composite (6.4) and two-phase PP/R blend (6.5).

The SEM micrograph of the three-phase PP/R/G composite (figure 6.4) reveals no encapsulation, since glass beads and EPR particles appear embedded side by side in the polypropylene matrix. The average diameter of the EPR particles in this system was approximately 0.6 μm as measured by an image analyser averaging from at least 800 particles. The EPR particles in the three-phase composites were found to be smaller than those in the two-phase PP/EPR blends where the average particle size of 1 μm was observed. The particle size decrease in the three-phase composite may be brought about by an increase in the melt viscosity due to filler addition, resulting in enhanced dispersion of the rubbery phase.

(ii) Dynamic mechanical analysis

Dynamic mechanical analysis (DMA) measures the storage modulus (E'), loss modulus (E") and damping (tan δ) as a function of temperatures. These dynamic mechanical properties, especially the damping, are extremely sensitive to all kinds of transitions, relaxation processes and structural heterogeneities. The damping, thus, is a powerful analytical tool for determining phase structures in multiphase polymer composites.

Figure 6.6 shows the temperature dependence of the damping or tan δ at 1 Hz. of an unmodified polypropylene, the two-phase systems of PP/R and PP/G, and the three-phase PP/R/G composites. The two tan δ peaks observed at -43 °C and 6 °C in both PP/R and PP/R/G samples, corresponded to the glass-transition temperatures of EPR and PP, respectively. The shift in the location of the rubber tan δ peak or any changes in maxima of this peak can infer the change in the composite structures (dispersion or encapsulation). For instance, in the structure where the filler particles were encapsulated by the rubber, the effect of rubber peak should be more pronounced by the incorporation of filler and one could expect a shift of the glass transition temperature of the rubber to a higher temperature due to the restriction of chain movement [148]. Since when a rubber is heated from low temperature to high temperature, the molecular chains in the frozen state acquire more freedom of movement due to the input heat energy. In the case where the rubber chains become adsorbed onto the filler surface or occluded in the filler structure, the freedom of movement is restricted or the free volume available will be less. In such a case the tan δ values, which reflect the free movement of molecular chains, will become distorted. Studies by Smit [266] showed that with the addition of a reinforcing filler like carbon black into a rubber matrix, the tan δ peak value diminished and the T_g of rubber shifted to a higher temperature due to the filler interaction with the rubber.

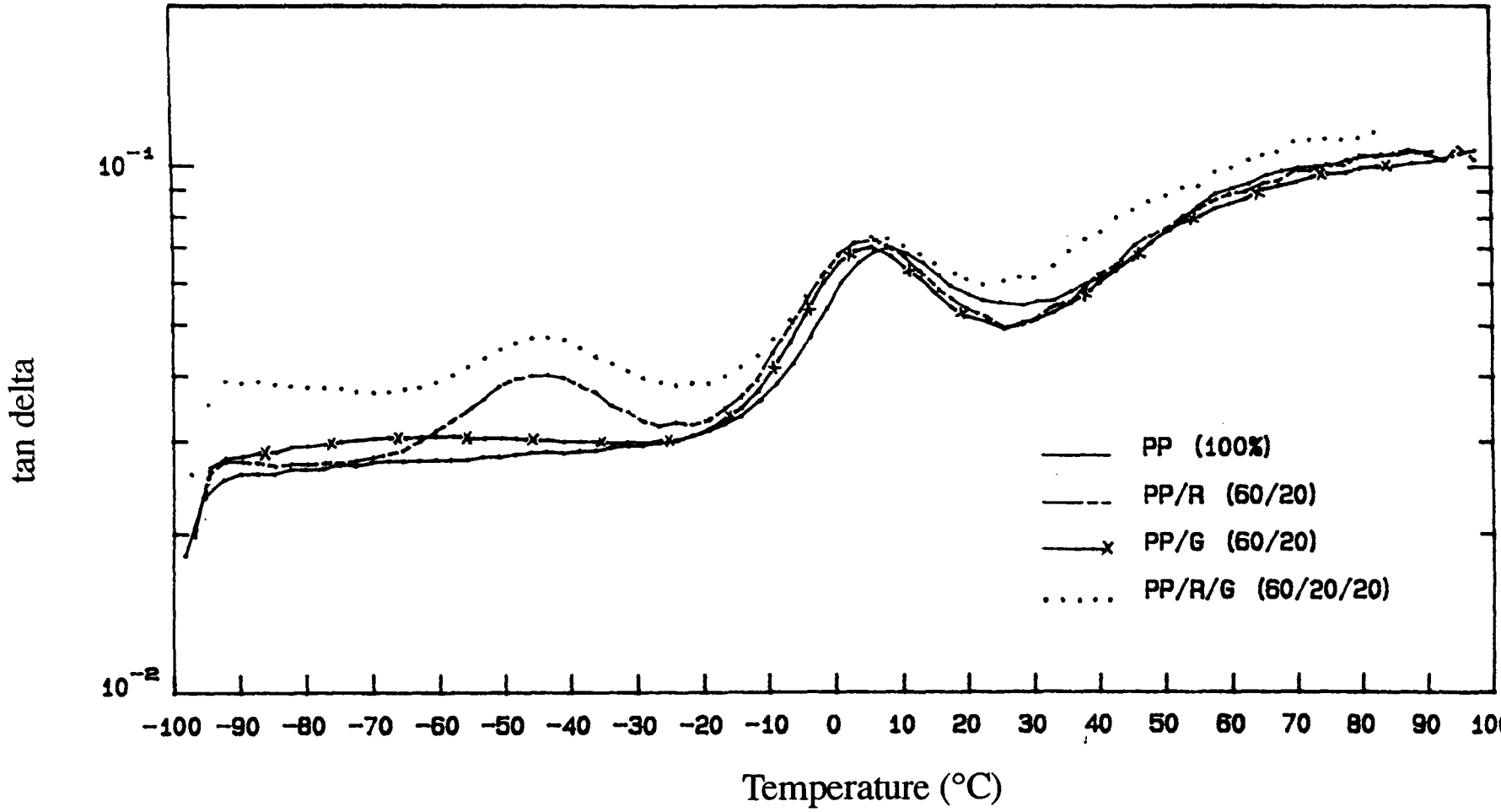

Figure 6.6 Temperature dependences of the damping (tan delta) at 1 Hz. of an unmodified polypropylene (PP), two-phase of PP/R and PP/G, and three-phase of PP/R/G composite.

As shown in *Figure 6.6*, the tan δ peak of EPR in the three-phase PP/R/G composite located at the same temperature as in the two-phase PP/R system. Also, the SEM micrograph of *Figure 6.4* revealed no cavity appeared around the glass-bead particles after etching. Taking all this evidence into account, it can be concluded that the glass bead particles were not encapsulated by EPR (no peak shift), on the other hand, EPR formed a discrete phase and is incompatible with PP (two T_g peaks). Thus, the final structure in the three-phase PP/R/G composite is "separate dispersion" where EPR and glass beads were separately dispersed in the polypropylene matrix.

6.3.1.2 Tensile and impact properties of the PP/R/G composites

The aim of this part of work was to evaluate whether a balance of tensile and impact properties can be achieved by physical blending of the polypropylene with EPR and glass beads. Some theoretical predictive models developed for two-phase composites will be applied in the explanation and comparison of the three-phase results.

The results from tensile and impact measurements presented in *Table 6.4* are for an unmodified polypropylene, two-phase polypropylene blends either with EPR or glass beads, and the three-phase PP/R/G composites. The data in this table show that the incorporation of EPR into polypropylene led to an improvement in impact strength, while addition of glass beads resulted in an increase in the composite modulus. In case of the three-phase PP/R/G composite, these properties are somewhat in between those of the PP/R and PP/G composites. However, at the composition studied (60/20/20 wt%) the properties of the three-phase composite are poorer than the same characteristics of the unmodified polypropylene. Varga [164] recently reported a similar observation for the PP/EPR/talc and PP/EVA/talc composites where the modulus and strength of the three-phase systems are lower than those of the neat polypropylene.

The tensile modulus and strength of the three-phase PP/R/G (60/20/20) composites were compared with the values calculated using some theoretical models for two-phase systems. In the calculation, the experimental data of the corresponding two-phase PP/R (60/20) blends were taken as the matrix values assuming that the filler and rubber particles act independently. *Table 6.5* presents the modulus values calculated from three selective models. Einstein's equation 6.1 for filled composites without adhesion [251-253]; Einstein's equation 6.2 which is a modified equation for the system with some

Table 6.4

Tensile modulus, yield stress, elongation at yield and falling weight impact fail energy at 23 °C of unmodified polypropylene and its composites

Sample (in weight %)	Modulus (GPa)	Yield Stress (MPa)	Elongation at yield (%)	Impact fail energy (J)
PP (100)	1.82 (0.03)[a]	36.59 (0.29)	5.49 (0.31)	3.64 (0.24)
PP/R (60/20)	1.32 (0.02)	22.93 (0.35)	4.66 (0.08)	4.91 (0.34)
PP/G (60/20)	2.05 (0.06)	29.33 (0.49)	4.08 (0.25)	2.34 (0.46)
PP/R/G (60/20/20)	1.36 (0.01)	16.93 (0.20)	4.26 (0.27)	3.28 (0.44)

[a] Standard deviations in parentheses, means from eight specimens.

adhesion between rigid spheres and the polymer matrix [111]; and the Kerner-Nielsen 's equation [114]. These equations are shown below.

$$E_c = E_m (1+\phi_f) \qquad (6.1)$$

$$E_c = Em (1+2.5\phi_f) \qquad (6.2)$$

$$E_c = E_m (1+AB\phi_f) / (1-\psi B\phi_f) \qquad (6.3)$$

where : $A = (7-5\nu_m) / (8-10\nu_m)$

$B = [(E_f/E_m)-1] / [(E_f/E_m)+A]$

$\psi = 1+[(1-P_f)/P_f^2]\ \phi_f$

E_c is the composite modulus. E_m of 1.32 GPa is the modulus of the polymer matrix (PP/R, 60/20). ϕ_f of 0.08 is the volume fraction of filler. P_f of 0.64 is the value for the random close packing of monodisperse spheres and ν_m of 0.27 is Poisson's ratio of the polypropylene matrix.

From the experimental work on glass bead filled polypropylene composites (chapter 5) it was found that the experimental data of such composites fit very well with the Einstein's equation without adhesion (eq.6.1). In case of the three-phase PP/R/G composites, the experimental modulus value is also in a reasonable accord with the prediction of the Einstein's equation (eq.6.1).

Table 6.5 - Comparison of experimental composite modulus to theoretical models

Equations	Experiment	Einstein (6.1)	Einstein (6.2)	Kerner (6.3)
Modulus (GPa)	1.36 (0.08)[a]	1.42	1.58	3.47

[a] Standard deviation in parentheses, means from ten specimens.

In the prediction of composite strength (σ_c) Nicolais and Nicodemo' equation was used and was expressed by the following equation [117].

$$\sigma_c = \sigma_m (1-1.21\phi^{2/3}) \qquad (6.4)$$

where σ_m of 23 MPa is the tensile strength of the polymer matrix (PP/R, 60/20), and ϕ of 0.08 is the volume fraction of filler.

A calculated tensile strength value of 17.7 MPa was obtained by this model. This calculated value was slightly higher than that obtained from the experiment (16.9 MPa). These results revealed no adhesion between glass beads and the polymer matrix. This may be the reason of the lower in tensile and impact strength values in the three-phase PP/R/G (60/20/20) composite, compared to the unmodified polypropylene.

The usual approach to overcome low properties due to the poor adhesion between phases, is to modify the interfaces using functionalised materials or surface-modified fillers. In this investigation, however, before approaching to the interfacial modification which makes the composite more complex and the interpretations more complicated, the composite properties were firstly modified by altering the processing parameters used during the compounding and also by varying compositions of rubber and filler used in the system.

6.3.2 Effect of Processing Variables on the Composite Properties

This part of the study considers twin-screw extrusion processing variables, such as screw configuration, screw speed, feed rate and mixing sequence, on the morphology and mechanical properties of the three-phase PP/R/G (60/20/20 by weight) composites. The morphology of polymer blends compounded by twin-screw extrusion has been shown in several studies to depend on the screw design [179, 267], screw speed and volume throughput [63, 268]. In many cases, the performance of the extruder with respect to blending was characterised in terms of the specific energy input and residence time distributions [268-270]. However, detailed studies on three-phase polymer composites involving both rubber and filler in the systems are not found in the literature.

6.3.2.1 Effect of screw configurations

The effect of screw geometry variations on the morphology and mechanical properties of the PP/R/G composites will be illustrated using two screw configurations shown in *Figures 6.1a-b*. They mainly differed in the contents of kneading disc blocks and their locations along the modular screw. The first screw configuration provided gentle mixing, while the second profile having more kneading blocks generated greater shear intensity.

It was expected that at equal screw speed and material feed rate, the different screw geometries and, hence, the different shear stresses generated would produce different mechanical and morphological results. *Figures 6.7 to 6.9* show the tensile modulus, yield strength and impact fail energy at 23 °C of the three-phase PP/R/G composites as well as corresponding two-phase PP/R and PP/G composites, prepared in the twin-screw extruder using the same two screw profiles (gentle and severe screw profile). A slight increase in the tensile and impact properties was observed in the PP/G and PP/R/G composites prepared by using the severe screw profile. Contrary results were found for the PP/R blend. The differences in the results, however, are not statistically significant according to the s-significance test (Appendix I). These differences only exceed the standard deviation of the measurements.

In the similar system, Bartilla et. al. [63] investigated the effect of screw geometry on the properties of PP/EPDM blends. They reported that to achieve good quality (fine dispersion and high impact property), such blends should be precompressed by use of a screw configuration in which the pitch decreased markedly toward the kneading blocks of the melting zone and baffles should be used to ensure sufficient particle size reduction and good mechanical properties. Narrow kneading discs were more likely to produce more uniform particle size distribution.

6.3.2.2 Effect of screw speed and feed rate

Since the quality of the composite also depends on screw speed and feed rate, these two parameters were also included in the test series.

Figures 6.10a to c and *Table 6.6* show the tensile modulus, yield stress, elongation at yield and impact fail energy at 23°C of various three-phase PP/R/G composites. The composition of PP/R/G was kept constant at 60/20/20 (%wt). All composites were prepared using a severe screw profile but using various screw speeds and feed rates. As seen from *Figures 6.10a and b* no significant difference in the effect of screw speed and feed rate was observed on the composite modulus and tensile yield stress. However, increasing the screw speed (from 100 to 170 rpm) with otherwise constant parameters resulted in an improvement in impact strength. The best results were obtained in the composite prepared using the 170 rpm screw speed with the feed rate of 19 kg/hr.

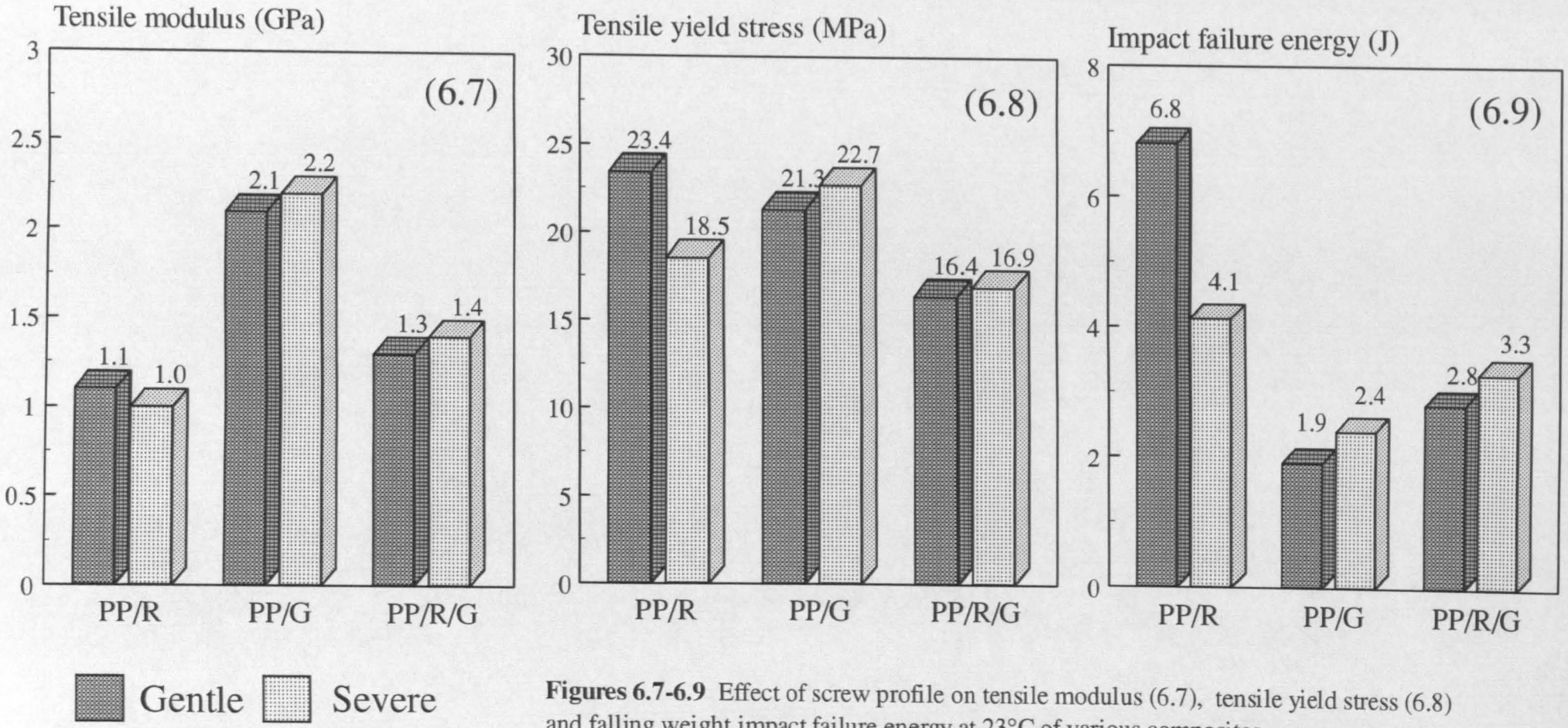

Figures 6.7-6.9 Effect of screw profile on tensile modulus (6.7), tensile yield stress (6.8) and falling weight impact failure energy at 23°C of various composites

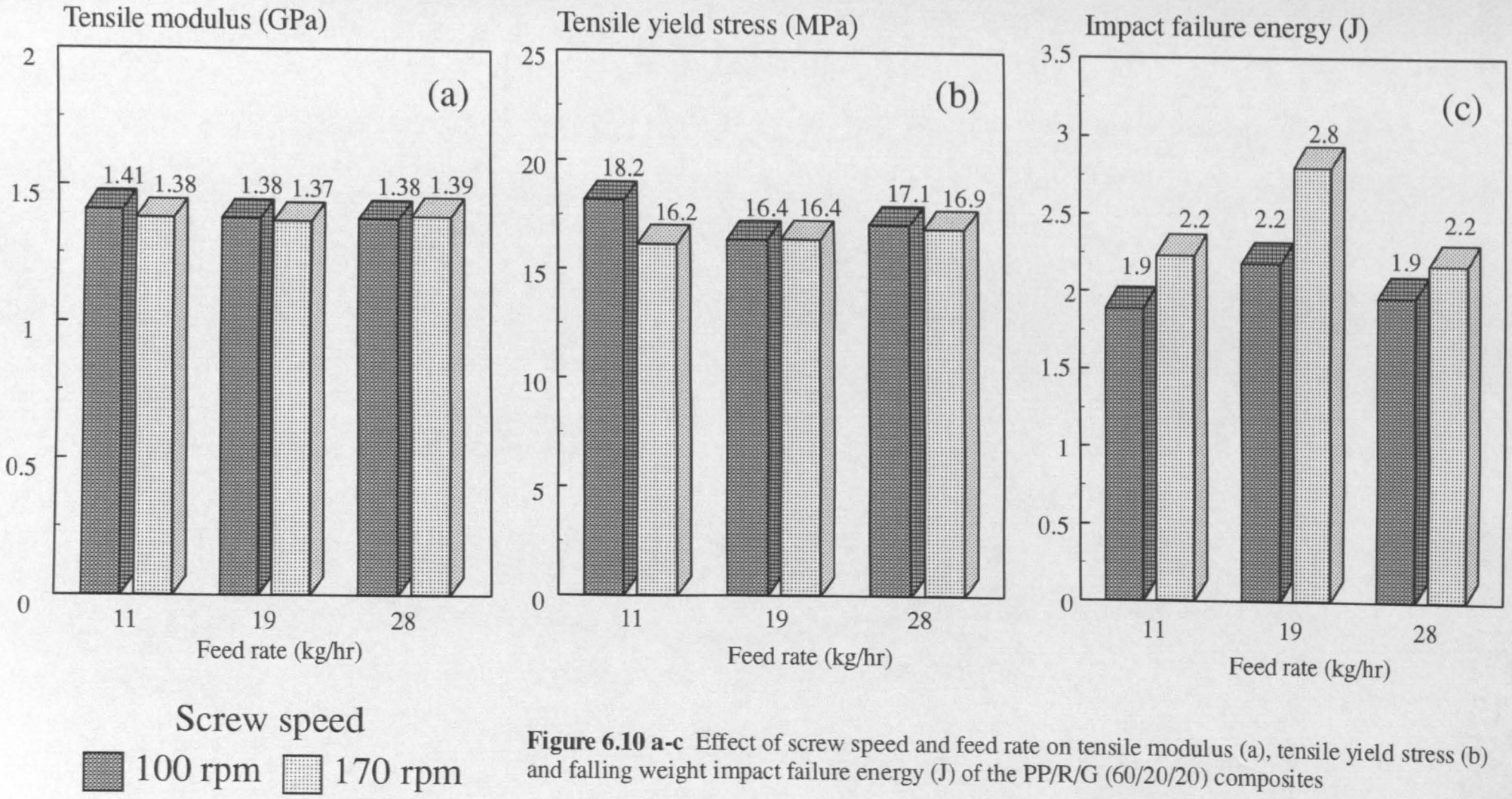

Figure 6.10 a-c Effect of screw speed and feed rate on tensile modulus (a), tensile yield stress (b) and falling weight impact failure energy (J) of the PP/R/G (60/20/20) composites

Table 6.6

Tensile modulus, yield stress, elongation at yield and falling weight impact fail energy at 23 °C of the 60/20/20 (%wt.) PP/R/G composites prepared by a twin-screw extruder using various screw speeds and feed rates

Sample	Speed (rpm)	Feed rate (kg/hr)	Modulus (GPa)	Yield stress (MPa)	Elongation at yield (%)	Impact fail energy (J)
S100F11	100	11	1.14 (0.05)[a]	18.16 (0.43)	3.64 (0.10)	1.89 (0.20)
S100F19		19	1.38 (0.17)	16.38 (1.19)	3.75 (0.60)	2.18 (0.26)
S100F28		28	1.38 (0.08)	17.10 (0.48)	3.69 (0.24)	1.96 (0.28)
S170F11	170	11	1.38 (0.04)	16.15 (0.48)	3.94 (0.31)	2.23 (0.20)
S170F19		19	1.31 (0.07)	16.41 (0.75)	3.91 (0.19)	2.80 (0.31)
S170F28		28	1.39 (0.04)	16.91 (0.43)	3.72 (0.23)	2.17 (0.19)

[a] Standard deviations in parentheses, means from six specimens.

In order to obtain more understanding of the influence of screw profile, screw speed and feed rate on the composite properties, studies were undertaken on influence of these variables on EPR particle size.

The size of the dispersed EPR particles was determined from the SEM micrographs of fracture surfaces using an image analyser as mentioned in chapter 3. No significant difference was observed in the number average particle size of EPR particles in the composites prepared using gentle (0.54 μm) or severe screw profiles (0.52 μm). The slightly smaller in the EPR particle size in the latter composite may be due to a higher shear stress generated by more intensive mixing from the severe screw profile. *Figure 6.11* demonstrates the average EPR particle sizes in the PP/R/G composites as a function of screw speeds and feed rates. At the lower screw speed (100 rpm) the average EPR particle size became bigger as the feed rates increased, while the opposite trend was found when the higher screw speed (170 rpm) was used.

In general, at higher screw speeds, polymer blends experience a greater shear stress which should ultimately yield a smaller dispersed rubbery phase. This follows Taylor's theory of particle deformation [96], where a droplet of a Newtonian dispersed phase in a Newtonian matrix will deform until the total force acting on the particle becomes equal to the surface tension. Bartilla [63] found that the morphology of polypropylene/EPDM blends became more homogeneous and the phase size of EPDM was smaller when the screw speed increased. In contrast, Willis et.al. [271] found the opposite trends in polystyrene/bromobutyl rubber blends. While Valsamis et.al. [268] found the phase size of low density polyethylene/polystyrene blends to be independent of screw speed.

The relationship between rubber particle size and mechanical properties of polymer blends has been reported [64-69]. For each type of material, there appears to be a critical particle size for the optimum property. For the investigated three-phase PP/R/G composite the optimum mechanical properties were achieved when the average particle size of EPR in the system was around 0.6 μm. The impact failure energy of 2.8 J was obtained in such a composite (S170F19). As the average particle size increased to 0.7 μm (in the S170F11) or dropped to 0.4 μm (in the S170F28), the impact fail energy fell down to around 2.2 J.

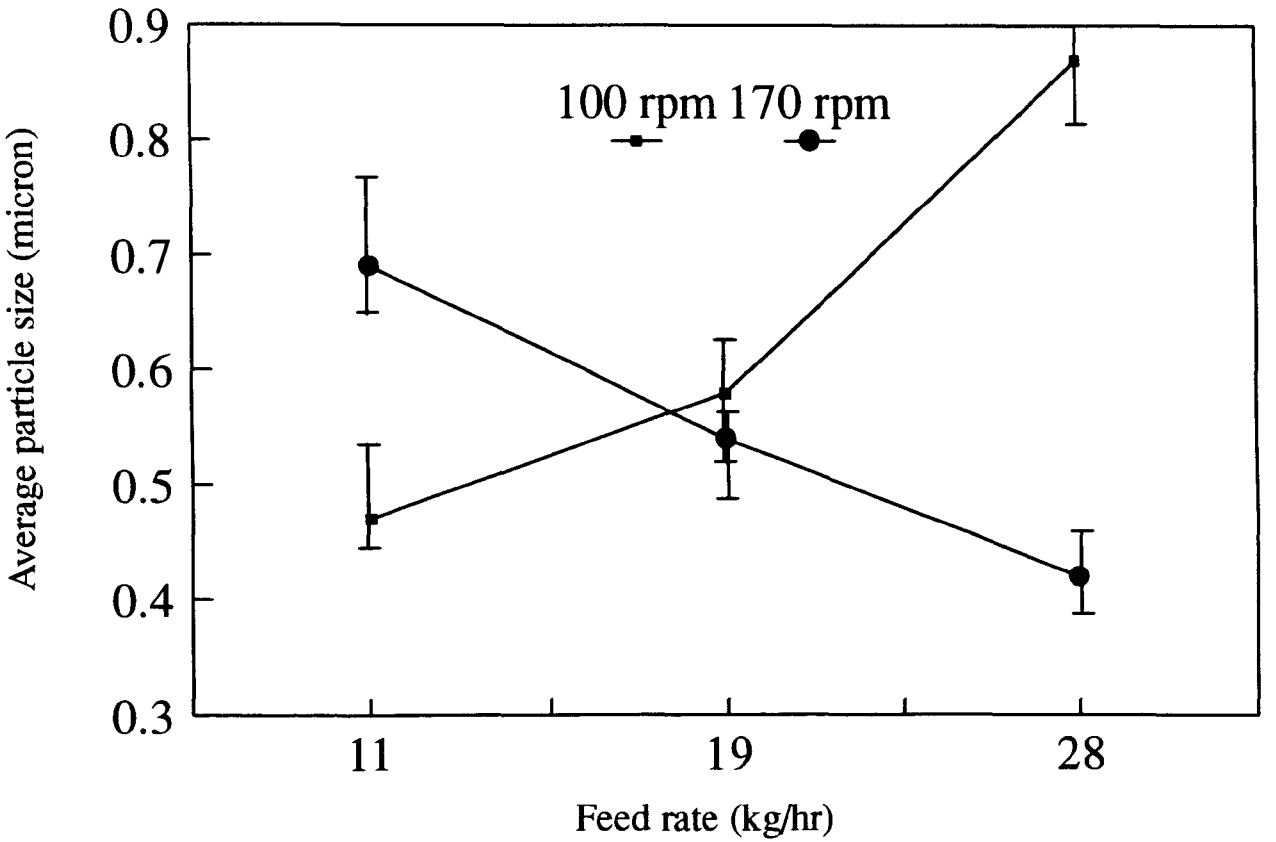

Figure 6.11 Number average rubber particle size in the PP/R/G (60/20/20) composites as a function of screw speed and feed rate

6.3.2.3 Effect of mixing sequence on the composite properties

In this part of experiment the effect of sequence in which the components (PP, EPR or G) were mixed in the twin-screw extruder, was investigated. From the previous studies on the influence of screw profile, screw speed and feed rate on the PP/R/G (60/20/20) composites, it was found that the best results were obtained in the composite prepared by using a severe screw profile and compounded at a screw speed of 170 rpm with a feeding rate of 19 kg/hr. This condition was, thus, selected for use throughout the rest of this study. The composites of constant composition (60/20/20, by weight) were prepared under the above conditions but using the five different ways of mixing, as shown in detail earlier in *section 6.2.2.*

Phase structures of these composites were studied by SEM on fractured and etched surfaces. The samples were fractured at liquid nitrogen temperature and then exposed to boiling heptane vapour for 3 sec to remove the EPR particles. The structures of these five composites were found to be very similar, although they were prepared in the different sequences of mixing. All five composites show separate dispersion structures.

Figures 6.12 and 6.13 are examples of phase structures observed in the PP+R+G, TC1 sample and (R+G)+PP, TC5 sample. In the TC1 sample, all components (PP, R and G) were fed into the extruder and mixed at the same time, while in the TC5 sample EPR and glass beads were introduced into the extruder and mixed together first. The extrudate was then cooled down and pelletised. These granules were subsequently fed into the extruder with polypropylene and mixed for a second time. The TC5 sample, although showing slightly more rubber particles adhering to the filler surfaces, both TC1 and TC5 samples had the same general "separate dispersion" structure as shown in *Figure 6.12 and 6.13.*

Thus it can be said that complete encapsulation of glass beads by EPR cannot be achieved by simple changing in the sequence of mixing. In the TC5 sample even when glass beads had been mixed with EPR first, the glass bead particles were finally wetted by the polypropylene matrix and resulted in the separate dispersion structure. Phase changing in this composite may be partly due to the poor adhesion between glass bead particles and EPR. During the second mixing with polypropylene, the high shear forces developed in the extruder were enough to separate them apart and at the same time the molten polypropylene which has a relatively lower viscosity or higher mobility than EPR was then being the first to adsorb onto the surfaces of glass bead particles. The distribution of glass beads in the polymer phases (PP or EPR phases) is more influenced

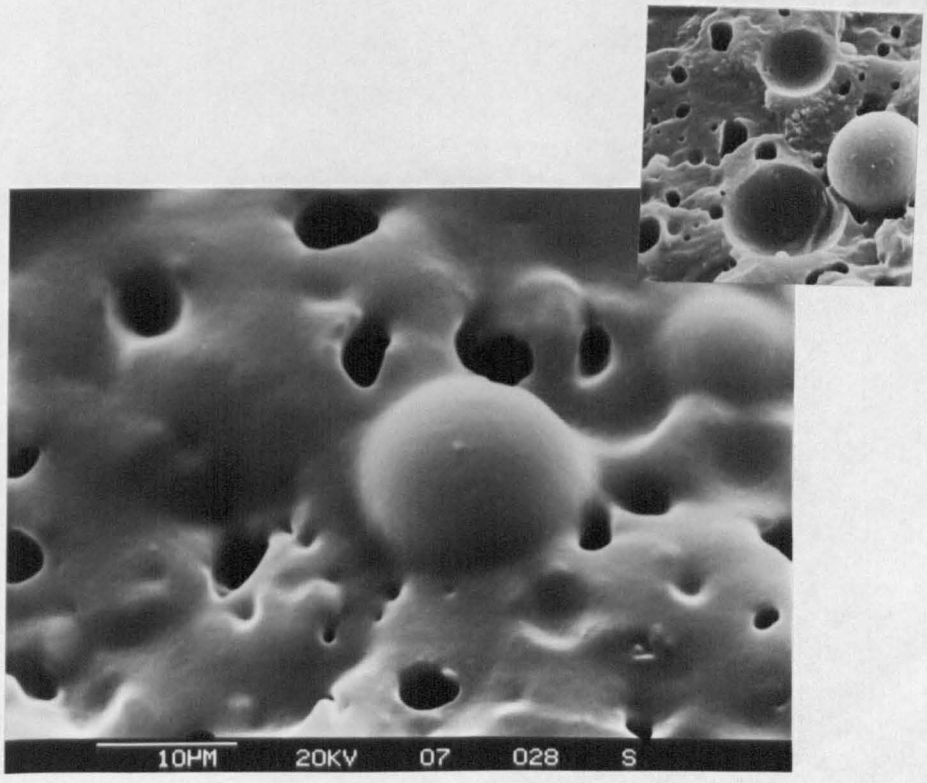

Figure 6.12 SEM micrograph of a cryogenic fractured and etched surface of a PP+R+G (TC1) sample showing a separate dispersion structure. Dark circular holes observed on the micrograph are the imprints of the EPR particles.

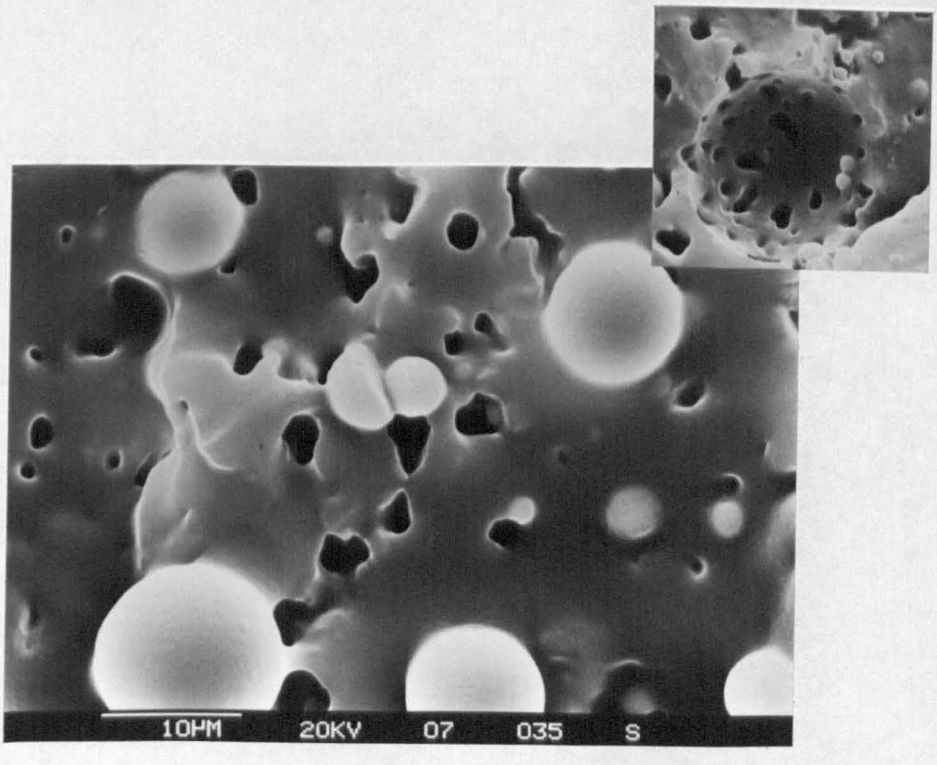

Figure 6.13 SEM micrograph of a (R+G)+PP, TC5 sample where EPR and glass beads were mixed in the extruder prior to PP, showing slightly more EPR particles adhering to the glass bead surfaces.

by the characteristics of the components than by the mixing technique. The similar observations had been reported by Varga [163] for the PP/elastomer/talc systems. The dispersion of talc in the polymer phases was mainly determined by the chemical characteristics of the components, and only slightly by the changes in the phase viscosity ratio or by the sequences of mixing. In his system encapsulation of talc by elastomer was observed. By using a polar elastomer a better wettability of talc was achieved. However, the final properties of these composites were poorer than those with a non-polar elastomer. This aspect will be considered later in Chapter 7.

Table 6.7 shows the tensile modulus, yield stress, elongation at yield and falling weight impact fail energy at 23°C of the PP/R/G composites prepared in five different sequences of mixing. The tensile modulus and yield stress values of these five composites were found to be lower than those of an unmodified polypropylene. The (PP+R)+G, TC3 composite showed the relatively lowest in both tensile modulus and yield stress values but highest in the elongation at yield. These differences, however, exceed only slightly the standard deviation of the measurements. The highest modulus and impact strength were found in the (R+G)+PP, TC5 composite. The slightly higher impact fail energy of the TC5 composite may be attributed to the presence of numbers of rubber particles adhering on the filler surface as shown by the SEM micrograph of *Figure 6.13*. Although the results from the SEM studies are in agreement with those of mechanical testing, it must be noted here that they do not provide enough quantitative evidence for the explanation of the higher in the tensile modulus and impact strength in the TC5 composite.

Further studies on the composite morphology were undertaken by DSC and DMA measurements in order to obtain more understanding on the structure/property relationships in these three-phase PP/R/G composites, especially in the TC5 composite where the relatively high impact strength was observed.

Figures 6.14 and 6.15 are the cooling and heating thermograms of the five PP/R/G composites prepared using different mixing sequences. Melting and crystallisation parameters calculated from these DSC thermograms are shown in *Table 6.8*. From preliminary studies of the two-phase systems of PP/R and PP/G, it was found that both EPR and glass beads have strong effects on the crystallisation behaviour of polypropylene. Addition of EPR to polypropylene led to a reduction in T_c and $T_{c\ onset}$ of polypropylene in the blends while glass beads caused an opposite effect. All five composites in this study showed a higher T_c and $T_{c\ onset}$ comparison to an unmodified

Table 6.7

Effect of mixing sequence on the tensile modulus, yield stress, elongation at yield and falling weight impact fail energy at 23 °C of the 60/20/20 (%wt.) PP/R/G composites

Sample	Mixing sequence	Modulus (GPa)	Yield stress (MPa)	Elongation at yield (%)	Impact fail energy (J)
PP	-	1.82 (0.03)[a]	36.59 (0.54)	5.49 (0.31)	3.64 (0.24)
TC1	PP+R+G	1.36 (0.01)	16.93 (0.20)	4.26 (0.27)	3.28 (0.44)
TC2	Reprocess of TC1	1.35 (0.01)	16.33 (0.26)	4.18 (0.41)	3.04 (0.32)
TC3	(PP+R)+G	1.24 (0.01)	15.90 (0.30)	4.57 (0.46)	2.82 (0.62)
TC4	(PP+G)+R	1.37 (0.01)	16.35 (0.35)	4.21 (0.46)	3.16 (0.43)
TC5	(R+G)+PP	1.38 (0.01)	16.19 (0.45)	4.02 (0.46)	4.39 (0.51)

[a] Standard deviations in parentheses, means from ten specimens.

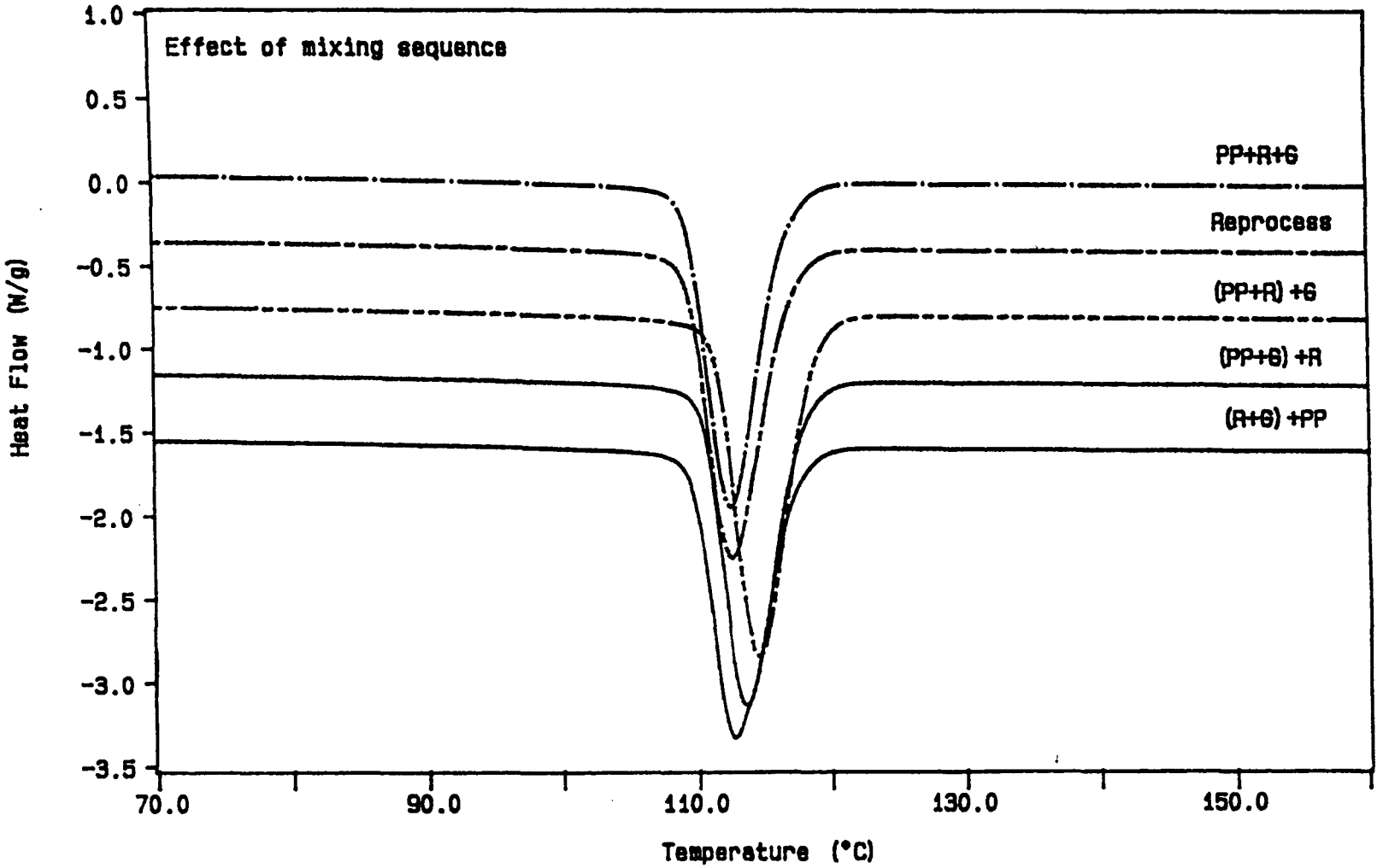

Figure 6.14 Crystallisation thermograms of the three-phase PP/R/G composites prepared using different mixing sequences.

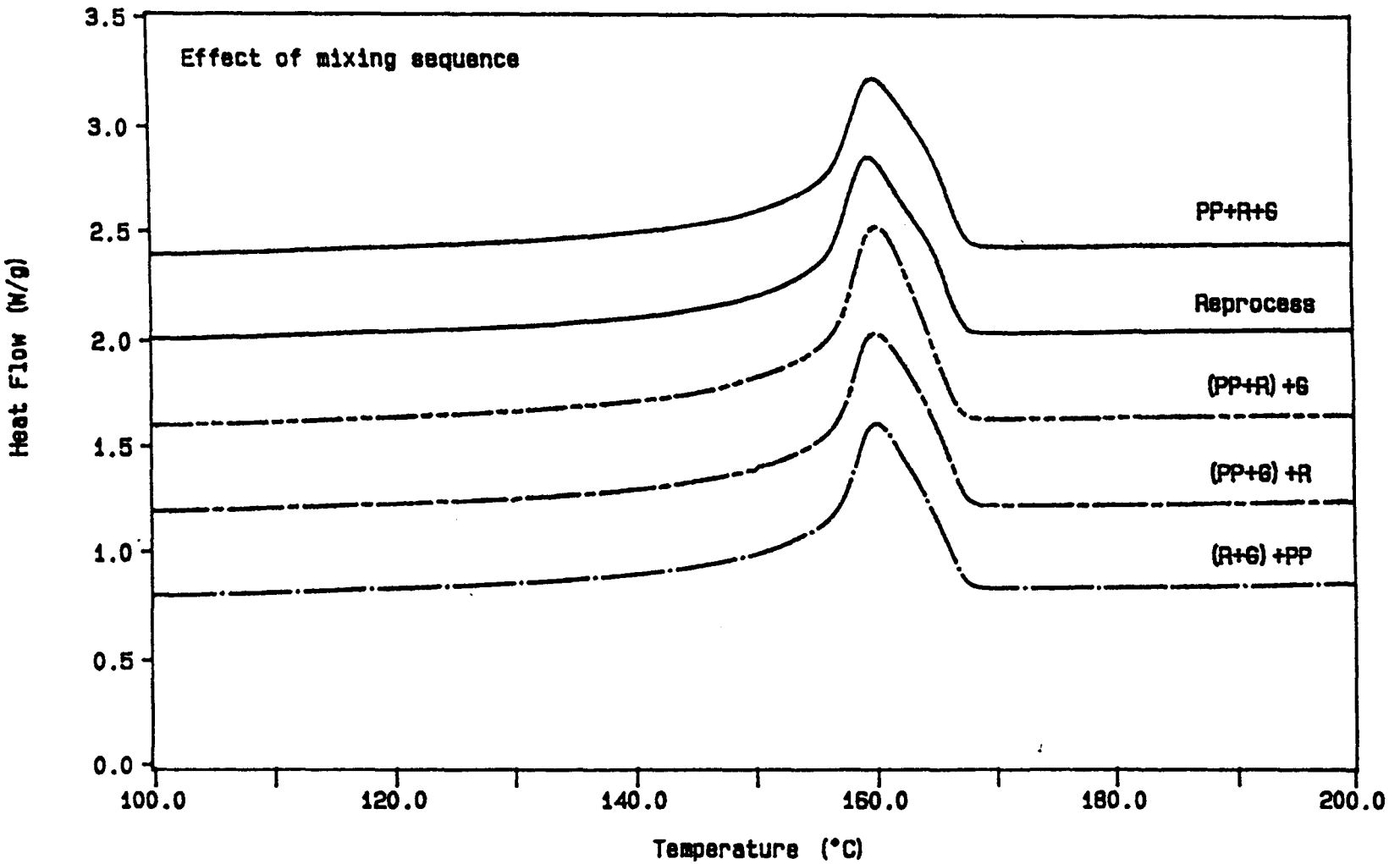

Figure 6.15 Melting endotherms of the three-phase PP/R/G composites prepared using different mixing sequences.

Table 6.8

The temperature of onset of crystallisation ($T_{c\ onset}$), crystallisation temperature (T_c), melting temperature (T_m), the difference between T_c and $T_{c\ onset}$ (T_1), degree of undercooling (T_2) and percentage crystallinity of unmodified polypropylene (PP) and the 60/20/20 (%wt.) PP/R/G composites prepared in a twin-screw extruder under differences of mixing sequence

Sample	Mixing sequence	$T_{c\ onset}$ (°C)	T_c (°C)	T_m (°C)	T_1 (°C)	T_2 (°C)	Crystallinity (%)
PP	-	114.6	109.2	163.3	5.4	54.1	48.9
TC1	PP+R+G	116.8	112.5	160.1	4.3	47.6	29.6
TC2	Reprocess of TC1	117.2	112.6	159.6	4.6	47.6	30.2
TC3	(PP+R)+G	118.8	114.5	160.2	4.3	45.7	31.7
TC4	(PP+G)+R	117.9	113.6	160.1	4.3	46.5	30.1
TC5	(R+G)+PP	117.4	112.8	160.1	4.6	47.3	28.2

polypropylene. This finding inferred that the glass bead particles had not been encapsulated by EPR since if so the effect of glass beads should be less pronounced in such composites.

According to Nielsen' s theory [108], the impact strength of polymers generally decreases as crystallinity increases. From this work, there is a good relationship between the impact strength and percentage of crystallinity. *Figure 6.16* is the plot of percentage crystallinity against impact strength. The TC5 composite which had been shown earlier as the composite of best impact properties has the lowest crystallinity while the TC3 composite which shows the lowest impact properties has the highest crystallinity.

Also, from the work by Hutley and Darlington [129-130] on filled composites, the high $T_{c\ onset}$ was observed in composites with low impact strength. The TC3 composite which has the lowest tensile and impact properties showed the highest $T_{c\ onset}$. However, there seems to be no correlation between $T_{c\ onset}$ and impact strength for the other four composites.

Quantitative studies on phase structures of the five PP/R/G composites were also undertaken by DMA measurement. *Figure 6.17* depicts the effect of mixing sequence on the damping (tan δ) of the PP/R/G (60/20/20) composites as a function of temperature. *Table 6.9* gives a quantitative representation of the EPR glass transition temperature (T_g) values and tan δ_{max} values with different mixing sequences.

Table 6.9 -Effect of mixing sequence on the EPR peak temperature values and tan δ values at peak of various three-phase PP/R/G composites.

Sample	Mixing sequence	EPR peak temperature (°C)	tan δ value ($\times 10^{-2}$)
TC1	PP+R+G	-43.4	4.75
TC2	Reprocess of TC1	-43.1	4.49
TC3	(PP+R)+G	-43.2	4.60
TC4	(PP+G)+R	-43.1	4.34
TC5	(R+G)+PP	-40.8	4.83

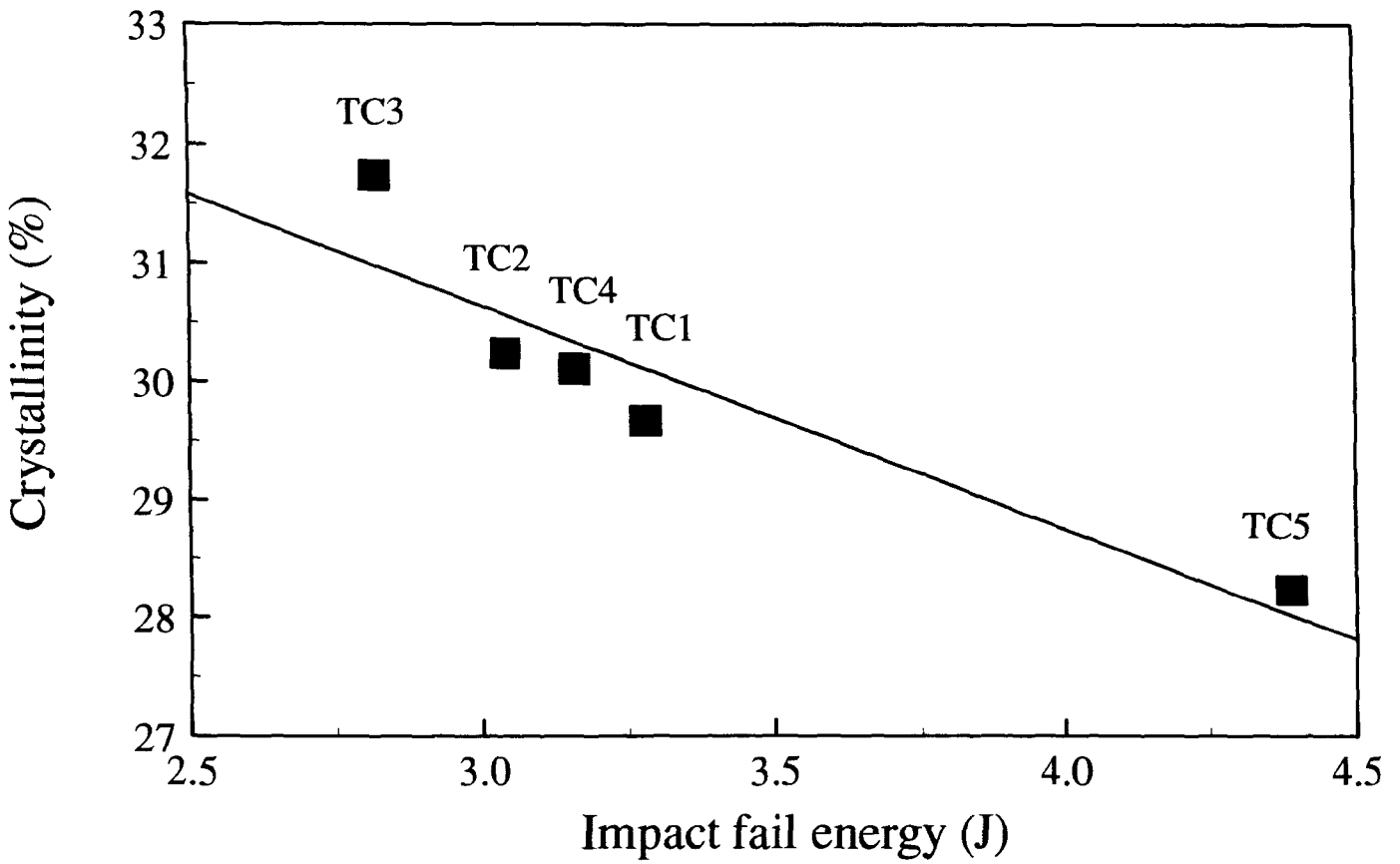

Figure 6.16 Percentage crystallinity of various PP/R/G composites as a function of falling weight impact fail energy at 23 °C. As the crystallinity decreased, the impact fail energy increased systematically.

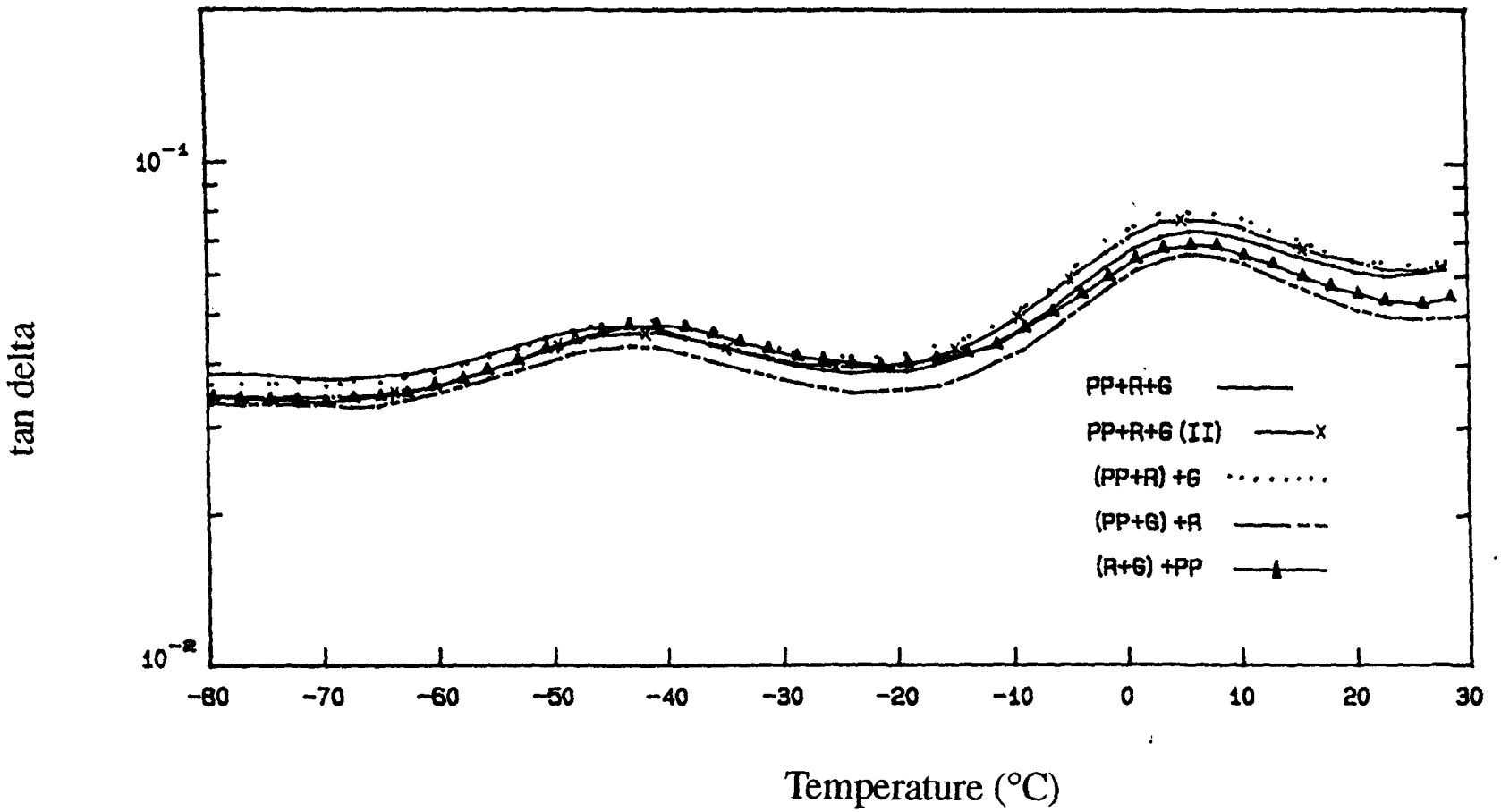

Figure 6.17 Temperature dependences of the damping (tan delta) at 1 Hz. of various PP/R/G composites prepared in a twin-screw extruder under different mixing sequence.

There is often a good correlation between the impact strength and the dynamic mechanical properties of polymer blends [272]. Impact strength generally increases with the size of the damping (tan δ) peak due to the rubber phase increases. In this study the EPR content was kept constant in all composites, thus, no significant difference was observed in the size of the damping peak. Apart from the size (maxima) of the damping peak, its location also indicates the phase structure of the composites. Due to the incompatibility of PP and EPR, two damping peaks were observed corresponding to the T_g of each component. The shift of these peaks can infer changes in the chain mobility of either PP or EPR. In this study, the (R+G)+PP,TC5 composite showed a shift of the EPR damping peak to a higher temperature. As shown in *Table 6.9* the T_g of EPR in the TC5 sample was observed at around -41°C which is 2°C higher than those observed in the other four composites (at -43°C).

The observation of the shift in the EPR damping peak, as well as those obtained from the SEM and DSC studies revealed that some encapsulation of glass beads by EPR had occurred, although this could not be fully achieved by simply changing the mixing sequence. The TC5 sample in which glass beads were mixed with EPR prior to mixing with PP, showed more EPR particles adhering to the glass bead surfaces. The result from this structure is more energy dissipation between phases resulting in a relatively higher in tensile and impact properties in this composite.

6.3.3 The Dependency of Composite Structure and Properties on Composition

PP/R/G composites of various compositions were prepared in the twin-screw extruder. All the three components (PP, EPR and G) were mixed in the extruder at the same time using a screw speed of 170 rpm with a feed rate of 19 kg/hr.

6.3.3.1 Study of composite structures by DSC and DMA

Figures 6.18 and 6.19 are the crystallisation and melting thermograms of various PP/R/G composites differing in the volume fraction of rubber and glass beads. The DSC data calculated from these thermograms are presented in *Table 6.10.* The incorporation of 30 vol% of EPR led to a decrease in the $T_{c\ onset}$ of crystallisation, inferring delayed nucleation. The crystallisation and melting temperatures as well as degree of undercooling also decreased, in comparison to those for an unmodified polypropylene. The percentage crystallinity observed in the PP/R (70/30) composite was lower than that

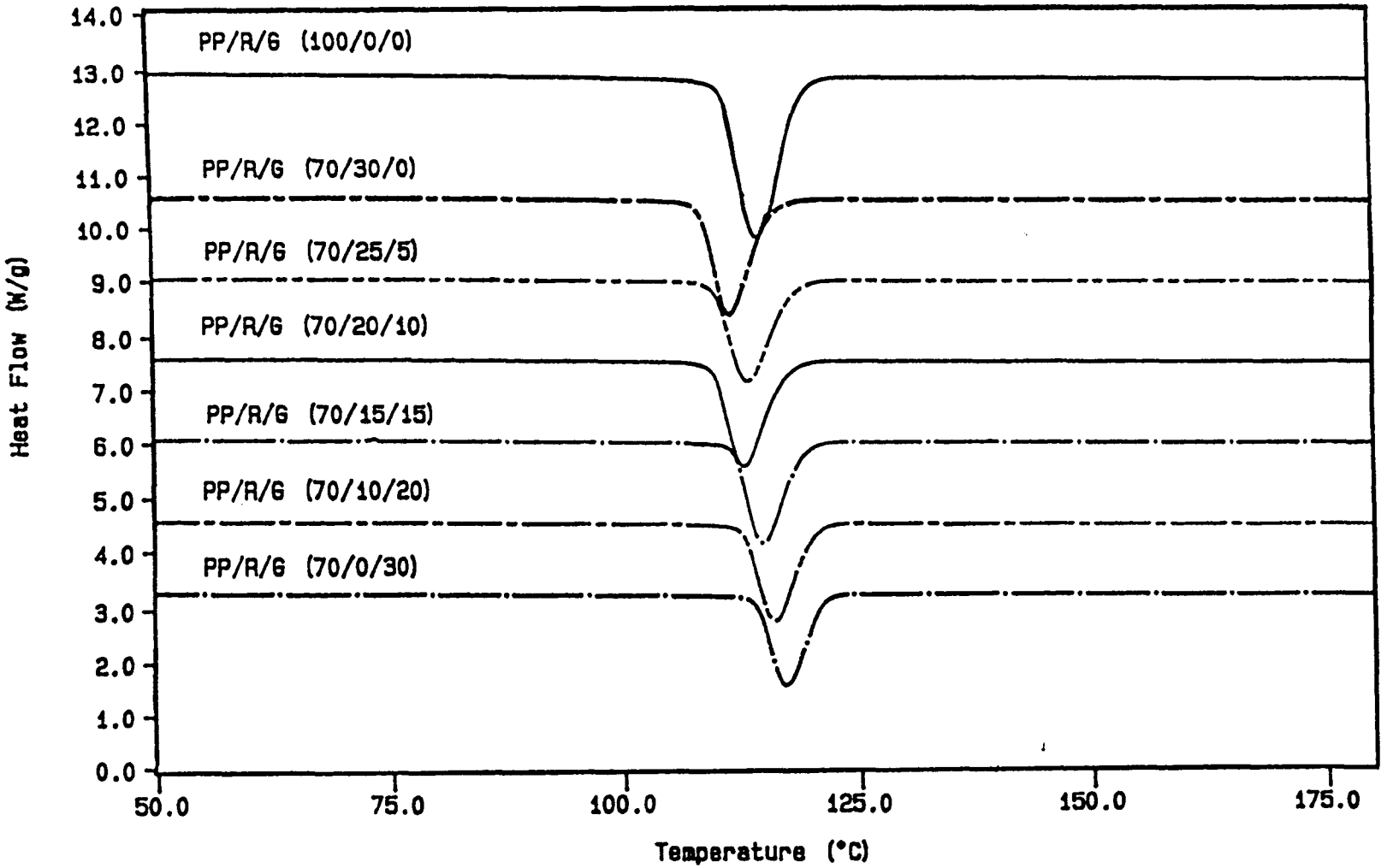

Figure 6.18 Crystallisation thermograms of the three-phase PP/R/G composites, showing the effect of composition

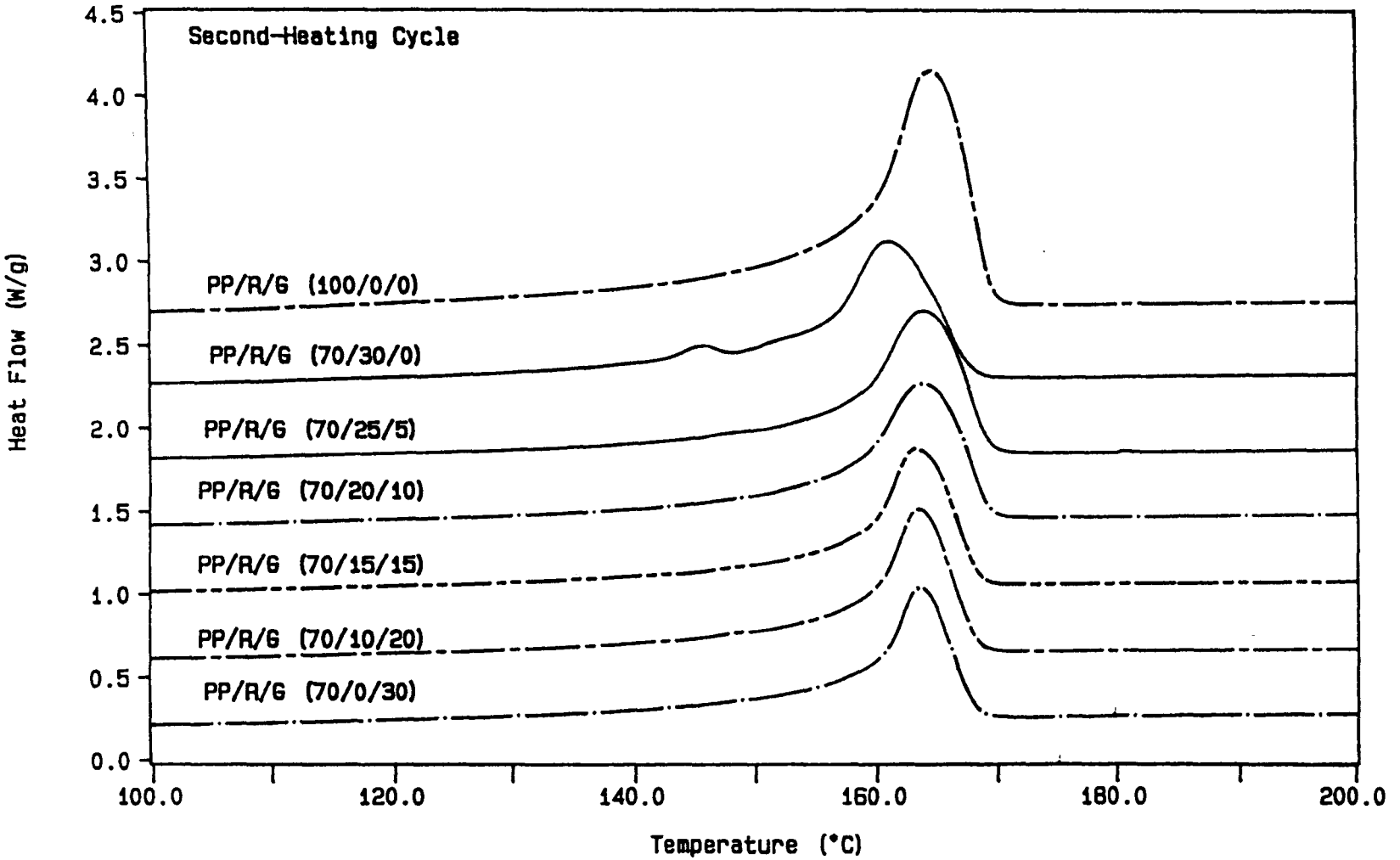

Figure 6.19 Melting endotherms of the three-phase PP/R/G composites of various compositions.

Table 6.10

The temperature of onset of crystallisation ($T_{c\ onset}$), crystallisation temperature (T_c), melting temperature (T_m), the difference between T_c and $T_{c\ onset}$ (T_1), degree of undercooling (T_2) and percentage crystallinity of various PP/R/G composites prepared by varying rubber and filler contents

Composition of PP/R/G		$T_{c\ onset}$	T_c	T_m	T_1	T_2	Crystallinity (%)	
(by vol)	(by wt)	(°C)	(°C)	(°C)	(°C)	(°C)	exper.[a]	recal.[b]
100/0/0	100/0/0	119.3	114.5	164.3	4.7	49.8	50.6	50.6
70/30/0	70/30/0	115.7	111.6	161.1	4.2	49.5	35.4	35.4
70/25/5	65/22/13	118.0	113.3	164.0	4.7	50.7	32.9	32.9
70/20/10	60/16/24	117.3	112.8	164.0	4.5	51.2	31.2	30.4
70/15/15	55/12/33	118.9	114.7	163.4	4.2	48.7	27.6	27.8
70/10/20	52/7/41	119.9	115.8	163.6	4.1	47.8	27.8	26.3
70/0/30	46/0/54	120.9	117.1	163.7	3.8	46.6	24.7	23.1

[a] Percentage crystallinity obtained from the experiments.

[b] Recalculated percentage crystallinity based on the weight % of polypropylene in the composites.

of the unmodified PP. This is attributed to the fact that 30% of polypropylene was substituted by EPR which acts as a diluent in the composite. However, no change in the percentage crystallinity was observed compared to PP when subtracting the wt.% of EPR in the composites and recalculating % crystallinity only on the wt.% of the PP component (70 wt.%), assuming EPR does not crystallise. As shown in *Table 6.10* 100 wt.% PP provides 50.6 % crystallinity, by subtracting 30 wt.% of EPR in the PP/R/G (70/30/0) composite so 70 wt.% of PP component should provide 35.4 % crystallinity. It can be seen that the recalculated crystallinity value was the same as that observed from the experiment. This result indicated that EPR has no effect on the extent of crystallinity in the PP/R/G composites.

Addition of 30 vol% (or 54 wt.%) of glass beads to polypropylene (PP/R/G, 70/0/30) led to an increase in T_c and $T_{c\ onset}$, and a decrease in melting temperature, the degree of undercooling (T_2) and the difference between T_c and $T_{c\ onset}$ (T_1). All these results indicated that glass beads increased the rate of crystallisation of polypropylene by acting as nucleating agents, promoting the formation of crystal nuclei and led to a decline in polypropylene spherulite size.

In the ternary phase systems where both EPR and glass beads were incorporated, as the glass bead contents increased $T_{c\ onset}$ and T_c increased systematically (*Figure 6.18*). In contrast, degree of undercooling (T_2) and the percentage crystallinity of the composites decreased. As the glass bead content increased, the crystallinity decreased systematically as shown in *Figure 6.20*. However, no significant change in crystallinity was observed compared to PP when subtracting the wt.% of glass beads in the composites. The investigated three-phase composites of different compositions show no significant difference in their melting temperatures. From these results, it can be concluded that both EPR and glass beads influenced the crystallisation behaviour of polypropylene but in different ways. EPR reduced the T_c and $T_{c\ onset}$ of polypropylene while glass beads had an opposite effect.

Dynamic mechanical analysis (DMA) undertaken was aimed at exploring whether the structure of the composites could be changed from separate dispersion to encapsulation by increasing the amount of rubber in the composites. *Figures 6.21 and 6.22* represent the temperature dependency of storage modulus and tan δ of various ternary PP/R/G composites. The expected increase in the composite modulus was observed as the glass beads content increased (*Figure 6.21*). Two tan δ peaks seen in *Figure 6.22* at about -43 °C and 6 °C corresponded to the glass transition temperatures of EPR and PP, respectively. As mention earlier the shift in EPR glass transition peak or any changes in

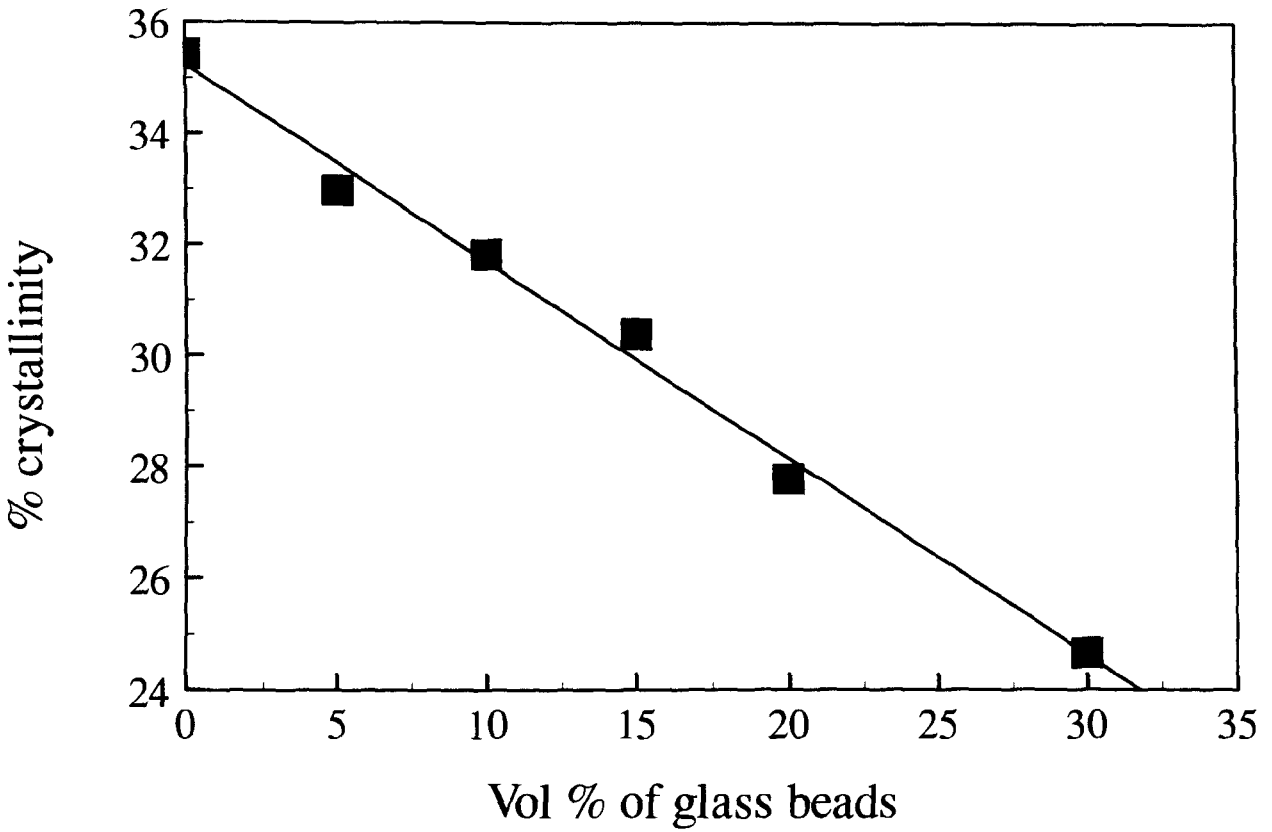

Figure 6.20 Percentage crystallinity of various PP/R/G composites as a function of vol % of glass beads

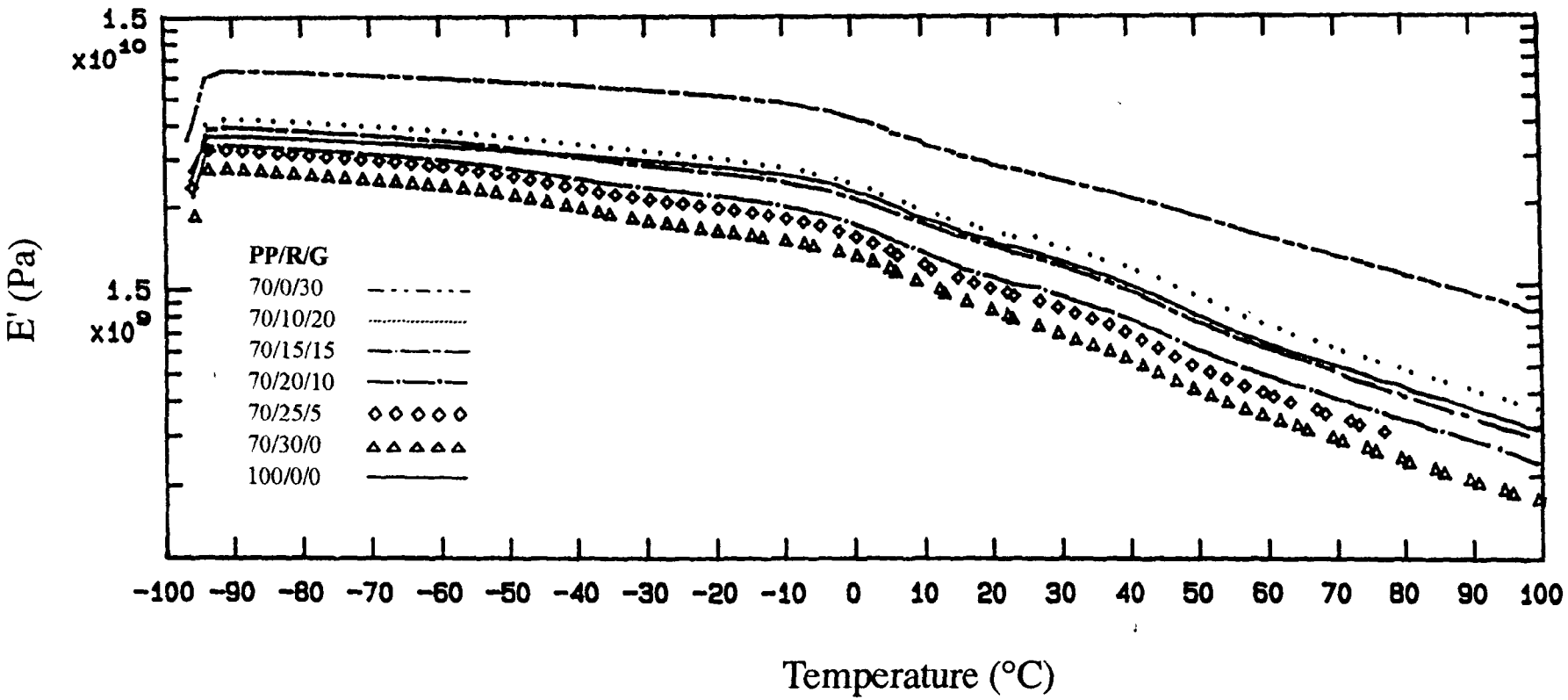

Figure 6.21 Temperature dependences of the storage modulus (E') at 1 Hz. of the three-phase PP/R/G composites of various compositions.

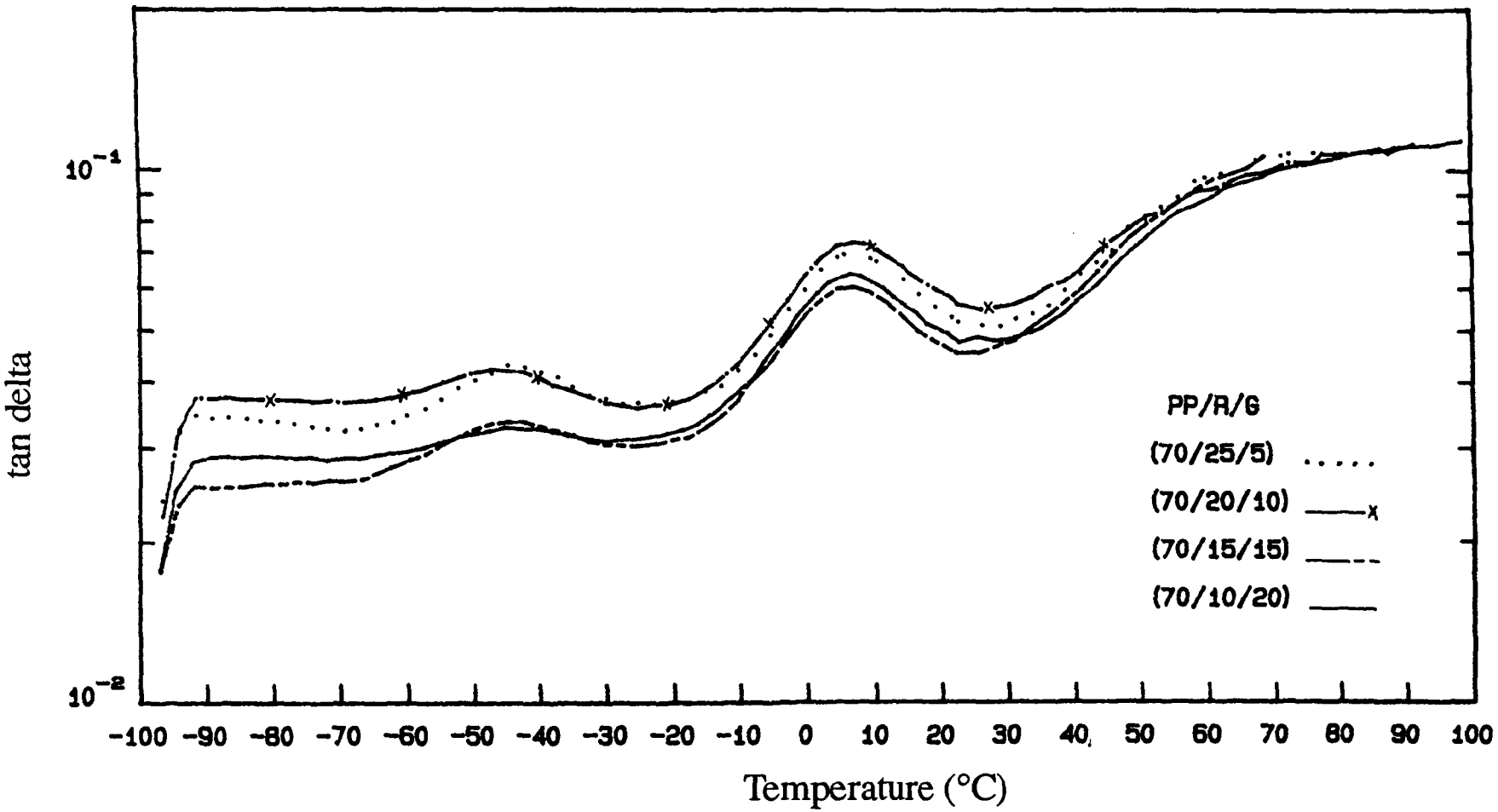

Figure 6.22 Temperature dependences of the damping (tan delta) at 1 Hz. of the three-phase PP/R/G composites of various compositions.

maxima of this peak can infer to the change in mobility of EPR chains. In this work the sum of filler and rubber contents was kept constant at 30 vol%. A reinforcing effect of the filler was still observed even at high rubber/filler ratio, i.e. in the 70/25/5 PP/R/G composite (where $V_r/V_f = 5$). These results proved the earlier findings that the structure of PP/R/G composites investigated involves separate dispersion of the additive phases. This structure could not be changed either by increasing the amount of rubber in the composites or by altering the sequence in which the components were mixed in the extruder .

6.3.3.2 The dependency of tensile and impact properties on composition

Tensile modulus, yield stress, percentage elongation at yield and falling impact fail energy of PP/R/G composites of various compositions are reported in *Table 6.11*. Unmodified polypropylene shows the tensile yield stress of 36.59 MPa. With addition of 30 vol% glass beads tensile yield stress dropped to 18.31 MPa or by a factor of 50%. A drop in the tensile strength can be explained by poor interfacial adhesion between the polypropylene matrix and glass beads. *Figures 6.23a -b* show the SEM micrographs of glass bead filled polypropylene composites. It is clearly seen from *Figure 6.23a* that the glass bead surface was very clean. There was almost no bonding between glass beads and the polypropylene matrix. *Figure 6.23b* revealed the tensile fracture surface of the same composite where the glass bead particles were torn out of the matrix leaving holes parallel to the drawing direction. In case of ternary phase composites where both rubber and filler are involved, if both components are spherical and their load bearing capacities are similar, additivity of component effects can be observed for yield and ultimate properties [273]. Thus, if yield stress or tensile strength is plotted against the total additive content, the experimental values lie on the same curve. For the PP/R/G composites investigated, the yield stress was found to be a unique function of the total concentration of rubber and filler as shown in *Figure 6.24*. Similar observation was found in PP/EPDM/talc composites [144].

The influence of EPR and glass beads on the composite modulus is shown in *Figure 6.25*. By incorporation of 30 vol% EPR the composite modulus reduced from 1.82 GPa (modulus of the PP matrix) to 1.14 GPa. This reduction can be ascribed to the substitution of the low modulus material such as EPR into the system. The addition of 30 vol% glass beads, on the other hand, increased this value to 2.87 GPa. Although the evidence from the SEM micrographs (figures 6.23a-b) revealed the lack of adhesion between the glass bead particles and the polypropylene matrix. It has to be pointed out, however, that the modulus of the composites is not affected by interfacial adhesion and

Table 6.11

Tensile modulus, yield stress, elongation at yield and falling weight impact fail energy at 23 °C of various PP/R/G composites prepared by varying rubber and filler contents

Sample (vol %)	Modulus (GPa)	Yield Stress (MPa)	Elongation at yield (%)	Impact fail energy (J)
PP/R/G (100/0/0)	1.82 (0.02)[a]	36.59 (0.29)	5.49 (0.31)	4.12 (0.46)
PP/R/G (70/30/0)	1.14 (0.05)	19.26 (0.23)	5.20 (0.27)	6.96 (0.39)
PP/R/G (70/25/5)	1.22 (0.06)	19.92 (0.31)	5.68 (0.32)	4.22 (0.19)
PP/R/G (70/20/10)	1.36 (0.05)	18.62 (0.28)	4.35 (0.04)	2.95 (0.56)
PP/R/G (70/15/15)	1.84 (0.03)	18.67 (0.18)	3.43 (0.17)	4.56 (0.43)
PP/R/G (70/10/20)	2.08 (0.10)	18.78 (0.21)	3.00 (0.29)	3.48 (0.29)
PP/R/G (70/0/30)	2.87 (0.05)	18.31 (0.46)	2.34 (0.24)	1.79 (0.54)

[a] Standard deviations in parentheses, means from ten specimens.

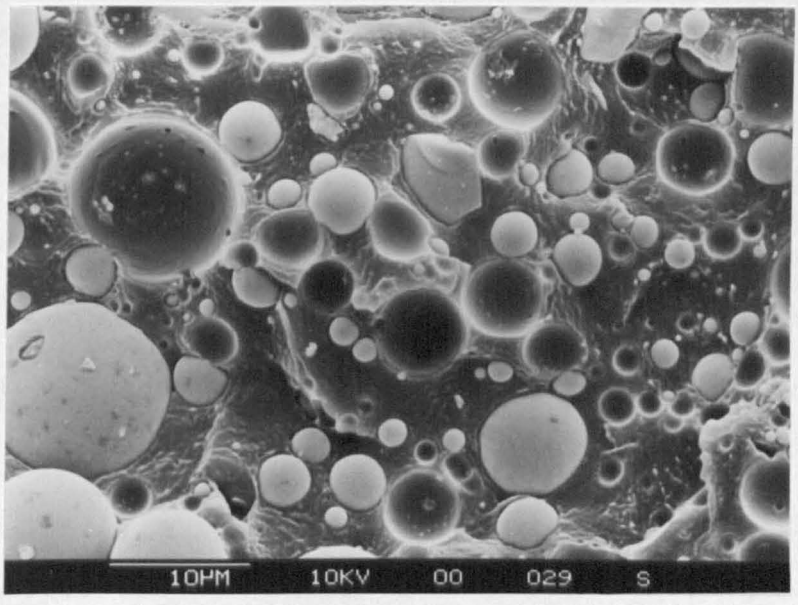

Figure 6.23a SEM micrograph of a cryogenic fractured surface of a polypropylene composite filled with 20 %vol of glass beads. Bead surfaces are very clean showing no bonding to the polypropylene matrix.

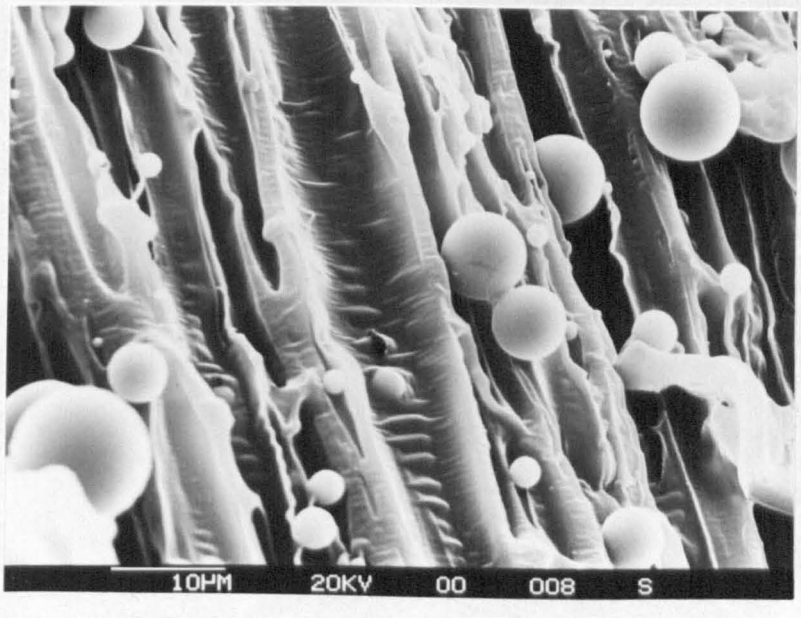

Figure 6.23b SEM micrograph of a tensile fractured-surface of a glass bead filled polypropylene composite (80/20) where the bead particles were torn out leaving holes parallel to the drawing direction.

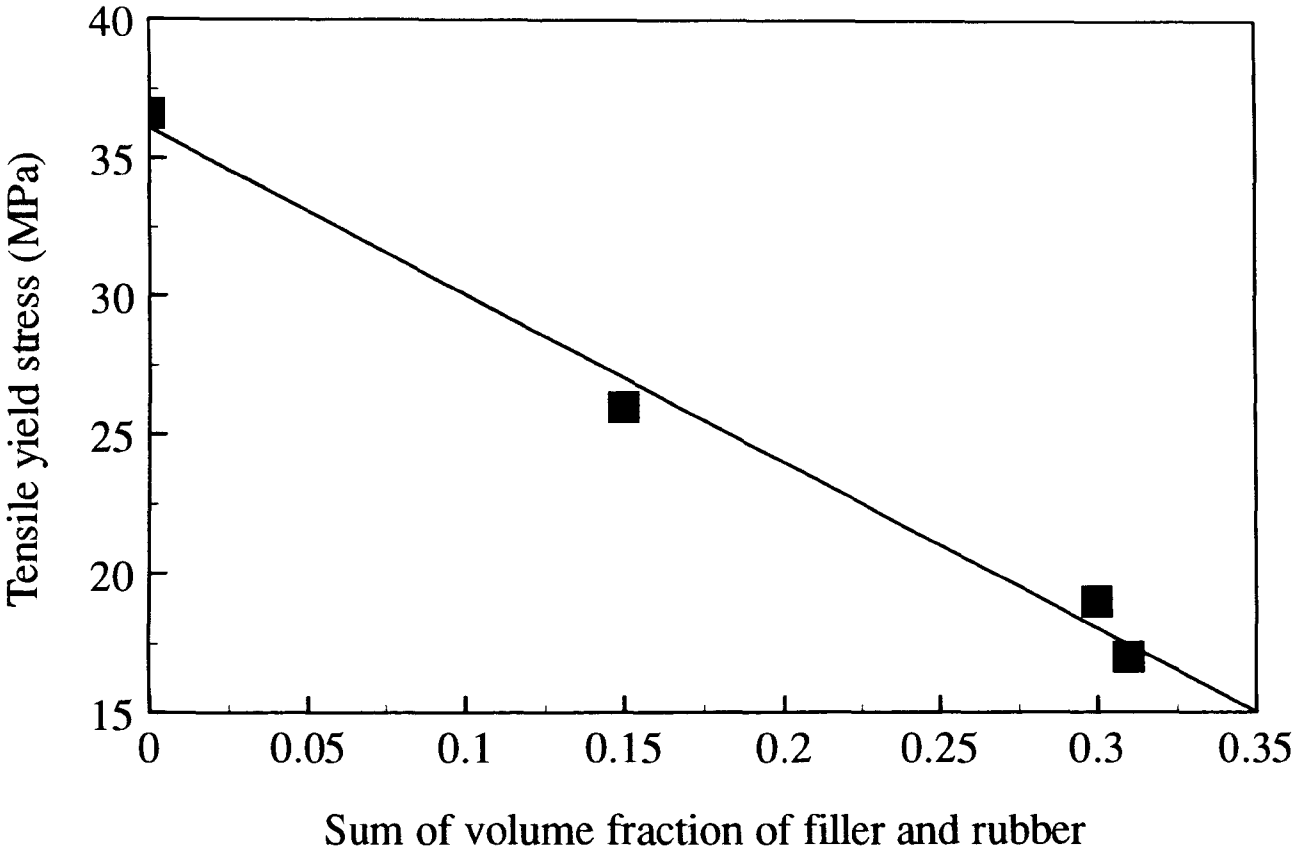

Figure 6.24 Tensile yield stress as a function of total filler and rubber contents

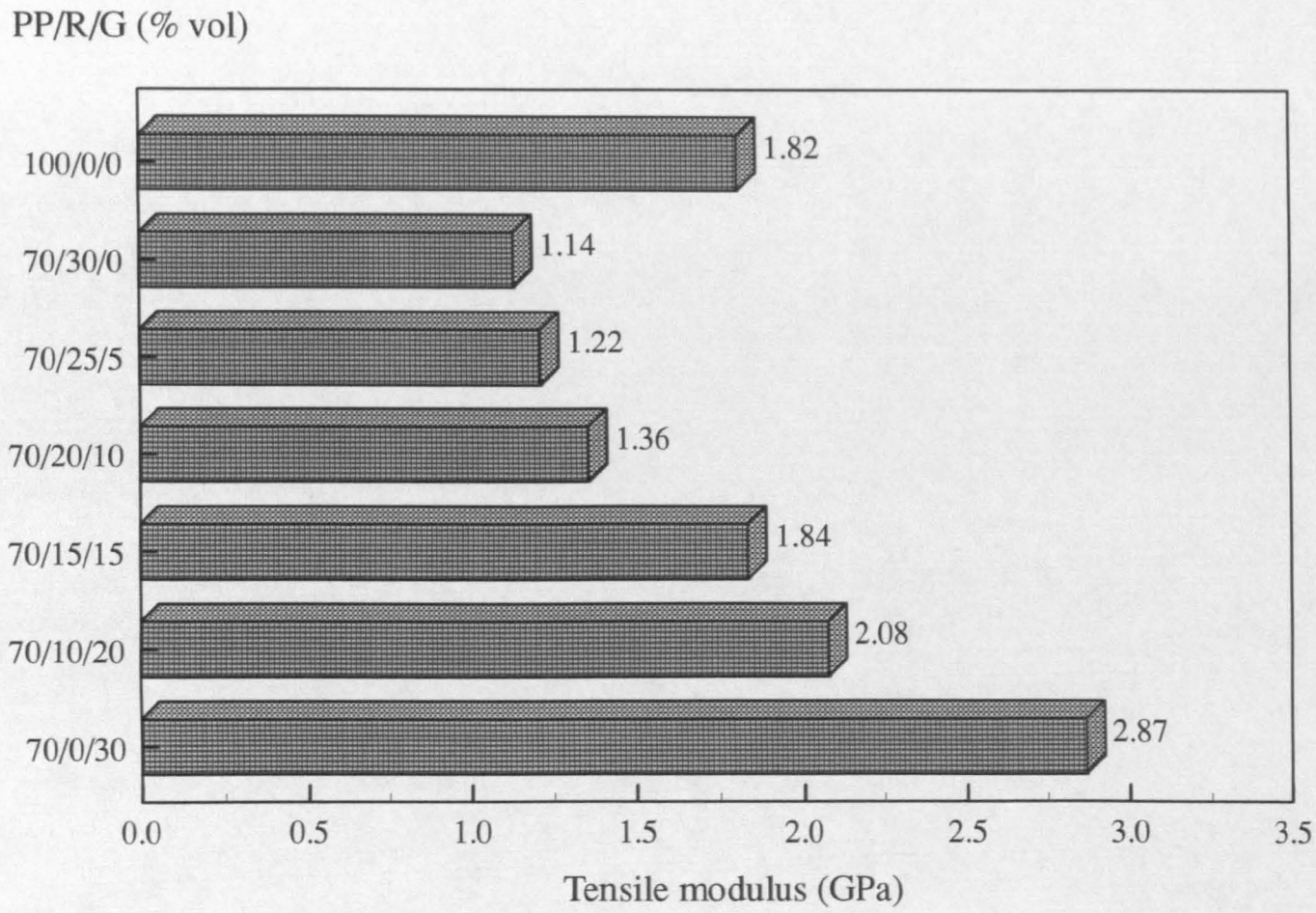

Figure 6.25 Effect of composition on the tensile modulus of PP/R/G composites

its variation because normal contact of the composites is sufficient to transmit stresses at very small strain [108]. Thus, the modulus of the filled composite is still higher than that of an unmodified polypropylene. Modulus of the ternary phase PP/R/G composites noticeably increased as the glass bead content increased. Although the results from the image analysis study showed that the rubber particles in the ternary phase PP/R/G composites were smaller than those in the binary (PP/R) system, the reduction in rubber particle size cannot lead to a drop in the composite modulus because of the strong reinforcing effect of the incorporated filler.

Both EPR and glass beads caused a reduction in the composite elongation, but at very different rates (*Table 6.11*). EPR has only a slight reduction effect, addition of 30 vol% EPR into the PP matrix caused the elongation at yield of the composite (70/30/0) reduced by 5.5%. While the incorporation of 30 vol% glass beads reduced this value sharply by 58%. With increasing the glass bead contents the elongation at yield reduced systematically.

In the case of effect on impact properties, as predicted addition of EPR raised the impact strength value of the 70/30/0 PP/R/G composite by 69%. On the other hand, with addition of 30 vol% glass beads a dramatic reduction in the impact strength value was observed. In the three-phase PP/R/G composites where both EPR and glass beads are involved in the systems, no significant difference between the impact strength values was found between the composites of different rubber and filler contents in the studied range of 5-25 vol%. Although the 70/15/15 PP/R/G composite gave a relatively higher in impact strength, it exceeds only slightly the standard deviation of the measurements.

From all these results it can be concluded that the balance of tensile and impact properties can be achieved by physical blending of the polypropylene with ethylene-propylene rubber and glass beads. The properties of these three-phase composites were mainly determined by the composition and phase structures of the composites. The investigated processing variables including screw configuration, screw speed and feed rate showed a minor influence on these properties. The evidence from SEM, DSC and DMA studies revealed separate dispersion structure in these three-phase PP/R/G composites. This structure could not be changed either by altering the sequence in which the components were mixed in the extruder or by introducing more rubber contents into the composite. However, by mixing the rubber and glass beads prior to polypropylene there was a tendency of more rubber particles adhering on the glass bead surface. This composite, interestingly, provided a slightly better in tensile and impact properties than the composite prepared by one-stage mixing.

CHAPTER 7

INTERFACIAL MODIFICATION OF TERNARY PHASE POLYPROPYLENE COMPOSITES

7.1 INTRODUCTION

In ternary phase polypropylene composites containing elastomer and rigid filler, two differing phase structures may assume : either a *"separate dispersion"* structure where elastomer and filler particles are dispersed separately in the polypropylene matrix, and/or an *"encapsulation"* structure where elastomer encapsulates filler particles, forming a low-modulus interlayer between matrix and filler. Formation of these structures depends on several factors including the properties of the polymers and fillers, especially their surface characteristics and mutual wettability; blend preparation techniques, including the sequence in which the components are introduced into the blend; and the relative viscosity of the polymer and elastomer phases, since the filler is thought to be generally encapsulated by the component of lower viscosity. The most important factor, reported by Pukanszky et.al. [145], is due to the surface treatment of the filler. In PP/EPDM/$CaCO_3$ systems [144,148], it was found that $CaCO_3$ fillers (without any surface treatment) were extensively encapsulated by an EPDM elastomer (up to 70% of incorporated filler). If the filler was surface-treated with stearic acid, fewer particles undergo encapsulation. As soon as the surface treatment (coverage) was completed, only a small percentage of particles remained encapsulated and the final structure was phase separated.

In the previous chapter, where ternary composites of PP/EPR/glass beads were investigated, separate dispersion of EPR and glass bead particles in the PP matrix was observed. The resulting structure could not be changed (from separate dispersion to encapsulation) either by alteration of the sequence in which the components were mixed in the extruder or by introduction of more rubber contents into the composites.

In the present study, surface-treated filler (silane-coated glass beads) and functionalised rubber (maleic-anhydride modified EPR) were investigated, in terms of their influence on morphological structures and mechanical properties of ternary phase polypropylene composites. Also, from the previous work of Chapter 6 the composite prepared by mixing the rubber and glass beads prior to polypropylene, showed slightly better in tensile and impact properties than the composite prepared by one-step mixing. In the present study effect of mixing step on composite structure and properties was also considered.

7.2 EXPERIMENTAL

7.2.1 Materials

Polypropylene homopolymer grade Novolen 1100HX, was used as a matrix polymer. Two grades of ethylene-propylene rubber (EPR) investigated, were Exellor PE808 and Exellor VA1803. The former is a medium viscosity semicrystalline grade, while the latter is a low viscosity amorphous maleic-anhydride grafted EPR, with 0.7 % of maleic-anhydride content. Glass beads used were the 5000CPOO which is a non surface-treated grade, and 5000CPO3 grade where the glass surface has been treated with silane coupling agent. Detail of their properties were reported earlier in Chapter 3 -section 3.2.

7.2.2 Blend preparation

One-step mixing. All the binary and ternary composites were prepared in a co-rotating twin-screw extruder, by melt-mixing of all the components at a temperature range from 185 to 200°C (from feeder to die), with a screw speed of 170 rpm and a feed rate of 20 kg/hr. The screw profile used was designated an "SM profile". The composite formulation was kept constant at 70/30 (by vol) for binary phase polypropylene composites both with rubber and with filler, and at 70/15/15 (by vol) for ternary phase composites.

Two-step mixing. This procedure was used only for ternary composites. Firstly, rubber and glass beads were premixed in the extruder. Secondly, the mixture obtained was melt mixed with polypropylene under the same operating conditions as listed in the above paragraph.

7.2.3 Sample preparation and testing

Samples for morphological and mechanical testing were prepared by compression-moulding. Direct observation of phase structure was carried out using SEM on fractured and etched surfaces. DMA and DSC were used as complementary methods for quantitative morphological information. FTIR was used in the characterisation of chemical functionalities in various polypropylene composites in order to investigate the chemical interaction and structure in the interphase region. Mechanical tests investigated included tensile and impact measurements at room temperature (23°C), and a fracture toughness test based on the J-integral method carried out at low temperature (-20°C). All testing procedures were reported in detail in Chapter 3.

7.3 RESULTS AND DISCUSSION

7.3.1 Effect of functionalised components on composite structure

7.3.1.1 Phase morphology by SEM observations

Effect of functionalised EPR (MaR) and surface-coated glass beads (coatG) on phase morphology of polypropylene composites were investigated. States of dispersion of the rubber and filler particles as well as the interfacial adhesion between phases were also considered.

Figure 7.1 shows phase structure of an unmodified PP/R/G composite. The sample was fractured at liquid nitrogen temperature, and then etched with heptane vapour for 3 sec. to remove the EPR particles. A separate dispersion structure was observed in this composite, where EPR does not encapsulate glass bead particles. Glass beads were very well dispersed without evidence of agglomeration.

A contrasting morphology is shown in *Figure 7.2*, where encapsulation of glass bead particles by MaR was observed in the PP/MaR/G composite. MaR adheres strongly to the surface of glass beads and remains bonded to glass even after heptane treatment.

The effect of silane-coated glass beads is shown in *Figure 7.3*. A separate dispersion structure was also observed in this system as with the PP/R/G composite. However, some glass bead particles were found to be partially wetted by EPR as seen in *Figure 7.4*. The small dark circular holes (~1 μm) shown on the micrographs are imprints of EPR particles, while large hemispherical dark areas (~5-7 μm) were due to the torn-off glass bead particles during the fracture. The fractured surface of this composite is very similar to that of the (R+G)+PP composite in which EPR was mixed with glass beads prior to polypropylene (*Figure 7.5*).

(i) Analysis of phase structure formation

Formation of these phase structures depends on several factors. However, the limits of ideal structure were reported to be determined by thermodynamic considerations [145]. The completeness and ease of wetting of the solid surface by liquid depends on the characteristics of the solid surface (such as surface energy and roughness), the viscosity and amount of liquid available, and the contact angle of the liquid on the solid. The

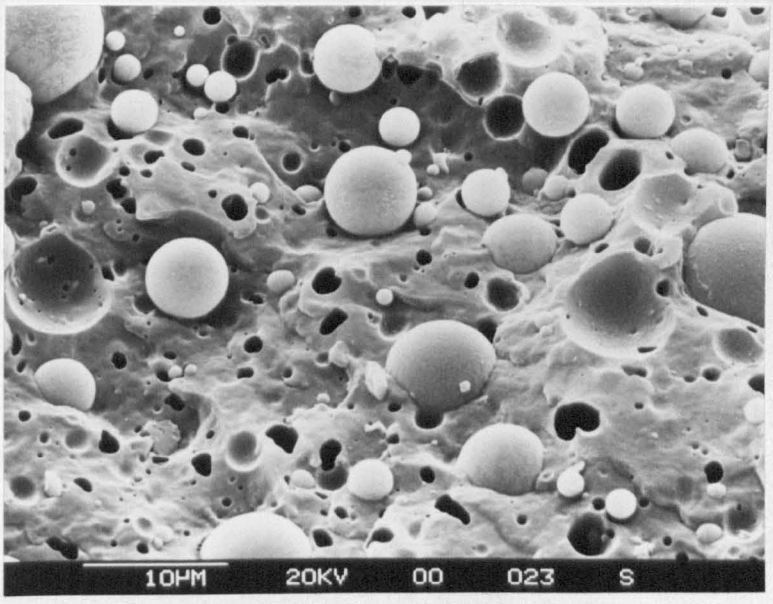

7.1

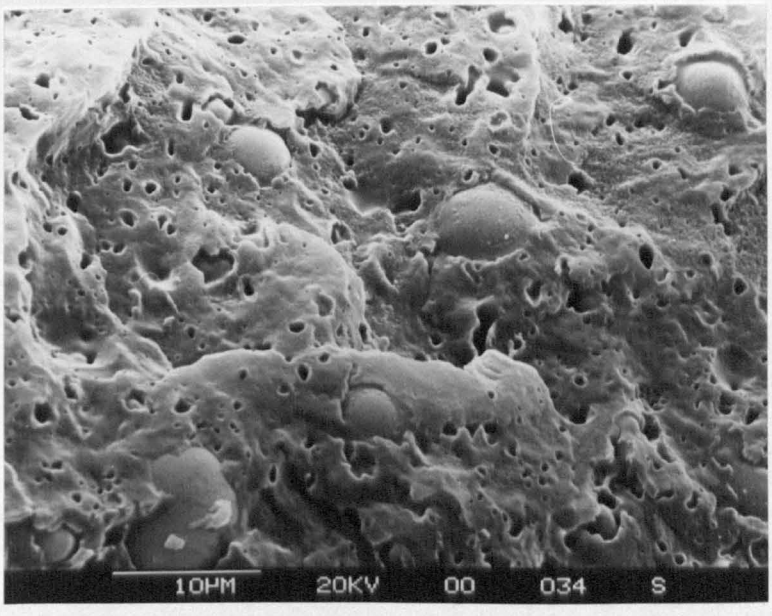

7.2

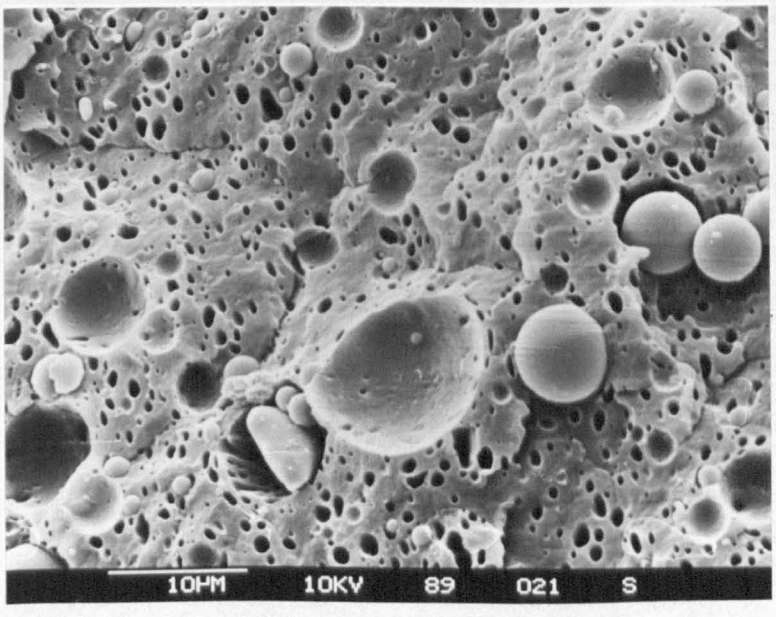

7.3

Figures 7.1 to 7.3 SEM micrographs of cryogenic fractured and etched surfaces of PP/R/G (7.1), PP/MaR/G (7.2), and PP/R/coatG composites (7.3).

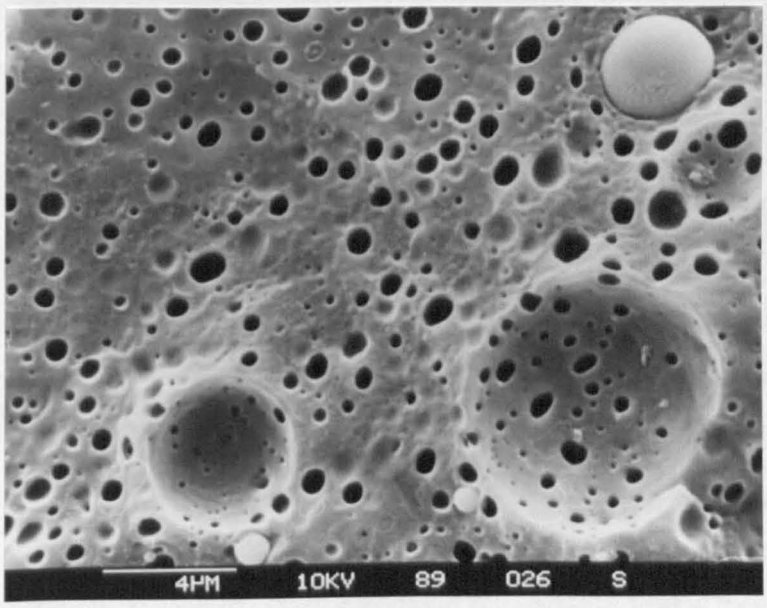

7.4

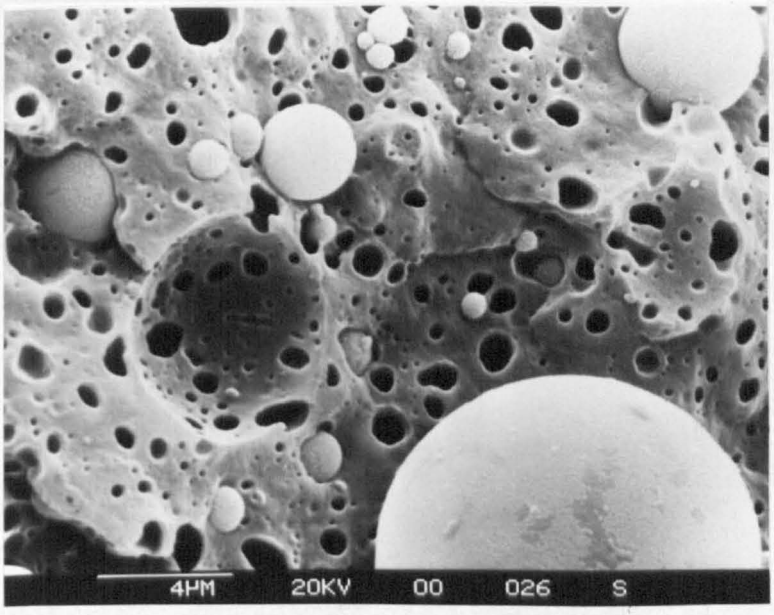

7.5

Figures 7.4 and 7.5 SEM micrographs of the PP/R/coatG composite (7.4) and (R+G)+PP composite (7.5), where glass bead particles were found to be partially wetted by EPR. Small dark circular holes observed on the micrograph are the imprints of the EPR particles, whereas large hemi-spherical areas were due to the torn-off of glass bead particles.

balance between the surface tension forces, which determines the contact angle (θ), is given by Young's equation [274].

$$\gamma_{SV} = \gamma_{SL} + \gamma_{LV}\cos\theta_{SL} \qquad (7.1)$$

Where : γ_{SV} is the solid surface energy, γ_{LV} is the liquid surface tension and γ_{SL} is solid/liquid interfacial energy. Ideally, for complete wetting θ should be zero. In systems where θ is high, more work is necessary to penetrate and wet out a filler. Young's equation, by definition, describes wetting at equilibrium. However, the rate at which equilibrium is approached depends on the balance between the driving force for wetting and the viscosity of the fluid. In the case of polymer melts viscosities can be very high, typically hundreds or thousands of pascal seconds (Pa.s), and it may take some time to reach the equilibrium contact angle. The wettabilities of filler surfaces can be determined indirectly in terms of Zisman's critical surface tension, γ_c [275].

According to thermodynamic criteria, a liquid with a given surface tension will wet any surface with a higher critical surface tension. In comparison with inorganic fillers, all polymers are low surface energy materials. Therefore, fillers might be expected to be wetted by polymer melts rather easily. The highest surface tension of a liquid will spread spontaneously on a given surface. Thus, in the case where there are two or more liquids (polymer melts) involved in the process, the high surface energy filler should be wetted by the liquid of highest surface tension.

Due to the similarity in the basic chemical components, PP and EPR have similar surface tension values. Critical surface tension (γ_c)of polypropylene were reported to be about 29-32 mJ/m^2, while γ_c of 28 mJ/m^2 was reported for EPR. Critical surface tensions of selected surfaces similar to those used in this study are reported in *Table 7.1*. The reported data inferred that both PP and EPR has similar probabilities to wet glass bead particles. However, due to the lower viscosity and higher amount of PP in the system, glass bead particles were finally wetted by PP instead of EPR and a separate dispersion structure was thus obtained in the PP/R/G composites.

In the PP/MaR/G composites, on the other hand, the glass bead particles were found to be wetted by MaR and resulted in an encapsulation structure. The reason for this observation can be explained by the higher surface tension of MaR than PP [145] brought about by the modification of EPR with maleic-anhydride. However, owing to the high viscosity of polymer melt, fully encapsulation is not reached and some of the particles were only partially encapsulated.

Table 7.1 Critical surface tensions (mJ/m^2) of selected surfaces

Surface	γ_c (mJ/m^2)	Reference
Polypropylene (PP)	29.0	[276]
	30.2	[277]
	32.0	[145]
Ethylene-propylene rubber (EPR)	28.0	[278]
Glass beads (wet)	30.0	[279]
Glass beads (dry)	47.0	[279]
Silane-coated glass beads	31-36	[280-281]

In the PP/R/coat G composite where glass beads had been treated with silane coupling agent, a separate dispersion structure was observed. Surface tension data of glass that had been treated with various silanes were reported by Lee [280] and by Sacher [281]. A rather broad range of surface tension values may be obtained with any silane, depending on the method of application, degree of silanol condensation, etc. However, it was found that most commonly used silane coupling agents led to critical surface tensions of coated glass around 31-36 mJ/m^2. It can be seen that even after surface treatment the filler still has considerably higher surface energy than the two polymer components (PP and EPR) and therefore the resulted structure remains the same as the structure observed in the PP/R/G composite.

It needs to be mentioned that the critical surface tension values used in this analysis were obtained from the works which have been reported in the literature. Problems associated with such data may be due to the variation of measurements. In this study, all composites were prepared in a twin-screw extruder and structure developed during mixing at around 190-200°C, while most of the surface tension data were determined at ambient temperature. However, by considering these data more understanding on phase structure formation was obtained.

(ii) Analysis of interfacial adhesion

The interfacial adhesion between phases in the composites was also examined using SEM. *Figure 7.6a* is a micrograph of a cryogenic fractured surface (non-etched) of unmodified PP/R/G composite. The fracture surface shows what is commonly referred to as an *interfacial failure*. Because the interface between PP and glass beads is weak, the propagating crack proceeded along this interface as well as along the PP/R interface. Some of the EPR particles were observed to be elongated and some were easily torn-off from the PP matrix, leaving small spherical holes on the fracture surface.

Comparing *Figures 7.6a* and *7.6b* reveals the fracture surface of a PP/MaR/G composite. In this system, the adhesion between the PP matrix and glass beads, also between PP matrix and EPR are stronger than the cohesion of the matrix and thus, the crack proceeds through the PP matrix resulting in a *cohesive failure*. No glass bead particle was observed on the fracture surface.

The fracture surface of the PP/R/coatG composite is shown in *Figure 7.6c*. Although glass beads had been treated with silane no significant improvement in adhesion to polypropylene was observed from the SEM micrograph, compared to that of the PP/R/G composite of *Figure 7.6a*. For quantitative information on interfacial adhesion in this composite, further investigation was undertaken using DMA. Similar observations were reported by Han et.al. [125] where γ-aminopropyl triethoxy silane coupling agent (Union Carbide, A1100) showed little effect on promoting interactions between glass beads and polypropylene, whereas N-octyl triethoxy silane coupling agent (Union Carbide, Y9187) appeared to have a stronger effect.

Failure in a filled composite often occurs in a boundary layer of filler and polymer (interphase region) rather than at the true interface. Even in the system in which there are apparently no strongly interacting groups, it appears that a polymer layer which differs from the bulk can adsorb at the interface. Several studies have focused on the presence of an interphase in filled polymer composites [121, 282]. Dolakova and Hudecek [282] studied composites of glass beads, silica and kaolin in polyethylene. After fracture of these composites, they observed fibrillar links on the filler surface, whose number depended on the filler used. Kendall and Sherliker [121] showed the presence of a layer of bound polymer a few nanometers thick which can not be removed by a solvent in silica filled polyethylene. Mechanical failure was observed not at the filler-polymer interface, but at a distance about 3 nm into the polymer [121]. This suggested that a weak interface between free and bound polymers may exist.

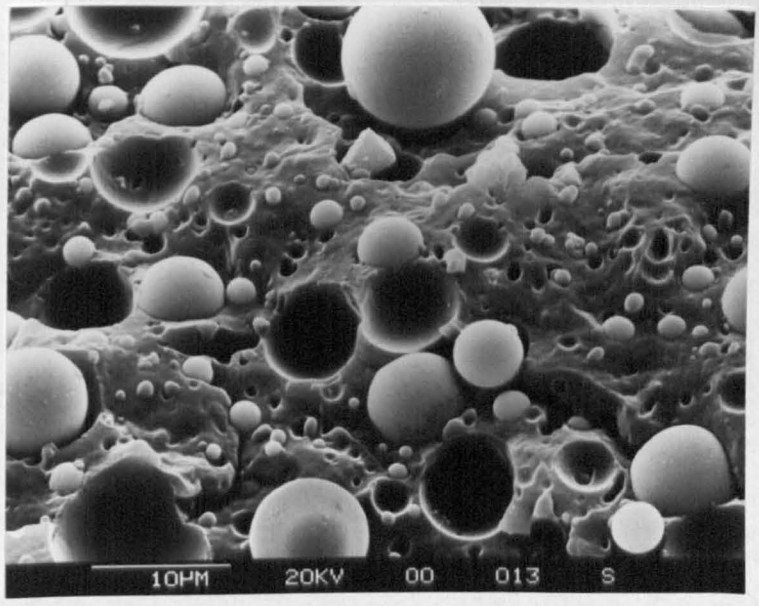

(a)

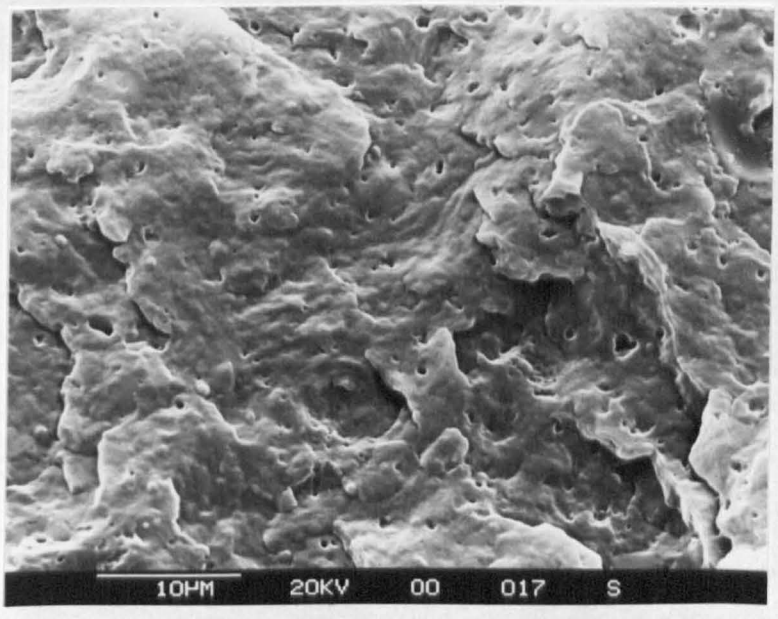

(b)

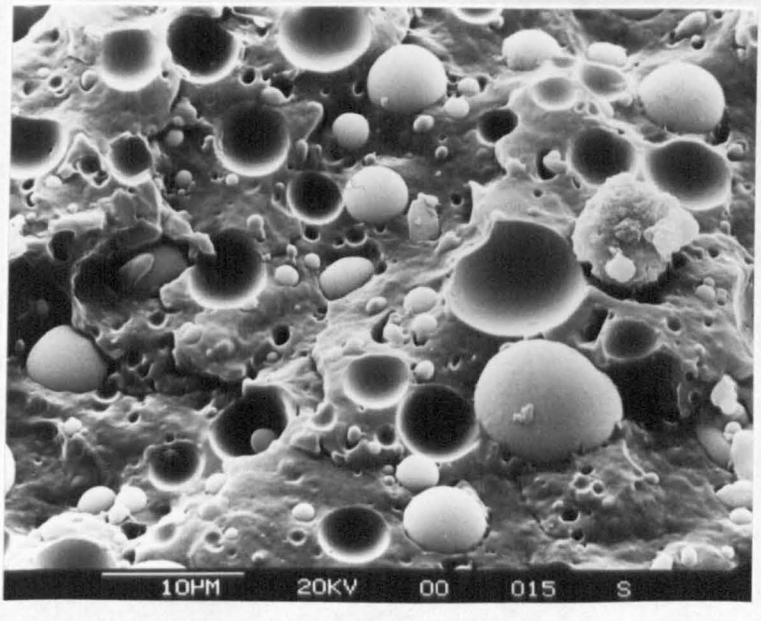

(c)

Figures 7.6 *a to c* SEM micrographs of cryogenic fractured surfaces (non-etched) of the PP/R/G *(a)*, PP/MaR/G *(b)*, and PP/R/coatG *(c)* composites.

It was believed that similar phenomena also occurred in the filled composites studied in this work. Evidence of the interphase region in the PP/R/G (70/15/15) composite is shown in *Figures 7.7a and b* where a patchy interphase region was observed on the glass surface. The sample was fractured at liquid nitrogen temperature and etched with heptane vapour for 3 sec. The observation of patchy (not smooth) interphase may be explained by the differences in the SiO_2 content on the glass surface. Although the chemical nature of the glass surface is not known in detail, its surfaces were reported [284] to compose mainly of hydroxyl groups. Ion such as Na^+, K^+, Ca^{2+}, Mg^{2+}, Fe^{2+}, Fe^{3+} may also be present in hydrated form at the surface, and there is evidence that some constituents tend to concentrate there. Some glasses tend to separate into phases differing in SiO_2 content and so giving a patchy surface.

7.3.1.2 Dynamic Mechanical Analysis

Dynamic mechanical analysis (DMA) was used as a complementary method for quantitative study of phase structures and interfacial adhesion in various ternary phase polypropylene composites. The temperature dependencies of tan δ at 1 Hz. of various composites are given in *Figures 7.8 to 7.11*, and a summary of the data is shown in *Table 7.2*.

Table 7.2 Glass transition temperatures of rubber and polypropylene in various PP composites

System	Sample	Rubber Tg peak (°C)	PP Tg peak (°C)
Raw material	PP	-	7.1
	EPR	-34	-
	MaR	-55	-
Binary phase (70/30)	PP/R	-43	6.8
	PP/MaR	-61	6.7
Ternary phase (70/15/15)	PP/R/G	-43	7.1
	PP/MaR/G	-56	6.7
	PP/R/coatG	-43	6.7

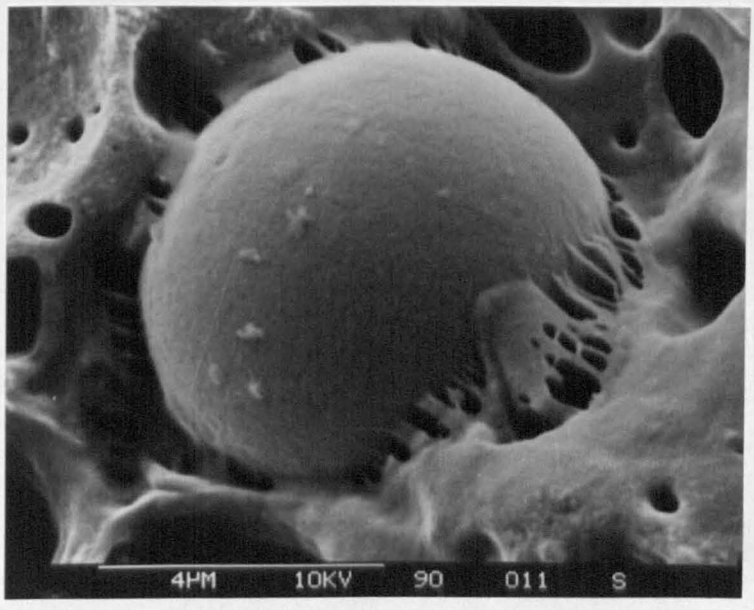

(a)

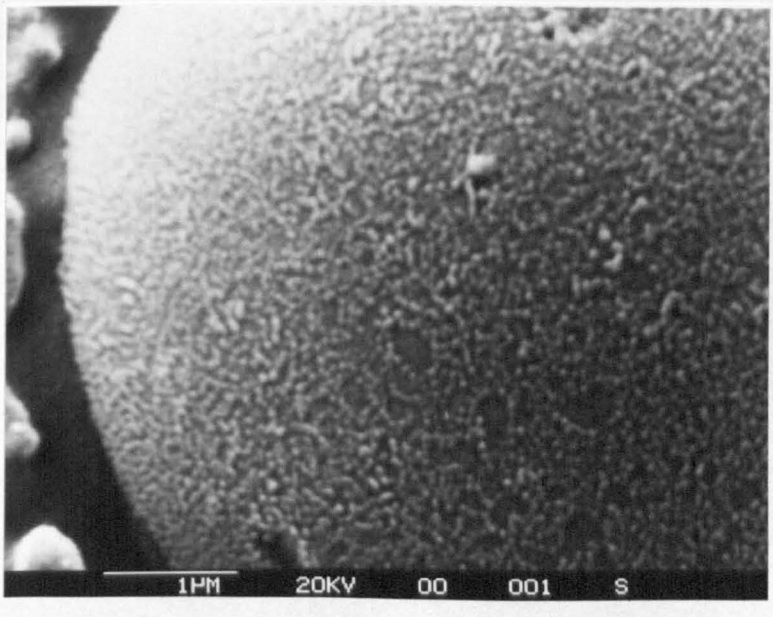

(b)

Figure 7.7 (**a**) Interphase region observed on the glass bead surfaces in the PP/R/G composite after being etched with n-heptane. (**b**) high magnification of (a)

The dynamic mechanical spectrum of EPR and MaR is shown in *Figure 7.8*. EPR shows a glass transition temperature peak at -34°C, whereas MaR exhibits a glass transition temperature at -55°C which is about 20°C lower than that of a non-functionalised rubber.

The tan δ curves for the binary blends of PP both with R and MaR are also shown in *Figure 7.9*. Two tan δ peaks were observed in both blends, inferring phase separation between PP and rubber in the blend. The low temperature peaks corresponded to glass transition temperatures of the incorporated rubbers, while the high temperature peaks reflected glass transition temperature of the PP matrix. In the PP/R blend R shows a broad-glass transition temperature at about -43°C, whereas the glass-transition of MaR in the PP/MaR blend was observed at -61°C. A small drop in the glass transition temperatures of both rubbers, compared to those observed in the raw materials (*Figure 7.8*), can be explained by their higher thermal expansion coefficient in comparison with the PP matrix. During the cooling, a negative hydrostatic pressure developed on the rubber particles and the thermal stress generated in the blend then caused a decrease in rubber glass transition temperature [43, 224]. For this reason, the glass transition temperature (T_g) values of various rubbers should be compared at the same rubber volume fraction in composites.

Temperature dependencies of tan δ at 1 Hz. of various PP/R/G composites are shown in *Figures 7.10 and 7.11*. Differences between R and MaR are seen in *Figure 7.10*. In both PP/R/G and PP/MaR/G composites, two tan δ peaks were observed corresponding to the T_g peaks of PP and the incorporated rubber. The location and the intensity of T_g peaks of PP in both composites, were the same at about 7°C. The T_g peak of rubber (R) in the PP/R/G composite was observed at -43°C which is similar to that observed in the binary PP/R blend, meaning that glass beads had no influence on the mobility of rubber chains, reflecting separate dispersion of EPR and glass beads in this composite. Whereas the T_g peak of MaR shifted from -61°C (in the binary blend) to -56°C (in the ternary blend). This suggested that with the incorporation of glass beads, there was immobilisation of rubber chains in the system. Also, DMA spectra of PP/MaR/G showed a much larger and broader rubber glass transition peak than similar composites of PP/R/G. This was attributed to the presence of more rubber around the filler particles in case of MaR since the size of the tan δ peak for the rubber phase was not determined by the amount of pure rubber but by the amount of rubber plus the inclusions inside the rubber phase. A significant immobilisation of the MaR chains occurs on the glass bead

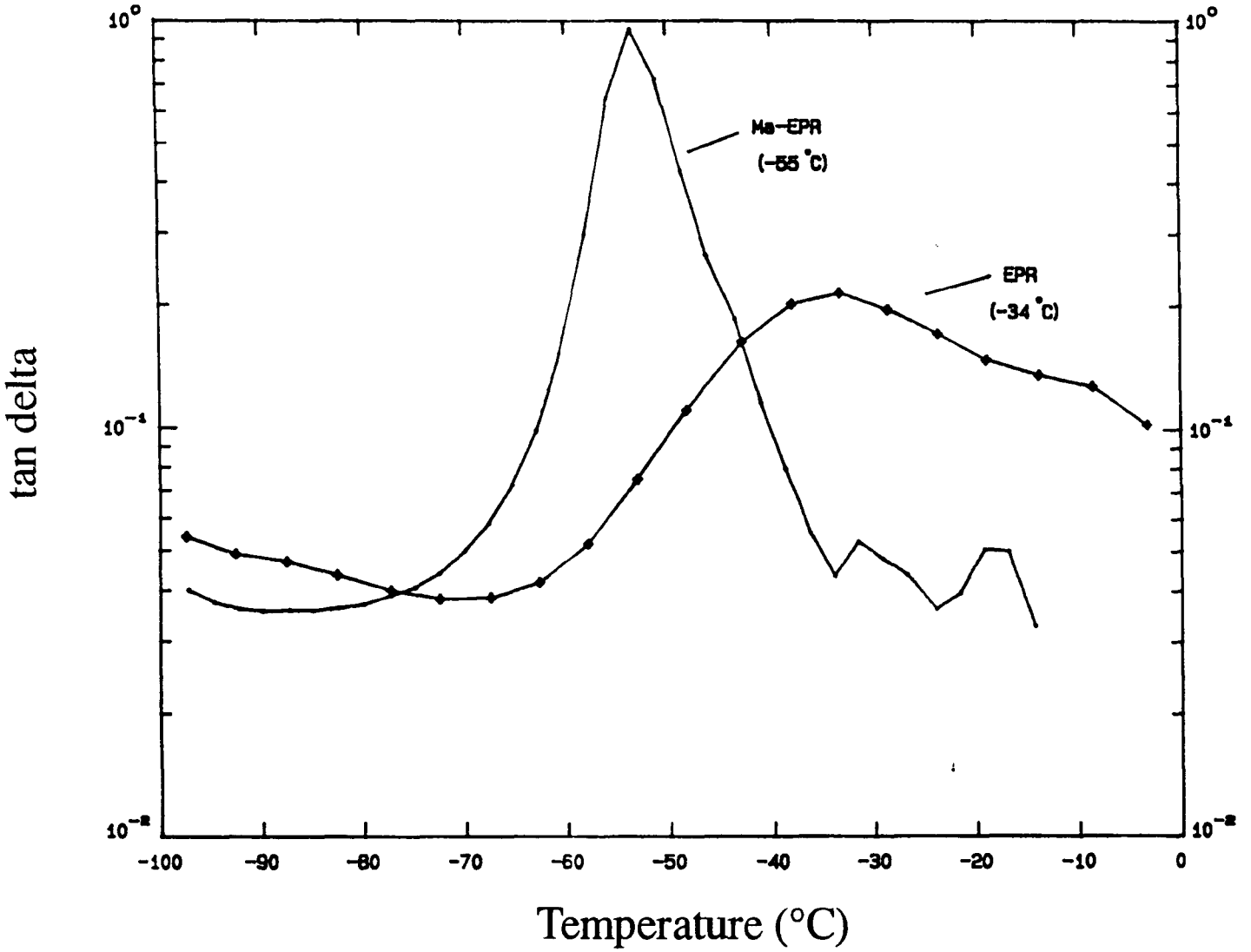

Figure 7.8 Temperature dependence of the damping (tan delta) at 1 Hz. of EPR and MaR raw materials.

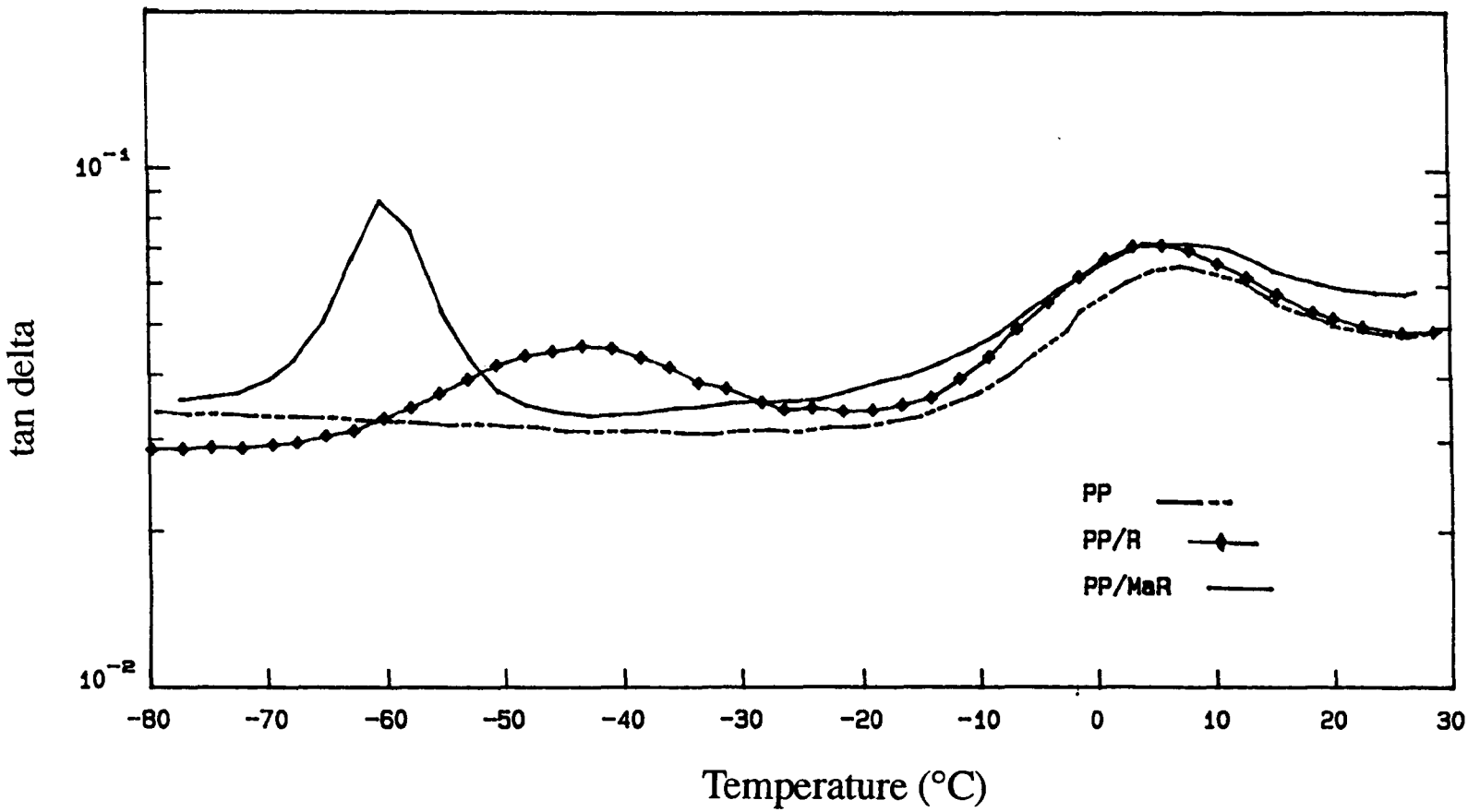

Figure 7.9 Temperature dependence of the damping (tan delta) at 1 Hz. of PP PP/R (70/30) and PP/MaR (70/30) blends

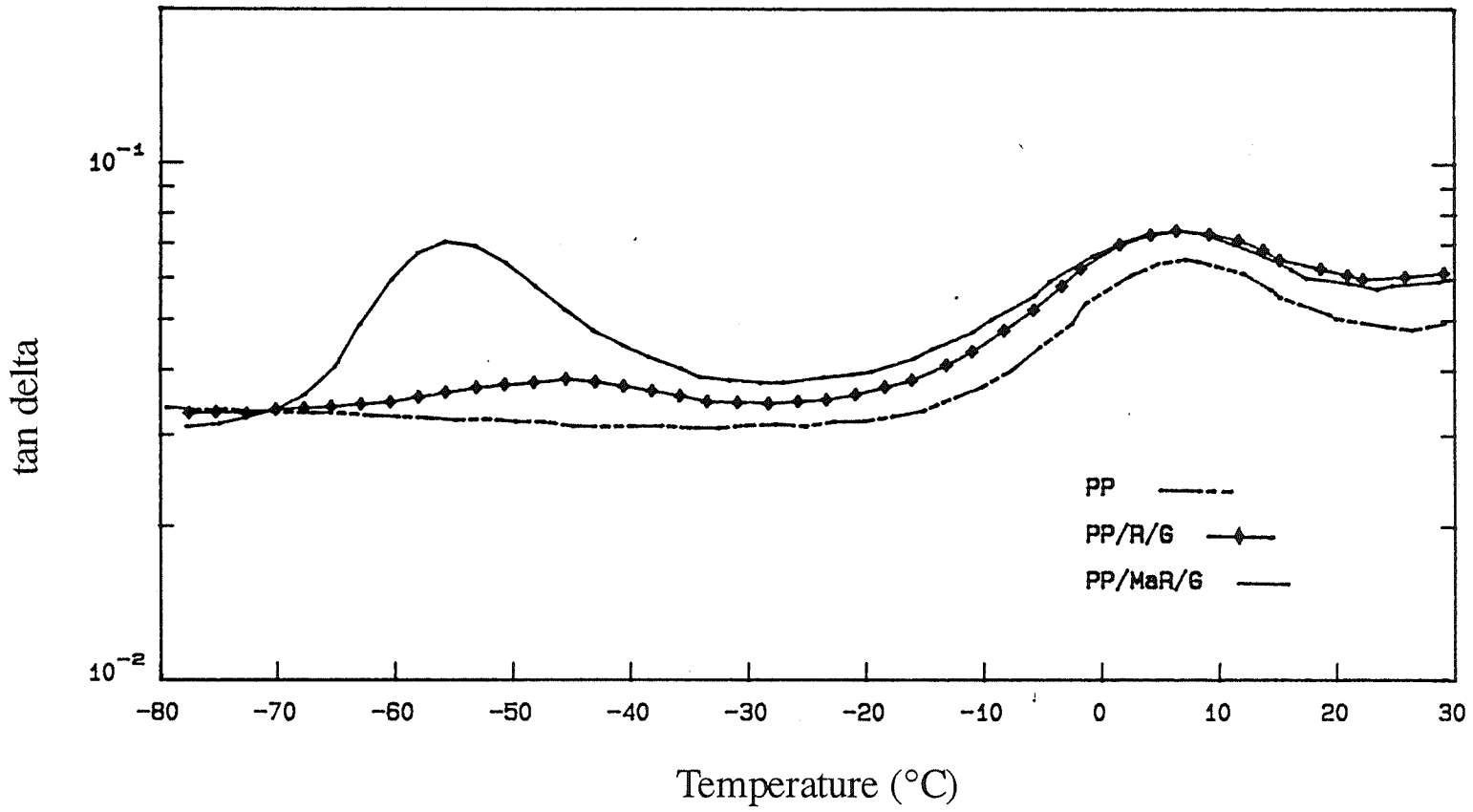

Figure 7.10 Temperature dependence of the damping (tan delta) at 1 Hz. of unmodified PP, ternary phase of PP/R/G (70/15/15), and PP/MaR/G (70/15/15) composites

surfaces, indicating some kind of interaction at the filler surface. Further studies on the interaction between these phases was undertaken using FTIR analysis.

The effect of surface-coated glass beads (coatG) on temperature dependence of tan δ of the ternary phase polypropylene composites is shown in *Figure 7.11*. There was essentially no difference in the dynamic mechanical spectra compared to the untreated filler. The use of coated glass beads do not appreciably affect the T_g of either PP or rubber, meaning that the filler and rubber are also dispersed separately in the PP matrix. However, the peak intensity (peak height) in the PP/R/coatG was considerably higher than those in the PP/R/G composite, inferring a slightly better adhesion between phases in this composite. Also, from *Figure 7.12* the observation of higher loss modulus in the PP/R/coatG composite revealed that more energy dissipated in this system. From the previous SEM study, some glass bead particles of the PP/R/coatG composite were partially wetted by EPR (*Figure 7.4*). A drop of the storage modulus at about -43°C and lower values of storage modulus above this temperature, confirmed the above SEM observation that there was some EPR wetted on the filler surface since the effect of glass beads on the storage modulus was hindered in such a composite.

7.3.1.3 DSC studies

The crystallisation and melting processes in various polypropylene composites were studied by differential scanning calorimetry (DSC), according to the thermal treatment (heat-cool-heat cycle) mentioned previously in Chapter 3-section 3.7. *Table 7.3* summarises the DSC results of an unmodified polypropylene, binary blends of polypropylene either with rubbers or with glass beads, and their corresponding ternary phase composites.

In the binary blends, addition of 30 vol% of R caused a reduction in the $T_{c\ onset}$ of PP, inferring delayed nucleation of PP by the incorporated R. The observed crystallisation and melting temperatures also decreased, in comparison to those for unmodified PP. This suggests the presence of smaller spherulites in such blends. The percentage crystallinity observed in the PP/R blend was found to be lower than that of unmodified PP. However, this reduction is attributed to the substitution of 30 wt.% of PP by R. No change in the percentage crystallinity was seen compared to PP when subtracting the wt.% of R and recalculating percentage crystallinity only on the wt.% of the PP in the blend, assuming R does not crystallise under the DSC testing conditions.

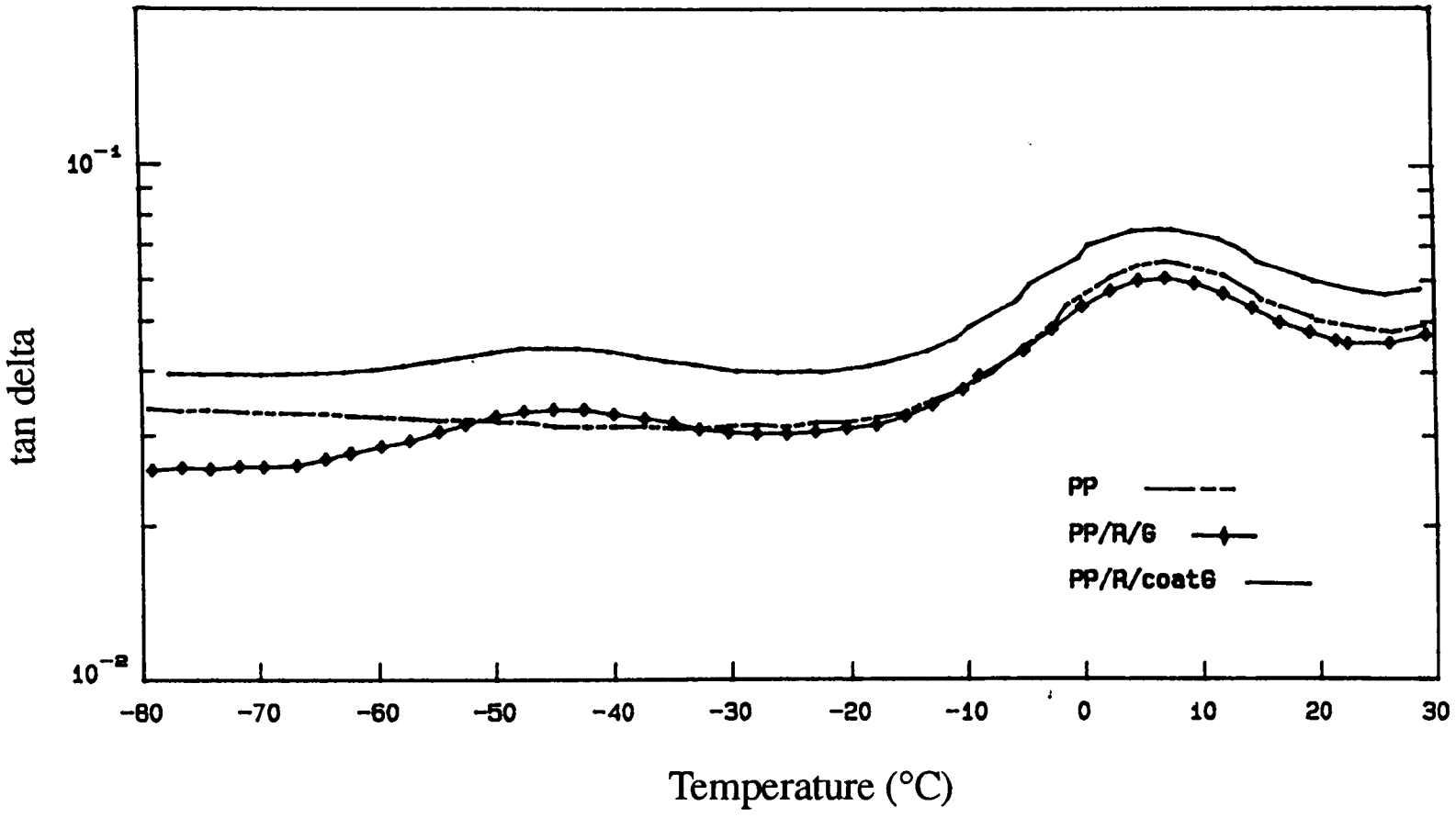

Figure 7.11 Temperature dependence of the damping (tan delta) at 1 Hz. of unmodified PP, ternary phase of PP/R/G (70/15/15), and PP/R/coatG (70/15/15) composites

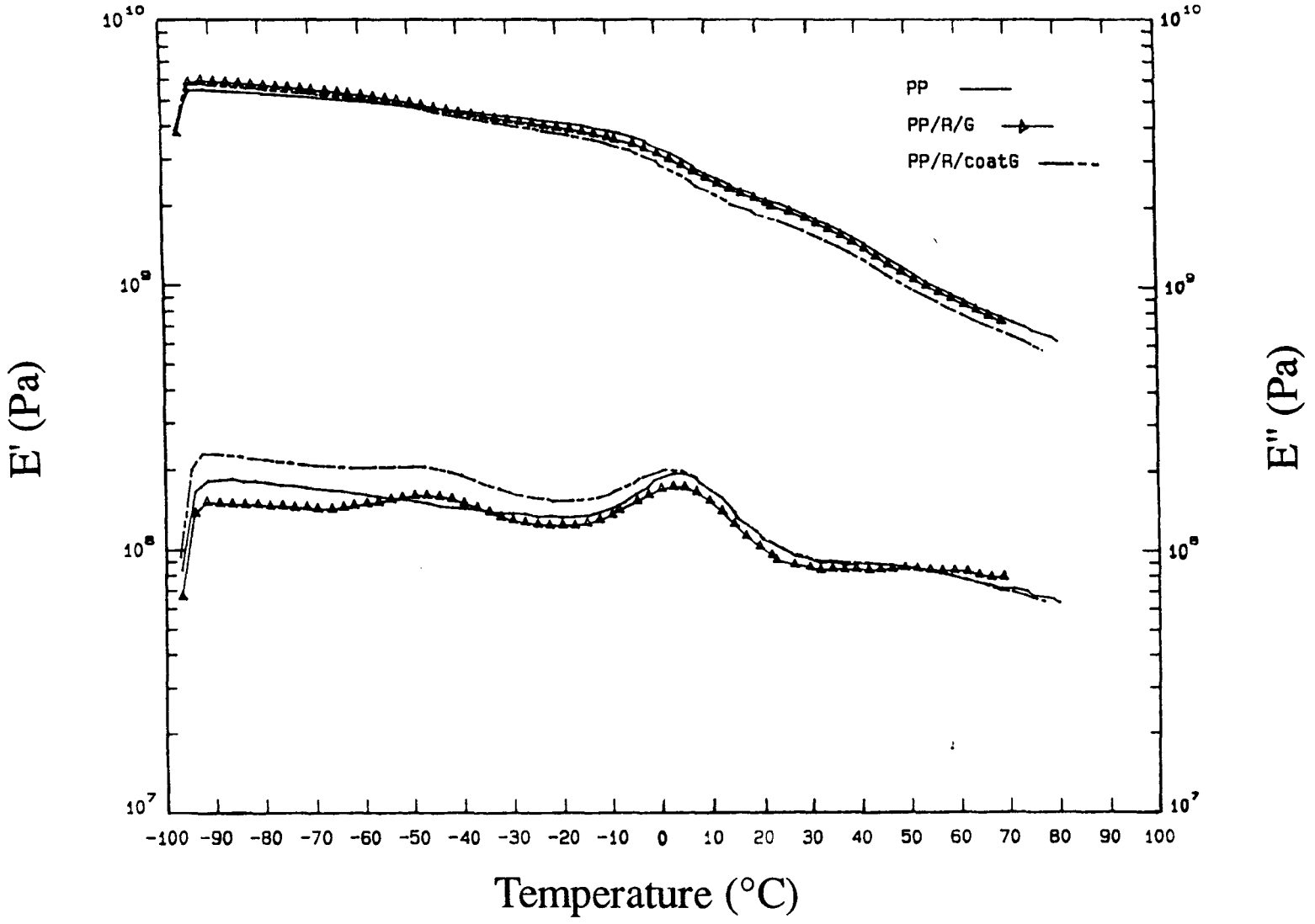

Figure 7.12 Temperature dependence of storage modulus (E') and loss modulus (E'') at 1 Hz. for PP, PP/R/G (70/15/15), and PP/R/coatG (70/15/15) composites

Table 7.3

The temperature of onset of crystallisation ($T_{c\ onset}$), crystallisation temperature (T_c), melting temperature (T_m), percentage crystallinity, the difference between $T_{c\ onset}$ and T_c (T_1) and degree of undercooling (T_2) of unfilled PP and its binary and ternary phase composites.

Sample	Composition (by vol)	$T_{c\ onset}$ (°C)	T_c (°C)	T_m (°C)	Crystallinity (%)	T_1 (°C)	T_2 (°C)
PP	100	114.6	109.5	164.3	49.0	5.1	54.8
PP/R	70/30	113.4	108.4	162.5	34.4	5.0	54.1
PP/MaR		114.5	109.9	160.5	35.4	4.6	50.6
PP/G		120.9	117.1	162.7	24.7	3.8	45.6
PP/R/G	70/15/15	116.7	111.8	162.3	26.2	4.9	50.5
PP/MaR/G		114.6	110.2	162.2	27.5	4.4	52.0
PP/R/coatG		119.5	114.8	162.6	26.3	4.7	47.8

Maleic-anhydride modified EPR (MaR) shows no effect on the $T_{c\ onset}$ and T_c values of PP. The difference between T_c and $T_{c\ onset}$ (T_1), also the degree of undercooling (T_2) were lower than those of unmodified PP. These results indicated that MaR increased the rate of crystallisation leading to the composites of smaller spherulites. As a consequence, by the presence of smaller spherulites having lower heat capacity, the melting temperature of the blend shifted to the lower temperature.

In the PP/G blends, opposite effect was observed. The incorporation of 30 vol% of glass beads to polypropylene led to an increasing in $T_{c\ onset}$ and T_c of PP. The degree of undercooling and the difference between T_c and $T_{c\ onset}$ was markedly reduced, inferring an increase in the rate of crystallisation of PP by the presence of glass beads. The percentage crystallinity observed in the PP/G composite was lower than that of unmodified PP. This was due to the substitution of PP by 30 vol% (or 54 wt.%) of glass beads.

In the ternary phase PP/R/G composite where both R and G were present, the $T_{c\ onset}$ and T_c as well as other DSC result values were somewhat between those of PP/R and PP/G composites. This means that both R and G exert separate effects on the crystallisation and melting behaviour of PP. This result can be explained by the separate dispersion structure in this composite. Contrary results were found for the PP/MaR/G composite. From the previous results of the binary PP/MaR blend, it was clearly seen that MaR has no effect on the $T_{c\ onset}$ of PP. Thus, in the corresponding ternary phase composite only glass beads will have an influence on the $T_{c\ onset}$ of PP and therefore its result should be similar to that observed in the PP/G composite (120.9°C). However, the observed $T_{c\ onset}$ value in the PP/MaR/G composite was only 114.6°C, revealing the suppression in the influence of glass beads on the $T_{c\ onset}$ of PP due to an encapsulation structure of the composite. In the PP/R/coat G composite, a strong effect from glass beads was observed on the crystallisation behaviour of PP. This observation confirmed the earlier finding that the structure in this composite was that of separate dispersion.

7.3.1.4 FTIR Analysis

In this study FTIR spectroscopy was used in the characterisation of chemical functionalities in various polypropylene composites in order to understand the structure of the glass-polymer interphase, especially in the PP/MaR/G composite in which an encapsulation of glass bead particles by EPR was observed.

The infrared spectra obtained in transmission from thin films (~15 μm) of PP and EPR raw materials are given in *Figure 7.13* over the spectral range from 2000 to 600 cm^{-1}. Polypropylene shows two large peaks at 1463 cm^{-1} due to the bending vibrations of C–H bonds in the methylene groups ($-CH_2$), and at 1375 cm^{-1} due to the symmetrical bending vibration of the methyl groups ($-CH_3$). EPR shows three main peaks at 1463, 1375 and 720 cm^{-1}. The strong absorbance at 720 cm^{-1} is due to the CH_2 rocking vibration in the rubber.

The infrared spectra of maleic-anhydride modified EPR (MaR) is given in *Figure 7.14* over the spectral range from 1800 to 1300 cm^{-1}. The large peaks at 1461 and 1375 cm^{-1} are due to the bending vibrations of the C–H bonds in the methylene and methyl groups in the rubber, respectively. The small peak observed at 1713 cm^{-1} is the acid peak of the maleic-anhydride modification. In general the anhydride modification may exist in the anhydride or acid form [285]. These two forms may be interchanged reversibly by the addition or removal of water as shown in *Figure 7.15a.* The anhydride form may slowly convert to the acid form by absorbing water from the atmosphere if the material is left in the laboratory environment. The acid may be converted to the anhydride by drying at high temperatures. The acid peak normally appears at around 1714 cm^{-1}. The anhydride form appears as two peaks, one at 1864 cm^{-1} and a larger one at 1789 cm^{-1}.

The infrared spectra of the PP/R/G composite is given in *Figure 7.16.* The C–H bending vibrations of methylene and methyl groups are seen at 1462 and 1375 cm^{-1}, respectively. The large and broaden peak at around 1160-1000 cm^{-1} is due to the Si–O stretching vibrations of glass beads.

Particular attention was paid to the 1800 to 1500 cm^{-1} region in composites including MaR in order to investigate the structure of the maleic-anhydride modification in the composites. *Figure 7.17* represents the spectra of PP/R and PP/MaR. The acid form of anhydride modification is apparent at 1714 cm^{-1} in the PP/MaR blend sample. In the case of ternary phase PP composites which contained only 15 vol% of rubber, in order to better resolve the bands due to the MaR thicker specimens (~50 μm) were used. *Figure 7.18a* shows the spectra of the MaR+G (1:1) and the PP/MaR/G composite. The anhydride peak at 1714 cm^{-1} was found to have disappeared (*Figure 7.18b*), and a new peak was detected at 1571 cm^{-1} (in the MaR+G composite) and at 1565 cm^{-1} (in the PP/MaR/G composite). This new peak was due to a asymmetrical stretching band of the carboxylate ion (CO_2^-) which is believed to have formed due to a reaction between MaR and glass beads during processing.

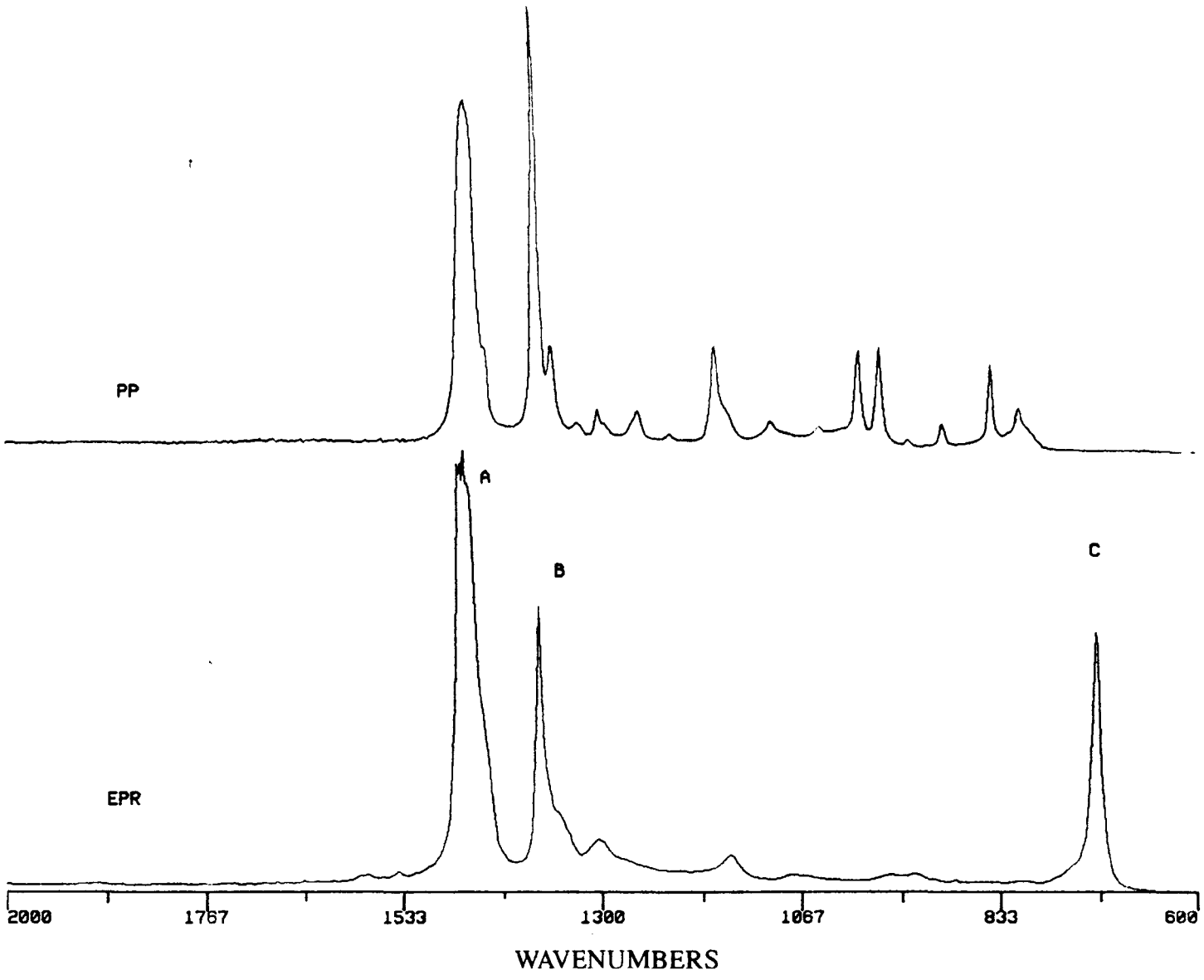

Figure 7.13 FTIR spectra of PP and EPR raw materials. **A.** C-H *stretch* - CH_2 group, **B.** C-H *stretch* -CH_3 group, and **C.** CH_2 *rock*.

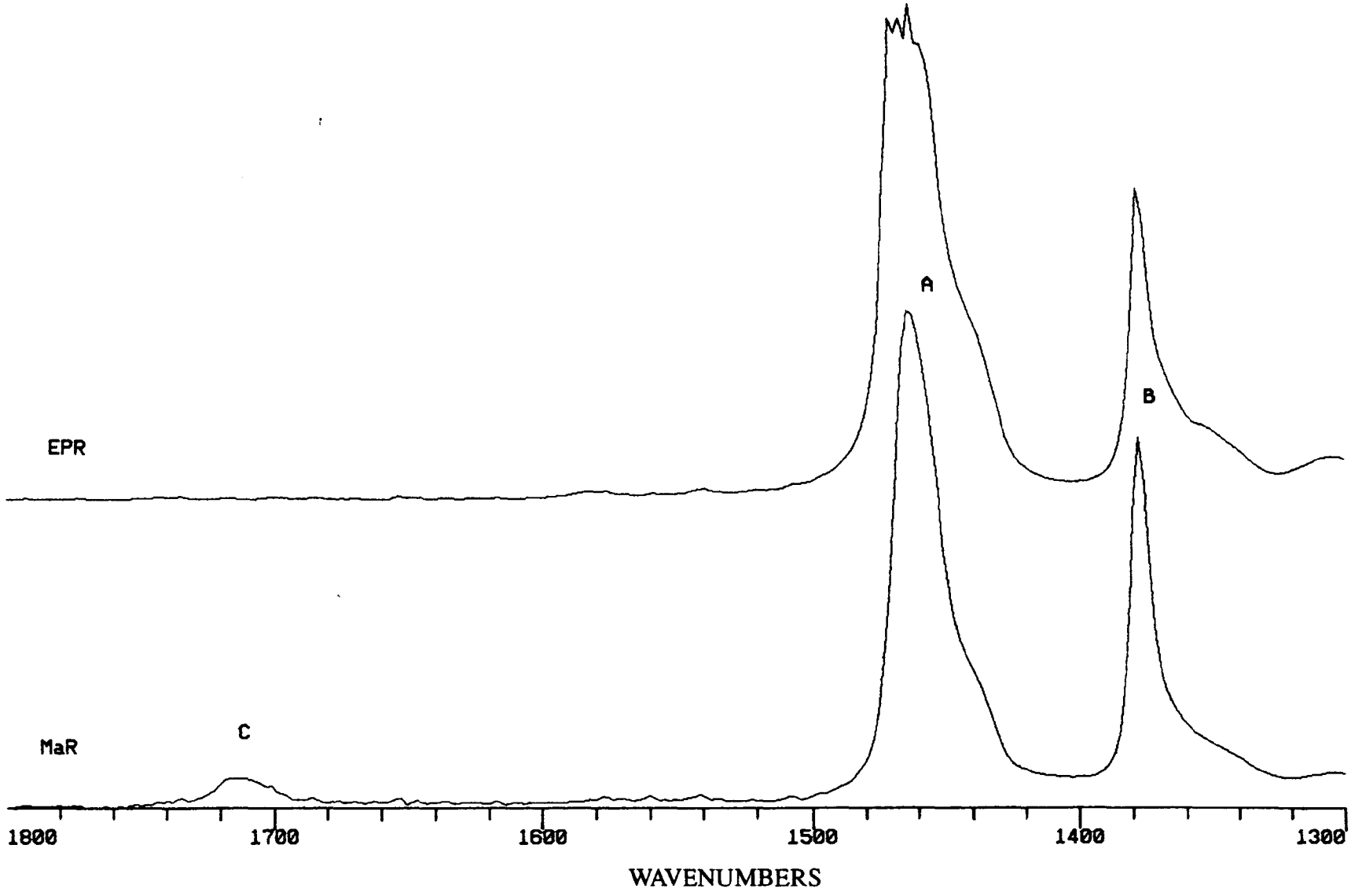

Figure 7.14 FTIR spectra of EPR and MaR. **A.** C-H *stretch* - CH_2 group, **B.** C-H *stretch* -CH_3 group in the rubber, and **C.** C=O *stretch* of anhydride modification.

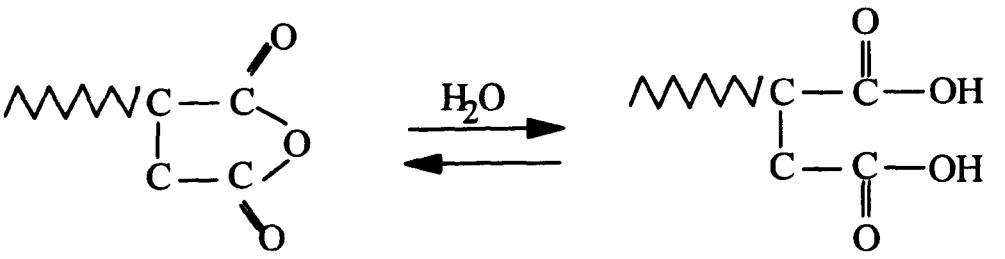

Acid form **Anhydride form**

Figure 7.15a Acid and anhydride forms in the maleic-anhydride modification

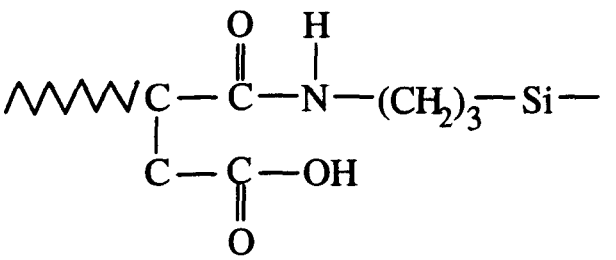

Amic acid

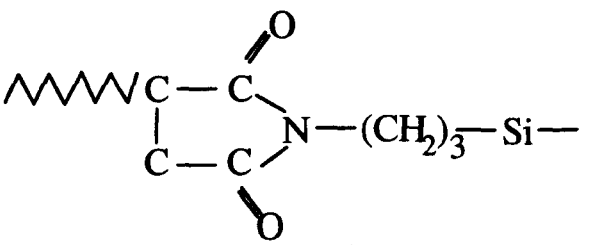

Cyclic imide

Figure 7.15b Possible products from the reaction between aminopropyl-triethoxy silane and maleic-anhydride modified EPDM [160].

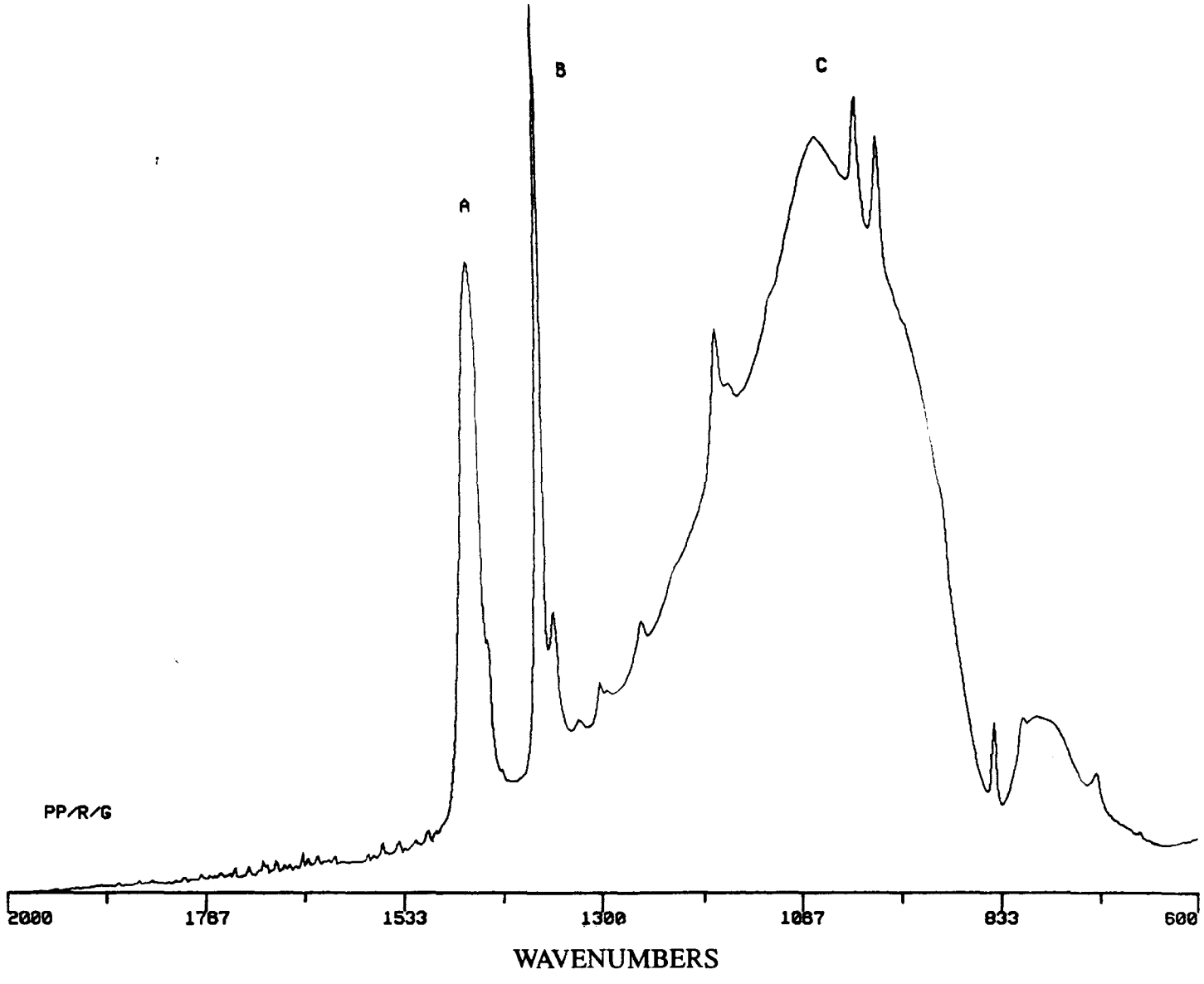

Figure 7.16 FTIR spectra of the PP/R/G composite. **A.** C-H *stretch* - CH_2 group, **B.** C-H *stretch* -CH_3 group, and **C.** Si-O *stretch.*

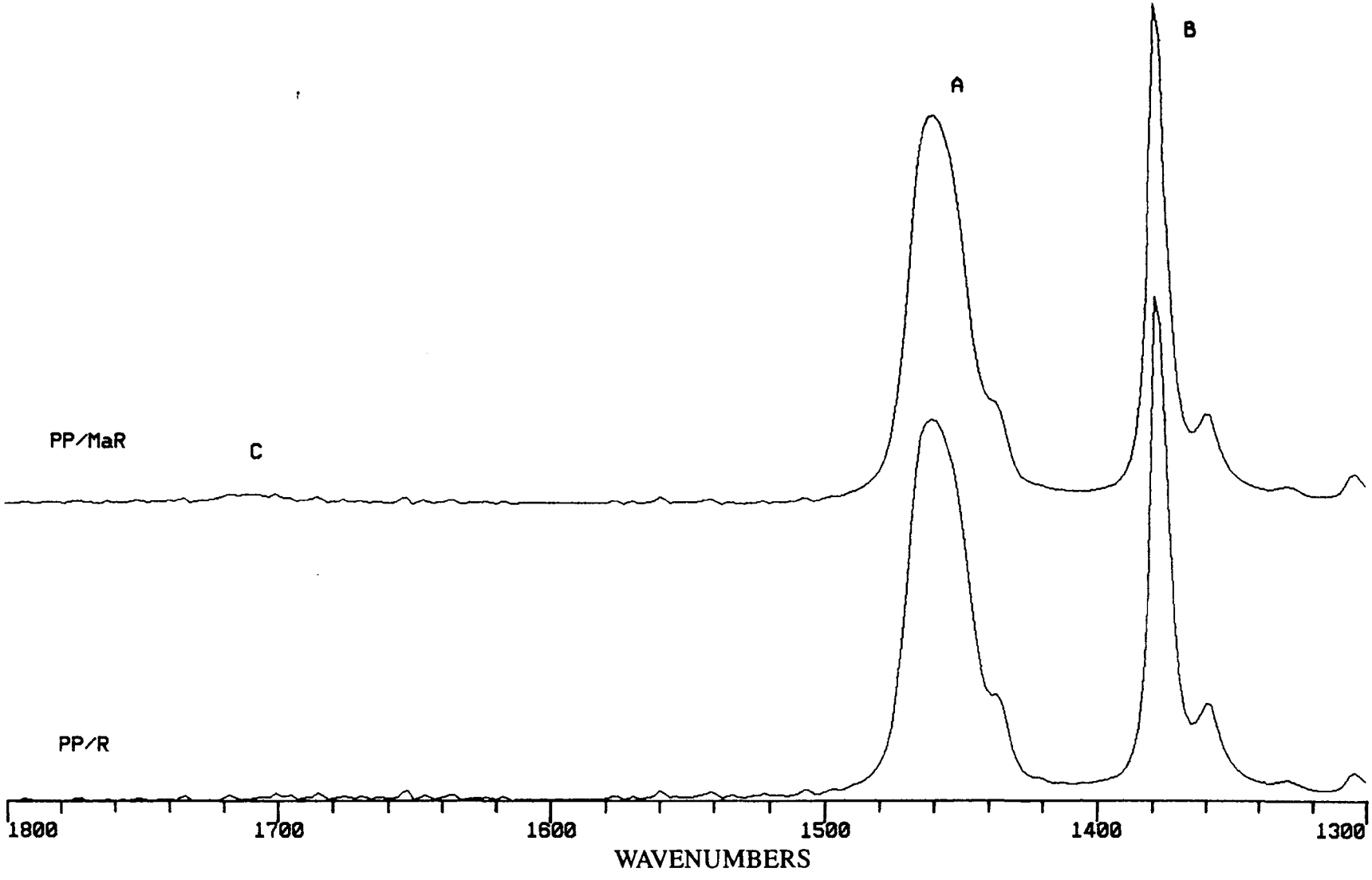

Figure 7.17 FTIR spectra of PP/R and PP/MaR. **A.** C-H *stretch* - CH_2group, **B.** C-H *stretch* -CH_3group and **C.** C=O *stretch* of anhydride modification.

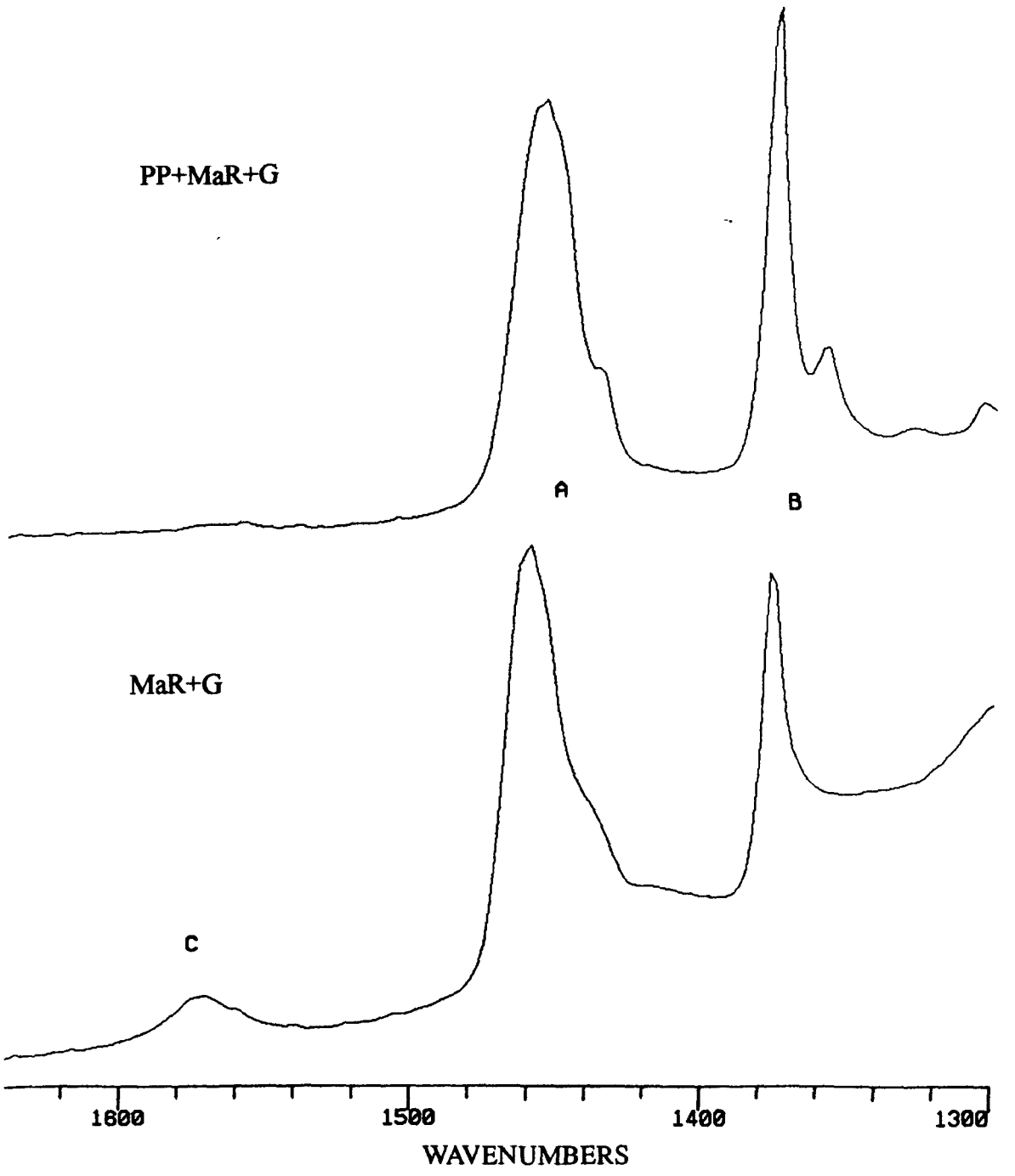

Figure 7.18a FTIR spectra of MaR+G and PP/MaR/G composite. **A.** C-H *stretch* -CH_2 group, **B.** C-H *stretch* - CH_3 group, and **C.** C=O *stretch* of carboxylate ion.

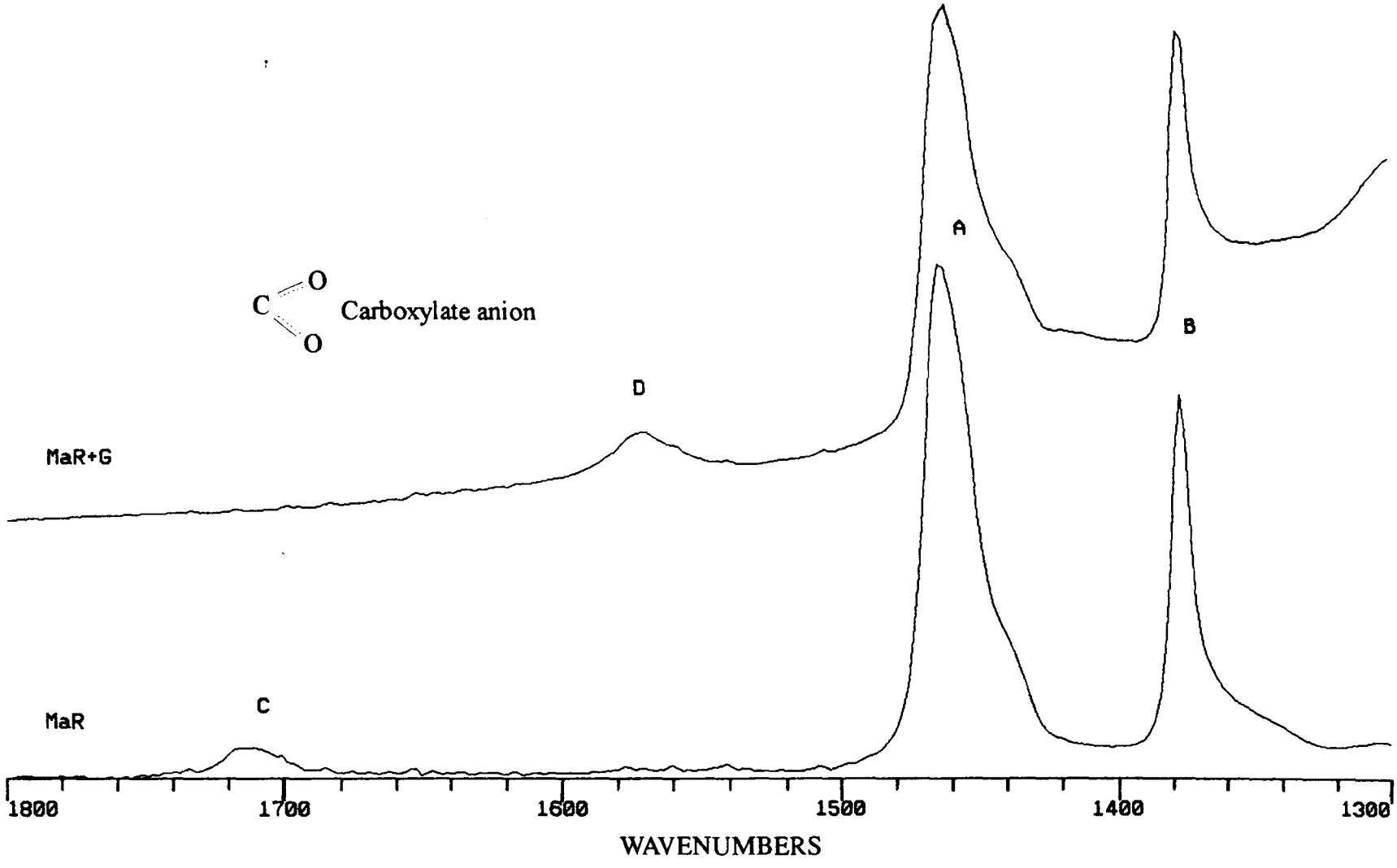

Figure 7.18b FTIR spectra of MaR and the blend of MaR and glass beads. **A.** C-H *stretch* - CH_2group **B.** C-H *stretch* -CH_3group, **C.** C=O *stretch* of anhydride, and D. C--O *stretch* of carboxylate anion.

A similar observation was reported by Scott et.al. [160] in which a new peak appeared at 1568 cm^{-1} due to the CO_2^- salt produced from the reaction of maleic-anhydride modified EPDM with γ-aminopropyltriethoxysilane (γ-APS). In the case of polyethylene based composites containing EPDM-Ma and γ-APS on silicon dioxide filler, the cyclic imide band was observed at 1742 cm^{-1}. The cyclic imide was reported as a product from the reaction between EPDM-Ma and γ-APS during processing on the roll mill. The interaction could be simple hydrogen bonding, salt formation, acid-base interactions, or chemical reaction. The most evident possibilities of reaction were reported to be the formation of amic acid or cyclic imide structures illustrated earlier in *Figure 7.15b*. Under the conditions of roll milling at 170°C, the formation of the amic acid was expected to be the rate-limiting step for the aliphatic diacid. The imide formation will occur quickly once the amide was formed and very little or no amic acid was found in the final composite.

The spectra of R+coat G and PP/R/coat G composites is given in *Figure 7.19*. No absorption band in the range of 1800 to 1500 cm^{-1} was observed. The spectra of the PP/R/coatG composite was found to be very similar to that of unmodified PP/R/G composite. Unlike MaR, the use of silane coated glass-beads did not promote a chemical reaction between glass beads and polymer. Bonding of silane coupling agents to the polymer is generally through interdiffusion of oligomeric siloxanes at the interface with possible crosslinking to interpenetrating polymer network (IPNs) in the interphase region [286], other than by chemical reaction. The concept of a diffused interphase region is shown in *Figure 7.20*.

7.3.2 Effect of functionalised components on composite mechanical properties

Generally, properties such as modulus, tensile strength, elongation at break, toughness, etc. of multiphase polymer composites are strongly influenced by interfacial properties. Indeed, this is one of the main reasons of the interest in modifying these interfaces.

7.3.2.1 Tensile and impact properties at ambient temperature

(i) Effect of maleic-anhydride modified EPR (MaR)

Tensile results of various polypropylene composites are shown in *Table 7.4*. Unmodified PP shows a Young's modulus of 1.72 GPa. Incorporation of 30 vol% of rubber (either R or MaR) into PP led to a reduction in composite modulus. This reduction can be

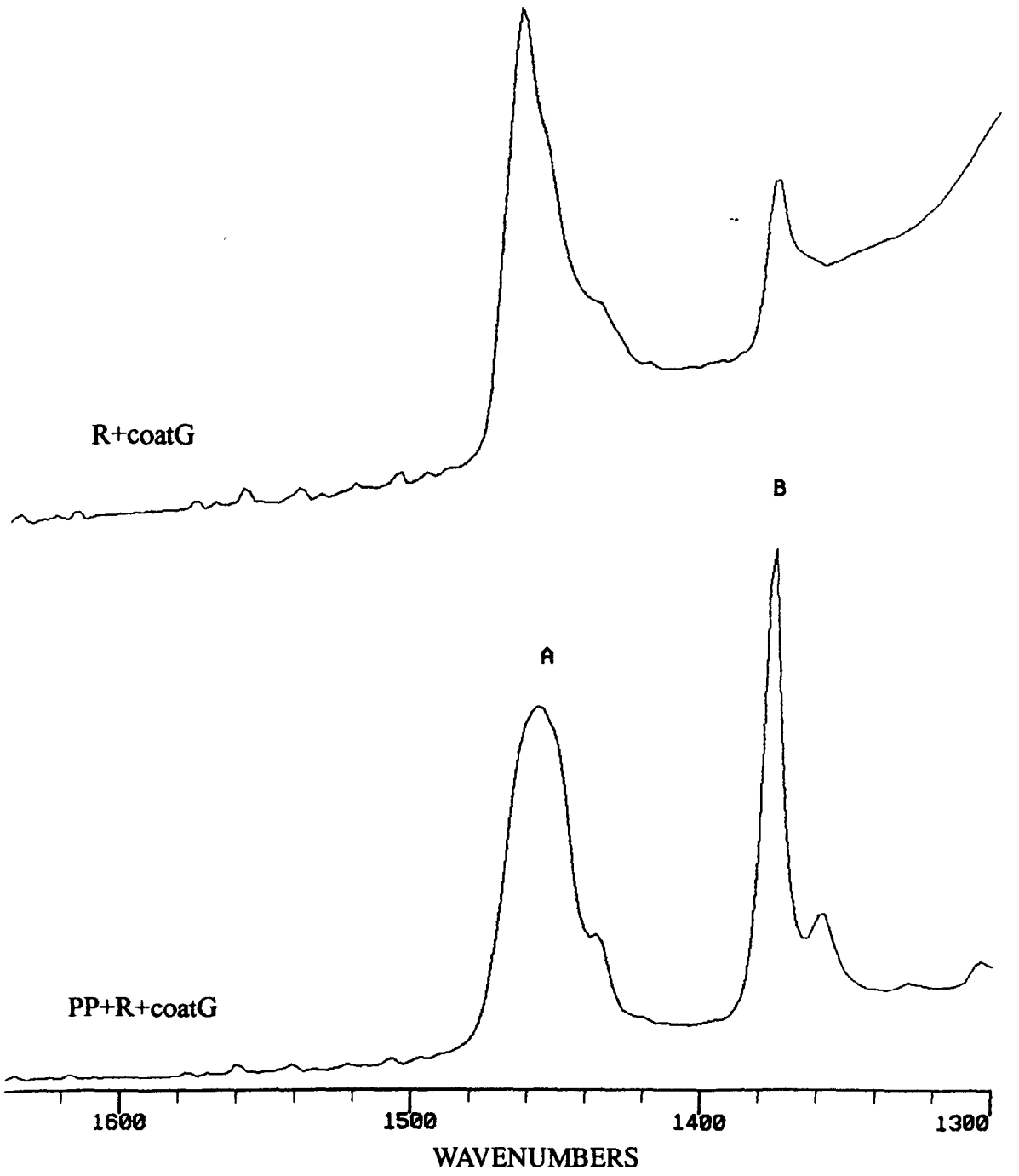

Figure 7.19 FTIR spectra of R+coatG and PP+R+coatG composite. **A.** C-H *stretch* -CH_2 group, and **B.** C-H *stretch* - CH_3 group.

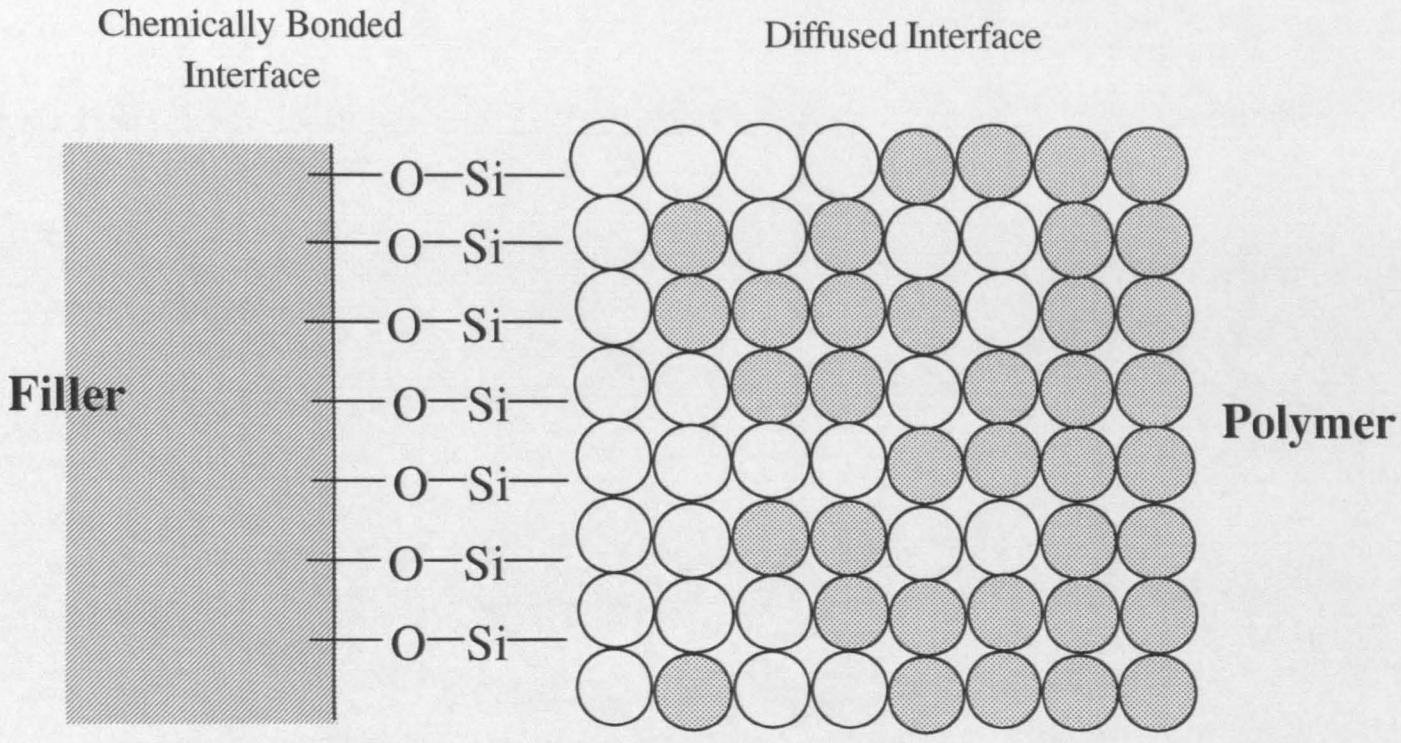

Figure 7.20 Interdiffusion model. Open circles indicate regions of coupling agent while filled circles indicate regions of polymer

Table 7.4

Young's modulus and tensile yield stress at 23°C of various polypropylene composites

Composition	Young's modulus (GPa)		Tensile yield stress (MPa)	
PP/R/G (by vol)	R	MaR	R	MaR
100/0/0	1.72 (0.06)[a]		33.24 (0.30)	
70/30/0	1.09 (0.02)	1.00 (0.06)	24.31 (0.35)	20.20 (1.10)
70/20/10	1.36 (0.05)	1.10 (0.05)	18.62 (0.28)	16.00 (0.46)
70/15/15	1.84 (0.05)	1.31 (0.03)	18.67 (0.18)	16.73 (0.24)
70/0/30	2.87 (0.05)		18.31 (0.46)	

[a] Standard deviations in parentheses, means from six specimens.

explained by the substitution of PP by a lower modulus material. No significant difference between the effect of R and MaR on modulus of the binary blends was observed. A number of investigations have shown that modulus is not sensitive to structural differences. Its value depends mostly on component properties and on the composition of the blend.

In contrast to binary blends, in ternary phase composites modulus is dependent on developed structure. If the components (R and G) are dispersed separately in the matrix, composition dependence of the modulus can be predicted by theoretical equations. In case of encapsulation the measured modulus is generally lower than the predicted one, due to the suppression in filler reinforcing effect by rubber. As shown in *Table 7.4* and *Figure 7.21a* the modified system (PP/MaR/G) exhibited lower modulus values than those of unmodified PP/R/G composites for both compositions studied. From the previous SEM studies, by introducing MaR into the composite filler encapsulation was observed. Maleic-anhydride in the MaR phase enhanced the interaction between rubber and glass beads through the formation of carboxylate salts. The transfer of rubber particles from the bulk matrix to the interlayer on the filler surface reduced the reinforcing efficiency of the filler. Therefore, the final result is a reduction of Young's modulus in such a composite. The effect of the two contrasting morphologies on storage and loss modulus is shown in *Figure 7.22*, for a PP/R/G (separation) and a PP/MaR/G (encapsulation), where a drop in composite modulus at and above the glass transition temperature of MaR (-56°C) was observed in the PP/MaR/G composite.

Also, results in *Table 7.5* confirm the suppression of the reinforcing effect of glass beads by MaR due to the encapsulation structure in the PP/MaR/G composite. The composite modulus was calculated using the Einstein' equation (eq.7.2) and Kerner's equation (eq.7.3) for rigid sphere filled polymer system. The measured modulus of the PP/MaR/G composite was found lower than those calculated from both predictive models.

Table 7.5 Calculated modulus values for the ternary phase PP/R/G and PP/MaR/G (70/15/15) composites

Sample	Experimental modulus (GPa)	Einstein eq.(7.2)[b]	Kerner eq.(7.3)[c]
PP/R/G	1.84 (0.05)[a]	1.74	1.65
PP/MaR/G	1.31 (0.03)	1.49	1.42

[a] Standard deviations in parentheses, mean from eight specimens.

[b] Einstein' eq (7.2) $E_c/E_m = 1 + 2.5\,\Phi_f$

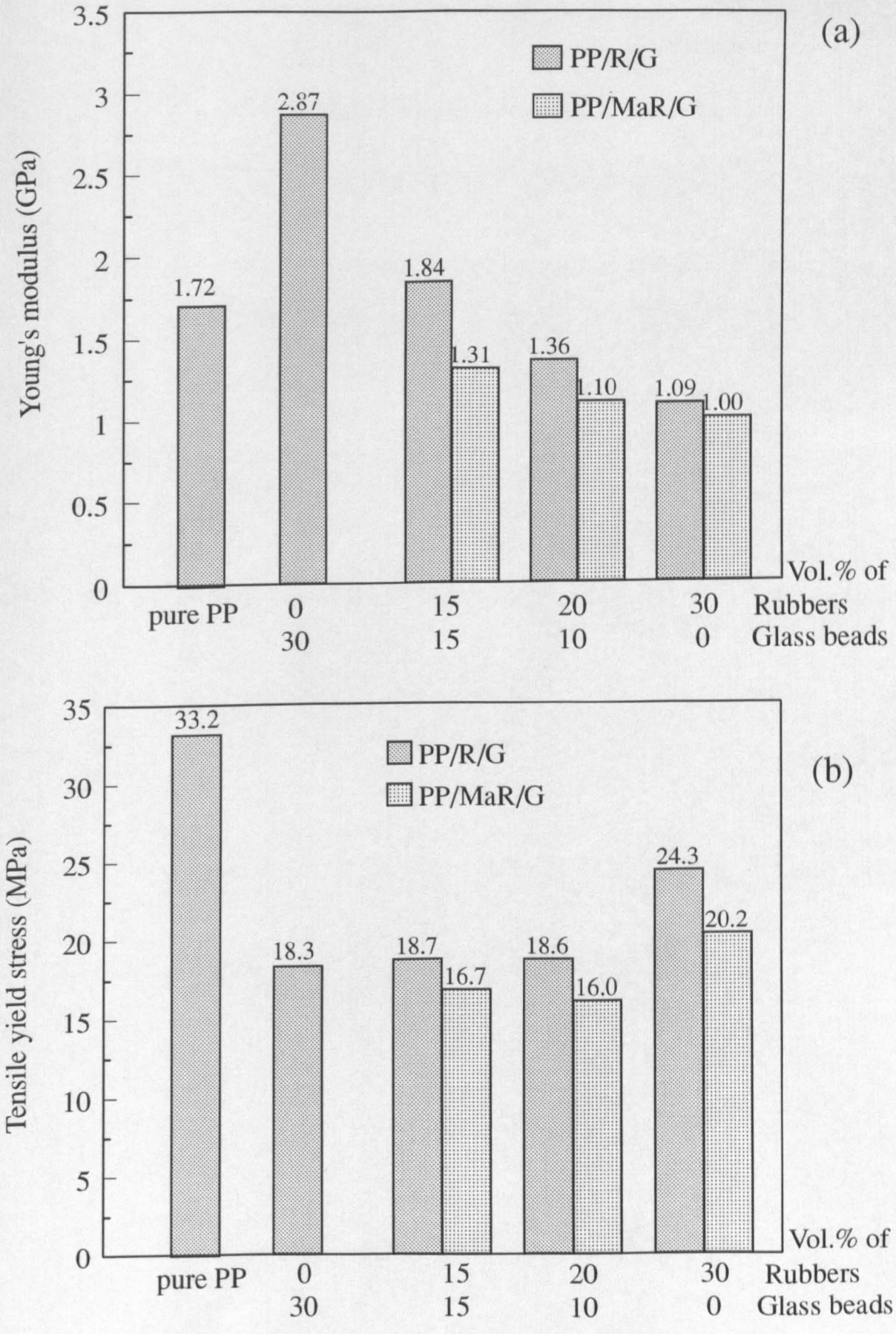

Figure 7.21 Effect of MaR on (a) Young's modulus, and (b) tensile yield stress of various polypropylene composites.

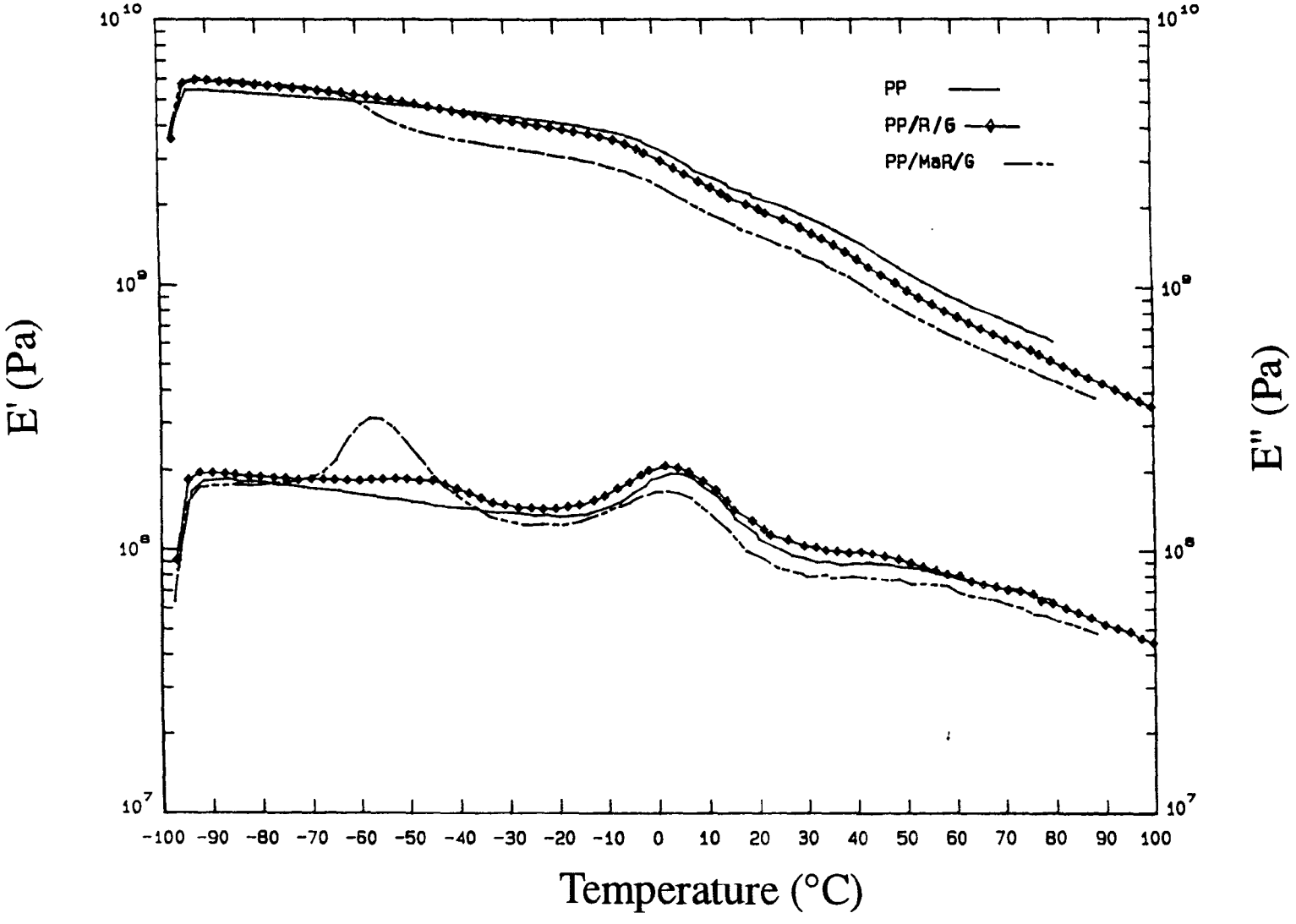

Figure 7.22 Temperature dependence of storage modulus (E') and loss modulus (E'') at 1 Hz. for PP, PP/R/G(70/15/15), and PP/MaR/G (70/15/15) composites

[c] Kerner's eq. (7.3) $E_c/E_m = 1 + \{15\,(1-\upsilon_m) / (8-10\Phi_f)\}\,\{\Phi_f / (1-\Phi_f)\}$

where : E_c is modulus of composite, E_m is the modulus of the polymer matrix. In this calculation the experimental data of corresponding two-phase PP/R (70/15) and PP/MaR (70/15) were taken as the matrix values for the PP/R/G (70/15/15) and PP/MaR/G (70/15/15), respectively. E_m (PP/R) = 1.27 GPa and E_m (PP/MaR) = 1.09 GPa, ϕ of 0.15 is the volume fraction of filler, and υ_m of 0.27 is Poisson's ratio of polypropylene.

Tensile yield stress of various polypropylene composites is shown in *Figure 7.21b*. Both rubber and glass beads caused a reduction in yield stress of the binary blends. This reduction was due to the decreased cross-sectional area of the polymer bearing the load. However, addition of 30 vol% of R led to a drop in yield stress to 24.31 MPa, while at the same additive volume fraction the yield stress values of PP/MaR and PP/G were only 20.2 and 18.31 MPa, respectively.

In ternary systems, PP/R/G composites showed a higher yield stress than PP/MaR/G composites, for both compositions studied. This difference is attributed mainly to the characteristics of rubber itself. To analyse the effect of MaR on the composite strength, some predictive models were undertaken. Equation 7.4 was proposed by Nielsen [108] where the filled composite strength (σ_c) can be calculated by

$$\sigma_c = \sigma_m (1- \phi) S \qquad (7.4)$$

where σ_m is the tensile strength of the matrix and ϕ is the volume fraction of filler in the composites. The parameter *S* was introduced to account for the weakness in the structure brought about by a discontinuity in stress transfer and the generation of stress concentration at the filler-polymer interface. The maximum value of *S* is unity for " no stress concentration effect". The lower the *S* value, the greater the stress concentration or poorer the adhesion.

Equation 7.5 was introduced by Nicolais and Nicodemo [117]. The strength of filled composite was expressed by :

$$\sigma_c = \sigma_m (1- a\phi^b) \qquad (7.5)$$

where *a* and *b* are constants. The value of *a* is related to the stress concentration or the quality of adhesion between the matrix and filler and *b* is related to the geometry of the filler. For spherical fillers with no adhesion and uniformly distributed, *a* becomes 1.21.

For the case of some adhesion, a becomes smaller than 1.21. The constant b is equal to 1 if the material fails by planar fracture and 2/3 if it fails by random fracture. *Table 7.6* shows the calculated S and a values of the PP/R/G and PP/MaR/G (70/15/15) composites.

Table 7.6 Values of stress concentration parameters, S (from eq.7.4) and a (from eq.7.5) in the PP/R/G and PP/MaR/G (70/15/15) composites.

Sample	σ_c (MPa)	σ_m (MPa)*	S	a
PP/R/G	18.67	26.75	0.80	1.07
PP/MaR/G	16.73	19.49	1.00	0.50

* In the calculation σ_m is the modulus of PP/R (70/15) and PP/MaR (70/15), respectively.

It can be seen that the calculated S value of the PP/MaR/G composite is equal to 1, also the calculated value of a is much smaller than 1.21. These results indicated a good interfacial adhesion between phases, leading to a continuity in stress transfer throughout the composite.

Table 7.7 shows the impact properties of various polypropylene composites. Impact strength of polypropylene was significantly increased by the incorporation of rubbers (both R and MaR). Initiation, propagation and failure energy of polypropylene increased markedly. Greater improvement in impact properties was observed using MaR. Differences between the effect of R and MaR on impact properties of polypropylene may be due to the characteristics of rubber itself, or due to the differences in melt rheology and morphology of the blends, as well as the adhesion of rubbers to the PP matrix. It has been suggested [283] for rubber filled polymer that the effect of reduced interfacial energy (by the use of functionalised material) in toughening is simply related to the effect that has on rubber particle sizes and therefore on average interparticular distance. The micrographs of *Figure 7.23 a and b* show a slightly difference in sizes of rubber particles in the PP/R and PP/MaR blends.

Impact strength (failure energy) of the ternary phase composites was also found to be strongly improved by MaR relative to unmodified R. Comparing the effect of R and MaR on the initiation, propagation and failure energy, it can be seen that the energy used for propagation of the crack in the PP/MaR/G composite (1.15 J) was lower than that in the PP/R/G composite (1.47 J). This means that the improvement in the total impact strength of the PP/MaR/G composite was due mainly to the strong interaction between MaR and

Table 7.7

Effect of maleic-anhydride modified EPR (MaR) on impact properties at 23°C for various polypropylene composites

Composition PP/R/G (by vol)	Initiation energy (J)		Propagation energy (J)		Failure energy (J)	
	R	MaR	R	MaR	R	MaR
100/0/0	3.08		1.04		4.12	
70/30/0	5.33	6.41	1.99	2.58	7.32	8.99
70/20/10	2.03	3.55	1.24	0.79	3.27	4.34
70/15/15	3.11	5.59	1.47	1.15	4.57	6.74

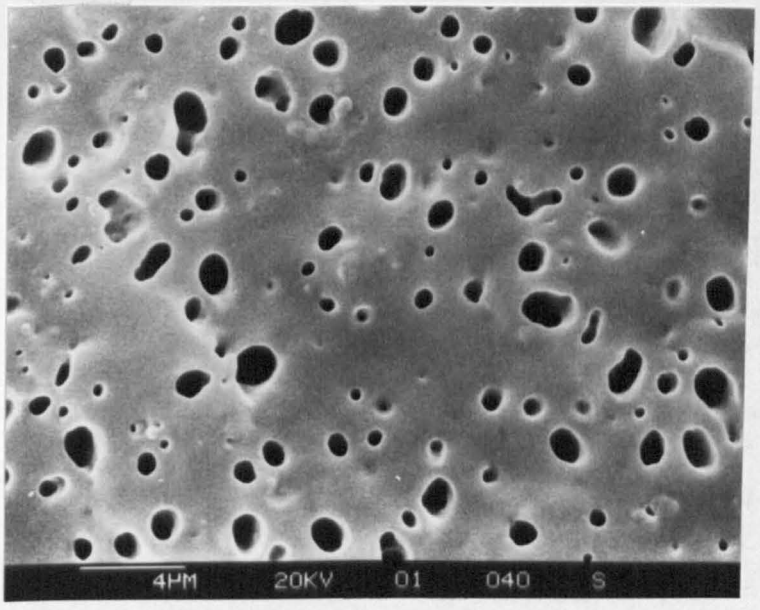

(a)

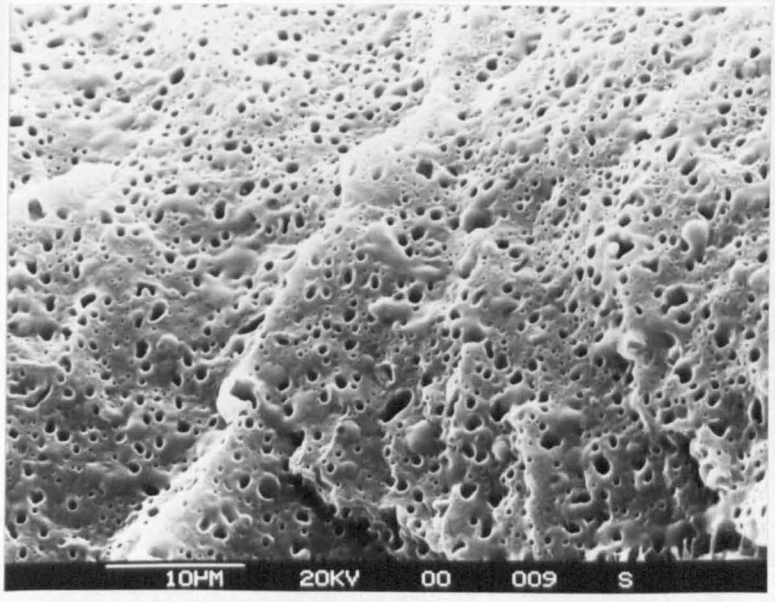

(b)

Figures 7.23 a-b SEM micrograghs of cryogenic fractured and etched surfaces of a PP/R blend *(a)*, and PP/MaR blend *(b)*.

glass beads in this composite. Thus, more energy was required for initiate cracks in such composite. Also, earlier observations by SEM revealed a cohesive failure in this composite, whereas an interfacial failure was observed in the PP/R/G composite.

(ii) Effect of silane-coated glass beads

Silane coupling agents are generally considered to be adhesion promoters between mineral fillers and polymer matrix and as such provide improved mechanical properties.

Table 7.8 shows the effect of silane-coated glass beads (coatG) on tensile and impact properties of ternary phase polypropylene composites. The ternary composite containing coatG shows higher elongation at yield and at break, also higher impact strength than the composite containing unmodified G. Generally, toughness and impact strength in filled composites is associated with good adhesion. Adhesion alone does not seem to be the reason for a higher impact strength in the PP/R/coatG composite, since adhesion is also a major parameter influencing tensile strength. In this study, the tensile yield stress of both PP/R/G and PP/R/coatG was very similar. The improvement of impact properties by coatG could be due to its influence on composite morphological structure, including dispersion of fillers, rubber particle size, also the interparticular-distance between particles. Interpretation of mechanical and morphological data in such composite, is complicated by the influence of several factors such as rheology and viscosity of the composite. Work by Han et.al.[125] showed that there was a possibility that coupling agent might have diffused into the polymer matrix, playing the role of an internal plasticiser leading to a decrease in the viscosity of the matrix phase. Also, owing to a reduction in interfacial energy by the surface modification, it is expected to lead to reduced dispersed phase size and greater ease of deformation of rubber particles [287]. At this stage, however, it is difficult to provide conclusion evidence for the mechanism of improvement in impact strength of the PP/R/coatG composite.

7.3.2.2 Fracture toughness at low temperature (-20° C)

One of the main reasons in addition of elastomer to polypropylene is to improve toughness at temperatures below its glass transition temperature (about 6°C). In this study, fracture toughness of various PP composites at -20°C was investigated, using the J-integral technique.

J-integral testing was carried out according to the multiple specimen method in ASTM E813-81 at -20°C and at the testing rate of 1 mm/min. Details of experimental procedure

Table 7.8

Effect of silane-coated glass beads (coat G) on tensile and impact properties at 23°C of ternary phase polypropylene composites

Sample	Composition (by vol)	Tensile properties				Impact properties		
		Modulus (GPa)	Yield stress (MPa)	Elongation at yield (%)	Elongation at break (%)	Initiation energy (J)	Propagation energy (J)	Failure energy (J)
PP/R/G	100/0/0	1.72 (0.06)[a]	33.24 (0.30)	5.77 (0.39)	146.88 (12.1)	3.08 (0.21)	1.04	4.12 (0.26)
PP/R/G	70/15/15	1.84 (0.05)	18.67 (0.18)	3.62 (0.04)	217.27 (32.3)	3.10 (0.31)	1.47	4.57 (0.33)
PP/R/coatG	70/15/15	1.73 (0.04)	18.80 (0.25)	3.83 (0.06)	254.64 (32.6)	4.10 (0.34)	1.93	6.03 (0.33)

[a] Standard deviations in parentheses, means from six specimens.

were discussed earlier in chapter 3. This method consists of loading and unloading several identical specimens to different values of load point deflection. The value of J can be determined from the area under load-deflection curve. The J-integral values were then plotted as a function of the length of the whitening region observed ahead the notch, as shown in *Figures 7.24 to 7.27.* The resistance curves were composed of two lines of different slopes, because the length of whitening ahead the initial notch tip is composed of the growing crack and the craze damage zone. In the lower J-value case, the energy put in is only dissipated to created crazes so that the craze zone increased rapidly with J-value. After the onset of crack growth, a part of energy was consumed by crack growth so that the craze damage zone extension was retarded. The intersection between these two lines of different slope is regarded as the onset of crack growth for the polymers to form the plastic craze zone. The critical J-integral value (J_c) was determined by this intersection. Plots of J values against stress-whitening length of polypropylene and its composites are shown in *Figures 7.24 to 7.27* and the J_c values obtained were presented in *Table 7.9.*

Table 7.9 The J value at the onset of crack growth (J_c) and the tensile yield stress (σ_y) at -20 °C of various polypropylene composites

Sample	Composition (by vol.)	J_c (kJ/m^2)	σ_y ($\times 10^{-6}$ N/m^2)
PP	100	1.75	51.8
PP/R	70/30	3.22	28.8
PP/MaR		6.13	25.5
PP/R/G	70/15/15	0.82	25.0
PP/MaR/G		3.33	20.1

At the testing temperature of -20°C polypropylene exhibited a brittle behaviour. The J_c value of 1.75 kJ/m^2 was observed in unmodified PP. By incorporation of 30 vol% rubbers (either R or MaR), a significant improvement in composite toughness was achieved. By using MaR instead of R, J_c was improved more than 200 %. In the ternary phase PP composites containing both rubber and rigid filler (PP/R/G), J_c value of 0.82 was observed. J_c fell down as the glass beads was incorporated and the incorporated R cannot prevent the usual fall in toughness due to filler addition. However, by the use of MaR composite toughness was found to be improved and this composite (PP/MaR/G) showed higher toughness than unmodified PP and, interestingly, higher than the PP/R blend.

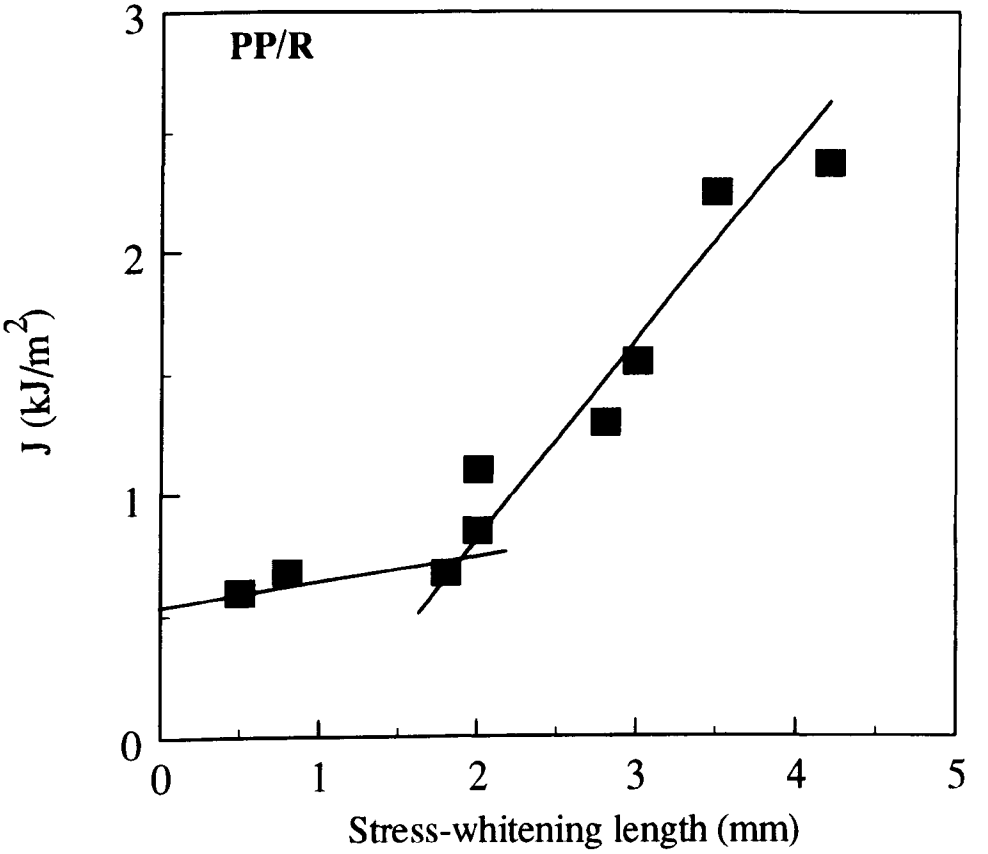

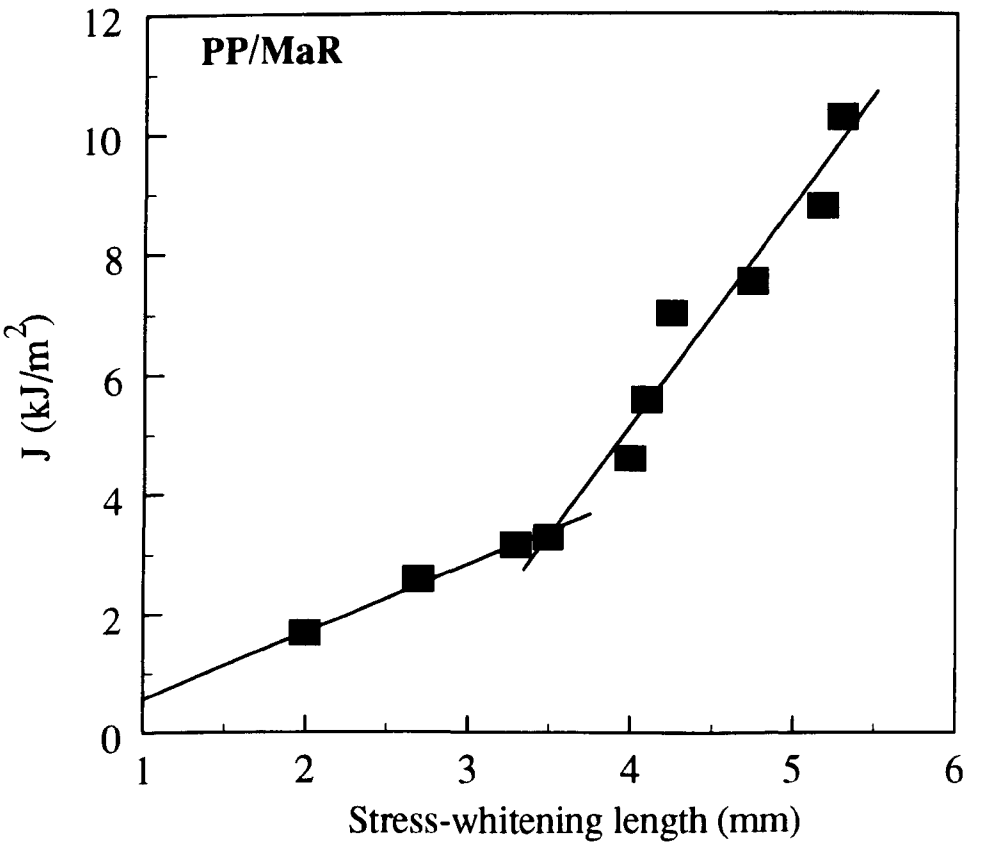

Figures 7.24 - 7.25 Plots of J against stress whitening length of a PP/R and PP/MaR blend (at -20°C).

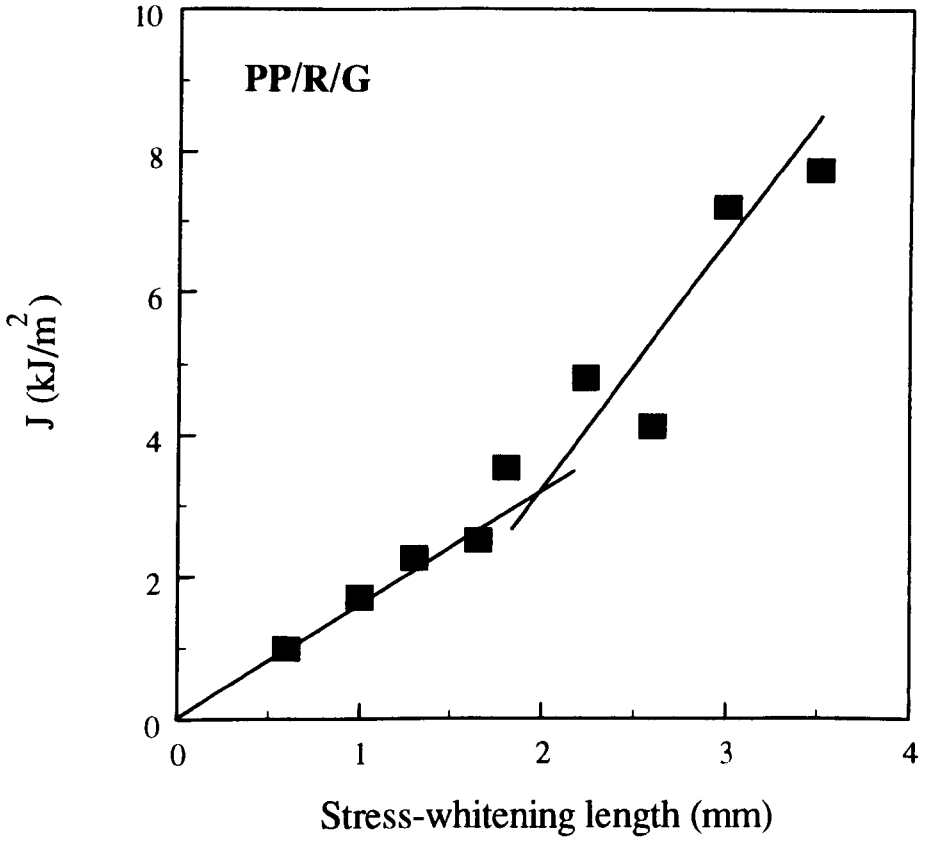

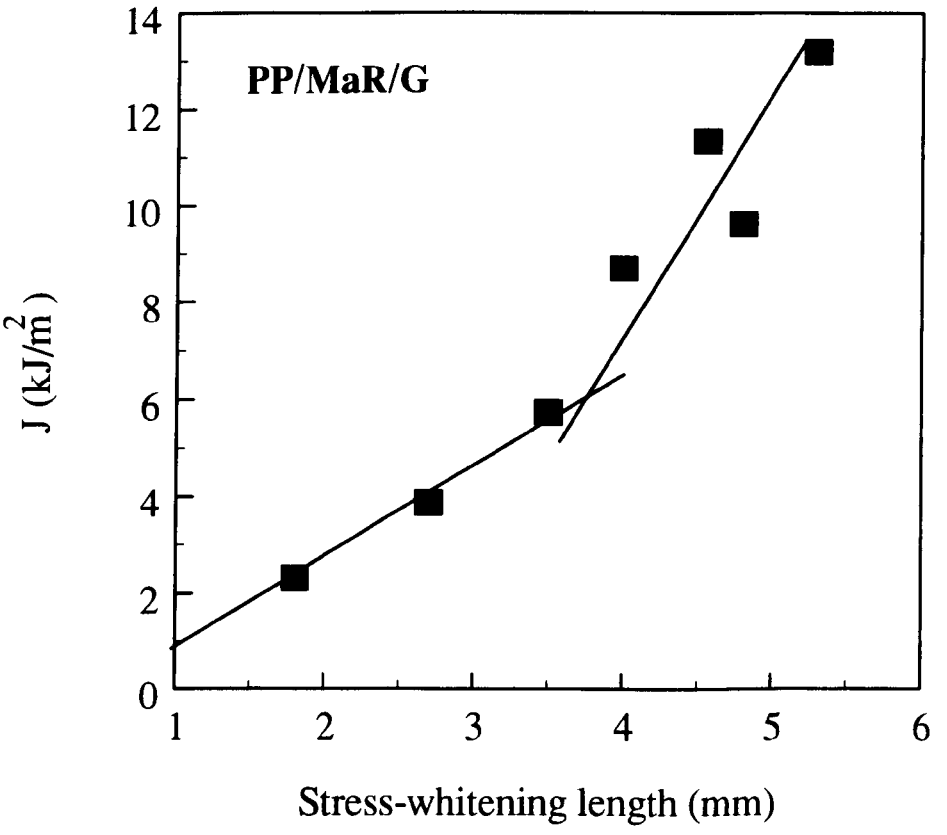

Figures 7.26 - 7.27 Plots of J against stress whitening length of ternary phase PP/R/G and PP/MaR/G composites (at -20°C).

In order to study the toughening mechanisms occurring during crack propagation in polypropylene and its composites, the microstructure of J-integral tested specimens was investigated. *Figure 7.28a* is a general view of a fracture surface showing three distinct zones. Zone I is a machined notch by a band saw, zone II is a sharp notch guided by a razor blade, and zone III is the fracture process which occurred during the J-integral testing. Higher magnifications showed the presence of further morphologically different areas, which can be distinguished proceeding from the notch tip towards the end of the fracture surface. The exact location of the details shown in *Figures 7.29 to 7.32* is indicated by the corresponding letters in *Figure 7.28b*. The arrows at the side of each micrograph show the direction of applied load.

Figure 7.29 shows a fracture surface of a 12 mm thick PP specimen. At the testing temperature of -20°C which is below its glass transition temperature, polypropylene failed in a brittle manner. A number of cracklike features were observed. Although no fracture nucleus can be clearly identified as in the case of most glassy polymers, it is apparent that fracture began ahead of the tip of the notch rather than at its tip. This behaviour has been observed in many semicrystalline polymers such as polyethylene [288].

With the incorporation of rubber to PP, cavitation associated with extensive plastic deformation was observed on the fracture surface of the rubber modified specimen. *Figure 7.30* is a micrograph of a fracture surface of a PP/MaR blend. The fractograph taken from the notch tip towards the end of the fracture surface showed general cavitation and the total absence of visible rubbery particles. A similar observation was also found in the PP/R blend and its fracture process has been discussed earlier in Chapter 4. In this case, a certain alignment among cavities can be seen suggesting the presence of a system of shear bands. Haaf et.al. [289] studied the deformation mechanisms in rubber-modified PVC. They concluded that the dispersed rubber phase initiated micro shear bands at an angle of 55 to 64° to the direction of applied stress, depending upon the particle size of the modifier in the blends. Speroni et.al. [290] also observed the angle of 76° between the void stretching and void alignment direction in rubber modified nylon-6. The intensity of rubber cavitation was extensive in the stress-whitening zone (area B). The structure of the material predominantly consists of voids surrounded by walls of drawn material. The large dimensions of some voids might be caused, at least partly, by coalescence between neighbouring cavities. From recent observations, the craze breakdown process has been described by Kramer and co-workers [291], and can be summarised as follows :

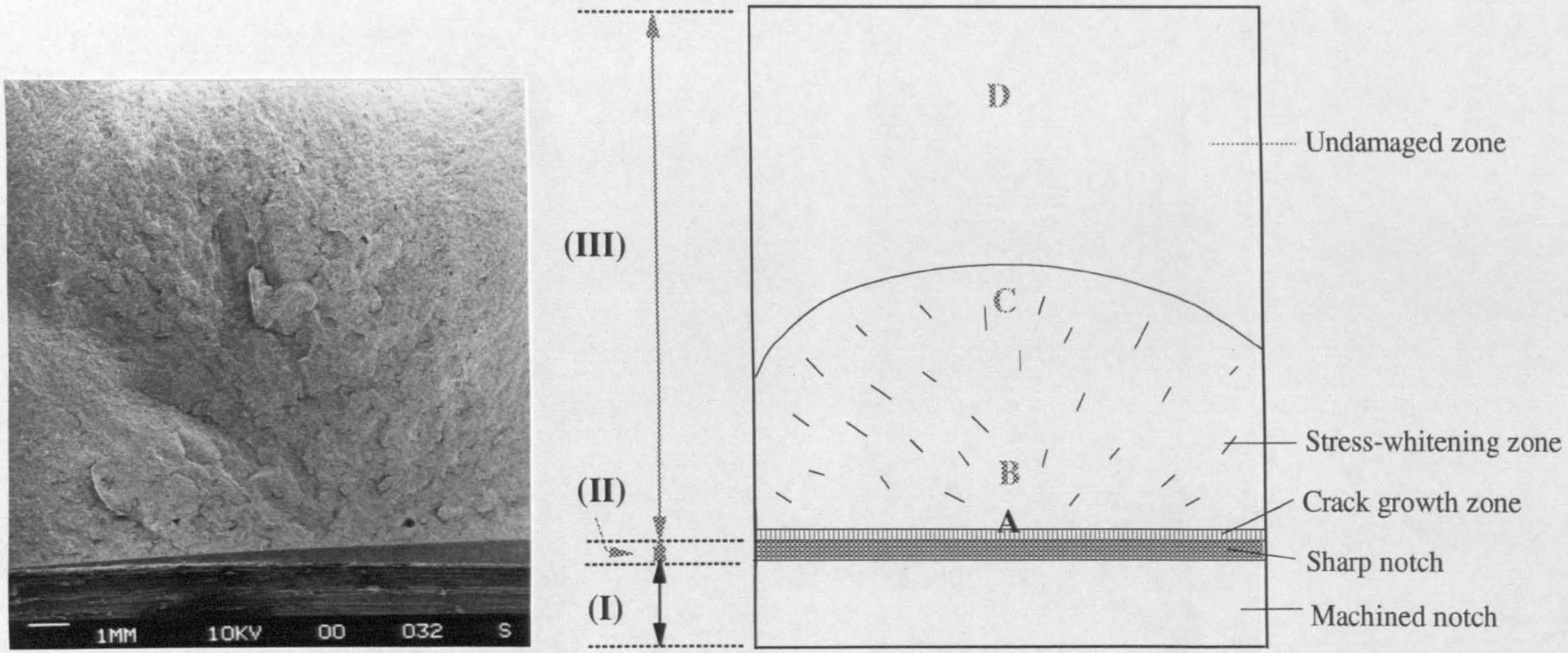

Figure 7.28 Typical fracture surface of J tested specimen showing three distinct zones. Zone (I) machined notch, zone (II) sharp notch, and zone (III) investigated fracture process area.

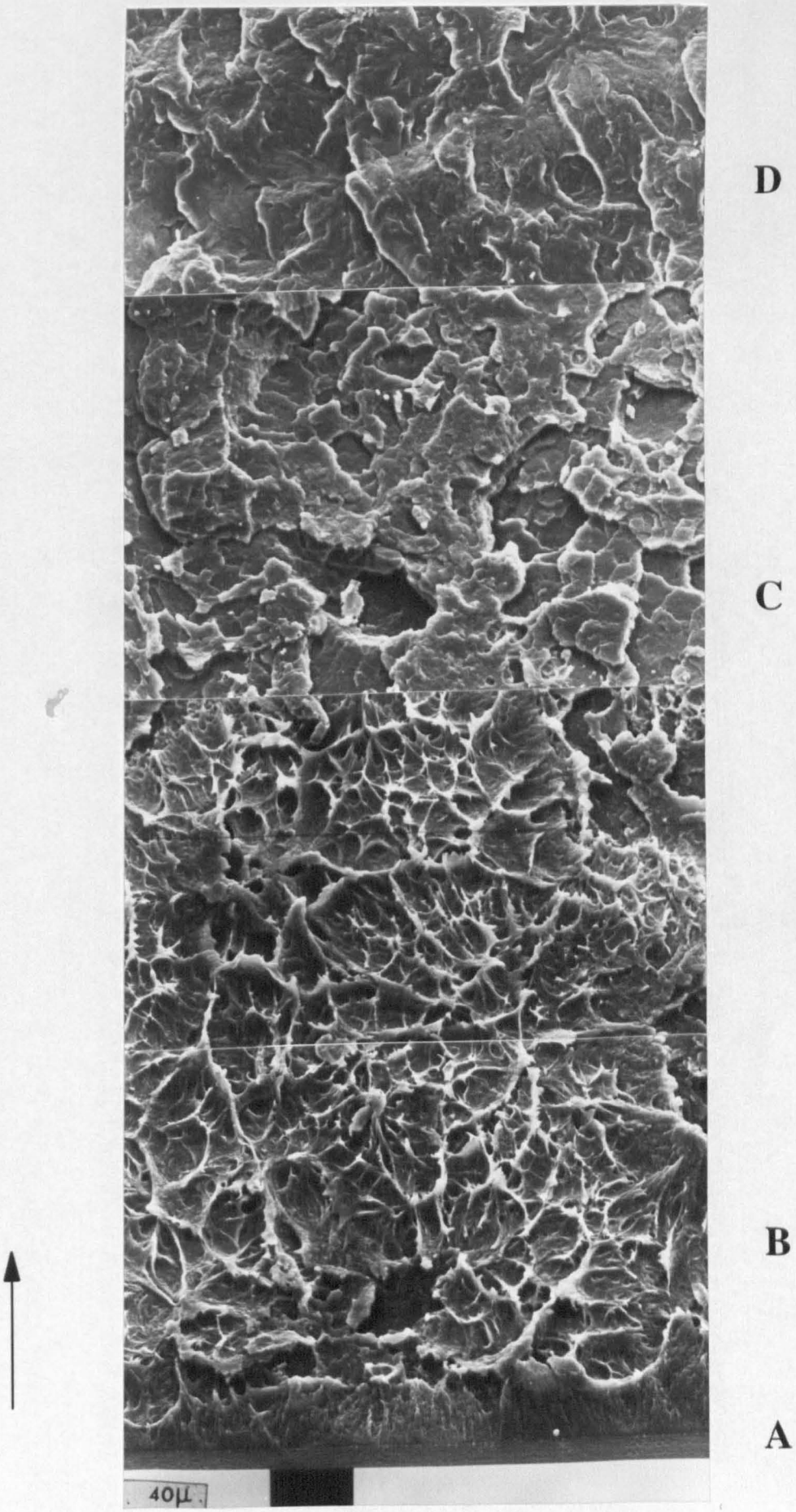

Figure 7.29 Fracture behaviour of polypropylene at -20°C

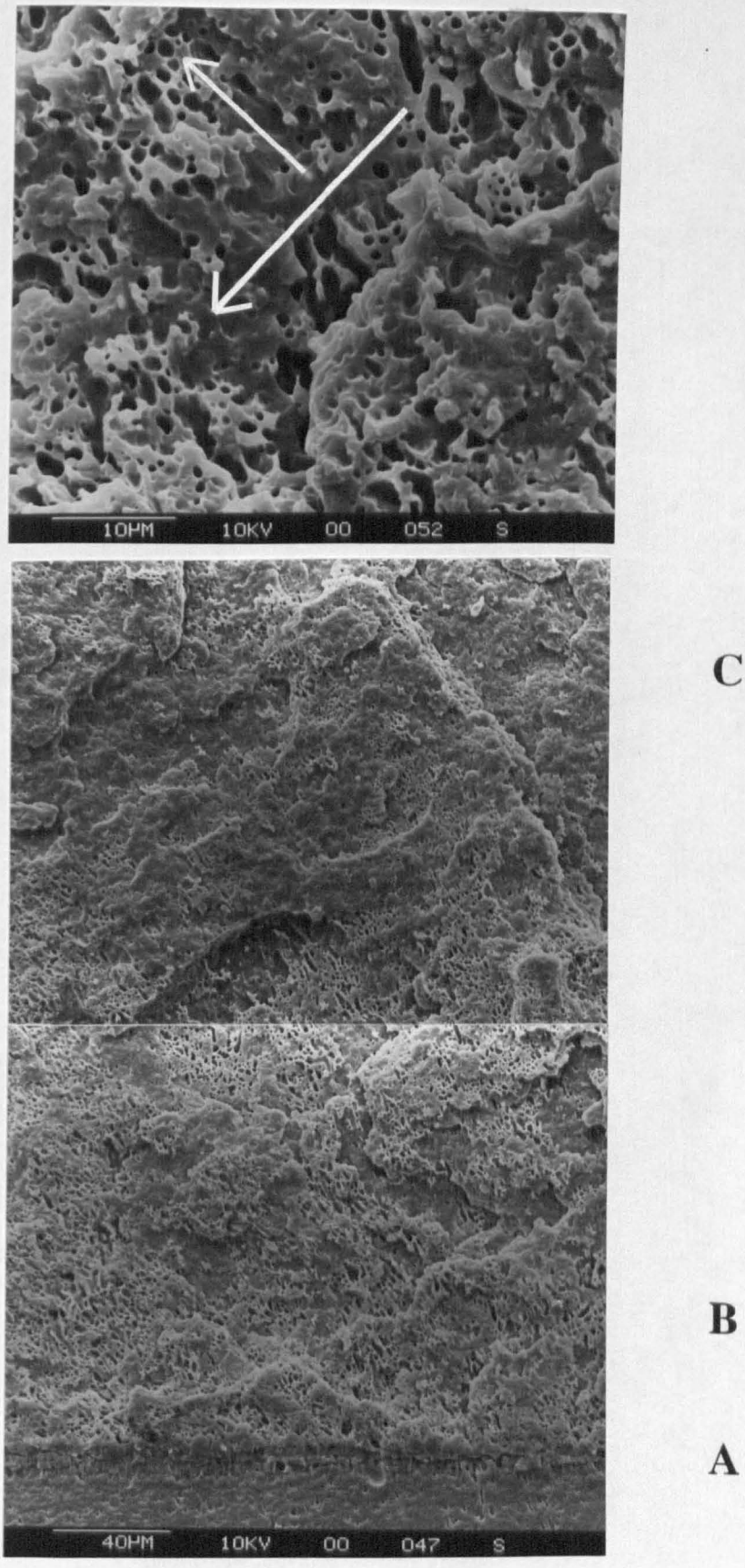

Figure 7.30 (top) High magnification of area B. The arrows show the orientation of the cavitation front. (bottom) Fracture behaviour of PP/MaR at -20°C

(1) As the craze grows, fibril breakage initiates at the craze-bulk interface, expanding to form larger voids. The initiation usually occurs around heterogeneities in the craze such as foreign matter and impurities.
(2) Each of these voids initially grows independently, but they eventually impinge on each other. Finally the crack is formed.
(3) Once the cracks reach a certain size, they pass through the interfacial regions between crazed and uncrazed materials along the craze plane and propagate by breaking more and more fibrils.
(4) Several cracks then become connected to each other, and this leads to macroscopic fracture.

Figures 7.31 and 7.32 show fracture processes in ternary phase PP/R/G and PP/MaR/G composites, respectively. Studies on particulate filled composites showed that crack propagation may occur by trans-particle fracture, by interfacial debonding or by cohesive failure of the matrix. In the case where filler material is sufficiently weak then instead of the crack propagation around the particles, the crack can pass directly through them. This effect has been reported for such fillers as aluminium trihydroxide [87] and dolomite [240]. The fracture surface of the PP/R/G composite (*Figure 7.31*) showed evidence that crack propagation occurred by particle-matrix debonding and pull-out, due to the poor adhesion between glass bead particles and the PP matrix.

In the PP/R/G composite, by using MaR instead of R the interfacial adhesion between glass bead particles and the polymer was improved. The micrograph of *Figure 7.32* revealed much less glass bead particles on the fracture surface. Evidence of good bonding can be clearly seen in the area of undamaged zone (area D) where the crack passed through the PP matrix and a cohesive failure was observed. Good interfacial adhesion between phases brought about by MaR is one of the reasons for a high impact strength and toughness in this composite. Also, the earlier SEM study showed an encapsulation structure in this composite. The presence of a rubber shell around the filler particles in the PP/MaR/G composite changed the stress distribution around the particles. For rigid spherical particles in a polymer matrix with good interfacial adhesion, the stress concentration is at the poles of the particles, and this is where the cracking will occur. For soft spherical particles such as rubber, the stress concentration is at the equator and it is where cracking or crazing will develop [86]. The difference in the stress fields is believed to be at least partially responsible for the differences between the impact behaviour commonly observed for addition of rigid spherical fillers and higher impact strength with the addition of rubber. The addition of rubber layers around the rigid filler in a polymer matrix ,altered the stress concentration from the poles to the equator of the

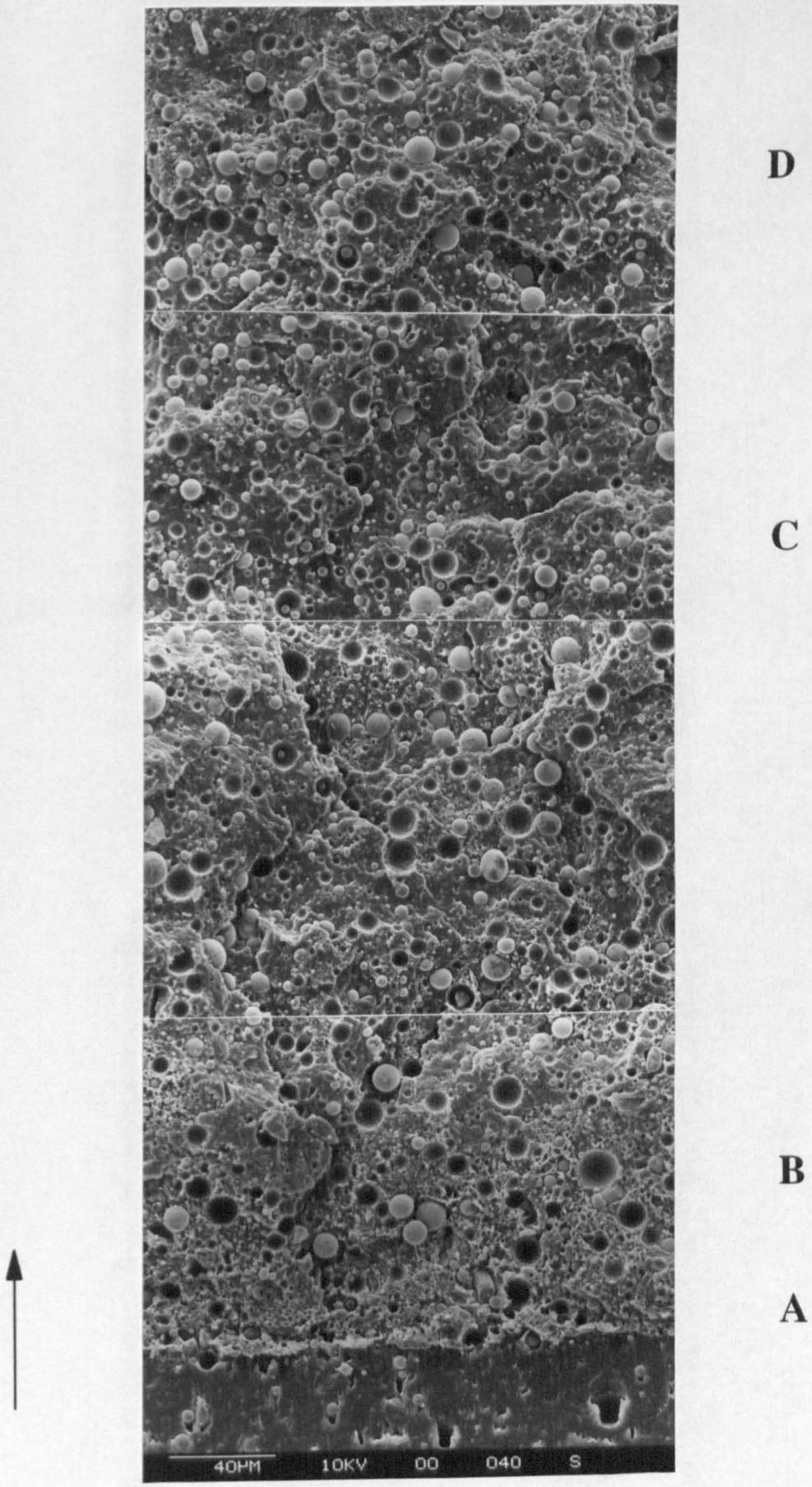

Figure 7.31 J-integral fracture surface of PP/R/G composite at -20°C

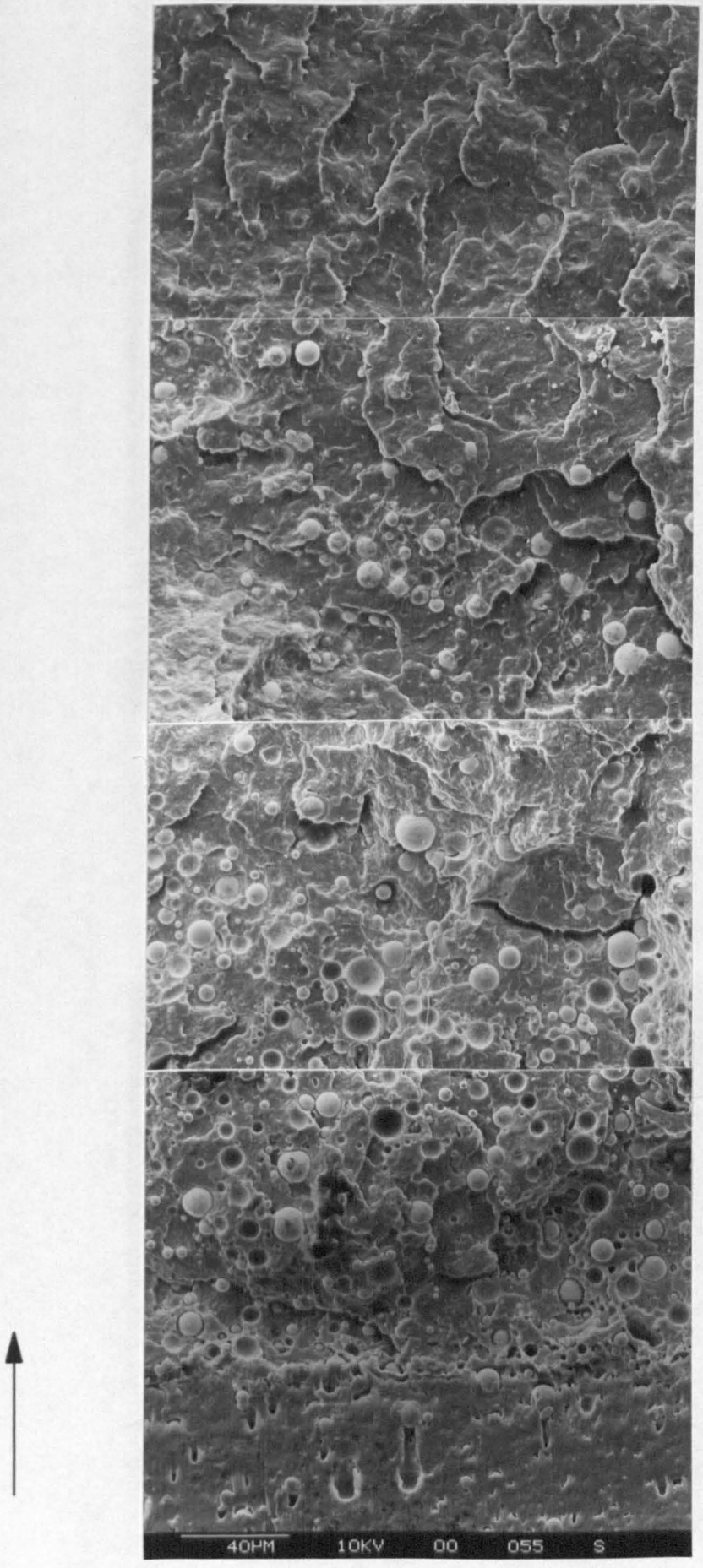

Figure 7.32 J-integral fracture surface of PP/MaR/G composite at -20°C

particles. Hence, the application of rubber layers to rigid fillers is expected to improve the impact strength and toughness due to a change in the location of the stress concentrations.

7.3.3 Effect of mixing step on composite structure and properties

Two mixing techniques were investigated : (i) one-step mixing, in which all the components were simultaneously mixed in the extruder, and (ii) two-step mixing, in which rubber and glass beads were premixed before the final mixing with polypropylene. The two mixing procedures are conceptually different. In the former, the mixing of the three components start simultaneously. In this case, the phase structure formation and arrangement of components is random, i.e. glass bead particles may be wetted by EPR and/or PP. Thus, the resulting structure could be separate dispersion or encapsulation. In the latter, rubber and filler were mixed together first. In this way, the formation of an encapsulated structure, in which glass bead particles were fully wetted by EPR, is experimentally controlled. The final structure, however, depends on the stability of the encapsulated units against shear forces in the melt during subsequent mixing with polypropylene.

Composites were prepared under the same processing conditions using the same extruder. The composite composition was kept constant at 70/15/15 (by vol%) PP/R/G. The following eight samples were prepared for this study.

System no.	Matrix	Rubber	Filler	one-step mixing	two-step mixing
1	PP	R	G	PP+R+G	(R+G)+PP
2	PP	R	coatG	PP+R+coatG	(R+coatG)+PP
3	PP	MaR	G	PP+MaR+G	(MaR+G)+PP
4	PP	MaR	coatG	PP+MaR+coatG	(MaR+coatG)+PP

7.3.3.1 Phase Structure Analysis

The aim of this analysis was to evaluate whether phase structures (separate dispersion or encapsulation) of ternary phase polypropylene composites can be changed by alteration of mixing step in which the components were mixed in the twin-screw extruder.

In the PP/R/G system (system no.1), by simultaneously mixing PP, R and G (PP+R+G) a separate dispersion structure was observed. EPR and glass bead particles were well dispersed in the polypropylene matrix. The interfaces between PP and G, as well as between PP and R were rather weak. The fracture surface shows an interfacial failure in this composite. By mixing EPR and glass beads prior to PP, (R+G)+PP, encapsulation of glass bead particles by EPR was not achieved, however, more EPR particles were observed adhering to the glass surface. *Figures 7.33a and b* are SEM micrographs of the PP+R+G (one-step mixing) and the (R+G)+PP (two-step mixing) fracture surfaces. The fracture surfaces were etched with heptane vapour to remove the EPR particles. The small dark circular holes (~1μm) shown on the micrographs are imprints of EPR particles, while large hemi-spherical dark areas (~5-7μm) were due to the torn-off glass bead particles during fracture. From *Figure 7.33b* a lot more dark holes were seen inside a large hemi-spherical area comparison to *Figure 7.33a*, meaning that more EPR particles were adhering to the glass surface prior to the fracture and etching processes. Quantitative phase-structure studies by DMA also showed the same phenomenon. Temperature dependencies of tan δ at 1 Hz. of these two composites are shown in *Figure 7.34*. Both composites showed two tan δ peaks, which are corresponded to the glass transition temperatures of EPR and PP. The T_g peaks of PP in both composites were of equal size (due to the same composition) and they were located at the same temperature (5.7°C). Contrary to the PP peaks, the EPR peak in the (R+G)+PP composite was observed at -40.5°C which was 3°C higher than that observed in the PP+R+G composite (-43.3°C). A shift in the EPR peak suggests less movement of EPR chains in such a composite. The DMA result, thus, supported the SEM observation that there were more EPR particles on the glass surfaces in the (R+G)+PP composites than in the PP+R+G composite.

A similar phenomenon was also observed in the system containing coated G (system no.2), SEM micrographs of fractured and etched surfaces of the PP+R+coatG (one-step mixing) and (R+coatG)+PP (two-step mixing) are shown in *Figures 7.35a and b*. Also, their DMA results are in *Figure 7.36*. Again, more rubber particles were found on the glass surface in the composite prepared by using a two-step mixing technique. A shift in the EPR glass transition peak from -45.4°C (in the PP+R+coatG) to -42.4°C (in the (R+coatG)+PP composite), quantitatively confirmed the observation from SEM.

Contrary phase structures were observed in the composites containing MaR (system no.3). Encapsulation of glass bead particles by MaR was observed in the PP+MaR+G composite (*Figure 7.37a*). However, due to the high viscosity of the polymer melt, full

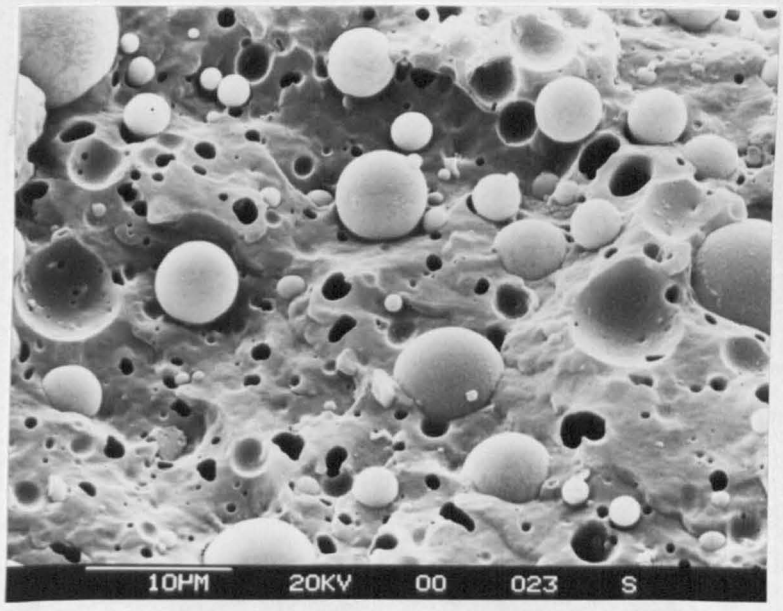

Figure 7.33a SEM micrograph of a cryogenic fractured and etched surface of a PP+R+G sample showing a separate dispersion structure. Dark circular holes observed on the micrograph are the imprints of the EPR particles.

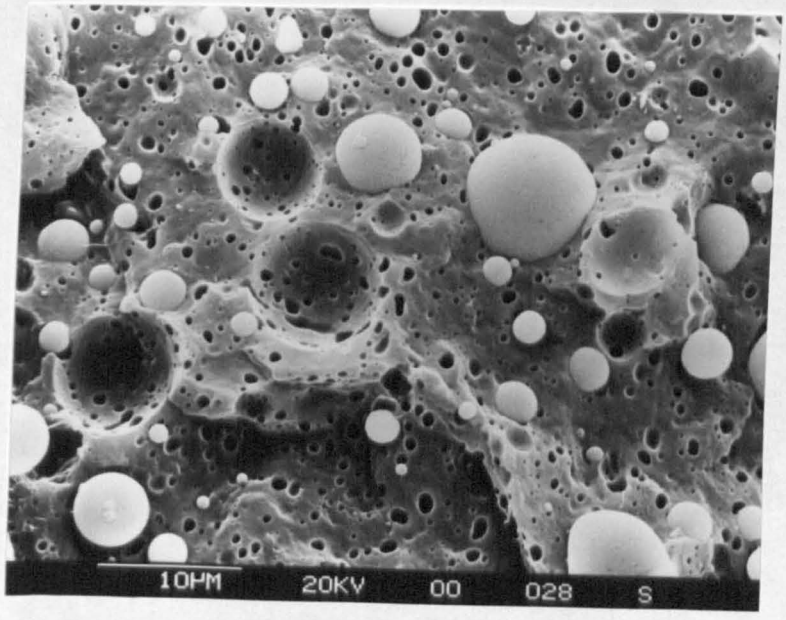

Figure 7.33b SEM micrograph of a (R+G)+PP (two-step mixing) sample where EPR and glass beads were mixed in the extruder prior to PP, showing slightly more EPR particles adhering to the glass bead surfaces.

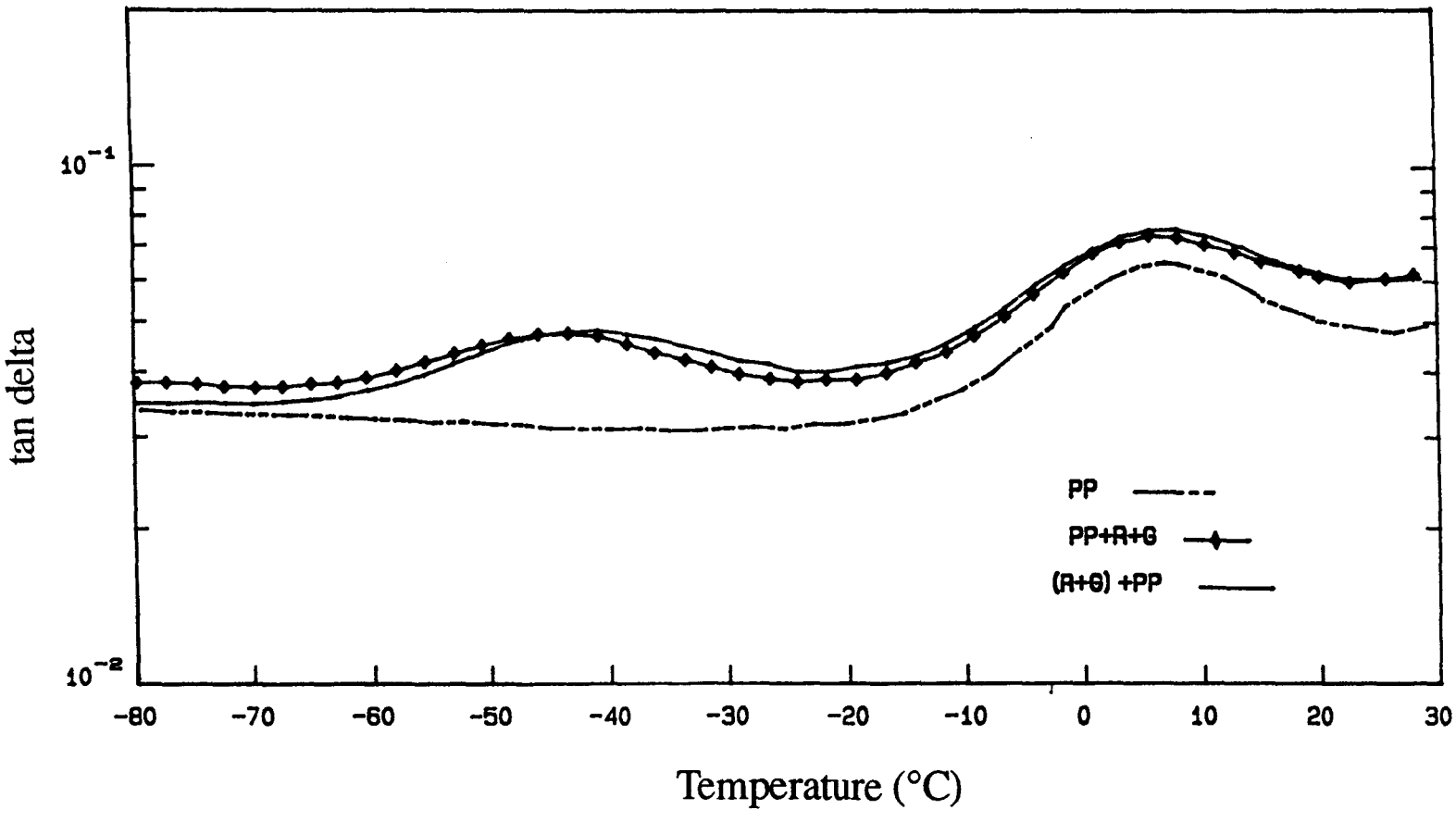

Figure 7.34 Temperature dependence of the damping (tan delta) at 1 Hz. of unmodified PP, ternary phase of PP/R/G (one-step mixing), and (R+G)+PP (two-step mixing) composites

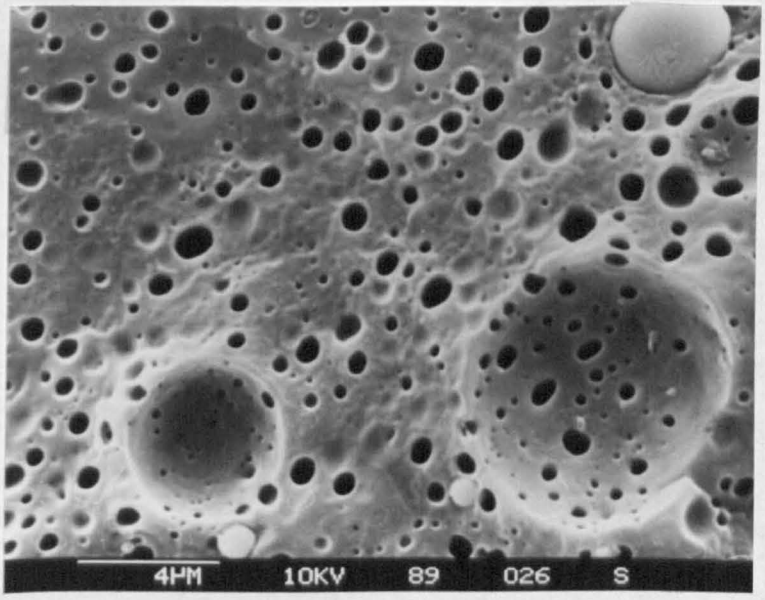

Figure 7.35a SEM micrograph of a cryogenic fractured and etched surface of a PP+R+coatG (one-step mixing) sample

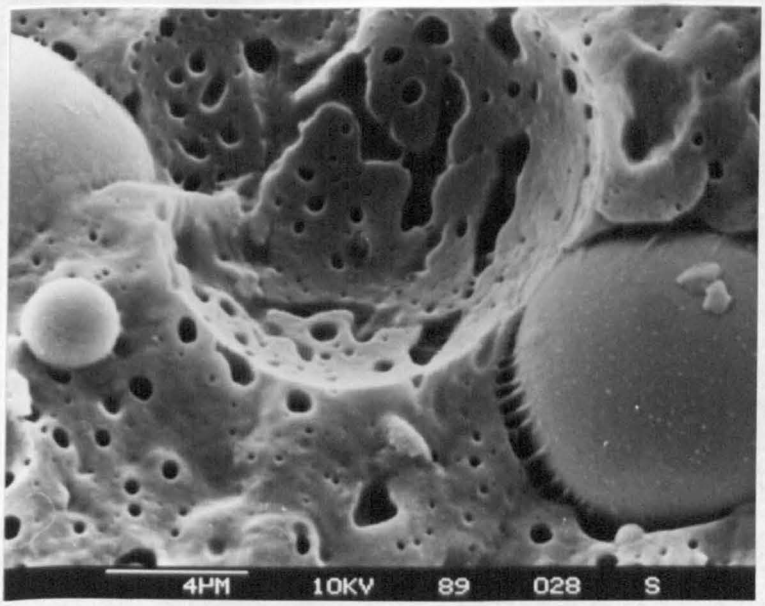

Figure 7.35b SEM micrograph of a (R+coatG)+PP (two-step mixing) sample, showing slightly more EPR particles adhering to the glass bead surfaces.

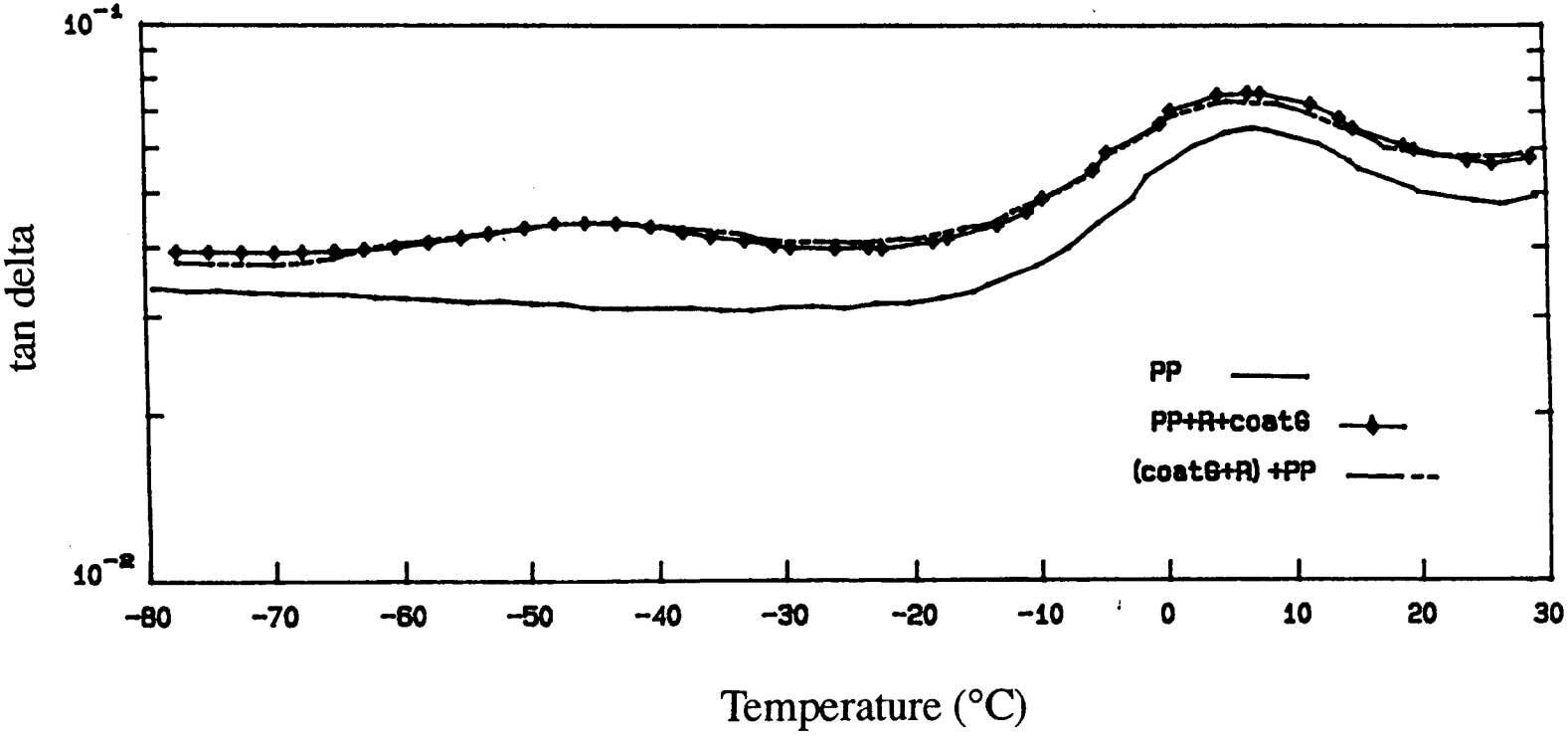

Figure 7.36 Temperature dependence of the damping (tan delta) at 1 Hz. of unmodified PP, ternary phase of PP/R/coatG (one-step mixing), and (R+coatG)+PP (two-step mixing) composites

encapsulation was not reached and some glass bead particles appeared only partially encapsulated. MaR was found to adhere strongly to the glass surface. As a result, a much larger rubber glass transition peak located at -55 °C was observed and presented in *Figure 7.38*. The use of MaR did not appreciably affect the tan δ peak of PP matrix. The tan δ peaks of the PP matrix in the PP/MaR and the PP/MaR/G composites were of equal size and both were located at ~ 6°C. In the two-step mixing technique, MaR and glass beads were mixed together prior to PP. In this case the encapsulation of glass bead by MaR was experimentally controlled before they (MaR+G) were final mixed with PP, and their result was expected to reach a fully encapsulation. Surprisingly, this was not observed. The effect of mixing step on phase structure of the ternary phase PP/MaR/G composites is shown in *Figures 7.37 to 7.39*. By using the two-step mixing technique, less interfacial adhesion between phases was observed. Glass bead particles were seen on the fracture (non-etched) surface of the (MaR+G)+PP composite (*Figure 7.39b*), comparison to the micrograph of *Figure 7.39a* where no glass bead particles was revealed on the fractured surface, reflecting a better adhesion in the PP+MaR+G composite. The DMA results of *Figure 7.38* show a reduction in size of the EPR tan δ peak in the (MaR+G)+PP composite. The glass transition temperature of EPR was observed at -60°C which is similar to that observed in the binary PP/MaR blends. Also, the FTIR results of *Figure 7.40* show a reduction in the peak intensity at 1565 cm^{-1}, demonstrating a small amount of carboxylate salt (CO_2^-) presented in the (MaR+G)+PP composite.

A similar observation on debonding of glass bead particles after the two-step mixing process, was also found in the ternary phase composite containing MaR and coatG. *Figures 7.41a and b* are the SEM micrographs of fractured and etched surfaces of the PP/MaR/coatG composites prepared using (a) one-step mixing, and (b) two-step mixing. A dewetting of glass bead particle can be clearly seen on the micrograph of *Figure 7.41b*. Their DMA results are presented in *Figure 7.42*.

7.3.3.2 Effect of mixing step on composite mechanical properties

Figures 7.43 to 7.45 show the effect of mixing step on tensile and impact properties of various polypropylene composites.

In the PP/R/G system (system no.1), the composite prepared by using the two-step mixing (R+G)+PP showed a lower Young's modulus value (1.71 GPa) than that observed in the composite prepared by one-step mixing (1.84 GPa) as shown in *Figure*

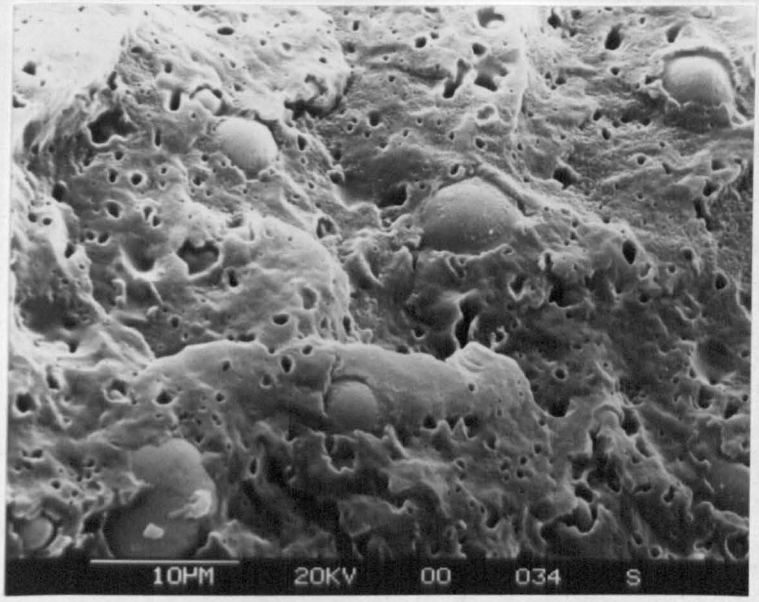

Figure 7.37a SEM micrograph of a cryogenic fractured and etched surface of a PP+MaR+G (one-step mixing) sample

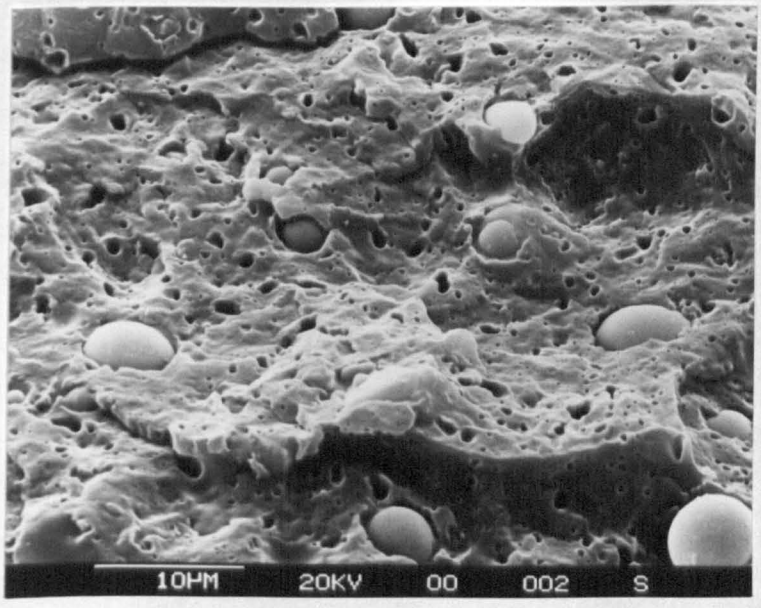

Figure 7.37b SEM micrograph of a cryogenic fractured and etched surface of a (MaR+G)+PP (two-step mixing) sample

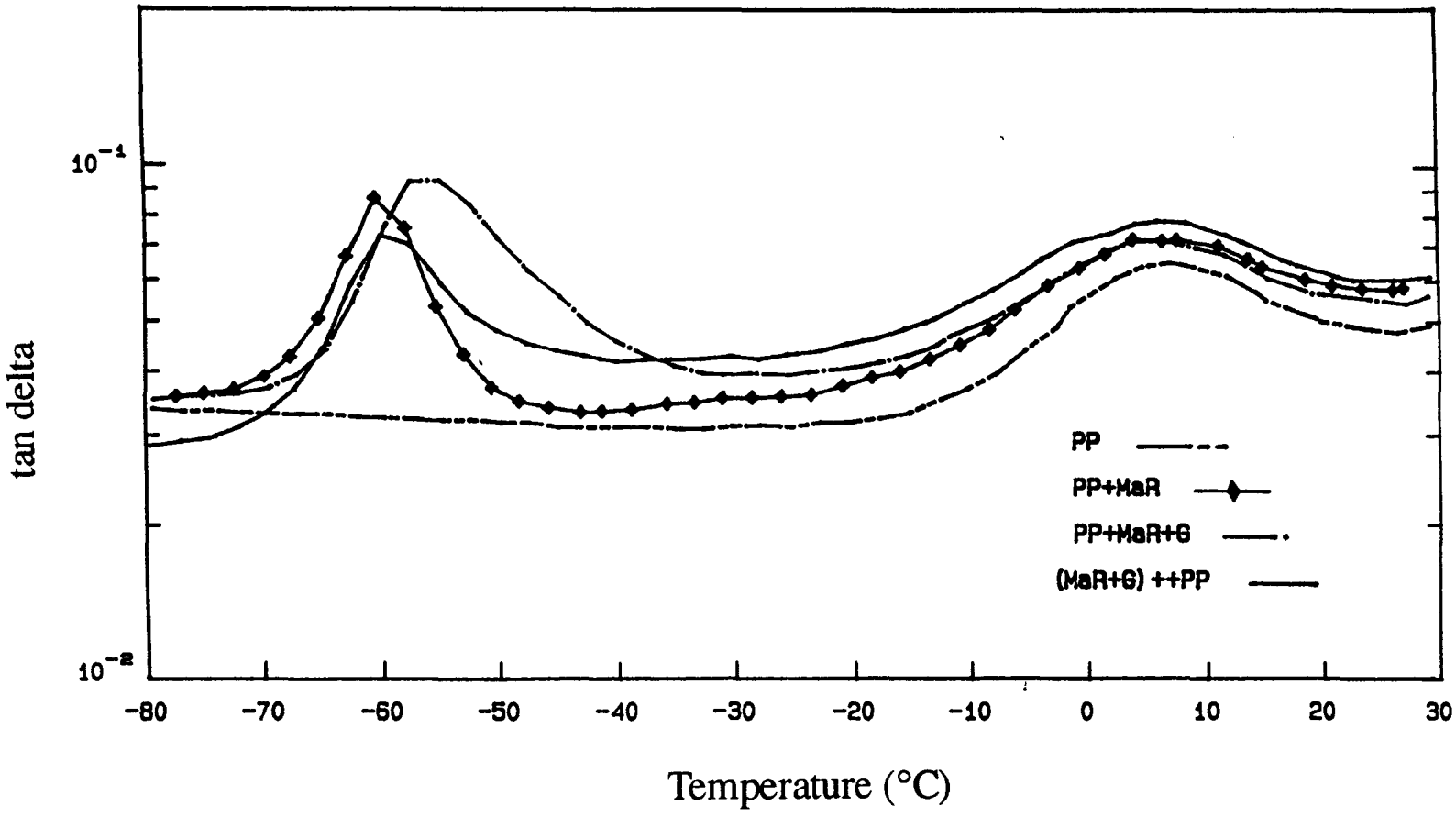

Figure 7.38 Temperature dependence of the damping (tan delta) at 1 Hz. of unmodified PP, PP/MaR blend, PP/MaR/G (one-step mixing), and (MaR+G)+PP (two-step mixing) composites

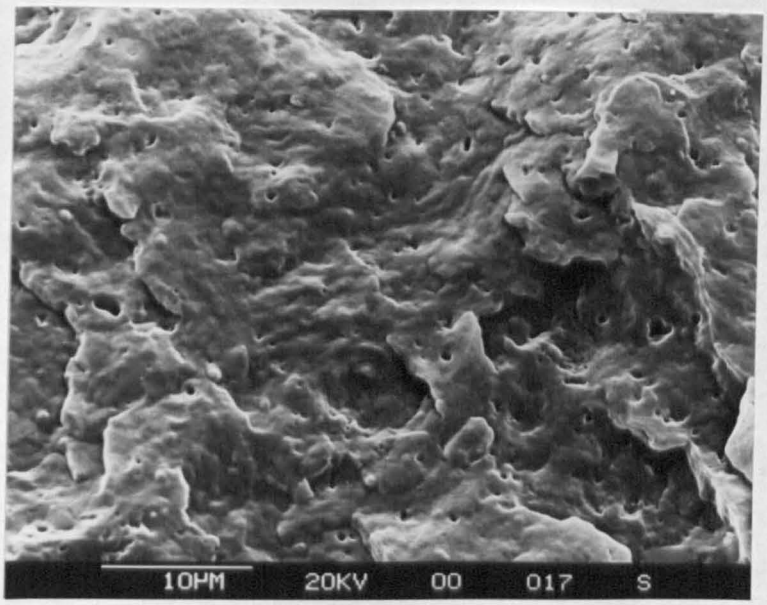

Figure 7.39a SEM micrograph of a cryogenic fractured surface of a PP+MaR+G (one-step mixing) sample, showing a cohesive failure where cracks pass through the PP matrix inferring a good interfacial adhesion.

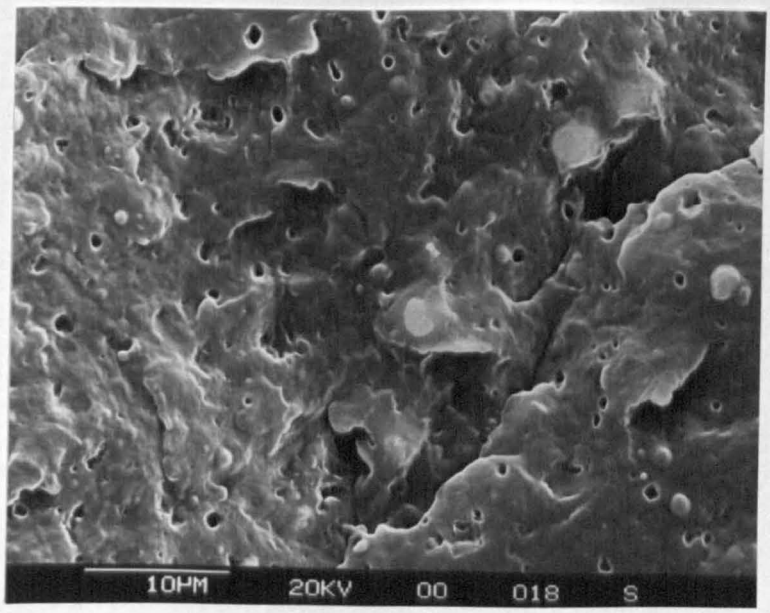

Figure 7.39b SEM micrograph of a (MaR+G)+PP (two-step mixing) sample, showing a reduction in interfacial adhesion between PP and glass bead.

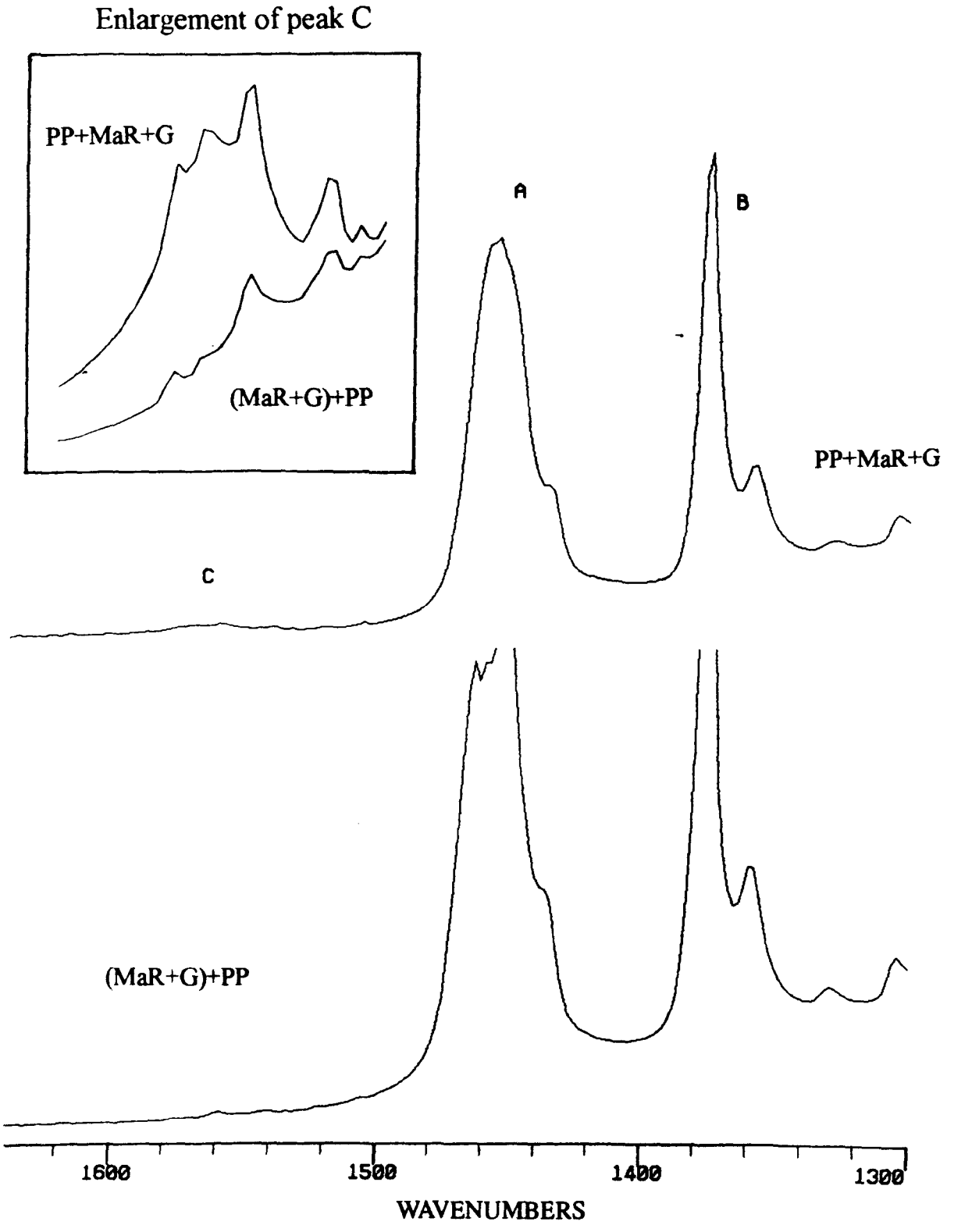

Figure 7.40 FTIR spectra of a PP+MaR+G (one-step mixing) composite and a (MaR+G)+PP (two-step mixing) composite, showing a reduction in carboxylate salt intensity peak at 1565 cm^{-1}

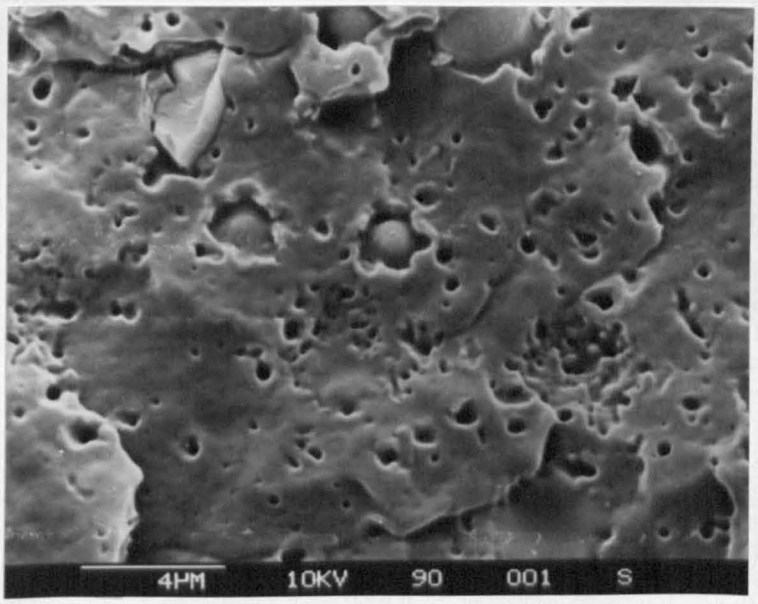

Figure 7.41a SEM micrograph of a cryogenic fractured and etched surface of a PP+MaR+coatG (one-step mixing) sample

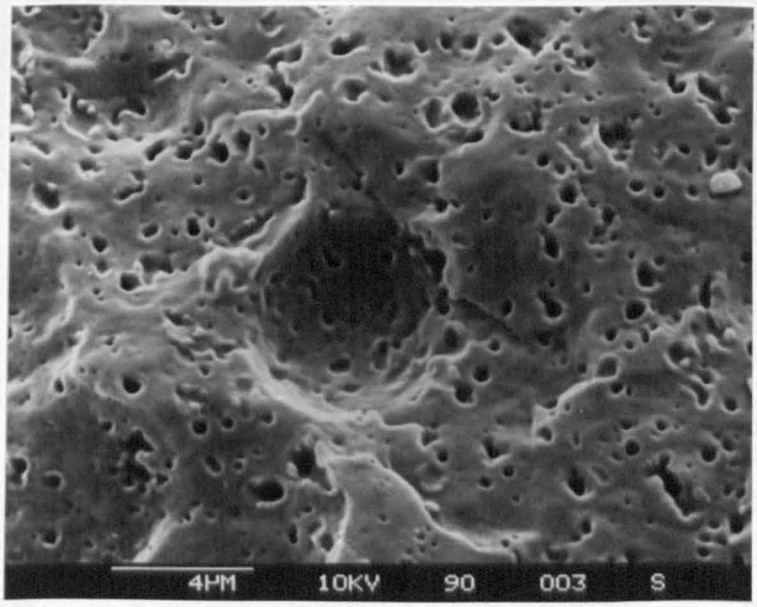

Figure 7.41b SEM micrograph of a cryogenic fractured and etched surface of a (MaR+coatG)+PP (two-step mixing) sample

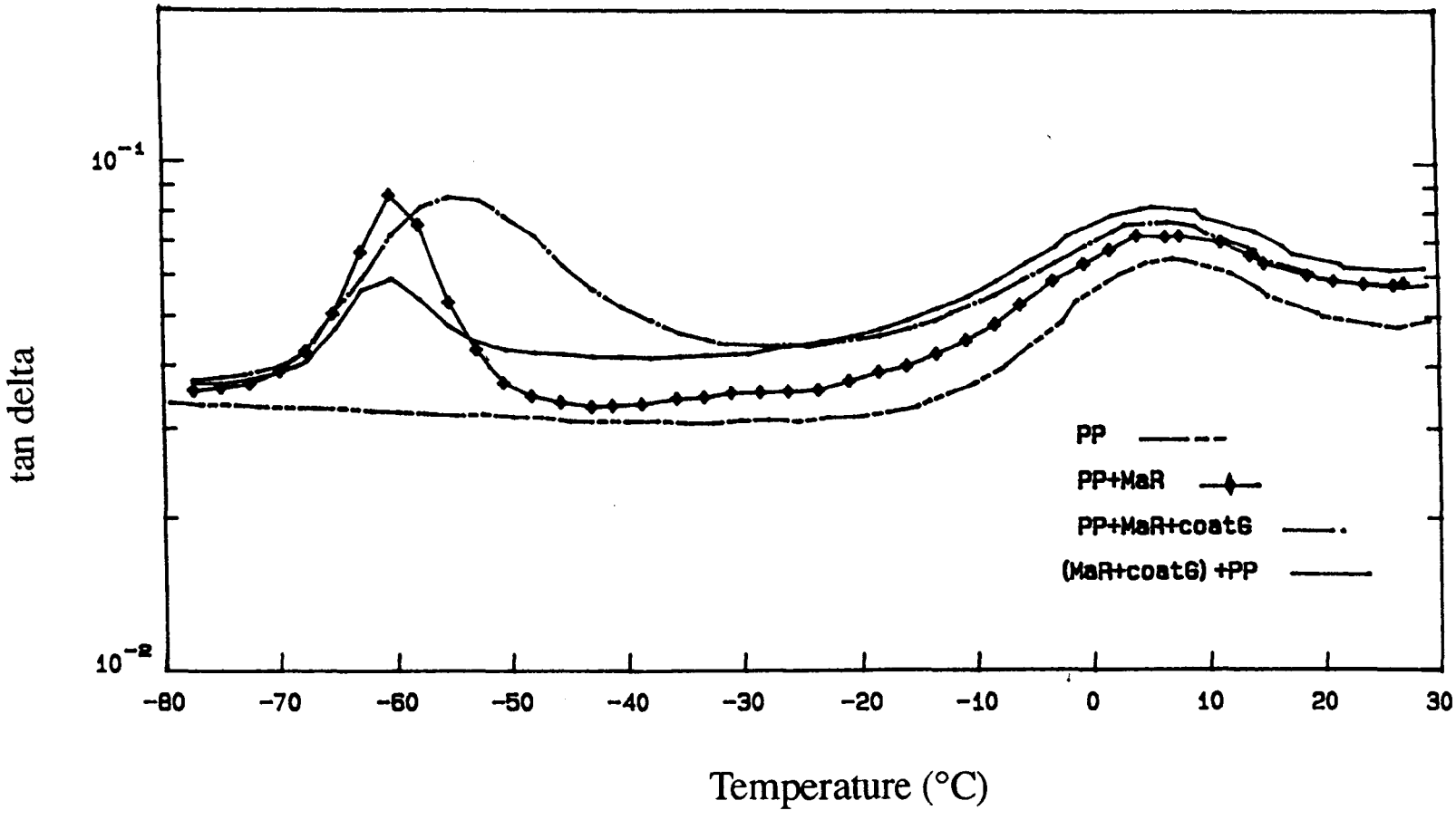

Figure 7.42 Temperature dependence of the damping (tan delta) at 1 Hz. of unmodified PP, PP/MaR blend, PP/MaR/coatG (one-step mixing), and (MaR+coatG)+PP (two-step mixing) composites

7.43. Differences in Young's modulus of the two composites may be explained by the difference in their morphological structure. Previous SEM and DMA results revealed more EPR particles adhering onto the glass bead surface in the (R+G)+PP composite. The increase in the amount of EPR particles on the glass surface reduced reinforcing efficiency of glass beads, causing a reduction in the effective filler modulus. Similar results were also found in the PP/R/coatG system (system no.2), in which the modulus of the (R+coatG)+PP composite (1.69 GPa) was lower than that of the PP+R+coatG composite (1.73 GPa).

Contrary results were found for composites containing MaR (both PP/MaR/G and PP/MaR/coatG systems). In these two composites, the composites prepared by using a two-step mixing technique showed higher modulus values than those of one-step mixing. This result can be explained in the same way which is due to their differences in morphological structures. In these two systems, encapsulation structure was obtained. MaR was found adhering strongly to the glass bead surfaces. However, by using the two-step mixing technique this interfacial adhesion reduced, also the EPR particles may be debonded from the glass surfaces due to the shear force generated during the second mixing with polypropylene in the extruder.

Among the four systems studied, no significant difference in the yield stress values was observed between composites prepared by a one-step mixing or two-step mixing technique as shown in *Figure 7.44*.

A greater effect of mixing step was found on composite impact properties. Impact strength improvement was observed in the composites containing unmodified R (system no.1 and 2) prepared by using the two-step mixing technique as shown in *Figure 7.45*. In the PP/R/G system, the PP+R+G composite (one-step mixing) showed an impact failure energy of 4.57 J, while that of 5.21 J was found for the (R+G)+PP composite (two-step mixing). A similar trend was also observed in the system of PP/R/coatG. Opposite results were found for the systems containing MaR (system no.3 and 4). In both systems, by using the two-step mixing technique impact strength was found to drop around 10% as shown in *Figure 7.45* and *Table 7.10*. This is more evidence which suggested that the presence of rubber around the filler particles instead of separate from the filler is favourable for better impact strength.

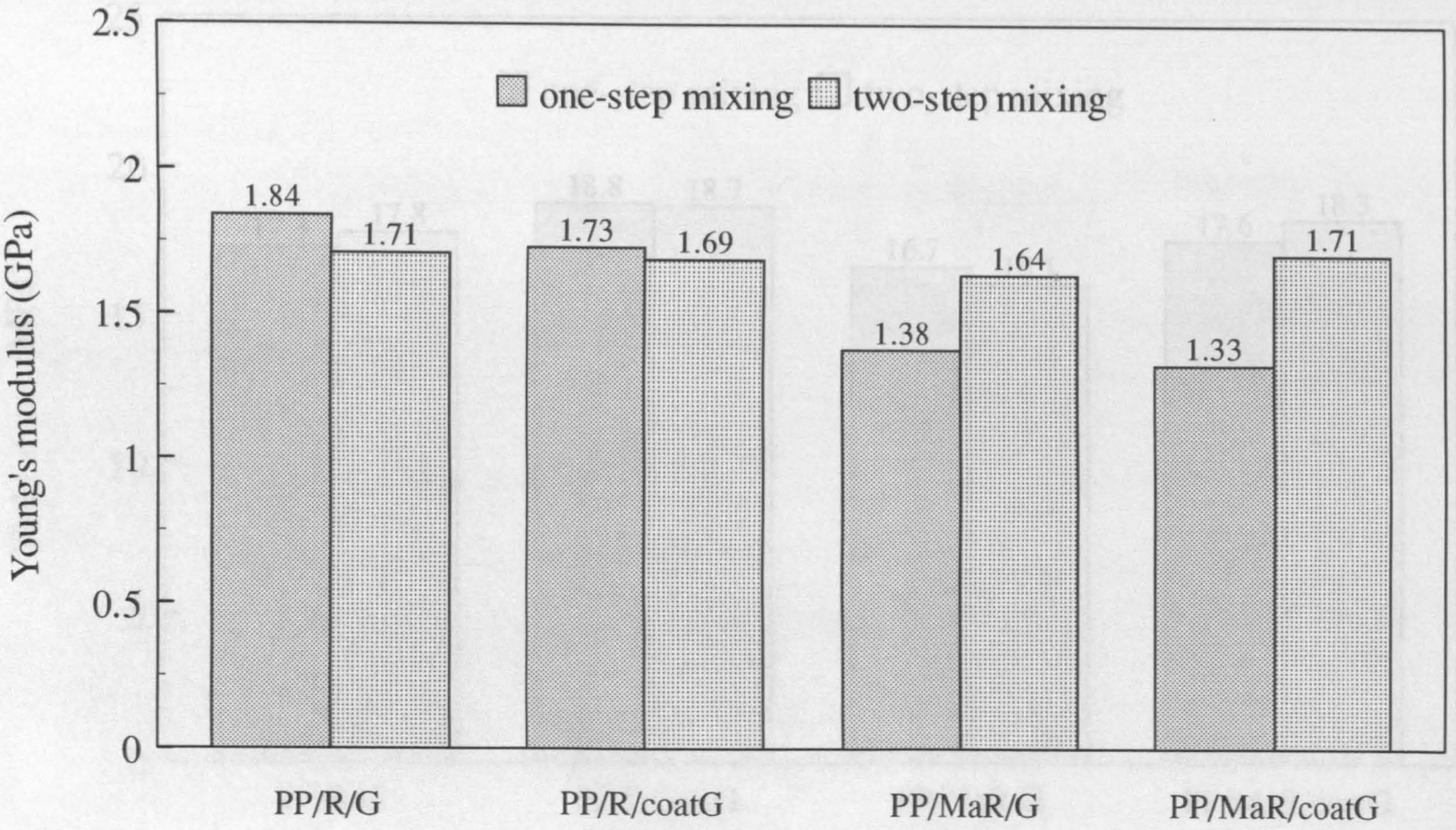

Figure 7.43 Effect of mixing step on Young's modulus of various ternary polypropylene composites

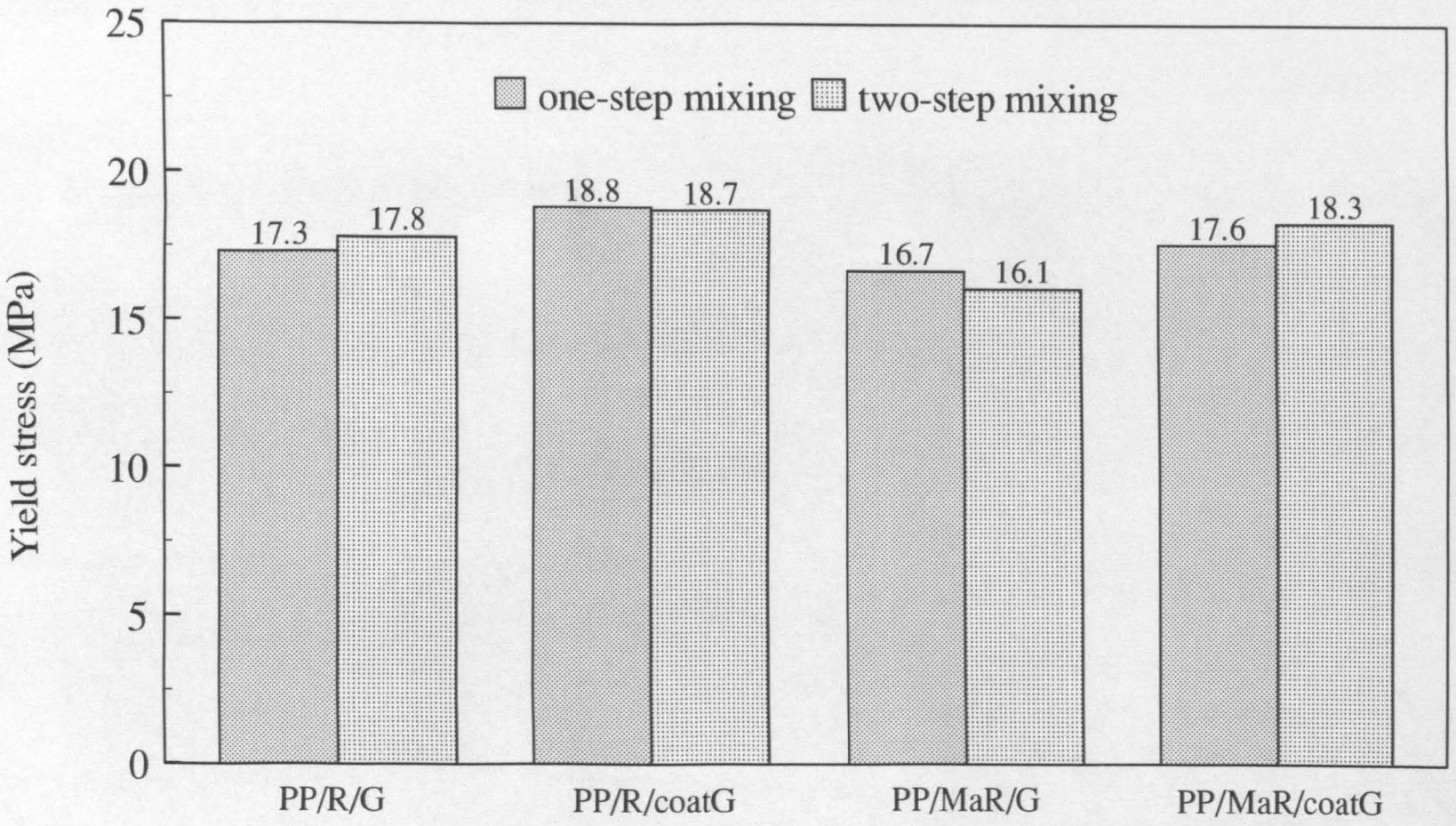

Figure 7.44 Effect of mixing step on tensile yield stress of various ternary polypropylene composites

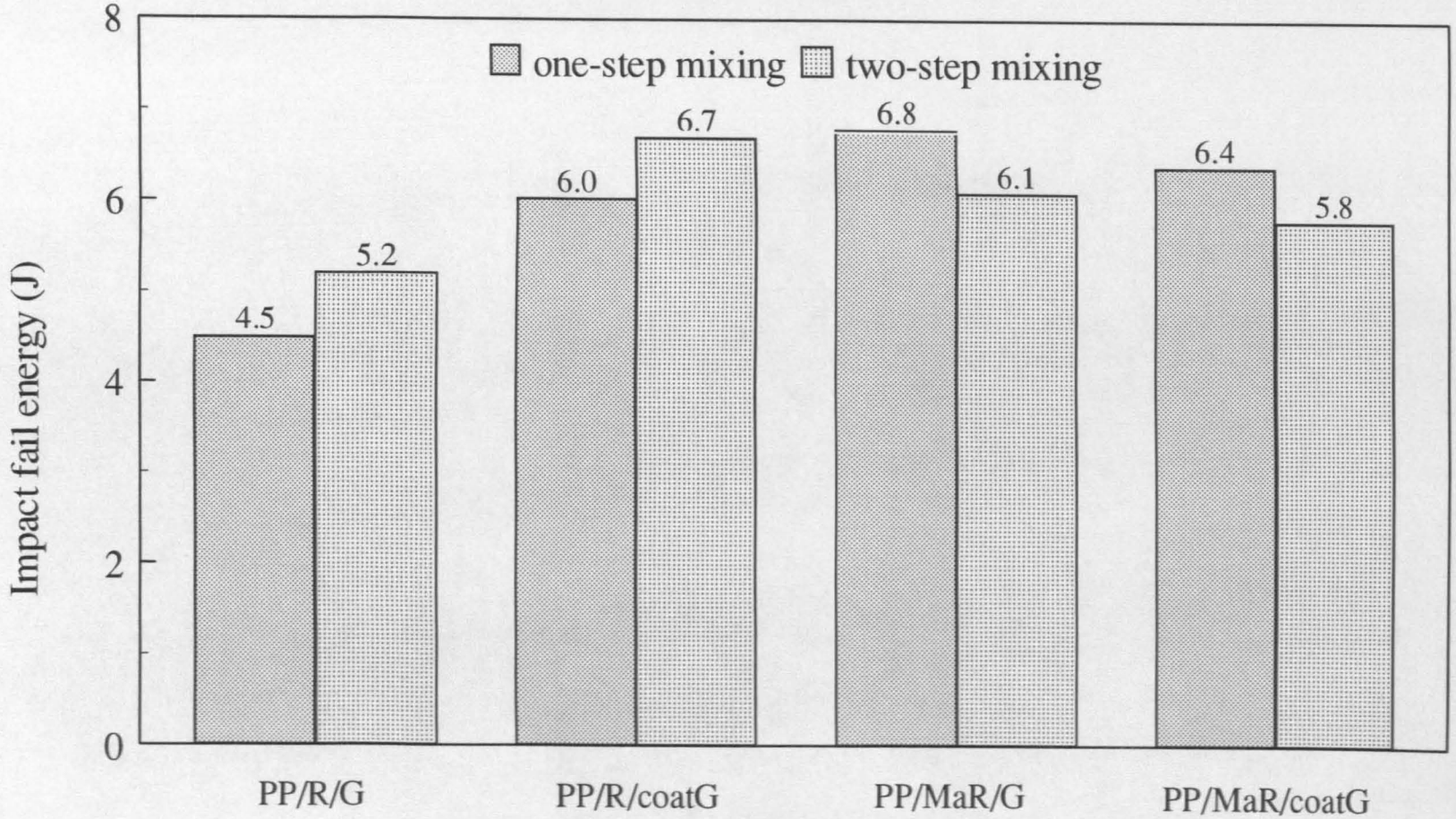

Figure 7.45 Effect of mixing step on the falling weight impact fail energy of various composites

Table 7.10

Effect of mixing step on impact properties at 23 °C of ternary phase polypropylene composites

Sample	Initiation energy (J)	Propagation energy (J)	Failure energy (J)
PP+R+G	3.10 (0.31)[a]	1.47	4.57 (0.23)
(R+G)+PP	3.71 (0.29)	1.50	5.21 (0.23)
PP+R+coatG	4.10 (0.34)	1.93	6.03 (0.33)
(R+coatG)+PP	4.86 (0.25)	1.79	6.65 (0.13)
PP+MaR+G	5.59 (0.32)	1.15	6.74 (0.21)
(MaR+G)+PP	4.98 (0.16)	1.10	6.08 (0.13)
PP+MaR+coatG	4.91 (0.28)	1.51	6.42 (0.32)
(MaR+coatG)+PP	3.97 (0.31)	1.88	5.85 (0.27)

[a] Standard deviations in parentheses, means from six specimens.

CHAPTER 8

CONCLUSIONS AND SUGGESTIONS FOR FURTHER WORK

8.1 CONCLUSIONS

Systematic investigations of polypropylene composites containing ethylene-propylene rubber and glass beads have been carried out. The effect of material characteristics, processing variables and formulations on the composite microstructure and properties were evaluated, from which the following conclusions were drawn.

1. An investigation of the effect of ethylene-propylene rubber (EPR) on the morphology and properties of an isotactic polypropylene (PP) has been carried out. SEM analysis on heptane-etched fracture surfaces showed that PP/EPR blends are two-phase systems consisting of spherical shaped EPR particles distributed in the continuous PP matrix. The average size of EPR particles were found to be determined by the value of the phase viscosity ratio. The particle size of the dispersed EPR was found to be proportional to the viscosity of the dispersed phase, and inversely proportion to the viscosity of the matrix phase.

The mechanical properties of polypropylene at ambient temperatures were found being modified by the incorporation of EPR. Incorporation of 30 %vol. EPR into PP improves impact strength and toughness in the blends, accompanying by a decrease in tensile modulus and tensile strength. The improvement in impact strength and toughness of PP can be explained either by the influence of EPR on the deformation mechanisms in the blends, or by the alteration of blend microstructures due to rubber addition. It was revealed by the investigations on fracture surfaces of PP/EPR blends that cavitation around the rubber particles and shear yielding of PP matrix were primary important toughening mechanisms during the ductile fracture of the PP/EPR blends. Also, the investigations on phase structure of PP/EPR blends by DSC and XRD revealed that incorporation of EPR to PP led to an increase in the degree of undercooling and resulted in a reduction in PP spherulite size. The presence of small PP spherulites interconnected by a large fraction of tie molecules gives more local transfer leading to ductile mechanical properties. The higher efficiency in toughening of PP was observed in the blends containing smaller EPR particles. The reasons for this observation may be explained in terms of more sites for cavitation and less interparticular distances compared to the blends containing large EPR particles of the same concentration.

2. The effect of glass beads on the microstructure of polypropylene has been investigated using SEM and DSC. Glass beads were found to be evenly dispersed in the polypropylene matrix, without evidence of agglomerations. The bead surfaces appeared very smooth and clean, revealing a poor adhesion to the PP matrix. The PP spherulite size in the filled systems was found to be smaller than that in the unfilled polypropylene. DSC results showed that glass beads influenced the crystallisation of polypropylene by acting as nucleating agents, promoting the formation of crystal nuclei. An increase in the number of nuclei, therefore, led to a decline in PP spherulite size.

Contrary to the effect of EPR, the incorporation of glass beads to polypropylene increased the composite modulus but led to a decrease in the composite strength and toughness. The effect of glass beads on the composite mechanical properties was found to be more pronounce as the concentration of glass beads increased, or as the bead particle size decreased. The experimental results obtained in the glass bead filled composites agreed well with some theoretical models. The fracture mechanism in such composites was found to be the dewetting process. SEM observations revealed crack propagation travelled along the interfaces between PP and glass bead particles. The correlation between impact properties and $T_{c\ onset}$, as reported by Hutley and Darlington [129-130], was also found for the filled composites studied in which high $T_{c\ onset}$ was observed in composites with poor impact properties. However, the reasons for this observation are not clear at present.

3. The balance of mechanical properties of polypropylene composites, as presented by tensile modulus and impact strength, was found to be achieved by physical blending of the PP with both EPR and glass beads. The properties of these three-phase composites were mainly determined by composition and phase structure of the composites. The investigated processing variables including screw configuration, screw speed and feed rate showed a minor influence on the composite properties.

Investigation of the morphology of ternary phase polypropylene composites has shown that two kinds of structures can be formed in such systems : either a separate dispersion structure where rubber and glass bead particles are dispersed separately in the PP matrix, or an encapsulation structure where rubber encapsulates glass bead particles, forming a layer between PP matrix and filler particles. The most important factor controlling these phase structures is believed to be due to the surface characteristics of the components, i.e. surface tension, work of adhesion and wettability.

4. It was revealed by SEM and DMA studies that by using maleic-anhydride modified EPR (MaR) instead of unmodified EPR, an encapsulation structure was achieved as a result of an increasing in the surface tension of the rubber phase. Glass bead particles were found to be wetted by MaR. The reaction between these phases was believed to produce the carboxylate salt (CO_2^-) as revealed by a new peak appearing at 1571 cm^{-1} in the FTIR spectrum. Due to a good interfacial adhesion between phases in the system, stress transfers continuously throughout the composites. The SEM fracture surfaces showed a cohesive failure in which the crack proceeded through the PP matrix.

In this encapsulation structure, the encapsulating rubber suppressed filler reinforcing effect and altered the stress concentration from the poles to the equator of the particles, resulting in a composite with a lower tensile modulus accompanying by a higher impact strength and toughness. Apart from the improvement in impact strength at ambient temperatures, the J-integral test at -20°C also revealed a significant improvement in composite fracture toughness by the incorporation of MaR. In the binary blends of PP and MaR, J_c of polypropylene was found being improved more than 200% and in the ternary phase composites containing MaR composite toughness at -20°C was found to be higher than in unmodified polypropylene and, interestingly, higher than in the binary PP/EPR blend.

5. In the unmodified PP, EPR and glass bead composites, on the other hand, a separate dispersion structure was observed. This structure could not be changed either by altering the sequence in which the components were mixed in the twin-screw extruder, or by introducing more rubber contents into the composites.

Composites with separate dispersion structure showed a higher tensile modulus but lower impact strength and toughness. Composition dependency of composite mechanical properties in this system was well predicted by theoretical models. Due to a poor interfacial adhesion between glass bead particles and the PP matrix in this system, SEM observations revealed crack propagation occurred by particle-matrix debonding or interfacial failure. Improvement in composite adhesion was found being achievable by the use of silane coated glass beads. The ternary phase composites containing coated glass showed higher elongation at yield and at break, also higher impact strength than the composites containing unmodified glass beads.

Although phase structure of ternary composites cannot be changed, from separate dispersion to encapsulation, by altering the sequences in which each component was

Although phase structure of ternary composites cannot be changed, from separate dispersion to encapsulation, by altering the sequences in which each component was mixed in the extruder. It was found for composites with separate dispersion structure that by mixing the rubber and glass beads prior to polypropylene there was a tendency of more rubber particles adhering on the glass bead surface. Such composite, interestingly, provided a slightly better impact strength than the composites prepared by one-step mixing. In the case of composites with encapsulation structure, contradictory results were observed. By using a two-step mixing technique impact strength was found to drop around 10%. This suggested that the presence of rubber around the filler particles instead of separate from the filler was favourable for better impact strength.

8.2 SUGGESTIONS FOR FURTHER WORK

In the view of present study considerable scope exists for further investigations in this area of research, areas of particular interest are summarised below.

1. The J-integral method based on stress-whitening length measurement described in this thesis has been shown being suitable for evaluating fracture toughness of tough materials including polypropylene blends and multiphase polypropylene composites. Owing to the time limitation, selected composites were investigated using this technique. It might be useful to apply this technique to evaluate the effect of mixing step on the low temperature fracture toughness of the composites, especially in composites with separate dispersion structure in which a slightly better impact strength (at 23°C) was observed in the composite prepared by two-step mixing technique.

2. Results from this research have shown that by using maleic-anhydride modified EPR (MaR) instead of unmodified EPR, a composite with an encapsulation structure was achieved. However, due to the high viscosity of polymer melt and small amount of MaR in the composite, fully (perfect) encapsulation is not reached. Future study on MaR content and/or the amount of maleic-anhydride in the rubber should emphasise their effect on composite structure and properties.

3. Investigations on the morphology of ternary phase of polypropylene, ethylene-propylene rubber and glass beads indicated a lack of adhesion between PP matrix and filler particles. Apart from using surface coated glass beads, improvement in this adhesion can be achieved by modification of polypropylene either with acrylic acid or

maleic-anhydride. In future study functionalisation of the polypropylene matrix may be considered.

4. The strength of multiphase polymer composites is strongly dependent upon the success with which applied loads are able to be transferred throughout the composite. This characteristic is in turn a function of the level of adhesion at the matrix-particle interface. Therefore, the development of an experimental procedure which would permit the quantitative characterisation of the level of interface bonding would contribute significantly to the mechanical behaviours of composites. On such procedures, extraction analysis and spectroscopy have been used. For multiphase polypropylene composites consisting of EPR or EPDM and fillers, extraction with n-heptane or xylene are customary used. The undissolved fractions after extraction process may be characterised using infrared spectroscopy and thermogravimetry to analyse the amount and/or thickness of the bound polymer layer in the interphase region.

REFERENCES

1. Vittoria, V., in **"Handbook of Polymer Science and Technology"**, vol. 2, edited by N.P. Cheremisinoff, Marcel Dekker, New York, 1989, pp.507-556.
2. Turner-Jones, A., Aizlewood, J.M. and Beckett, D.R., ***Macromol. Chem.***, 1964, 75, 134.
3. Natta, G. and Corradini, P., ***Nuovo Cim. Supp.***, 1960, 15, 1.
4. Keith, H.D., Padden, F.J., Walter, N.M. and Wycoff, M.W., ***J.App.Phys.***, 1959, 30, 1485.
5. Turner-Jones, A. and Cobbold, A.J., ***J.Polym.Sci.***, 1968, 6, 539.
6. Samuels, R.J. and Yee, R.Y., ***J.Polym.Sci.-Polym.Phys.***, 1972, 10, 385.
7. Dragaun, H., Hubeny, H. and Muschik, H., ***J.Polym.Sci.Phys.***, 1977, 15, 641.
8. Lovinger, A.J., Chua, T.O. and Gryte, C.C., ***J.Polym.Sci.***, 1977, 15, 641.
9. Varga, J., ***J.Thermal.Anal.***, 1986, 31, 165.
10. Varga, J., Schlek-Toth, F. and Ille, A., ***Colloid Polym.Sci.***, 1991, 269, 655.
11. Ullmann, W. and Wendorff, J.H., ***Progr.Coll.Polym.Sci.***, 1979, 66, 25.
12. Garbarczyk, J. and Paukszta, D., ***Colloid Polym.Sci.***, 1965, 263, 985.
13. Leugering, H.J., ***Macromol.Chem.***, 1967, 109, 204.
14. Duswalt, A., ***Amer.Chem.Soc.Div.Org.Coat.***, 1970, 30, 93.
15. Addink, E.J. and Beintema, J., ***Polymer***, 1961, 2, 185.
16. Phillips, P.J. and Campbell, R.A., ***SPE ANTEC Tech.Papers***, 1991, 896.
17. Mc Allister, P.B., Carter, F.J. and Hinde, R.M., ***J.Polym.Sci.Polym.Phys.***, 1978, 16, 49.
18. Corradini, P., De Rosa, C., Guerra, G. and Petracco, V., ***Polym.Commun.***, 1989, 30, 281.
19. Varga, J., ***J.Mat.Sci.***, 1992, 27, 2557.
20. Padden, F.J. and Keith, H.D., ***J.Appl.Phys.***, 1959, 30, 1479.
21. Norton, D.R. and Keller, A., ***Polymer***, 1985, 26, 704.
22. Khoury, F.J., ***J.Res.Nat.Bur.Stand.***, 1966, A70, 29.
23. Rybnikar, F., ***J.Macromol.Sci-Phys.***, 1991, B30 (3), 201.
24. Wunderlich, B., **"Macromolecular Physics"**, Vol.2, Academic Press, London, 1976.
25. Plochocki, A.P., in **"Polymer Blends"**, edited by D.R. Paul and S. Newman, Acadymic Press, New York, 1978, chapter 21.
26. Karger-Kocsis, J., Kallo, A., Szafner, A., Bodor, G. and Senyei, Zs., ***Polymer***, 1979, 20, 37.

27. Vernon, W.D., in **"Advance in Polymer Blends and Alloys Technology"**, vol.2, edited by M.A. Kohudic and K.Finlayson, Technic Publishing Company, USA, 1989, pp. 12-24.
28. Lohse, D.J., ***Polym.Eng.Sci.***, 1986, 26 (21), 1500.
29. Karger-Kocsis, J., Kiss, L. and Kuleznev, V.N., ***Polym. Commun.***, 1984, 25, 122.
30. Pukanszky, B., Tudos, F., Kallo, A. and Bodor,G., ***Polymer***, 1989, 30, 1399.
31. Speri, W.M. and Patrick, G.R., ***Polym.Eng.Sci.***, 1975, 15(9), 668.
32. Goizueta, G., Chiba, T. and Inoue, T., ***Polymer***, 1992, 33(4), 886.
33. Tervoort-Engelen, Y. and Van Gisbergen, J., ***Polym. Commun.***, 1991, 32, 261.
34. Sain, M.M., Hudec, I., Beniska, J. and Rosner, P., ***Mat. Sci. Eng.***, 1989, 108, 63.
35. Hudec, I., Sain, M.M. and Kozankora, J., ***Polym. testing***, 1991, 10, 387.
36. D'Orazio, L., Mancarella, C., Martuscelli, E. and Polato, F., ***Polymer***, 1991, 32, 1186.
37. Greco, R., Mancarella, C., Martuscelli, E., Ragosta, G. and Jinghua, Y., ***Polymer***, 1987, 28, 1929.
38. Karger-Kocsis, J., Kallo, A. and Kuleznev, V.N., ***Polymer***, 1984, 25, 279.
39. Martuscelli, E., Silvestre, C. and Bianchi, L., in **"Polymer blends: Processing Morphology and Properties"**, vol.2, edited by Kryszewski, M., Galeski, A. and Martuscelli, E., Plenum Press, New York, 1984, pp. 57-71.
40. Laus, Th., ***Makro. Chem.***, 1977, 60/61, 87.
41. Avgeropoulos, G.N., Weissert, F.C., Biddison, P.H. and Bohm, G.G.A., ***Rubber Chem.Technol.***, 1976, 49, 93.
42. Hlavata, D., Plestil, J., Zuchowska, D. and Steller, R., ***Polymer***, 1991, 32, 3313.
43. Choudhary, V., Varma, H.S. and Varma, I.K., ***Polymer***, 1991, 32(14), 2534.
44. Kammer, H.W., Kummerloewe, C., Grego, R., Mancarella, C. and Martuscelli, E., ***Polymer***, 1988, 29, 963.
45. Bartczak, Z., Galeski, A., Martuscelli,E. and Janik, H., ***Polymer***, 1985, 26, 1843.
46. Karger-Kocsis, J. and Kiss, L., ***Polym.Eng.Sci.***, 1987, 27, 4.
47. Danesi, S. and Porter, R.S., ***Polymer***, 1978, 19, 448.
48. Han, C.D., **"Multiphase Flow in Polymer Processing"**, Academic Press, New York, 1981.
49. White, P.L., Plochocki, A.P. and Tanaka, H., ***Polym.Eng.Rev.***, 1981, 1, 217.
50. Alle, N. and Lyngaae-Joergensen, J., ***Rheol.Acta.***, 1980, 19, 94.
51. Hayashida, K., Takahashi, J. and Matsui, M., in **"Proc. 5th Int. Rheological Congress"**, Vol.4, edited by S. Onogi, University of Tokyo Press, Tokyo, 1970, pp. 523-35.
52. Pukanszky, B., Tudos, E., Kallo, A. and Bodor, G., ***Polymer***, 1989, 30, 1407.

53. Fortelny, I. and Kovar, J., ***Eur. Polym. J.***, 1992, 28, 85.
54. Bucknall, C.B., **"Toughened Plastics"**, Applied Science Publishers, London, 1977.
55. Maurer, F.H.J., in **"Polymer Composites"**, edited by Sedlacek, B., Walter de Gruyter, Berlin, 1986, pp.399-412.
56. Paakkonen, E.J., Magonov, S.N. and Tormala, P., in **"Polymer Composites"**, edited by Sedlacek, B., Walter de Gruyter, Berlin, 1986, pp.199-206.
57. Pukanszky, B., Tudos, F., Kolarik, J. and Lednicky,F., ***Polym. Compos.***, 1990, 11(2), 98.
58. Jang, B.Z., Uhlmann, D.R. and Vander Sande, J.B., ***J. Appl. Polym. Sci.***, 1984, 29, 4377.
59. Onogi, S., Asada, T. and Tanaka, A., ***J.Polym.Sci.(A)***, 1969, 2, 171.
60. Bartczak, Z., Galeski, A. and Martuscelli, E., ***Polym.Eng.Sci.***, 1984, 24, 1115.
61. Martuscelli, E., Silverstre, C. and Abate, G., ***Polymer***, 1982, 23, 229.
62. Kalfoglou, N.K., ***Agew.Macromol.Chem.***, 1985, 129, 103.
63. Bartilla, T., Kirch, D., Nordmeier, J., Promper, E. and Strauch, Th., ***Adv. Polym. Tech.***, 1986, 6, 339.
64. Ho, W-J. and Salovey, R., ***Polym.Eng.Sci.***, 1981, 21(13), 839.
65. Fortelny, I., Kamenicka, D. and Kovar, J., ***Angew. Makro. Chem.***, 1988, 164, 125.
66. Baer, M., ***J.Appl.Polym.Sci.***, 1972, 16, 1109.
67. Dao, K.C., ***Polymer***, 1984, 25, 1527.
68. Dao, K.C., ***J.Appl.Polym.Sci.***, 1982, 27, 4799.
69. Stehling, F.C., Huff, T., Speed, C.S. and Wissler, G., ***Appl.Polym.Sci.***, 1981, 26, 2693.
70. Rice, J.R, ***J.Appl.Mech.***, 1968, 35, 379.
71. Williams, J.G , ***Polym.Eng.Sci.***, 1977, 17(3), 144.
72. Hashemi, S. and Williams, J.G, ***J.Mat.Sci.***, 1984, 19, 3746.
73. Fernando, P.L and Williams, J.G, ***Polym.Eng.Sci.***, 1980, 20(3), 215.
74. Hashemi, S. and Williams, J.G, ***Polym.Eng.Sci.***, 1986, 26(11), 760.
75. Hashemi, S. and Williams, J.G, ***Plas.Rubb.Proc.App.***, 1986, 6, 363.
76. Kim, B.H, Joe, C.R and Otterson, D.M, ***Polym.Testing***, 1989, 8, 119.
77. Huang, D.D and Williams, J.G, ***J.Mat.Sci.***, 1987, 22, 2503.
78. Lee, C.B and Chang, F.C, ***Polym.Eng.Sci.***, 1992, 32(12), 792.
79. Narisawa, I. and Takemori, M.T, ***Polym.Eng.Sci.***, 1989, 29(10), 671.
80. Zhang, M-J, Zhi, F-X and Su, X-R, ***Polym.Eng.Sci.***, 1989, 29(16), 1142.
81. Kim, B.H and Joe, C.R, ***Int.J.Fracture***, 1987, 34, 57.
82. Hashemi, S. and William, J.G, ***Polymer***, 1986, 27, 384.

83. Narisawa, I., ***Polym.Eng.Sci.***, 1987, 27(1), 41.
84. Ha, C., Kim, Y. and Cho, W., ***J.Polym.Sci.***, 1994, 51, 1381.
85. Bucknall, C.B., in **"Polymer Blends"**, Vol.2, edited by D.R. Paul and S. Newman, Academic Press, New York, 1978, Chapter 14.
86. Kinloch, A.J. and Young, R.J., **"Fracture Behaviour of Polymers"**, Applied Science Publisher, London, 1983.
87. Lange, F.F. and Radford, K.C., ***J.Mat.Sci.***, 1971, 6, 1197.
88. Wu, S., ***J.Polym.Sci.-Polym.Phys.***, 1983, 21, S699.
89. Wu, S., ***J.Appl.Polym.Sci.***, 1988, 35, 549.
90. Jang, B.Z., Uhlmann, D.R. and Vader Sande, J.B., ***J.Appl.Polym.Sci.***, 1985, 30, 2485.
91. Merze, E.H., Claver, G.C. and Baer, M.J., ***J.Polym.Sci.***, 1956, 22, 325.
92. Newman, S. and Strella, S., ***J.Appl.Polym.Sci.***, 1965, 9, 2297.
93. Kambour, R.P., ***Macromol.Rev.***, 1971, 7, 134.
94. Wu, S., ***Polymer***, 1985, 26, 1855.
95. Pukanszky, B., Fortelny, I., Kovar, J. and Tudos,F.,***Plas.Rubb.Comp.Proc.Appl.***, 1991, 15, 31.
96. Taylor, G.I., ***Proc.Roy.Soc.***, 1934, A146, 501.
97. Tokita, N., ***Rubber Chem.Technol.***, 1977, 50, 292.
98. Walczak, Z.K., ***J.Appl.Polym.Sci.***, 1973, 17, 169.
99. Han, C.D., Villamizar, C.A. and Kim, Y.W., ***J.Appl.Polym.Sci.***, 1977, 21, 353.
100. D'Orazio, L., Greco, R., Mancarella, C., Martuscelli, E., Ragosta, G. and Silvestre, C., ***Polym.Eng.Sci.***, 1982, 22, 536.
101. ASTM standard E813-81, 1982.
102. Schlumpf, H.P., in **"Plastic Additives Handbook"**, edited by Gachter, R. and Muller, H., Hanser Publishers, New york, 1990, Chapter 9.
103. Jilken, L., Malhammer, G. and Selden, R., ***Polym. Testing***, 1991, 10, 329.
104. Pukanszky, B., Tudos, F. and Kelen, T., in **"Polymer Composites"**, edited by Sedlacek, B., Walter de Gruyter, Berlin, 1986, pp. 167-182.
105. Chartoff, R.P. and Eriksen, E.H., in **"Polymer Composites"**, edited by Sedlacek, B., Walter de Gruyter, Berlin, 1986, pp. 89-104.
106. Busigin, C., Lahtinen, R., Matinez, G.M., Thomas, G. and Woodhams, R.T., ***Polym.Eng.Sci.***, 1984, 24(3), 169.
107. Riley, A.M., Paynter, C.D., McGenity, P.M. and Adams, J.M., ***Plast.Rubb.Proc.App.***, 1990, 14, 85.
108. Nielsen, L.E., **"Mechanical Properties of Polymers and Composites"**, vol.2, Marcel Dekkar, New York, 1974.

109. Manson, J.A. and Spering, L.H., **"Polymer Blends and Composites"**, Plenum Press, New York, 1976.
110. Chacko, V.P., Farris, R.J. and Karasz, F.E., ***J.Appl.Polym.Sci.***, 1983, 28, 2701.
111. Einstein, A., ***Ann.der Phys.***, 1906, 19, 289.
112. Guth, E., ***J.Appl.Phys.***, 1944, 15, 758.
113. Mooney, M., ***J.Colloid Sci.***, 1951, 6, 162.
114. Kerner, E.H., ***Proc.Phys.Soc.London***, 1956, B69, 808.
115. Nielsen, L.E., ***J. Appl. Phys.***, 1970, 41, 4626.
116. Bigg, D.M., ***Polym.Eng.Sci.***, 1979, 16, 1188.
117. Nicolais, L. and Nicodemo, L., ***Polym.Eng.Sci.***, 1973, 13, 469.
118. Leidner, J. and Woodhams, R.T., ***J.Appl.Polym.Sci.***, 1974, 18, 1639.
119. Nielsen, L.E., ***J. Appl. Polym. Sci.***, 1966, 10, 97.
120. Vu-Khanh, T. and Decharentenay, F.X., ***Polym.Eng.Sci.***, 1985, 25, 841.
121. Kendall, K. and Sherliker, F.R., ***Brit. Polym. J.***, 1980, 12, 85.
122. Miller, J.D. and Ishida, H., in **"Polymer Composites"**, edited by B. Sedlacek, Walter de Gruyter, Berlin, 1986, pp. 449-456.
123. Miller, J.D., Ishida, H. and Maurer, F.H.J., ***Rheol.Acta***, 1988, 27, 397.
124. Pukanszky, B., Fekete, E. and Tudos, F., ***Makro.Chem.***, 1989, 28, 165
125. Han, C.D., Weghe, T., Shete, D. and Haw, J.R., ***Polym.Eng.Sci.***, 1981, 21(4), 196.
126. Szijarto, K. and Kiss,P., in **"Polymer Composites"**, edited by B. Sedlacek, Walter de Gruyter, Berlin, 1986, pp. 473-478.
127. Kalay, G., Allan, P.and Bevis, M.J., ***Polymer***, 1994, 35(12), 2480.
128. Alonso, M., Gonzalez, A., de Saja, J.A. and Requejo, A., ***Plas.Rubb.Comp.Proc.App.***, 1993, 20, 165.
129. Hutley, T.J. and Darlington, M.W., ***Polym. Commu.***, 1984, 25, 226.
130. Hutley, T.J. and Darlington, M.W., ***Polym. Commu.***, 1985, 26, 264.
131. Khunova, V., Smatko, V., Hudec, I. and Beniska, J., ***Prog. Colloid Polym. Sci.***, 1988, 78, 188.
132. Xavier, S.F., Schultz, J.M. and Friedrich, K., ***J.Mat.Sci.***, 1990, 25, 2411.
133. Morale, E., Ojeda, M.C., Linares, A. and Acosta, J.L., ***Polym.Eng.Sci.***, 1992, 32(12), 769.
134. Jancar, J., ***J.Mat.Sci.***, 1991, 26, 4123.
135. Dao, K.C. and Hatem, R.A., ***SPE ANTEC Tech.Papers***, 1984, 30, 198.
136. Kitamura, H., ***Proc.4th Intl.Conf.Composite Mater.***, ICCM-IV, Tokyo, 1982, 1787.
137. Comitov, P.G., Nicolova, Z.G., Simeonov, I.S., Naidenova, K.V. and Siarova, A.D., ***Eur.Polym.J.***, 1984, 20, 405.

138. Ronca, G., **PhD Thesis**, Brunel University, London, 1985.
139. Utracki, L.A., **"Polymer Alloys and Blends - *Thermodynamics and Rheology*"**, Hanser Publisher, Munich, 1989.
140. Miles, I.S. and Rostami, S., **"Multicomponent Polymer Systems"**, Polymer Science and Technology Series, Longman, U.K., 1992.
141. Stamhuis, J.E., ***Polym.Compos.***, 1984, 5(3), 202.
142. Stamhuis, J.E., ***Polym.Compos.***, 1988, 9(1), 72.
143. Stamhuis, J.E., ***Polym.Compos.***, 1988, 9(4), 280.
144. Pukanszky, B., Kolarik, J. and Lednicky, F., in **"Polymer Composites"**, edited by B. Sedlacek, Walter de Gruyter, Berlin, 1986, pp.553-560.
145. Pukanszky, B., Tudos, F., Kolarik, J. and Lednicky, F., ***Polym.Compos.***, 1990, 11(2), 98.
146. Kolarik, J., Lednicky, F., Jancar, J. and Pukanszky, B., ***Polym.Comm.***, 1990, 31, 201.
147. Kolarik, J. and Jancar, J., ***Polymer***, 1992, 33(23), 4961.
148. Kolarik, J. and Lednicky, F., in **"Polymer Composites"**, edited by B. Sedlacek, Walter de Gruyter, Berlin, 1986, pp.537-544.
149. Kolarik, J., Pukanszky, B. and Lednicky, F., ***Compos.Polym.***, 1990, 2, 271.
150. Marosi, Gy., Bertalan, Gy., Rusznak, I., Anna, P. and Molnar, I., in **"Polymer Composites"**, edited by B. Sedlacek, Walter de Gruyter, Berlin, 1986, pp.457-464.
151. Marosi, Gy., Bertalan, Gy., Rusznak, I. and Anna, P., ***Colliod and Surfaces***, 1986, 23, 185.
152. Faulkner, D.L., ***J.Appl.Polym.Sci.***, 1988, 36, 467.
153. Chiang, W-Y, Yang, W. and Pukanszky, B., ***Polym.Eng.Sci.***, 1992, 32(10), 641.
154. Kosfeld, R., Schaefer, K., Kemmer, E.A., Hess, M., Theinsen, A. and Uhlenbroich, T.H., in **"Controlled Interphases in Composite Materials"**, edited by H.Ishida, Elsevier Science Publishing Company, 1990, pp.385-390.
155. Kosfeld, R., Schaefer, K., Kemmer, E.A. and Hess, M., in **"Integration of Polymer Science and Technology-4"**, edited by P.J.Lemstra and L.A.Kleintjens, Elsevier Applied Science, London, 1990, pp.326-334.
156. Schaefer, K., Hess,M., Kosfeld, R. and Uhlenbroich, T.H., ***Kunststoffe***, 1990, 80(12), 19.
157. Schaefer, K., Theinsen, A., Hess, M. and Kosfeld, R., ***Polym.Eng.Sci.***, 1993, 33(16), 1009.
158. Theisen, A., Heβ, M. and Kosfeld, R., in **"Integration of Polymer Science and Technology-5"**, edited by P.J.Lemstra and L.A.Kleintjens, Elsevier Applied Science, London, 1990, pp.72-76.

159. Speri, W.M. and Patrick, G.R., ***Polym.Eng.Sci.***, 1975, 15(9), 668.
160. Scott, C., Ishida, H. and Maurer, F.H.J., ***J.Mat.Sci.***, 1987, 22, 3963.
161. Scott, C., Ishida, H. and Maurer, F.H.J., ***Rheol. Acta***, 1988, 27(3), 273.
162. Scott, C., Ishida, H. and Maurer, F.H.J., ***J.Mat.Sci.***, 1991, 26, 5708.
163. Varga, J., ***J.Polym.Eng.***, 1991, 1(1-3), 231.
164. Varga, J., ***J.Thermal.Anal.***, 1989, 35, 1891.
165. Janssen, L.P.B.M., **"Twin Screw Extrusion"**, Elsevier, Amsterdam, 1978.
166. Rauwendaal, C., **"Polymer Extrusion"**, Hanser Publishers, New York, 1986.
167. White, J.L., Szydlowski, W., Min, K. and Kim, M-H, ***Adv.Polym.Tech.***, 1987, 7(3), 295.
168. White, J.L., **"Twin Screw Extrusion - Technology and Principles"**, Hanser Publishers, New York, 1990.
169. Cheremisinoff, N.P., **"Polymer Mixing and Extrusion Technology"**, Marcel Dekker, Inc., New York, 1987, Chapter 6.
170. Martelli, F.G., **"Twin-Screw Extruders"**, Van Nostrand Reinhold Company Inc., New York, 1983.
171. Sakai, T., Hashimoto, N. and Kobayashi, N., ***SPE ANTEC Tech.Paper***, 1987, 146.
172. Rauwendaal, C., ***Polym.Eng.Sci.***, 1981, 21(16), 1092.
173. Hornsby, P.R., ***Plast.Compounding***, 1983, Sept/Oct, 65.
174. Ess, J.W., Hornsby, P.R., Lin, S.Y. and Bevis, M.J., ***Plast.Rubb.Proc.Appl.***, 1984, 4, 7.
175. Hornsby, P.R., ***Plast.Rubb.Proc.Appl.***, 1987, 7, 237.
176. Ess, J.W. and Hornsby, P.R., ***Plast.Rubb.Proc.Appl.***, 1987, 8, 147.
177. Ess, J.W. and Hornsby, P.R., ***Polym.Testing***, 1986, 6, 205.
178. Hornsby, P.R. and Sothern, G.R., ***Plast.Rubb.Proc.Appl.***, 1984, 4(2), 165.
179. Lim, S. and White, J.L., ***Intern.Polym.Processing***, 1993, 2, 119.
180. Reynolds, G.E.J., ***Rubb.Proc.Appl.***, 1987, 7, 237.
181. Encyclopedia of Polymer Science and Engineering, 2nd ed., vol.6, John Wiley & Sons, Inc., USA, 1986, pp. 617.
182. Folkes, M.J., **"Short Fibre Reinforced Thermoplastics"**, Research Studies Press, Letchworch, UK, 1982.
183. Folkes, M.J., in **"Multicomponent Polymer Systems"**, edited by I.S.Miles and S.Rostami, Polymer Science and Technology Series, Longman, U.K., 1992, Chapter 8.
184. Plueddemann, E.P., in **"Fundamental of Adhesion"**, edited by L-H. Lee, Plenum Press, New York, 1991, Chapter 9.
185. BASF data sheets for Novolen 1100HX and Novolen 1100L.

186. Exxon Chemical Company data sheets for Exellor PE805, Exellor PE808 and Exellor VA1803.
187. Croxton & Garry Ltd. data sheets for Spherical 3000CPOO, Spherical 5000 CPOO and Sperical 5000CPO3.
188. Wu, S., ***Polym.Eng.Sci.***, 1987, 27, 335.
189. Kantz, M.R., Newman, H.D. and Stigale, F.H., ***J.Appl.Polym.Sci.***, 1972, 16, 1249.
190. Fujiyama, M., Awaya, H. and Kimura, S., ***J.Appl.Polym.Sci.***, 1977, 21, 3291.
191. Fujiyama, M. and Wakino, T., ***J.Appl.Polym.Sci.,*** 1988, 35, 29.
192. Fujiyama, M. and Azuma, K., ***J.Appl.Polym.Sci.***, 1979, 23, 2807.
193. Michaeli, W., Cremer, M. and Aachen, R.B., ***Kunststoffe***, 1993, 83(12), 992.
194. Jones, D.P., Leach, D.C. and Moore, D.R., ***Plast.Rubb.Proc.Appl.***, 1986, 6, 67.
195. Reed, P.E., ***Plast.Rubb.Comp.Proc.Appl.***, 1992, 17, 157.
196. Mooij, J.J., ***Polym.Testing***, 1981, 2, 69.
197. Begley, J.A and Landes, J.D, in **"Fracture toughness"** ASTM STP 514, American Society for Testing and Materials, 1972.
198. Kim, B.H. and Joe, C.R., ***Polym. Testing***, 1987, 7, 355.
199. Kim, B.H. and Joe, C.R., ***Eng.Fracture Mech.***, 1989, 32(2), 225.
200. Kim, B.H. and Joe, C.R., ***Eng.Fracture Mech.***, 1989, 32(1), 155.
201. Begley, J.A and Landes, J.D, ***ASTM STP 560***, 1974, 170.
202. Rivin, R.S. and Thomas, A.G., ***J.Polym.Sci.***, 1953, 10, 291.
203. Oh, H.L., ***ASTM STP 590***, 1976, 104.
204. Paris, P.C., Tada, H., Zahoor, A. and Ernst, H., ***ASTM STP 668***, 1979, 5.
205. Jancar, J. and Dibenedetto, A.T., ***J.Mat.Sci.***, 1994, 29, 4651.
206. Bershtein, V.A. and Egorov, V.M., **Differential Scanning Calorimetry of Polymers - *physics, chemistry, analysis, technology***, Ellis Horwood Ltd., Chichester, 1994.
207. Fitchman, D.R.and Newman, S., ***J.Polym.Sci.***, 1970, 8, 1545.
208. Palmer, R.P. and Cobbold, A.J., ***Macromol.Chem.***, 1969, 74, 174.
209. Olley, R.H., Hodge, A.M. and Basset, D.C., ***J.Polym.Sci.-Polym Phys.***, 1979, 17, 627.
210. Basset, D.C., in **"Comprehensive Polymer Science : *The Synthesis, Characterisation, Reactions and Applications of Polymers*"**, edited by G.Allen, Pergamon Press, Oxford, 1989, pp.841-865.
211. Aboulfaraj, M., Ulrich, B., Dahoun, A. and G'Sell, C. ***Polymer***, 1993, 34(23), 4817.
212. Basset, D.C. and Hodge, A.M., ***Proc.Roy.Soc.***, 1981, A377, 25.
213. Rybnikar, F., ***J.Appl.Polym.Sci.***, 1985, 30, 1949.

214. Olley, R.H. and Basset, D.C., ***Polymer***, 1982, 23, 1707.
215. Franke, B., ***J.Prakt.Chem.***, 1887, 36, 31.
216. Carrington, A. and Symons, M.C.R., ***Chem.Rev.***, 1973, 63, 443.
217. Underwood, E.E., in **"Quantitative Microscopy"**, edited by R.T. Dehoff and F.N. Rhines, McGraw-Hill, New York, 1968, pp. 162-167.
218. Allen, T., **"Particle Size Measurement"**, 3rd ed.- Powder technology series, Chapman and Hall, London, 1981, pp. 210-211.
219. Covas, J.A. and Gilbert, M., ***Polym.Eng.Sci.***, 1992, 32(11), 743.
220. Covas, J.A., Gilbert, M. and Marshall, D.E., ***Plast.Rubb.Proc.Appl.***, 1988, 9(2), 107.
221. Takayanagi, M., Imada, K., Nagai, A., Tatsumi, T. and Matsuo, T., ***J.Polym.Sci.***, 1967, 16, 867.
222. Inamura, I., Ochiai, H. and Yamamura, H., ***J.Polym.Sci. Polym. Phys.***, 1976, 14, 1221.
223. Wetton, R.E. and Corish, P.J., ***Polym.Testing***, 1989, 8, 303.
224. Bales, F.S., Cohen, R.E. and Argon, A.S., ***Macromolecules***, 1983, 16, 1108.
225. Gezovich, D.M. and Geil, P.H., ***Polym.Eng.Sci.***, 1968, 8(3), 202.
226. Samuels, R.J., ***J.Polym.Sci.-Polym.Phys.***, 1972, 10, 385.
227. Dao, K.C., ***SPE ANTEC Tech.Papers***, 1983, 49.
228. Danusso, F. and Gianotti, G., ***Eur.Polym.J.***, 1986, 4, 165.
229. Encyclopedia of Polymer Science and Engineering, 2nd ed., vol.6, John Wiley & Sons, Inc., USA, 1986, pp. 532-533.
230. Ogawa, T., ***J.Appl.Polym.Sci.***, 1992, 44, 1869.
231. Way, J.L., Atkinson, J.R. and Nulting, J., ***J.Mat.Sci.***, 1974, 9, 293.
232. Roark, R.J. and Young, W.C., **Formular for stress and strain**, 5th ed., McGraw-Hill, NewYork, 1975.
233. Jang, B.Z., Uhlmann, D.R. and Vander Sande, J.B., ***J.Appl.Polym.Sci.***, 1984, 29, 3409.
234. Borggreve, R.J.M., Gaymans, R.J., Schuijer, J. and Ingen Housz, J.F., ***Polymer***, 1987, 28, 1489.
235. Ramsteiner, F. and Heckmann, W., ***Polym.Commu.***, 1985, 26, 199.
236. Bucknall, C.B., Heather, P.S. and Lazzeu, A., ***J.Mat.Sci.***, 1989, 16, 2255.
237. Friedrich, K., ***Fracture***, ICF4, 1977, 3, 1119.
238. Gallagher, M.T., ***SPE ANTEC Tech.Papers***, 1991, 2389.
239. Reiw, C.K. and Kinloch, A.J., **Toughened Plastics I**, Advance in Chemistry Series 233, American Chemical Society, Washington, DC, 1993.
240. Maloney, A.C., Kausch, H.H. and Stieger, H.R., ***J.Mat.Sci.***, 1983, 18, 208.

241. Burke, M., Young, R.J. and Standford, J.L., ***Plast.Rubb.Comp.Proc.Appl.***, 1993, 20, 121.
242. Mandelkern, L., **"Crystallisation in Polymers"**, McGraw-Hill, New York, 1964.
243. Avrami, M., ***J.Chem.Phys.***, 1941, 9, 177.
244. Hoshino, S., Meinecke, E., Powers, J. and Stein, R.S., ***J.Polym.Sci.***, 1965, 3, 3041.
245. Young, R.J. and Lovell, P.A., **"Introduction to Polymers"**, 2nd edition, Chapman & Hall, London, UK, pp.283.
246. Sharples, A., **"Introduction to Polymer Crystallisation"**, Publishers Ltd., London, 1966.
247. Avella, M., Martuscelli, E. and Pracella, M., ***J.Thermal Anal.***, 1983, 28, 237.
248. Avella, M., Martuscelli, E. and Selliti, C., ***J.Mat.Sci.***, 1987, 22, 3185.
249. Dekkers, M.E.J. and Heikens, D., ***J.Appl.Polym.Sci.***, 1983, 28, 3809.
250. Mitsuishi, K., Kodama, S. and Kawasaki, H., ***Polym.Eng.Sci.***, 1985, 25(17), 1069.
251. O'Connor, P.D.T., **"Practical Reliability Engineering"**, 2nd ed., A Wiley-Interscience Publication, John Wiley & Sons, 1985, pp. 49-52.
252. Kova-Svehlova, V.D., ***J.Macromol.Sci.Phys.***, 1982, B21(2), 231.
253. Maiti, S.N. and Lopez, B.H., ***J.Appl.Polym.Sci.***, 1992, 44, 353.
254. Nicolais, L., Drioli, E. and Landel, R.F., ***Polymer***, 1973, 14, 21.
255. Faulker, D.L. and Schmidt, L.R., ***Polym.Eng.Sci.***, 1977, 17(9), 657.
256. Friedrich, K. and Karsch, U.A., ***Fibre Sci.Tech.***, 1983, 18, 37.
257. Pukanszky, B., Belina, K., Rockenbauer, A. and Maurer, F.H.J., ***Composites***, 1994, 25(3), 205.
258. Hay, J.N., ***Br.Polym.J.***, 1971, 3, 74.
259. Hay, J.N., ***J.Polym.Sci.-Polym.Lett.***, 1976, 14, 543.
260. Sharples, A., ***Polymer***, 1962, 3, 250.
261. Hay, J.N. and Przekop, Z., ***J.Polym.Sci.-Polym.Phys.***, 1979, 17, 951.
262. Brown, L.M. and Embury, J.D., in ***"Proc. 3rd Int.Conf. on Strength of Materials"***, Cambridge, 1973, paper 33, pp. 164.
263. Paynter, C.D., McGenity, P.M. and Adams, J.M., ***Filplas***, 12-13 Apr 1989, Manchester, UK, paper 14.
264. Friedrich, K., ***Progr.Colloid Polym.Sci.***, 1978, 64, 103.
265. Tadmor, Z., in **"Integration of fundamental Polymer Science and Technology"**, edited by L.A. Kleintjens and P.J. Lemstra, Elseveir Applied Science Publishers, London, 1986, pp. 367-380.
266. Smit, P.A., ***Rheol.Acta***, 1966, 5, 277.
267. Lim, S. and White, J.L., ***Intern.Polymer Processing***, 1994, 1, 33.

268. Valsamis, L.N., Kenney, M.R., Dagli, S.S., Merhta, D.D. and Plochacki, A.P., ***Adv.Polym.Technol.***, 1988, 8, 115.
269. Agur, E.E., ***Adv.Polym.Technol.***, 1986, 6, 225.
270. Kao, S.V. and Allison, G.R., ***Polym.Eng.Sci.***, 1984, 24, 645.
271. Willis, J.M., Favis, B.D. and Lunt, J., ***Polym.Eng.SCi.***, 1990, 30(17), 1073.
272. Murayama, T., **"Dynamic Mechanical Analysis of Polymeric Materials"**, Elsevier Scientific Publishing Company, Netherlands, 1978.
273. Pukanszky, B., Tudos, F, Kolarik, J. and Lednicky, F., ***Compos.Polym***, 1989, 2, 491.
274. Myers, D., **"Surface, Interfaces, and Colloids - Principles and Applications"**, VCH Publishers, Inc., USA, 1991, pp.357.
275. Zisman, W.A., ***J.Paint Technol.***, 1972, 44(564), 43.
276. McGregor, A. and Penins, L.E., ***Plast.Polym.***, 1970, 38, 192.
277. Owens, D.K., ***J.Appl.Polym.Sci.***, 1970, 14, 1725.
278. Lee, L.H., ***J.Polym.Eng.Sci.***, 1967, 5, 1103.
279. Plueddemann, E.P., **"Silane Coupling Agents"**, Plenum Press, New York, 1982.
280. Lee, L.H., **"Adhesion Science and Technology"**, vol.9B, Plenum Press, New York, 1975, pp.647.
281. Sacher, E., **"Symposium on Silylated Surfaces"**, Gordon & Breach, London, 1983.
282. Dolakova, V. and Hudecek, F., ***J.Macromol.Sci.-Phys.***, 1978, B15(3), 337.
283. Borrgreve, R.J.M., Gaymans, R.J. and Luttmer, A.R., ***Makromol.Chem.Macromol.Sym.***, 1988, 16, 195.
284. Norman, R.H., Stone, M.H. and Wake, W.C., in **"Glass Reinforced Plastics"**, edited by B. Parkyn, Iliffe Books, London, 1970, Chapter 15.
285. Trivedi, B.C. and Culbertson, B.M., **"Maleic Anhydride"**, Plenum Publishing Corporation, New York, 1982.
286. Plueddemann, E.P., in **"Interface in Polymer, Ceramic, and Metal Matrix Composites"**, edited by H. Ishida, Elvier Science Publishing Co., 1988, pp.17.
287. Miles, I.S., in **"Multicomponent Polymer Systems"**, edited by I.S. Miles and S. Rostami, Longman Scientific & Technical, UK, 1992, Chapter 2.
288. Narisawa, I., Ishikawa, M., Ogawa, M. and Sato, T., ***Materials***, 1979, 28, 543.
289. Haaf, F., Breuer, H. and Stabenow, J., ***J.Macromol.Sci.-Phys.***, 1977, B14, 387.
290. Speroni, F., Castoldi, E., Fabbri, P. and Casiraghi, T., ***J.Mat.Sci.***, 1989, 24, 2165.
291. Kramer, E.J. and Berger, L.L., ***Adv.Polym.Sci.***, 1990, 91/92, 1.

APPENDIX I

Tests for differences in means (z test) [251]

The *z* test is a very common *s*-significance test for the hypothesis that the mean of a set of data is the same as that of an assumed *s*-normal population, with know μ and σ . The *z*-statistic is given by

$$z = (|\mu - \chi|) / S_{\chi}$$

$$\text{or } z = (|\mu - \chi|) / \sigma n^{-1/2}$$

where *n* is the sample size, μ is the population mean, χ is the sample mean and σ is the population standard deviation. The *s*-significance level then can be derived from the normal cumulative normal distribution function table.

z	0.00	0.01	0.02	0.03	0.04	0.05	0.06	0.07	0.08	0.09
0.0	0.5000	0.5040	0.5080	0.5120	0:5160	0.5199	0.5239	0.5279	0.5319	0.5359
0.1	0.5398	0.5438	0.5478	0.5517	0.5557	0.5596	0.5636	0.5675	0.5714	0.5753
0.2	0.5793	0.5832	0.5871	0.5910	0.5948	0.5987	0.6026	0.6064	0.6103	0.6141
0.3	0.6179	0.6217	0.6255	0.6293	0.6331	0.6368	0.6406	0.6443	0.6480	0.6517
0.4	0.6554	0.6591	0.6628	0.6664	0.6700	0.6736	0.6772	0.6808	0.6844	0.6879
0.5	0.6915	0.6985	0.6985	0.7019	0.7054	0.7088	0.7123	0.7157	0.7190	0.7224
0.6	0.7257	0.7291	0.7324	0.7357	0.7389	0.7422	0.7454	0.7486	0.7517	0.7549
0.7	0.7580	0.7611	0.7642	0.7673	0.7703	0.7734	0.7764	0.7794	0.7823	0.7852
0.8	0.7881	0.7910	0.7939	0.7967	0.7995	0.8023	0.8051	0.8078	0.8106	0.8133
0.9	0.8159	0.8186	0.8212	0.8238	0.8264	0.8289	0.8315	0.8340	0.8365	0.8389
1.0	0.8413	0.8438	0.8461	0.8485	0.8508	0.8531	0.8554	0.8577	0.8599	0.8621
1.1	0.8643	0.8665	0.8686	0.8708	0.8729	0.8749	0.8770	0.8790	0.8810	0.8830
1.2	0.8849	0.8869	0.8888	0.8907	0.8925	0.8944	0.8962	0.8980	0.8997	0.9015
1.3	0.9032	0.9049	0.9066	0.9082	0.9099	0.9115	0.9131	0.9147	0.9162	0.9177
1.4	0.9192	0.9207	0.9222	0.9236	0.9251	0.9265	0.9279	0.9292	0.9306	0.9319
1.5	0.9332	0.9345	0.9357	0.9370	0.9382	0.9394	0.9406	0.9418	0.9430	0.9440
1.6	0.9452	0.9463	0.9474	0.9485	0.9495	0.9505	0.9515	0.9525	0.9535	0.9545
1.7	0.9554	0.9564	0.9573	0.9582	0.9591	0.9599	0.9608	0.9616	0.9625	0.9633
1.8	0.9641	0.9649	0.9656	0.9664	0.9671	0.9678	0.9686	0.9693	0.9700	0.9706
1.9	0.9713	0.9719	0.9726	0.9732	0.9738	0.9744	0.9750	0.9756	0.9762	0.9767
2.0	0.9773	0.9778	0.9783	0.9788	0.9793	0.9798	0.9803	0.9808	0.9812	0.9817
2.1	0.9821	0.9826	0.9830	0.9834	0.9838	0.9842	0.9846	0.9850	0.9854	0.9857
2.2	0.9861	0.9865	0.9868	0.9871	0.9875	0.9878	0.9881	0.9884	0.9887	0.9890
2.3	0.9893	0.9896	0.9898	$0.9^{2}010$	$0.9^{2}061$	$0.9^{2}035$	$0.9^{2}086$	$0.9^{2}111$	$0.9^{2}134$	$0.9^{2}158$
2.4	$0.9^{2}180$	$0.9^{2}202$	$0.9^{2}224$	$0.9^{2}245$	$0.9^{2}266$	$0.9^{2}286$	$0.9^{2}305$	$0.9^{2}324$	$0.9^{2}343$	$0.9^{2}361$
2.5	$0.9^{2}379$	$0.9^{2}396$	$0.9^{2}413$	$0.9^{2}430$	$0.9^{2}446$	$0.9^{2}461$	$0.9^{2}477$	$0.9^{2}492$	$0.9^{2}506$	$0.9^{2}520$
2.6	$0.9^{2}534$	$0.9^{2}547$	$0.9^{2}560$	$0.9^{2}573$	$0.9^{2}586$	$0.9^{2}598$	$0.9^{2}609$	$0.9^{2}621$	$0.9^{2}632$	$0.9^{2}643$
2.7	$0.9^{2}653$	$0.9^{2}664$	$0.9^{2}674$	$0.9^{2}683$	$0.9^{2}693$	$0.9^{2}702$	$0.9^{2}711$	$0.9^{2}720$	$0.9^{2}728$	$0.9^{2}737$
2.8	$0.9^{2}745$	$0.9^{2}752$	$0.9^{2}760$	$0.9^{2}767$	$0.9^{2}774$	$0.9^{2}781$	$0.9^{2}788$	$0.9^{2}795$	$0.9^{2}801$	$0.9^{2}807$
2.9	$0.9^{2}813$	$0.9^{2}819$	$0.9^{2}825$	$0.9^{2}831$	$0.9^{2}836$	$0.9^{2}841$	$0.9^{2}846$	$0.9^{2}851$	$0.9^{2}856$	$0.9^{2}861$